
Novel Bulky Bis(benzoxazol-2-yl)methane Ligands in s-Block Metal Coordination

Dissertation

zur Erlangung des mathematisch-naturwissenschaftlichen Doktorgrades

„Doctor rerum naturalium“

der Georg-August-Universität Göttingen

im Promotionsprogramm Catalysis for Sustainable Synthesis (CaSuS)

der Georg-August University School of Science (GAUSS)

vorgelegt von

Ingo Köhne

aus Soltau

Göttingen, 2018

Betreuungsausschuss:

Prof. Dr. Dietmar Stalke, Institut für Anorganische Chemie

Prof. Dr. Franc Meyer, Institut für Anorganische Chemie

Prof. Dr. Matthias Tamm, Institut für Anorganische und Analytische Chemie, TU Braunschweig

Mitglieder der Prüfungskommission:

Referent: Prof. Dr. Dietmar Stalke, Institut für Anorganische Chemie

Korreferent: Prof. Dr. Franc Meyer, Institut für Anorganische Chemie

Weitere Mitglieder der Prüfungskommission:

Prof. Dr. Inke Siewert, Institut für Anorganische Chemie

Prof. Dr. Konrad Koszinowski, Institut für Organische und Biomolekulare Chemie

Prof. Dr. Manuel Alcarazo, Institut für Organische und Biomolekulare Chemie

Prof. Dr. Lutz Ackermann, Institut für Organische und Biomolekulare Chemie

Tag der mündlichen Prüfung: 06.04.2018

Für meine Familie

Research is the process of going up alleys to see if they are blind.

Marston Bates

TABLE OF CONTENTS

ABBREVIATIONS	vii
1 INTRODUCTION	1
1.1 Development of the β -Diketiminato Ligand System	1
1.2 Alkali- and Alkaline-Earth-Metal β -Diketiminato Complexes	4
1.3 Low Oxidation State Magnesium β -Diketiminato Complexes	9
1.4 β -Diketiminato Related Ligand Platforms	14
1.5 Outline	21
2 RESULTS AND DISCUSSION	23
2.1 Important Structural Features	23
2.2 Bis(4-Me-benzoxazol-2-yl)methanide (1) Based s-Block Complexes	24
2.2.1 Ligand Synthesis	24
2.2.2 Group 1 Complexes	25
2.2.2.1 [K(THF){(4-Me-NCOC ₆ H ₃) ₂ CH}] _∞ (2)	25
2.2.3 Group 2 Complexes	28
2.2.3.1 [Mg{(4-Me-NCOC ₆ H ₃) ₂ CH}] ₂ (3)	28
2.2.3.2 [Ca(THF) ₂ {(4-Me-NCOC ₆ H ₃) ₂ CH}] ₂ · THF (4)	31
2.2.4 Comparison of Complexes 2-4 and Conclusions	33
2.3 Syntheses of the Bis(4,6- <i>t</i> Bu-benzoxazol-2-yl)methane (7) Ligand and its s-Block Complexes	34
2.3.1 Ligand Synthesis	34
2.3.1.1 3,5-di- <i>tert</i> -butyl-2-nitrophenol (5) & 3,5-di- <i>tert</i> -butyl-2-aminophenol (6)	35
2.3.1.2 Bis(4,6- <i>t</i> Bu-benzoxazol-2-yl)methane (7)	36
2.3.1.3 Excursus: Attempts for Bis(4,6- <i>t</i> Bu-benzoxaphosphol-2-yl)methane (12)	39
2.3.2 Group 1 Complexes	42
2.3.2.1 [Li(THF){(4,6- <i>t</i> Bu-NCOC ₆ H ₂) ₂ CH}] (13)	42
2.3.2.2 [K{ η^5 -(4,6- <i>t</i> Bu-NCOC ₆ H ₂) ₂ CH}] _∞ (14)	47
2.3.2.3 [K(18-crown-6){(4,6- <i>t</i> Bu-OCNC ₆ H ₂) ₂ CH}·(H ₂ O) _{0.352} (16)	52
2.3.3 Group 2 Complexes	61
2.3.3.1 [MgX(THF) ₂ {(4,6- <i>t</i> Bu-NCOC ₆ H ₂) ₂ CH}] (X = Cl, Br: 18/18a)	61
2.3.3.2 [Mg{(4,6- <i>t</i> Bu-NCOC ₆ H ₂) ₂ CH}] ₂ (19)	65
2.4 Syntheses of the Bis(4,6- <i>i</i> Pr-benzoxazol-2-yl)methane (26) Ligand and its s-Block Complexes	71
2.4.1 Ligand Synthesis	71
2.4.1.1 3,5-diisopropylphenol (23)	71
2.4.1.2 3,5-diisopropyl-2-nitrophenol (24) & 3,5-diisopropyl-2-aminophenol (25)	72
2.4.1.3 Bis(4,6- <i>i</i> Pr-benzoxazol-2-yl)methane (26)	73
2.4.2 Group 1 Complexes	74
2.4.2.1 [Li(THF) ₂ {(4,6- <i>i</i> Pr-NCOC ₆ H ₂) ₂ CH}] (27)	75
2.4.2.2 [K{ η^5 -(4,6- <i>i</i> Pr-NCOC ₆ H ₂) ₂ CH}] _∞ (28)	77
2.4.3 Group 2 Complexes	78
2.4.3.1 [MgCl(THF) ₂ {(4,6- <i>i</i> Pr-NCOC ₆ H ₂) ₂ CH}]·hexane (29)	78

2.4.3.2	Excursus: Percent Buried Volume (%V _{bur}) Calculations	80
2.4.3.3	Excursus: Electronic Structure Analyses	83
2.4.3.4	[M(THF) _n]{(4,6- <i>i</i> Pr-NCOC ₆ H ₂) ₂ CH ₂] ₂ (30-33) (M = Mg, Ca, Sr, Ba; n = 0-1)	85
3	SUMMARY & OUTLOOK	90
4	EXPERIMENTAL PART	95
4.1	Work Techniques and Experimental Setups	95
4.1.1	Handling of Air- and Moisture-Sensitive Compounds	95
4.1.2	Preparation and Workup of Starting Materials	95
4.1.1	Elemental Analyses	96
4.1.2	Mass Spectrometry	96
4.1.3	NMR Techniques and Experiments	96
4.1.3.1	¹ H-DOSY-ECC-MW Estimation: Sample Preparation and Measuring Parameters	97
4.1.3.2	Clean-Inphase HSQC Measurements for Residual Dipolar Coupling Calculations	97
4.1.3.3	¹ H NMR Water Titration Experiments	98
4.1.4	Computational Details of Electronic Structure Analyses	98
4.1.5	Percent Buried Volume (%V _{bur}) calculations	98
4.1.6	Single Crystal X-ray Diffraction Experiments	99
4.2	Syntheses and Characterizations	99
4.2.1	Syntheses of Bis(4-Me-benzoxazol-2-yl)methane based s-Block Complexes	100
4.2.1.1	[K(THF){(4-Me-NCOC ₆ H ₃) ₂ CH}] _∞ (2)	100
4.2.1.2	[Mg{(4-Me-NCOC ₆ H ₃) ₂ CH}] ₂ (3)	101
4.2.1.3	[Ca(THF) ₂]{(4-Me-NCOC ₆ H ₃) ₂ CH}] ₂ ·THF (4)	101
4.2.2	Syntheses of the Bis(4,6- <i>t</i> Bu-benzoxazol-2-yl)methane Ligand and its s-Block Complexes	102
4.2.2.1	3,5-di- <i>tert</i> -butyl-2-nitrophenol (5)	102
4.2.2.2	3,5-di- <i>tert</i> -butyl-2-aminophenol (6)	103
4.2.2.3	Bis(4,6- <i>t</i> Bu-benzoxazol-2-yl)methane (7)	104
4.2.2.4	[Li(THF){(4,6- <i>t</i> Bu-NCOC ₆ H ₂) ₂ CH}] (13)	105
4.2.2.5	[K{η ⁵ -(4,6- <i>t</i> Bu-NCOC ₆ H ₂) ₂ CH}] _∞ (14)	106
4.2.2.6	1,1,2,2-tetrakis(4,6- <i>t</i> Bu-benzoxazol-2-yl)ethene (15)	107
4.2.2.7	[K(18-crown-6){(4,6- <i>t</i> Bu-OCNC ₆ H ₂) ₂ CH}·(H ₂ O) _{0.35} ·(THF) ₂] (16)	107
4.2.2.8	[K(18-crown-6){(4,6- <i>t</i> Bu-OCNC ₆ H ₂) ₂ C(OH)}] (17)	108
4.2.2.9	[MgCl(THF) ₂]{(4,6- <i>t</i> Bu-NCOC ₆ H ₂) ₂ CH}]·pentane (18)	109
4.2.2.10	[MgBr(THF) ₂]{(4,6- <i>t</i> Bu-NCOC ₆ H ₂) ₂ CH}] (18a)	110
4.2.2.11	[Mg{(4,6- <i>t</i> Bu-NCOC ₆ H ₂) ₂ CH}] ₂ (19)	111
4.2.3	Syntheses of the Bis(4,6- <i>i</i> Pr-benzoxazol-2-yl)methane Ligand and its s-Block Complexes	112
4.2.3.1	4-Bromo-2,6-diisopropylaniline (20)	112
4.2.3.2	1-Bromo-3,5-diisopropylbenzene (21)	113
4.2.3.3	(3,5-Diisopropylphenyl)boronic acid (22) / 2,4,6-Tris(3,5-diisopropylphenyl)cyclo-triboroxane (22a)	114
4.2.3.4	3,5-diisopropylphenol (23)	115
4.2.3.5	3,5-diisopropyl-2-nitrophenol (24)	116
4.2.3.6	3,5-diisopropyl-2-aminophenol (25)	117

4.2.3.7	Bis(4,6- <i>i</i> Pr-benzoxazol-2-yl)methane (26)	118
4.2.3.8	[Li(THF) ₂ {(4,6- <i>i</i> Pr-NCOC ₆ H ₂) ₂ CH}] (27)	119
4.2.3.9	[K{ η^5 -(4,6- <i>i</i> Pr-NCOC ₆ H ₂) ₂ CH}] _∞ (28)	120
4.2.3.10	[MgCl(THF) ₂ {(4,6- <i>i</i> Pr-NCOC ₆ H ₂) ₂ CH}]·hexane (29)	121
4.2.3.11	[M(THF) _n {(4,6- <i>i</i> Pr-NCOC ₆ H ₂) ₂ CH}] ₂ (30-33) (M = Mg, Ca, Sr, Ba; n = 0-1)	122
5	APPENDIX	126
5.1	Crystallographic Data	127
5.1.1	[K(THF){(4-Me-NCOC ₆ H ₃) ₂ CH}] _∞ (2)	127
5.1.2	[Mg{(4-Me-NCOC ₆ H ₃) ₂ CH}] ₂ (3)	128
5.1.3	[Ca(THF) ₂ {(4-Me-NCOC ₆ H ₃) ₂ CH}] ₂ ·THF (4)	129
5.1.4	Bis(4,6- <i>t</i> Bu-benzoxazol-2-yl)methane (7)	130
5.1.5	[Li(THF){(4,6- <i>t</i> Bu-NCOC ₆ H ₂) ₂ CH}] (13)	131
5.1.6	[K{ η^5 -(4,6- <i>t</i> Bu-NCOC ₆ H ₂) ₂ CH}] _∞ (14)	132
5.1.7	1,1,2-tetrakis(4,6- <i>t</i> Bu-benzoxazol-2-yl)ethene (15)	133
5.1.8	[K(18-crown-6){(4,6- <i>t</i> Bu-OCNC ₆ H ₂) ₂ CH}·(H ₂ O) _{0.352} (16)	134
5.1.9	[MgCl(THF) ₂ {(4,6- <i>t</i> Bu-NCOC ₆ H ₂) ₂ CH}]·pentane (18)	135
5.1.10	[Li(THF) ₂ {(4,6- <i>i</i> Pr-NCOC ₆ H ₂) ₂ CH}] (27)	136
5.1.11	[MgCl(THF) ₂ {(4,6- <i>i</i> Pr-NCOC ₆ H ₂) ₂ CH}]·hexane (29)	137
5.1.12	[Mg{(4,6- <i>i</i> Pr-NCOC ₆ H ₂) ₂ CH}] ₂ ·hexane (30)	138
5.1.13	[Ca(THF){(4,6- <i>i</i> Pr-NCOC ₆ H ₂) ₂ CH}] ₂ (31)	139
5.1.14	[Sr(THF){(4,6- <i>i</i> Pr-NCOC ₆ H ₂) ₂ CH}] ₂ (32)	140
5.1.15	[Ba(THF){(4,6- <i>i</i> Pr-NCOC ₆ H ₂) ₂ CH}] ₂ (33)	141
5.2	DOSY NMR Data	142
5.3	Spectra of ¹ H NMR Water Titration Experiments	144
5.4	Structural Models of 19 and 19a	145
6	REFERENCES	146
	Danksagung	158
	CURRICULUM VITAE	159

ABBREVIATIONS

Å	Ångstrom
Adam	Adamantyl
Ae	Alkaline-earth-metal(s)
ATR	Attenuated Total Reflection
Bis(4-Me-benzoxazol-2-yl)methane / -methanide	(4-Me-NCOC ₆ H ₃) ₂ CH ₂ / (4-Me-NCOC ₆ H ₃) ₂ CH
Bis(4,6-R-benzoxazol-2-yl)methane / -methanide (R = <i>t</i> Bu, <i>i</i> Pr)	(4,6-R-NCOC ₆ H ₂) ₂ CH ₂ / (4,6-R-NCOC ₆ H ₂) ₂ CH (R = <i>t</i> Bu, <i>i</i> Pr)
CIP	Contact Ion Pair
CS	Compact Spheres / Compact Spherical
CSD	Cambridge Structural Database
CCDC	Cambridge Crystallographic Data Base
DCM	Dichloromethane
dev.	Deviation(s)
diox	1,4-Dioxane
Dipp/Dip	2,6-Diisopropylphenyl
DMAP	4-Dimethylaminopyridine
DMSO	Dimethylsulfoxide
DOSY	Diffusion-Ordered Spectroscopy
DSE	Dissipated Spheres and Ellipsoids
Dur	Duryl (2,3,5,6-Tetramethylphenyl)
ECC	External Calibration Curve
ED	Expanded Discs
EI	Electron Ionization
ESI	Electrospray-ionization
Et ₂ O	Diethyl ether
EtOAc	Ethyl acetate
eq.	Equivalent(s)
GUI	Graphical User Interface
HMDS	Hexamethyldisilazane
HSAB	Hard and Soft Acids and Bases
HSQC	Heteronuclear Single Quantum Correlation
<i>i</i> pp	2-Isopropylphenyl
<i>i</i> Pr	Isopropyl
IR	Infrared
LIFDI	Liquid Injection Field Desorption Ionization
M	Molar
MHz	Megahertz
MS	Mass Spectrometry

Abbreviations

<i>MW</i>	Molecular Weight
<i>m/z</i>	Mass/charge ratio
NacNac	β -Diketiminato
NBO	Natural Bonding Orbital
<i>n</i> BuLi	<i>n</i> -Butyllithium
NMR	Nuclear Magnetic Resonance
NOESY	Nuclear <i>Overhauser</i> Enhancement Spectroscopy
NPA	Natural Population Analysis
NRT	Natural Resonance Theory
PMDETA	<i>N,N,N',N'',N'''</i> -Pentamethyldiethylenetriamine
ppm	Parts per million
Py	Pyridyl
RDC	Residual Dipolar Coupling
SSIP	Solvent-Separated Ion Pair
<i>t</i> Bu	<i>tertiary</i> -Butyl
<i>t</i> BuLi	<i>tertiary</i> -Butyllithium
THF	Tetrahydrofuran
TMEDA	<i>N,N,N',N'</i> -Tetramethylethylene-1,2-diamine
TMS	Tetramethylsilane

Major parts of this Ph.D. thesis have been published separately:

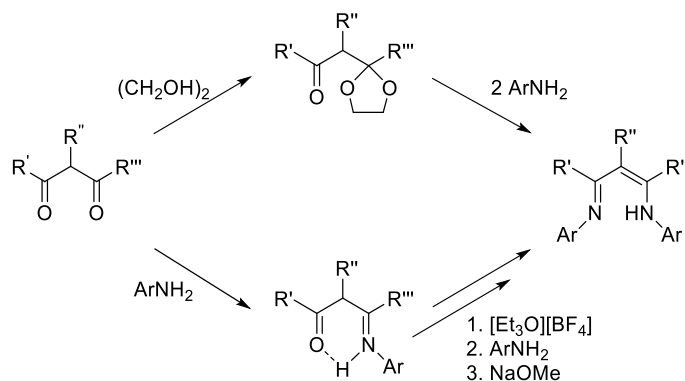
- [1] **I. Koehne**, R. Herbst-Irmer, D. Stalke, “*Bis(4-methylbenzoxazol-2-yl)methanide in s-Block Metal Coordination*”, *Eur. J. Inorg. Chem.* **2017**, 2017, 3322-3326.^[1]
- [2] **I. Koehne**, S. Bachmann, T. Niklas, R. Herbst-Irmer, D. Stalke, “*A Novel Bulky Heteroaromatic-Substituted Methanide Mimicking NacNac: Bis(4,6-tert-butylbenzoxazol-2-yl)methanide in s-Block Metal Coordination*”, *Chem. Eur. J.* **2017**, 23, 13141-13149.^[2]
- [3] **I. Koehne**, S. Bachmann, R. Herbst-Irmer, D. Stalke, “*A Water-Containing Organopotassium Compound Based on Bis(4,6-tBu-benzoxazol-2-yl)methanide and Its Unexpected Stability to Hydrolysis*”, *Angew. Chem.* **2017**, 129, 15337-15342; *Angew. Chem. Int. Ed.* **2017**, 56, 15141-15145.^[3]
- [4] **I. Koehne**, N. Graw, T. Teuteberg, R. Herbst-Irmer, D. Stalke, “*Introducing NacNac-Like Bis(4,6-isopropylbenzoxazol-2-yl)methanide in s-Block Metal Coordination*”, *Inorg. Chem.* **2017**, 56, 14968-14978.^[4]

1 INTRODUCTION

The development of novel, sustainable and efficient catalysts begins with the synthesis of a tailor-made ligand platform. In this context, the ligand framework has to satisfy several requirements like to guaranty a high turnover number of the catalyst and a sufficient product selectivity and yield.^[5,6] The ligand should be able to undergo metal-ligand cooperative processes,^[7,8] as well as to exhibit a redox non-innocent behavior.^[9] Moreover, it should be able to host differently sized metal ions in high as well as low oxidation states, to provide a sufficient flexibility as well as different coordination sites to address both, hard and soft metal centers. A multifunctional ligand platform has to provide an efficient charge delocalization and to promote the formation of metal complexes with different coordination numbers and geometries.^[6,10] In addition, a well-considered ligand backbone should supply adequate steric shielding to a coordinated cation to prevent the complex from oligomerization and to enhance its solubility.^[5,6] The β -diketiminato or NacNac ligand family represents a well-established compound class that combines most of these features. Hence, it finds widespread application in transition- as well as main-group metal mediated catalysis.^[11,12] This thesis focuses on the development of novel NacNac-like ligand platforms comprising additional donor sites, the ability to show redox non-innocent behavior as well as to assist in metal-ligand cooperative substrate activation. Furthermore, on their introduction to s-block coordination for future applications in small molecule activation and homogeneous catalysis.

1.1 Development of the β -Diketiminato Ligand System

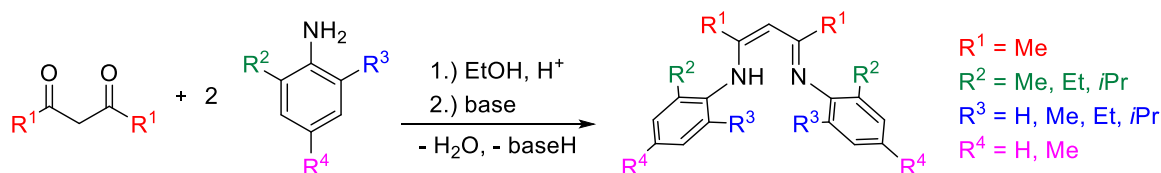
Initially, *McGeachin*,^[13] *Bonnett*^[14] and *Parks* and *Holm*^[15] reported the preparation of β -diketiminato-based transition-metal complexes in 1968. Two fundamental synthetic routes for the preparation of this ligand class that are known for several decades are depicted in Scheme 1-1.^[16]



Scheme 1-1. Simplified generation of NacNac ligands from their related β -diketones.

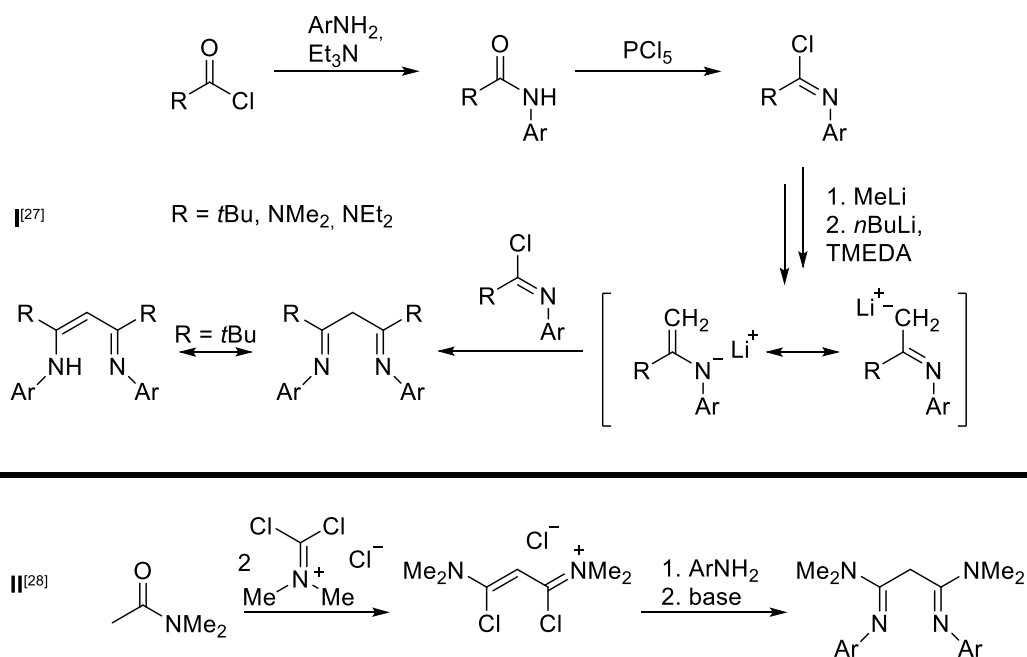
The upper route consists of the simple reaction of one of the ketone functions with ethylene glycol leading to the formation of the corresponding cyclic acetal moiety. Subsequently, the formed ketal is converted *via* a double condensation reaction with two equivalents of a primary amine forming the β -diketiminato.^[17] The bottom route starts with a mono condensation reaction of a primary amine at one of the ketone moieties of the starting material. A clear disadvantage of this pathway is the necessity of two additional steps to prevent the reaction from stopping at the stage of this β -enaminoketonato product. To realize the second imine condensation, a metalation with the help of a *Meerwein* salt has to be carried out, followed by the addition of a base.^[13,18] Furthermore, in a method to prepare β -diketiminates that do not bear any further substituents at the ligand backbone, 1,1,3,3-tetraethoxy propane is used as starting material. On addition of an aromatic amine hydrochloride the corresponding β -diketimin hydrochloride salt is obtained and subsequently deprotonated with sodium hydroxide, giving the target ligand.^[19]

Until the late 1990s, NacNac-based ligand systems remained mainly unattended in coordination chemistry, which was put to an end by the initial synthesis of the famous Dipp-substituted DippNacNac by *Marshall* et al. in 1997.^[20] Also due to a new and straightforward synthesis method for *N*-arylated ligands with yields around 80%, this derivative should become one of the most frequently used and best studied NacNac platforms in the following years (Scheme 1-2). In detail, the steric strain supplied by two-fold *N*-aryl substituted β -diketiminates is compared to that offered by terphenyl systems.^[21] The latter established a reputation in successfully stabilizing multiple bonded low-valent group 13 and 14 compounds.^[22,23]



Scheme 1-2. General procedure for the preparation of *N*-arylated β -diketiminates.

As can be seen from Scheme 1-2, ligand preparation consists of a simple acid-catalyzed double condensation reaction of differently substituted aniline derivatives and acetylacetone followed by basic workup to obtain the desired ligand.^[20,24,25] While this approach covers a wide range of anilines, only limited modifications at the ligand backbone of the 2,4-pentanedione are tolerated.^[26] The introduction of sterically demanding substituents like *t*Bu groups at the β -carbons of the C_3N_2 framework still requires several but fortunately high-yielding steps to build up the diketiminato scaffold (Scheme 1-3, I, *vide infra*). In the course of the procedure, pivaloyl chloride is reacted with a corresponding aniline derivative. A subsequent chlorination with PCl_5 affords the *N*-methyl-pivalimidoyl chloride. Subsequent methylation and lithiation reactions pave the way for a C-C coupling with a second equivalent of the pivalimidoyl chloride to yield the related β -C-substituted diketiminato.^[27]



Scheme 1-3. Synthesis procedures of *N*-arylated NacNac ligands bearing β -carbon substituents.

Most recently, route **I** was additionally used to implement NR_2 groups ($\text{R} = \text{Me}, \text{Et}$) at the ligand backbone forming highly electron-rich so-called *N*-NacNac ligand systems.^[28] A second, less elaborate preparation method was presented as well, that based on a procedure by *Viehe* et al.^[29] (Scheme 1-3, **II**). Starting from *N,N*-dimethylacetamide, in a reaction with two equivalents of *Viehe's* salt, a bifunctional backbone is pre-assembled. Subsequent condensation with the desired aryl amine forms the corresponding *N*-NacNac ligand derivative. In contrast to the NacNac ligands that usually exhibit an imino-enamin tautomerism in the protonated form, in the *N*-NacNac congeners the diimine form was found to be favored.^[28]

The residues at the nitrogen donor atoms (*e.g.* hydrogen-, alkyl-, silyl- or bulky aryl substituents) in direct proximity to the coordination pocket are known to have a strong influence on the ligands steric and electronic capabilities. They play a major role in controlling the coordination sphere of a metal ion enabling access to low-valent compounds. Thus, even slide variations are reported to provoke significant changes in complex reactivity.^[9, 30] Typically, β -diketiminates are used as monoanionic chelate ligands that bind in a $\kappa^2-(\text{N},\text{N}')$ fashion to a coordinate metal ion, forming a six-membered metalla-heterocycle (**A**^[9] in Figure 1-1). Additionally, in this form, the established aromaticity throughout the ligand backbone allows a metal to interact with the offered π -electron density. This results in manifold possible coordination motifs up to a maximum η^5 -hapticity, depending on the nature of the metal ion as well as the nitrogen substituents (**B-I**^[31–38] in Figure 1-1, *vide infra*).^[16]

Despite a vast amount of readily accessible *N*-alkylated NacNacs,^[39] metal ions hosted by *N*-arylated coordination pockets form the majority. Dominated by the latter ligand class, a variety of structures stabilizing main-group, d- and f-block metal ions of diverse oxidation states were successfully synthesized in the last two decades. Many of these compounds proved to show a high activity and selectivity in catalytic reactions like cross-couplings, alkene polymerization and functionalization as well as to contain unprecedented low-valent and/or low oxidation state metal ions. This process has been summarized in several excellent review articles.^[12, 16, 26, 40–44] Moreover, it was shown by *Lappert* et al. in 2003 that β -diketiminato ligands exhibit a redox non-innocent character which was investigated in detail in the last fifteen years.^[9, 45]

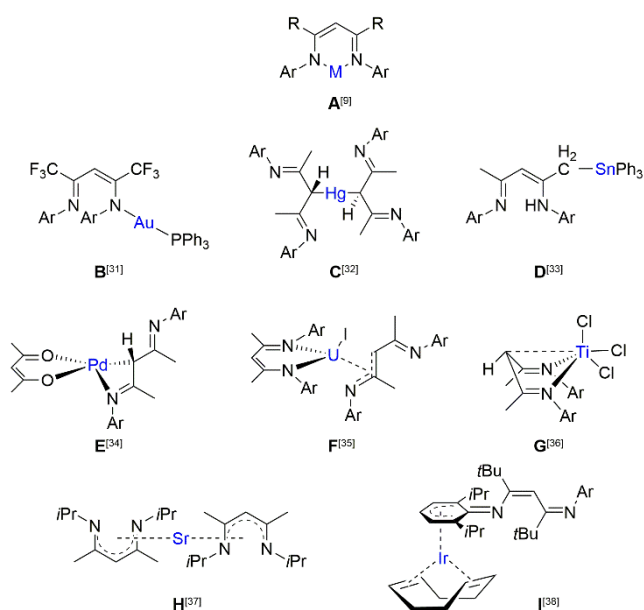


Figure 1-1. Selection of different coordination modes in mononuclear β -diketiminato-based complexes. **A:** κ^2 -(*N,N'*); **B:** κ^1 -(*N*); **C:** κ^1 -(γ -C); **D:** κ^1 -(β -Me); **E:** κ^2 -(γ -C,*N*); **F:** κ^2 -(*N,N'*) + η^3 -(*NCC*); **G:** κ^3 -(γ -C,*N,N'*); **H:** (η^5 -(*C*₃*N*₂))₂; **I:** κ^2 -(*N*, η^6 -Ar). Adapted with permission from reference^[9]. Copyright 2016, The Royal Society of Chemistry.

1.2 Alkali- and Alkaline-Earth-Metal β -Diketiminato Complexes

The sophisticated steric and electronic fine-tuning of the NacNac ligand,^[30] and the manifold catalytic applications found for its derived transition-metal^[12, 26, 43] compounds put the focus on the extension of these applications to the corresponding late and early main-group metal complexes in current research topics.^[11] In this context, the following chapter focuses on the area of s-block β -diketiminato compounds.

In particular, lithium and potassium compounds are commonly used as versatile starting materials for metathesis reactions with metal halides or –amides to access other metal complexes.^[16, 46–48] Lithiated β -diketiminates are easily obtained by deprotonation of the corresponding NacNacH ligand with lithium organics like *n*- or *t*BuLi, LiN(*i*Pr)₂ or LiHMDS.^[16] The structural features of these products strongly depend on the bulkiness of the ligand itself and the presence of additional donor molecules.^[42] In particular, in less hindered structures like [Li(THF)₂{ⁱPrNacNac}] that bears 2-*isopropylphenyl*-substituted nitrogen donor atoms, a four-coordinate, tetrahedral complex was obtained in the presence of THF (Figure 1-2, left).^[49]

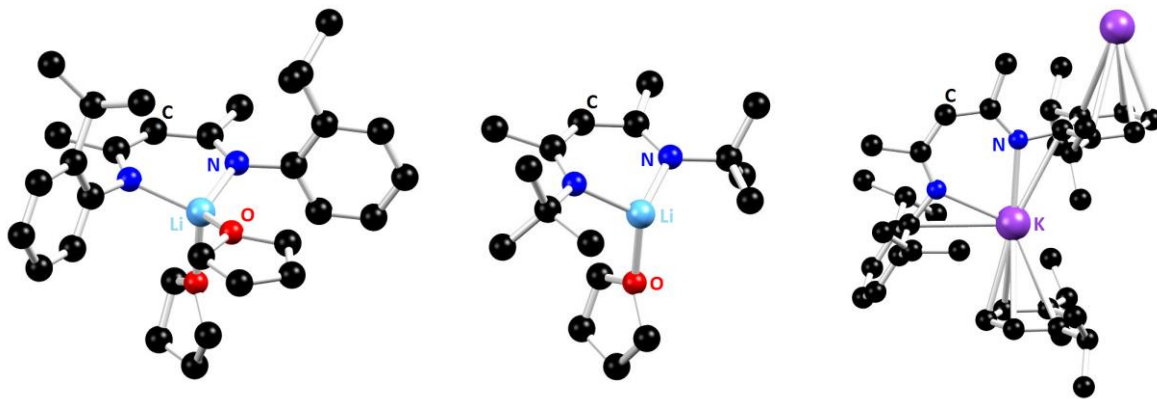
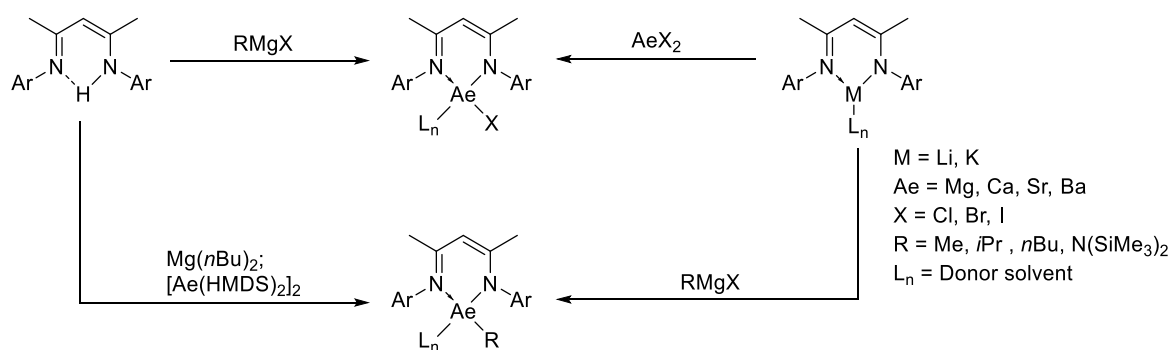


Figure 1-2. Isotropic solid-state structures of the alkali metal complexes $[\text{Li}(\text{THF})_2\{\text{DippNacNac}\}]^{[49]}$ (left), $[\text{Li}(\text{THF})\{t\text{BuNacNac}\}]^{[50]}$ (middle) and polymeric $[\text{K}\{\kappa^2(\eta^2)\text{-C,N,C',N'}\text{-DippNacNac}\}]_\infty^{[51]}$ (right). The Hydrogen atoms are omitted for clarity.

By incremental increase of steric demand around the cation, low-valent species are accessible. Starting from a *t*Bu *N*-alkylated NacNac derivative, the three-coordinate, trigonal-pyramidal compound $[\text{Li}(\text{THF})\{t\text{BuNacNac}\}]$ was obtained (Figure 1-2, middle).^[50] Here, the inflexible *t*Bu substituents successfully block one of the coordination sites of the lithium ion preventing it from being coordinated in a tetrahedral fashion by a second THF donor molecule. Additionally, comparable three-fold coordinated structures were reported for the lithiation of the corresponding Dipp *N*-arylated β -diketiminates which bear either *tert*-butyl or methyl groups at the β -carbon atoms.^[25, 27] Interestingly, lithiation of the latter in absence of any donor molecules led to the formation of $[\text{Li}\{\text{DippNacNac}\}]_n^{[25]}$ that crystallized in two different but associated structural motifs. One is described as a dimer in which the lithium ions, along with a $\kappa^2\text{-N,N'}$ coordination, exhibit a $\text{Li}\cdots\text{C}$ interaction to one of the carbon atoms of a 2,6-diisopropylphenyl substituent of a second molecule. The other motif consists of two linked hexameric chains that form in total a dodecameric so-called slipped ladder structure.^[25]

Generally, in concerted deprotonation-metalation reactions with simple potassium hydride or other organometallic KR compounds (*e.g.* R = CH_2Ph , $\text{N}(i\text{Pr})_2$ or $\text{N}(\text{SiMe}_3)_2$), potassium-containing β -diketiminates are as easily accessed as their lithium congeners. The obtained potassium complexes tend to form multi-hapto binding modes like reported for compound $[\text{K}\{\kappa^2(\eta^2)\text{-C,N,C',N'}\text{-DippNacNac}\}]_\infty^{[51]}$ (Figure 1-2, right). In the solid-state, this structure exhibits on the one hand a $\kappa^2(\eta^2)\text{-C,N,C',N'}$ coordination to one DippNacNac ligand as well as an $\eta^5\text{-K}\cdots\text{aryl}$ interaction to the Dipp residue of a second molecule. This satisfies the coordination sphere of the potassium ion forming infinite zig-zag strands.^[51] Interestingly, usage of a sterically demanding DippNacNac ligand system that carries additional *t*Bu substituents at the β -carbons in the ligand periphery, forced the potassium ion in $[\text{K}(\text{THF})_3\{\text{DippNacNac}(\beta\text{-C}(t\text{Bu}))\}]$ into a $\kappa^1\text{-N} + \eta^2\text{-aryl}$ coordination. Presumably to avoid steric congestion, this binding motif is preferred over the formation of a low-valent compound like in the corresponding lithium derivatives.^[52]

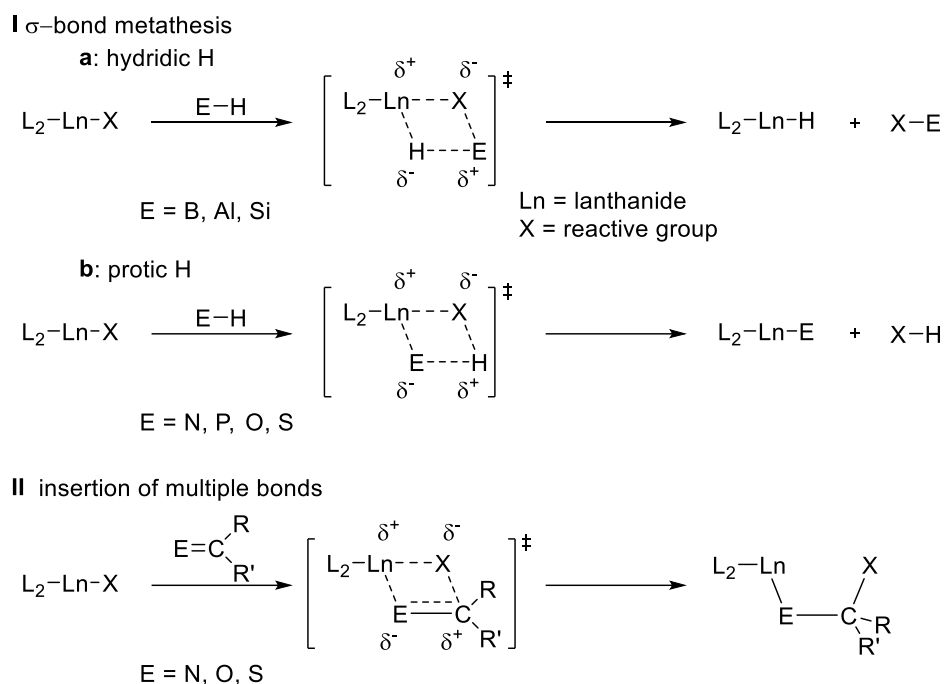


Scheme 1-4. Selected preparation methods for different β -diketiminato-based alkaline-earth-metal halide compounds (top routes), and -alkyl or -amide pre-catalysts (bottom routes).

As illustrated in Scheme 1-4 (top), β -diketiminato-supported alkaline-earth-metal halide compounds are mainly accessed *via* two different procedures. These complexes are versatile platforms for further transformations like the activation of small molecules (*e.g.* H₂, CO₂), or reduction to access low oxidation state magnesium(I) compounds (see next chapter). Magnesium-based halide compounds can be obtained from reaction of a *Grignard* reagent RMgX (X = Cl, Br, I) with a corresponding protonated NacNacH ligand.^[53] The heavier NacNac -based alkaline-earth-metal halides are commonly prepared through salt metathesis of a lithium or potassium β -diketiminato precursor complex with a group 2 halide AeX_2 (X = Cl, Br, I).^[54] If a halide compound is obtained as a monomer or in a dimeric form, with bridging halide ions, strongly depends on cation size, the steric bulk offered by the β -diketiminato ligand as well as the presence of additional donor molecules (*e.g.* THF, Et₂O).^[55–57]

Most advances of group 2 catalysis are strongly influenced by the aspect that Ae^{2+} metal centers should be able to promote a lanthanide-like catalysis, due to an analogous d^0 valence-shell configuration. With this in mind, the construction of similar catalytic cycles like for trivalent, redox inactive d^0 lanthanide compounds is feasible.^[11] In transition-metal-mediated mechanisms, variation of the catalysts oxidation state is a crucial feature in the process of catalytic bond activation. In contrast to that, with σ -bond metathesis and polarized insertion the catalytic reactivity of lanthanide metals features two fundamental mechanistic steps, which do not alter the d^0 configuration of the metal fragment (Scheme 1-5, *vide infra*).^[58, 59] Starting with reaction type **Ia**, lanthanide hydrides are obtained *via* σ -bond metathesis from substrates comprising a hydridic E–H bond. Substrates that exhibit a protic E–H bond undergo protonolysis to give an $\text{L}_2\text{Ln–E}$ species (**Ib**). In combination with reaction type **II**, two catalytic cycles for the heterofunctionalization of unsaturated bonds can be derived. In the case of the metal hydride $\text{L}_2\text{Ln–H}$, the catalytic cycle proceeds *via* insertion into the unsaturated bond, affording $\text{L}_2\text{LnEC}(\text{X})\text{RR}'$ (X = H) as intermediate species. Subsequent σ -bond metathesis with a second equivalent of the hydridic E–H bonded substrate yields the *Markovnikov* product $\text{E–E'–CHRR}'$. In the case of the $\text{L}_2\text{Ln–E}$ species, obtained from a reaction with a protic E–H substrate, the intermediate $\text{L}_2\text{LnEC}(\text{X})\text{RR}'$ (X = E) is formed by

insertion into the parent multiple bond. The catalytic cycle is closed *via* protonolysis with a second molecule of the protic E–H substrate affording the anti-*Markovnikov* addition product HE'–C(E)RR'.^[11]

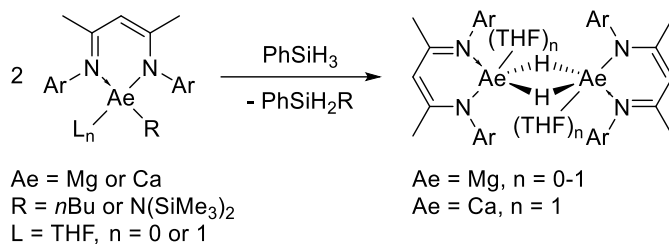


Scheme 1-5. Overviews of catalytic key steps in trivalent, lanthanide mediated σ -bond metathesis. **I:** Utilization of a substrate that comprises either a hydridic (**a**) or a protic (**b**) E–H bond. **II:** Insertion of an unsaturated E=C bond into a Ln–X σ -bond. Adapted with permission from reference ^[11]. Copyright 2016, The Royal Society of Chemistry.

With an emphasis on the practicability of alkaline-earth-metal-mediated protonolysis reactions (Scheme 1-5, **IIb**), different β -diketiminato-based group 2 alkyl- and amide pre-catalyst species were prepared.^[11] These complexes are usually accessed by reaction of a protonated NacNacH ligand with a group 2 alkyl or –amide precursor compound.^[53, 56, 60] In the case of magnesium, preparation may also proceed *via* salt metathesis of an alkali β -diketiminato complex with a *Grignard* reagent RMgX (X = Cl, Br, I) (Scheme 1-4, bottom routes).^[55] Many of these compounds already found a versatile catalytic application, for example, in the field of ring opening polymerization reactions of cyclic esters (*e.g.* *rac*-lactide)^[61, 62] or inter- and intramolecular hydroamination^[63–65] and -phosphination reactions.^[66]

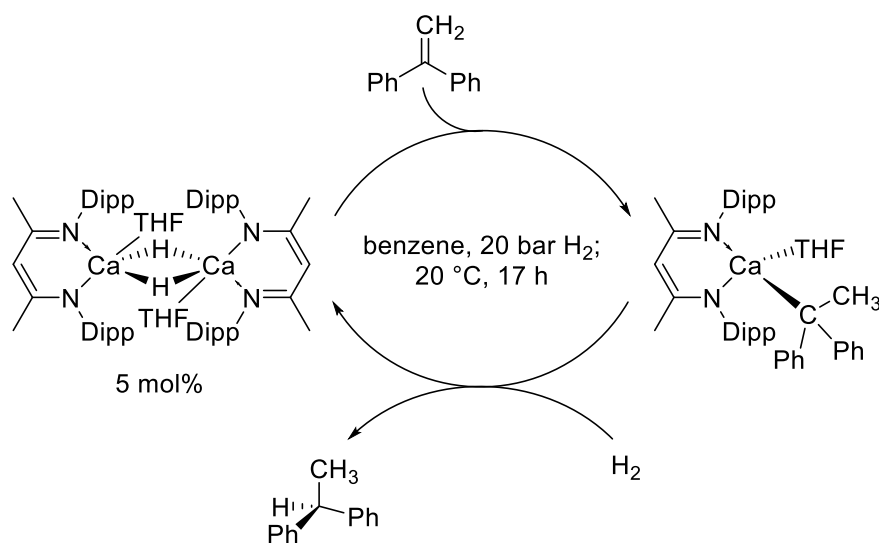
In order to exceed the variety of heterofunctionalizations of unsaturated substrates to hydrogenation as well as hydrosilylation and –boration reactions, the search for well-defined group 2 hydride complexes capable of a lanthanide analogous reactivity was started. Initiated by the groundbreaking synthesis of the dimeric ^{Dipp}NacNac-based calcium hydride complex [Ca(THF)-(μ -H)]₂{^{Dipp}NacNac} by *Harder* and co-workers in 2006,^[67] preparation of the corresponding

magnesium-based congeners was independently reported by *Jones* and *Stasch* shortly after (Scheme 1-6).^[53, 68]



Scheme 1-6. Preparation of β -diketiminato-based magnesium^[68] and calcium^[69] hydrides.

According to pathway **Ia** in Scheme 1-5, the calcium as well as the magnesium complexes were obtained through σ -bond metathesis with phenylsilane as hydride source. Due to an intrinsic higher reactivity of the heavier strontium and barium homologues, associated with decomposition reactions, the synthesis of the related β -diketiminato hydride complexes remains elusive. Here, an increasing cation size is assumed to provoke faster ligand exchange as well as to hamper the ability of a sterically demanding ligand framework to prevent the complex from *Schlenk* equilibrium redistribution.^[11] Building up on this work, also a couple of higher magnesium hydride clusters were introduced, for example, by the groups of *Hill* and *Harder*.^[70-72] Remarkably, *Harder* and co-workers also succeeded in the synthesis of the first higher strontium hydride cluster only very recently.^[73] Simple treatment of $[\text{Sr}(\text{N}(\text{SiMe}_3)_2)_2]$ with phenylsilane and PMDTA led to the formation of a hexanuclear “inverse cryptant”-like cage structure in $[\text{Sr}_6\text{H}_9(\text{N}(\text{SiMe}_3)_2)_3(\text{PMDTA})_3]$. These findings simultaneously underscore that bulky spectator ligands are obviously no basic requirement to stabilize heavier group 2 hydride species. The analogous higher calcium hydride cluster was obtained as well.



Scheme 1-7. Exemplary and simplified catalytic hydrogenation of 1,1-diphenylethylene with the dimeric calcium hydride complex $[\text{Ca}(\text{THF})(\mu\text{-H})\{\text{DippNac}\}_2]_2$ by *Harder* et al.^[74]

Additionally, an initial reactivity study was carried out on the calcium hydride complex $[\text{Ca}(\text{THF})(\mu\text{-H})\{\text{Dipp}^{\text{NacNac}}\}]_2$ by *Harder et al.*^[75, 76] Reactions with stoichiometric amounts of different unsaturated substrates supplied precise data on its insertion reactivity, paving the way for heavier alkaline-earth-metal hydrides in catalytic applications.^[69] In later implementations of this compound to catalytic hydrogenations of diverse diphenylethylene and styrene substrates, even at mild conditions conversions of 99% and higher were achieved (Scheme 1-7, *vide supra*).^[72] Also for the corresponding magnesium congeners, successful application to hydroboration^[77] and -amination^[63] reactions of aldehydes, ketones and pyridines as well as the dehydrocoupling of amines and boranes was reported.^[11]

1.3 Low Oxidation State Magnesium β -Diketiminato Complexes

The isolation and characterization of the first dimeric Zn^{I} complexes $[\text{Zn}\{\text{Cp}^*\}]_2$ ^[78] ($\text{Cp}^* = \text{C}_5\text{Me}_5^-$) and $[\text{Zn}\{\text{Dipp}^{\text{NacNac}}\}]_2$ ^[79] was reported in 2004 and 2005, respectively. Encouraged by this development and due to a chemical analogy between both elements, attempts to prepare related $\text{Mg}^{\text{I}}\text{-Mg}^{\text{I}}$ dimers were carried out.^[80] Finally, this research peaked in the synthesis of the first “bottleable” dimeric low oxidation state magnesium compounds $[\text{Mg}\{\text{Dipp}^{\text{NacNac}}\}]_2$ (Figure 1-3, **b**) and $[\{\text{Mg}(i\text{Pr}_2\text{NC}(\text{N-Dipp})_2)\}_2(\text{Et}_2\text{O})]$ by *Jones and Stasch* in 2007.^[81] The preparation proceeded *via* potassium-metal-mediated reduction, starting from the related magnesium iodide precursor complexes.

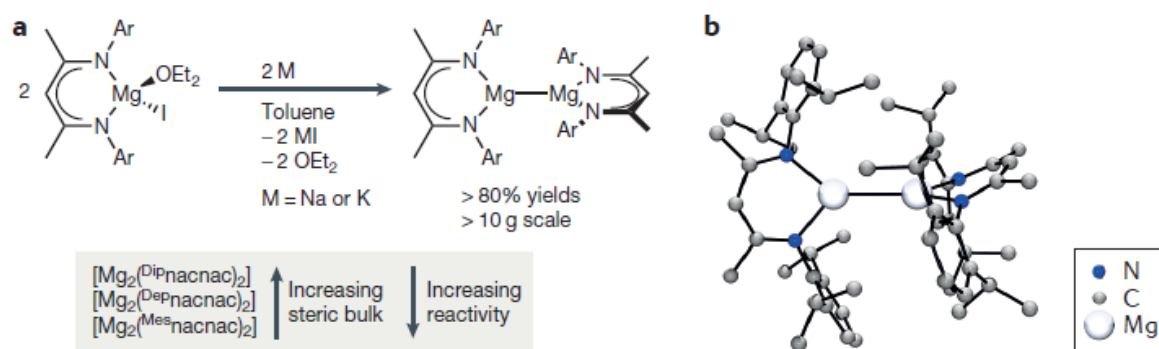


Figure 1-3. **a** (top): General preparation of dimeric β -diketiminato-based Mg^{I} compounds of the form $[\text{Mg}\{\text{Ar}^{\text{NacNac}}\}]_2$ ($\text{Ar} = \text{Dip}, \text{Dep}, \text{Mes}$) by reduction of the corresponding divalent magnesium iodide precursors with sodium or potassium metal. **a** (bottom): Schematic relationship between the steric demand of the ligand scaffold and the reactivity of its derived $\text{Mg}^{\text{I}}\text{-Mg}^{\text{I}}$ dimer. **b**: Solid-state structure of the first β -diketiminato-supported dimagnesium(I) complex $[\text{Mg}\{\text{Dipp}^{\text{NacNac}}\}]_2$. Reprinted with permission from reference^[82]. Copyright 2017, Springer Nature.

The utilized bulky β -diketiminato and guanidinate ligand systems are assumed to play a key role in stabilizing these reactive species by rather favoring the formation of a reduced heteroleptic than a homoleptic divalent magnesium compound.^[42] In the following years, many other $\text{Mg}^{\text{I}}\text{-Mg}^{\text{I}}$ compounds featuring different *N*-arylated β -diketiminato ligand scaffolds were prepared in high

yields from their respective divalent magnesium iodide precursors (Figure 1-3, **a** (top), *vide supra*).^[53, 81] Due to the variety in *N*-aryl substituents, the reactivity of the corresponding reduced magnesium(I) dimer can be simply adjusted. Thus, a clear trend of increasing reactivity accompanied by a decreasing steric congestion of the coordination pocket was derived from the most commonly used species, featuring 2,6-diisopropyl-, 2,6-diethylphenyl (Dep) or mesityl (Mes) substituents. (Figure 1-3, **a** (bottom)).^[83] Inspired by this development, several comparable dimagnesium(I) complexes supported by related anionic ter- di- and even monodentate ligand systems were synthesized and intensively studied during the last decade. As one can see from Figure 1-4, these range from tripodal diimine-enolate derived species (**a**),^[84] over a bulky double negatively charged α -diimine supported complex (**b**),^[85] to Mg^I-Mg^I dimers stabilized by highly sterically demanding monodentate amido ligands (**c**).^[86]

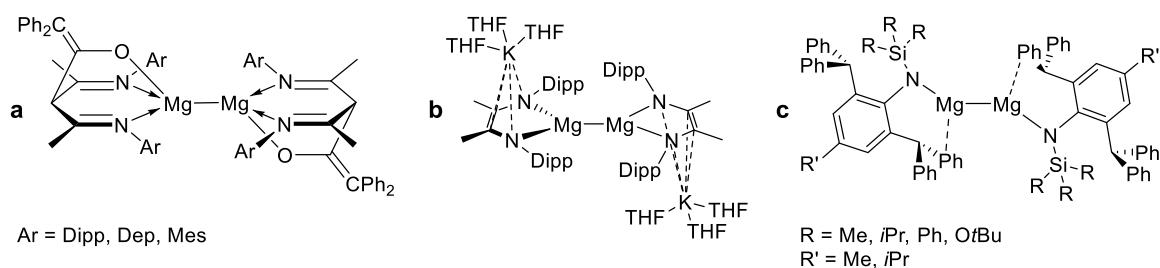


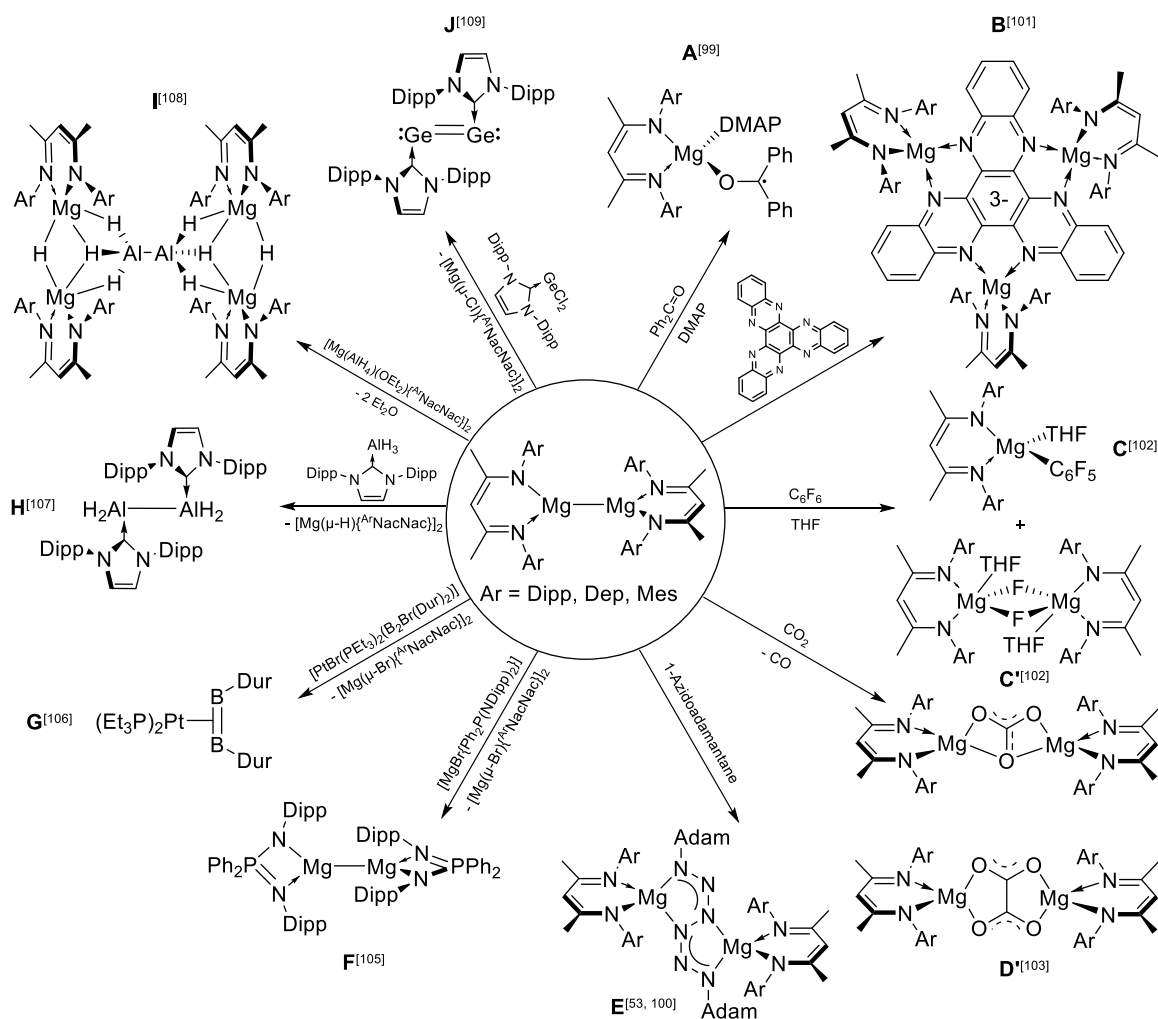
Figure 1-4. Diversity of dimagnesium(I) compounds derived from other ter- (**a**),^[84] di- (**b**)^[85] and monodentate (**c**)^[86] supporting ligands.

The preparation of other $[Ae^{Ar}NacNac]_2$ species, *e.g.* from the respective beryllium or calcium iodide precursors failed so far. The preferred formation of the corresponding homoleptic $[Ae^{Ar}NacNac]_2$ compounds has been affiliated to the size and reduction potential of the alkaline-earth-metal being crucial for the preparation of the desired reduced Ae^I-Ae^I bound dimer.^[53] After its first preparation, the nature of the Mg^I-Mg^I bond in $[Mg^{DippNacNac}]_2$ was investigated in detail. X-ray structure analysis revealed a molecular geometry similar to the corresponding dimeric Zn^I species exhibiting two almost perfectly perpendicular arranged C_3N_2 ligand planes. This directly excluded the hypothesis of a hydride bridged $Mg-Mg$ moiety, because in this case these planes would be arranged in an almost co-planar fashion with an orthogonally oriented pair of hydride ions (see Scheme 1-6).^[68, 81] The absence of an Mg_2H_2 moiety was additionally corroborated by the lack of any hydride signals in the compounds 1H NMR spectrum. Furthermore, only marginal residual electron-density was observed between the magnesium ions, and no hydride species were detected in high resolution mass spectrometry experiments.^[87] Computational as well as crystallographic studies further affirmed an unsupported, high *s*-character, covalent Mg^I-Mg^I bond.^[88] Because of a pronounced polarization of the $Mg-N$ bonds, the two monovalent magnesium ions can also be seen as a Mg_2^{2+} dication supported by negatively charged β -diketiminate ligands that readily form stable donor-base adducts.^[68, 81, 83]

Moreover, experimental charge density studies revealed the presence of a local maximum in the electron density between the two magnesium ions that does not arise from a present atom. Hence, the $\text{Mg}^{\text{I}}\text{-Mg}^{\text{I}}$ bond represents a rare case of a structure containing a so-called non-nuclear attractor.^[89, 90]

In the last decades, a variety of compounds have distinguished themselves as powerful lab-tools to access synthetic targets in organic-, inorganic and organometallic transformations, that are nowadays used on a daily routine by synthetic chemists.^[82] Besides simple s-block elements (*e.g.* Na, K or *Rieke*-magnesium),^[91] the utilization of different organometallic reagents has gained wide acceptance. Among others, these range from potassium graphite (KC_8)^[92] and sodium- or potassium naphthalenides,^[93] over magnesium anthracene $[\text{Mg}(\text{C}_{14}\text{H}_{10})(\text{THF})_3]$ as source of elemental magnesium,^[94, 95] to decamethylsamarocene $[\text{Sm}(\text{Cp}^*)_2]$ ^[96] or simple samarium iodide.^[97, 98] Despite their unabated preparative significance, most of them share some disadvantages like an insolubility in conventional organic solvents accompanied by a strongly negative redox potential. The latter often results in poor selectivity control and over-reduction of the substrate. Furthermore, a general instability and highly pyrophoric character makes them hard to store. Even soluble reducing agents like sodium naphthalenide still exhibit harsh cathodic redox potentials that promote side-product formation.^[82] As a result, there had been a strong urge for readily accessible and more controllable reducing agents, which was satisfied with the synthesis of the first magnesium(I) dimers in 2007.^[81] These compounds and their derivatives are easily prepared under mild conditions, they show a high solubility and stability in common aprotic organic solvents and exhibit some stability against air and hydrolysis. Since then, this compound class, and in particular the NacNac-based complexes, have proven to be reliable and controllable two-electron sources. Experiments to determine the redox potential of dimeric $\text{Mg}^{\text{I}}\text{-Mg}^{\text{I}}$ species have failed so far, but they are assumed less reductive than the corresponding group 1 metals used for their preparation. Based on redox potentials of -2.61 V and -2.29 V for the respective $\text{Mg}^{\text{II}/0}$ and $\text{Mg}^{\text{II}/\text{I}}$ redox couples, it is anticipated that those of the magnesium(I) dimers range in a similar scale.^[82]

Continuing this development, $[\text{Mg}\{\text{ArNacNac}\}]_2$ dimers have been implemented as versatile reducing agents in organic- and inorganic syntheses. In Scheme 1-8 (*vide infra*), selected reactions of β -diketiminato-supported dimagnesium(I) compounds with different organic substrates and their striking adaptation in the synthesis of other low oxidation state main-group complexes are summarized. Thus, the following paragraph focuses on recent highlights of this novel class of more user-friendly reducing agents.



Scheme 1-8. Selected reactions of $[\text{Mg}\{\text{Ar}^{\text{NacNac}}\}]_2$ ($\text{Ar} = \text{Dipp}, \text{Dep}, \text{Mes}$) reductants with organic substrates and their application in the preparation of low oxidation state group 2, 13 and 14 compounds.^[82]

In general, $[\text{Mg}\{\text{Ar}^{\text{NacNac}}\}]_2$ dimers are reported to be able to perform one-, two- or even three electron reductions of a variety of unsaturated organic materials.^[82] Starting with complex **A** in Scheme 1-8, a reaction of benzophenone in the presence of DMAP led to the formation and first description of a magnesium ketyl-radical which was subsequently affirmed by solid-state structure determination.^[99] So far, this reduction represents the only example of a one-electron delivery process promoted by a dimagnesium(I) reductant. In contrast to that, the insertion of an organic material into the $\text{Mg}^{\text{I}}\text{-Mg}^{\text{I}}$ bond under formation of dimagnesiated products involve a more common two-electron transfer onto the substrate. For example, this is reported for unsaturated compounds like azides, carbodiimides, ketenimines and cyclooctatetraene,^[53,100] or anthracene.^[99] The ter-magnesiated complex **B** is a prominent representative for a three-electron reduction by a dimeric Mg^{I} complex.^[101] Here, three monomeric β -diketiminato supported magnesium(II) fragments are bridged by the nitrogen donor atoms of a triple negatively charged hexaazatri-naphthylene system. Continuing in clockwise direction, it was shown that dimeric Mg^{I} reductants are capable of the activation of stable carbon-fluoride bonds of partially- or perfluorinated aromatic

substrates under formation of arylated (**C**) and dimeric, fluoride bridged, Mg^{II} complexes (**C'**).^[102] If the mechanism of the reductive C–F bond cleavage is mediated by preliminary Mg^{I} radical formation or by simple ligand-scrambling, still is subject to current investigations. Moreover, a reaction of a magnesium(I) dimer with CO_2 was reported to promote the reductive disproportionation of carbon dioxide under formation of carbon monoxide and the related carbonato complex **D** as kinetic main products. In addition, minor amounts of the thermodynamic oxalato compound **D'** were detected as a result of reductive coupling between CO_2 molecules.^[103] In this context, a striking study on the possibility to use magnesium(I) dimers in the transformation of feedstock gases into value-added products was carried out.^[104] In the course of the study, 1,3-cyclohexadiene (a molecular source of H_2) was treated with $[\text{Mg}\{\text{ArNacNac}\}]_2$ (Ar = Dipp, Dep) reductants under a CO atmosphere at room temperature. As a result, magnesium complexes coordinated by alkoxy ligands were obtained, that are assumed to form in a *Fischer-Tropsch*-like C–C coupling process. As suggested by experimental and computational studies, the reaction is mediated by intermediary hydride bridged $[\text{Mg}(\mu\text{-H})\{\text{ArNacNac}\}]_2$ species. These undergo a subsequent reaction with CO under formation of the corresponding alkoxy ligands after several further reaction steps. This work underscores the possible future application of dimeric Mg^{I} compounds in the stoichiometric or catalytic *Fischer-Tropsch*-like transformation of synthesis gas into higher alcohols.^[82] A further remarkable reaction product of a magnesium(I) dimer with an organic substrate is visualized with structure **E**. Here, a reductive coupling of two 1-azideadamantane molecules takes place, affording a dianionic $\text{Adam}_2\text{N}_6^{2-}$ hexaazadiene ligand.^[53, 100] Straight organic compounds that contain covalently bound N_6 -chains are known to be prone to spontaneous explosive decomposition. In stark contrast to that, the $[\text{Mg}^{\text{II}}\{\text{ArNacNac}\}]$ supported hexaazadienes do not appear to be subject to shock- or thermally induced detonations.^[42]

Besides utilization as reductants in organic substrate transformation, dimagnesium(I) compounds also found a widespread application in tailored syntheses of other low oxidation state main-group complexes. A compound class that promises to be a serious alternative for small-molecule activation and catalysis – transformations that usually require the presence of a rare and toxic transition-metal.^[82] So far, complex **F** represents the only example for the synthesis of another low oxidation state group 2 compound mediated by a dimeric $\text{Mg}^{\text{I}}\text{-Mg}^{\text{I}}$ species (Scheme 1-8, *vide supra*).^[105] Analogous to the synthesis of the reducing agent itself, a halide precursor complex $[\text{MgBr}\{\text{Ph}_2\text{P}(\text{NDipp})_2\}]$ is converted to the respective magnesium(I) dimer $[\text{Mg}\{\text{Ph}_2\text{P}(\text{NDipp})_2\}]_2$, which in this case is based on a $\text{Mg}^{\text{I}}/\text{Mg}^{\text{II}}$ redox couple. Continuing with group 13 elements, in a reduction of a platinum(II)-based boryl compound, the corresponding multiple reduced complex **G** was obtained.^[106] Compound **G** features both, a now neutrally charged platinum metal center as well as the first η^2 -bound diborene ligand in any metal complex. It was shown by computational and experimental investigations that there is π -back donation from the Pt(0) metal to a vacant π -bonding orbital of the perpendicularly arranged diborene, strengthening the boron-boron double

bond. Therefore, the bonding situation in complex **G** can be seen as a rare and unusual exception from the *Dewar-Chatt-Duncanson* model.^[82] Moreover, in the reaction of two equivalents of an *N*-heterocyclic carbene (NHC) supported AlH_3 adduct with a $[\text{Mg}^{\{\text{Mes}\}\text{NacNac}}]_2$ dimer, the first thermally stable NHC adduct of highly elusive dialane(4) (Al_2H_4) (**H**) and the respective dimagnesium(II) hydride $[\text{Mg}(\mu\text{-H})^{\{\text{Mes}\}\text{NacNac}}]_2$ are formed.^[107] Treatment with potassium metal, revealed the hydrogenation of the magnesium(I) dimer to be reversible, indicating a possible future application of this compound as hydrogen storage material in fuel cell driven units. Remarkably, preparation of structure **I** allowed the isolation of the dialanate dianion structural fragment ($[\text{Al}_2\text{H}_6]^{2-}$) as a CIP supported by two singly hydride bridged dimagnesium(II) counter ions.^[108] Computational studies revealed that the stability of the dialanate (an isoelectronic analogue of ethane) strongly depends on the coordination and support of the sterically demanding dimagnesium(II) cations. Complex **J** is one of the first examples of the preparation of a low oxidation state group 14 compound accessed *via* reduction with a dimagnesium(I) reagent.^[109] In particular, from a reaction with NHC supported germanium(II) chloride the respective dimeric germanium(0) fragment featuring a $\text{Ge}^0=\text{Ge}^0$ double bond was obtained. In a similar reaction, the related $\text{Sn}^0=\text{Sn}^0$ NHC adduct was accessed as well.^[110] Furthermore, there are several reported examples in which dimeric $\text{Mg}^{\text{I}}-\text{Mg}^{\text{I}}$ species were successfully applied to generate low oxidation state group 15 as well as d-block element complexes. An excellent review summarizing these approaches has been published recently.^[82]

1.4 β -Diketiminato Related Ligand Platforms

The archetypical β -diketiminato ligand scaffold is characterized by a pronounced modularity with respect to the substituents attached to its nitrogen donors (see Scheme 1-2).^[30] Moreover, by the sweeping capability of its main-group^[11, 111] and transition-metal^[12] compounds to perform in catalysis, as well as its ability to host low oxidation state group 2 and late main-group metals.^[82, 83] The corresponding group 13 and 14 complexes are also known as metallylenes, due to their analogy to *N*-heterocyclic carbenes.^[21, 112] Inspired by these features and its applicability, the search for related auspicious ligand platforms was started. So far, the synthesis of novel ligand systems has mainly focused on the ability to maintain the formation of a NacNac-like six-membered metallaheterocycle. Another point of interest was to mimic the excellent shielding that is supplied to a metal ion by the residues residing at the NacNacs nitrogen Lewis-donor atoms. Especially, as it is the case for the famous 2,6-diisopropylphenyl substituted DippNacNac ligand system.

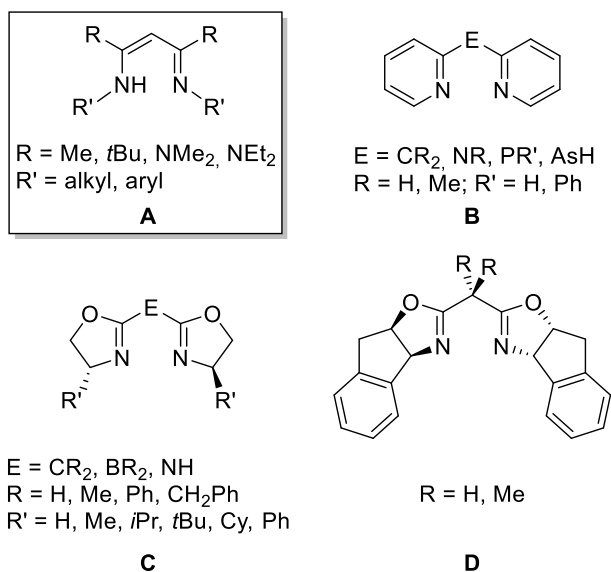


Figure 1-5. The archetype β -diketiminato ligand system (**A**) in comparison to selected derived ligand scaffolds featuring heterocyclic side arms with endocyclic C=N imine moieties (**B-D**).

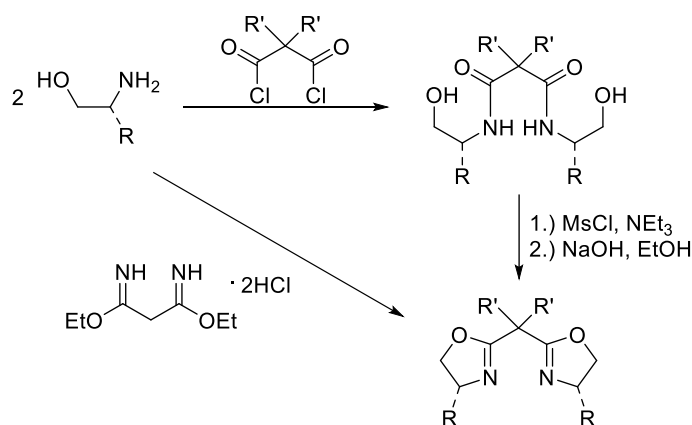
In this context, several different NacNac-related ligand systems featuring heterocyclic side arms with fused C=N imine moieties were synthesized that are summarized in Figure 1-5. Starting with ligand class **B**, the β -diketiminato side arms are formally replaceable by 2-pyridyl units. The resulting 2,2'-dipyridylmethane ligand is readily accessed by heating 2-picolylithium with either 2-bromopyridine or an excess of neat pyridine.^[113] The corresponding amine bridged derivatives are obtained in a *Buchwald-Hartwig* type reaction of, for example, 2-bromo- with 2-aminopyridine.^[114, 115] In the case of the group 15 homologues, synthesis is started from the triple substituted phosphide or arsenide compounds $(2\text{-NC}_5\text{H}_4)_3\text{E}$ ($E = \text{P, As}$). A treatment with lithium chips followed by hydrolysis from aqueous workup affords the secondary phosphanes or arsines *via* reductive fission of an aryl substituent. Accompanied by X-ray structure analysis-based structure-reactivity investigations as well as computational and charge density studies, these ligand scaffolds were intensively studied by our group from the early 1990s to the late 2000s. During that time, focus was put on the introduction of the monoanionic ligands to group 1 and 13 metal coordination. Among others, a variety of different complexes of the form $[\text{MR}_2\{((2\text{-NC}_5\text{H}_4)_2\text{E})\}]$ ($M = \text{Li, Cs, Al, Ga, In, Tl}$; $R = \text{THF, Me, Et}$, $E = \text{CH, N, P, As}$)^[10, 116–118] were obtained. Especially for the heavier group 13 metals and the soft cesium cation, these showed versatile coordination motifs under incorporation of the bridging heteroatom.

In addition to this development, some recent highlights in the utilization of ligand class **B** are mentioned in the following paragraph. Regarding the neutral 2,2'-dipyridylmethane ligand, in 2013, a derived platinum-based complex of the form $[\text{PtPh}(\text{THF})\{2\text{-NC}_5\text{H}_4)_2\text{CH}_2\}][\text{B}\{3,5\text{-(CF}_3)_2\text{-C}_6\text{H}_3\}_4]$ was reported to be one of the most active catalysts to perform in the hydrophenylation of ethene.^[126] Moreover, the formation of a variety of ionic structures as well as neutral adducts obtained from 1:1 and 1:2 molar ratios of the parent neutral ligand and group 13 (B, Al, Ga, In)

chlorides were introduced by Vasko and co-workers in 2015. Their molecular and electronic structures were examined in detail.^[127] Lately, copper- and platinum dichloride complexes supported by different neutral 2,2'-dipyridyls featuring various substituted carbon bridges (CH₂, CHMe and CMe₂) were evaluated with respect to their anti-proliferative character for possible future anti-cancer drug application.^[128] Moreover, iridium(III) complexes of differently substituted 2,2'-dipyridylamine and -amide ligands were reported to show photo-catalytic activity in, for example, CH-functionalizations of organic substrates.^[129] Interestingly, in a recent screening study on copper(I) NHC adducts supported by aryl-functionalized 2,2'-dipyridylamines, the first blue copper(I) based LECs (light-emitting cells) were presented and thoroughly investigated in terms of their photo-physical features.^[115]

With respect to the heavier 2,2'-dipyridylphosphane congener, the neutral phosphide analogue is accessed if the hydrogen atom at the bridging position is replaced, for example, by an phenyl substituent. Lately, zinc(II) chloride complexes supported by such a neutral (2-NC₅H₄)₂PPh phosphide were investigated in terms of their capability to activate and electrochemically reduce carbon dioxide.^[130] Starting from the same phosphide bridged ligand and copper(I) halides, in a mechanochemical synthesis under crucial addition of a few drops of aceto- or benzonitrile, highly emissive dinuclear copper(I) species of the form [CuX{(2-NC₅H₄)₂PPh}]₂ (X = Cl, Br, I) were quantitatively obtained. In a same manner, these complexes were accessed starting from the dimeric copper(I) tetrafluoroborates [Cu(MeCN){(2-NC₅H₄)₂PPh}]₂[BF₄]₂ and the corresponding potassium halides. Based on experimental and theoretical studies, the emission observed at low temperature around 77 K could be assigned to phosphorescence. In contrast to that, at ambient temperature so-called thermally activated delay fluorescence (TADF) processes are reported to take place.^[131]

From a formal replacement of the NacNacs RC=NR' substituents by oxazoline side arms, the family of bis(oxazoline-2-yl)methane or BOX ligands (C in Figure 1-5, *vide supra*) and its derivatives become available.^[132]



Scheme 1-9. Two exemplary preparation methods of carbon bridged bis(oxazoline) ligand systems.^[132]

For example, these ligand platforms are readily accessible through a one-step double cyclocondensation reaction starting from an ethylbisimidate dihydrochloride linker unit and a adequately substituted 1,2-aminoalcohol (Scheme 1-9, *vide supra*). Another method starts from malonyl dichloride as linker yielding a yet non-cyclized bis(hydroxy) amide intermediate. Activation with mesityl chloride (MsCl) affords the corresponding bis(mesylate) that forms the desired bis(oxazoline) upon two intramolecular cyclocondensation reactions.^[132] Because of a partially saturated ligand backbone, in association with bulky substituents adjacent to the coordination pocket, these ligands carry chiral information. Based on the prototypical ligand C, versatile ligand systems featuring substituents with varying degree of steric demand (*e.g.* Me, *i*Pr, *t*Bu, Cy, Ph) adjacent to the imine nitrogen atoms have been prepared. These platforms soon proved to be efficient asymmetric catalysts that are now widely utilized in transition-metal-mediated catalytic reactions.^[133–137] Despite that most of these catalysts carry neutral BOX systems, a variety of monoanionic oxazolinato-based main-group-^[138, 139] and transition-metal^[140–144] complexes were synthesized as well. As a highlight, the only crystallographically characterized bis(oxazoline-2-yl)methanide group 2 complex $[\text{Ca}(\text{THF})_2\{\text{N}(\text{SiMe}_3)_2\}\{\text{PhBOX}\}]$ ^[145] was synthesized by *Harder* and co-workers in 2008 (Figure 1-6).^[146] A subsequent evaluation of its applicability in the catalytic hydrosilylation and intramolecular hydroamination of alkenes revealed a high substrate turnover but only a poor enantiomeric excess of the obtained products. It is assumed that the poor enantioselectivity of the catalyst is due to the catalytically active species being mainly homoleptic. As a landmark in biomimetic applications, in the group of *Meyer*, neutral BOX-supported copper(I) complexes were successfully used for a hemocyanin-like dioxygen activation. The formed $\mu\text{-}\eta^2\text{-}\eta^2$ -peroxido-dicopper(II) complexes were shown to reversibly release dioxygen at elevated temperatures.^[147] Most recently, these peroxido-dicopper(II) compounds (Scheme 1-10, left, *vide infra*) were readily transformed into their bis(μ -oxido)-dicopper(III) (Scheme 1-10, right) derivatives by simple deprotonation of the ligand backbones and *vice-versa*.^[148] Subsequently, extensive spectroscopic, crystallographic and computational studies were carried out to shed light on these proton coupled electron transfers. As a result, rare insights into key intermediates in copper-mediated dioxygen activation were gained, which are proposed model compounds for pH responsive histidine-supported dicopper proteins.

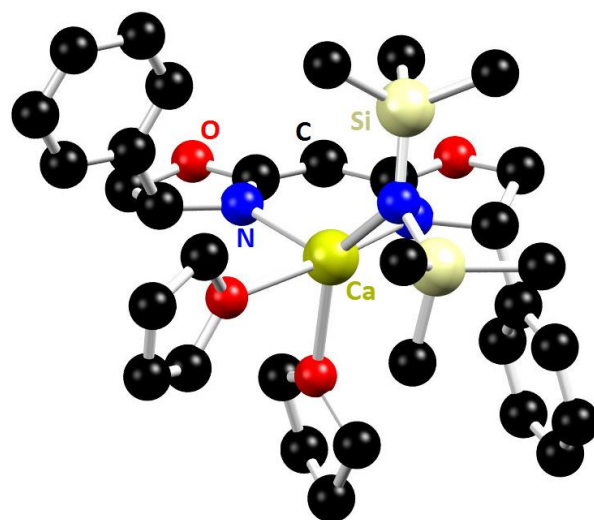
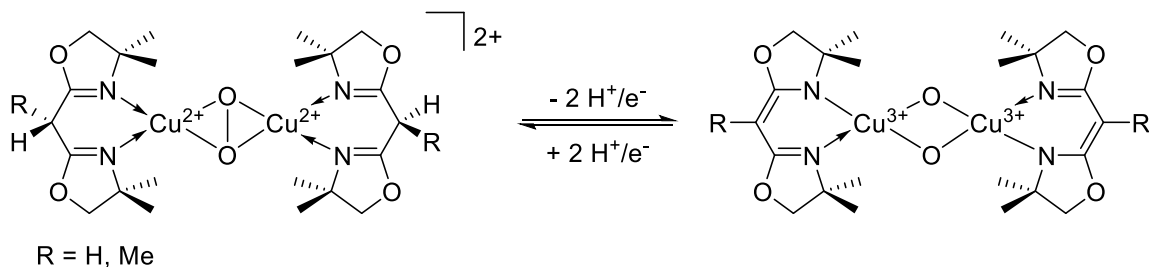


Figure 1-6. Isotropic solid-state structure of the bis(oxazolinato)-based alkaline-earth metal complex $[\text{Ca}(\text{THF})_2\{\text{N}(\text{SiMe}_3)_2\}\{\text{PhBOX}\}]$ by *Harder* et al.^[145]



Scheme 1-10. Acid/base induced transformation between μ - η^2 - η^2 -peroxido-dicopper(II) complexes (left) and their oxidized bis(μ -oxido)-dicopper(III) congeners (right).^[148]

In analogy to the archetypal β -diketiminate ligand scaffold, if the CR_2 spacer in **C** carries at least one hydrogen atom, a tautomerism between the imino-enamine and the diimine form was detected. The former is fostered especially by the presence of a phenyl substituent at the bridging unit.^[149]

Regarding variations in the backbone spacer, a formal replacement of the CR_2 moiety with a BR_2 ^[150] or NH ^[151] group gives access to the corresponding lighter group 13 and 15 bridged BOX derivatives of **C**. In association with modifications at the ring system, so-called bis(indaoxazoline-2-yl)-methanes were introduced (**D** in Figure 1-5, *vide supra*). Preparation in a one-pot procedure can be carried out by condensation of the aforementioned ethylbisimidate dihydrochloride salt with (1S, 2R)-aminoindane-2-ol.^[132] In addition, these extended bis-oxazolines found implementation as versatile platforms for asymmetric catalysts, for example, in a diastereo- and enantioselective cyclopropanation of 1,2-disubstituted alkenes.^[152–154]

The formal replacement of the unsupported $\text{C}=\text{N}$ imine residues of the β -diketiminate framework by benzannulated five-membered heterocycles gives access to the related bis(heterocyclo)methane ligand family (**E** and **F** in Figure 1-7).

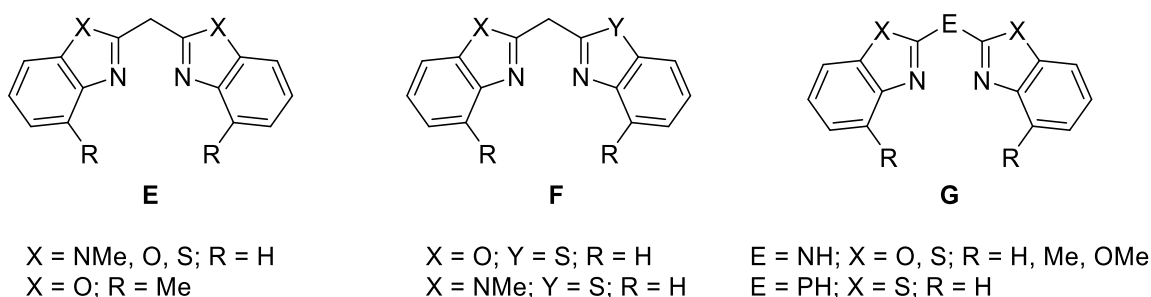


Figure 1-7. Bis(heterocyclo)methane, -amine and -phosphane derivatives mimicking the five-membered coordination pocket of the paragon NacNac ligand. Adapted with permission from reference ^[1]. Copyright 2017, John Wiley and Sons.

The preparation of bis(benzothiazole-2-yl)methanes was established many decades ago,^[155] and bis(heterocyclo)methanes and –methanides have proven to be suitable hosts for transition-metal complexation, forming salt- or neutral chelate complexes. Despite that, this ligand class has gained only minor attention in the field of coordination chemistry.^[156, 157] Nevertheless, a wide range of bis(heterocyclo)methanes and –methanides featuring benzimidazol, -oxazol, benzothiazol and asymmetrically substituted side arms were prepared and investigated in detail during the last decades.^[157–159] However, research predominantly focused on comprehensive NMR spectroscopic studies in order to determine the intrinsic π -electron-withdrawing ability of each heterocyclic residue. In order to gain a reliably experimental charge distribution mapping, extensive ^{13}C - and ^{15}N NMR shift-to-charge ratio calculations were carried out in comparison to related heterocyclic substituted platforms.^[160–165] Despite a neglected implementation in coordination chemistry, in recent years, our group successfully introduced differently shaped bis(heterocyclo)methanides $(\text{NCXC}_6\text{H}_4)_2\text{CH}_2$ ($\text{X} = \text{NMe}, \text{O}, \text{S}$) as well as $(4\text{-Me-NCOC}_6\text{H}_3)_2\text{CH}_2$ (**E** in Figure 1-7, *vide supra*) to selected group 1 (Li) and 13 (Al, Ga, In) coordination.^[166, 167] A preparation can be carried out similar to the one-step procedure depicted in Scheme 1-9, using different linker units like the aforementioned bisimidate dihydrochloride salt or malonodinitrile. Additionally, this chemistry was successfully extended to selected asymmetric platforms $\{(\text{NCXC}_6\text{H}_4)(\text{NCYC}_6\text{H}_4)\}\text{CH}_2$ ($\text{X} = \text{O}, \text{NMe}; \text{Y} = \text{S}$) featuring two different heterocyclic side arms (**F** in Figure 1-7).^[168] All obtained metal complexes contain MRR' fragments ($\text{M} = \text{Li}$: $\text{R}, \text{R}' = \text{THF}$; $\text{M} = \text{Al}$: $\text{R} = \text{Me}, \text{R}' = \text{Me}, \text{Cl}, \text{I}$; $\text{M} = \text{Ga}$: $\text{R}, \text{R}' = \text{Me}$) and were studied in detail in comparative crystallographic and NMR spectroscopic investigations with respect to their coordinative features. On the way to low oxidation state group 13 compounds similar to those already established for the $\text{D}^{\text{ipp}}\text{NacNac}$ ligand system in $[\text{M}\{\text{D}^{\text{ipp}}\text{NacNac}\}]$ ($\text{M} = \text{Al}$,^[169] Ga ,^[170] In ,^[171] Tl ^[172]), especially the $(4\text{-MeNCOC}_6\text{H}_3)_2\text{CH}_2$ ligand system bearing methyl groups adjacent to the coordination pocket turned out to be most promising. Its group 13 metal complexes that contain MMe_2 fragments ($\text{M} = \text{Al}^{3+}, \text{Ga}^{3+}, \text{In}^{3+}$) exhibit almost no dislocation of

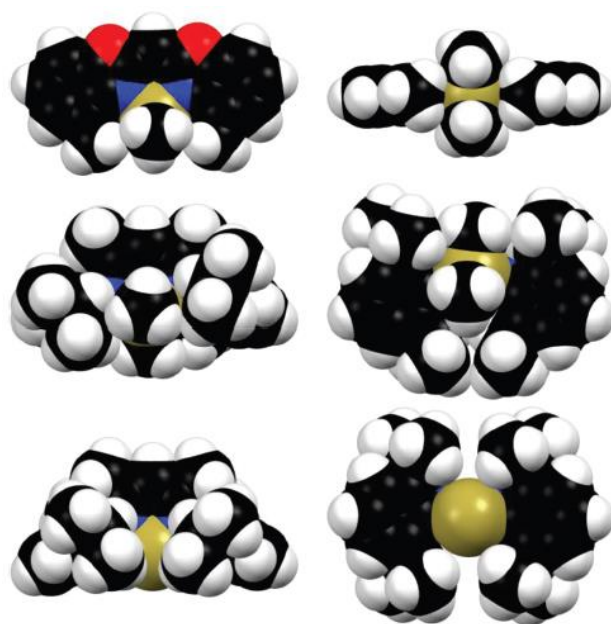
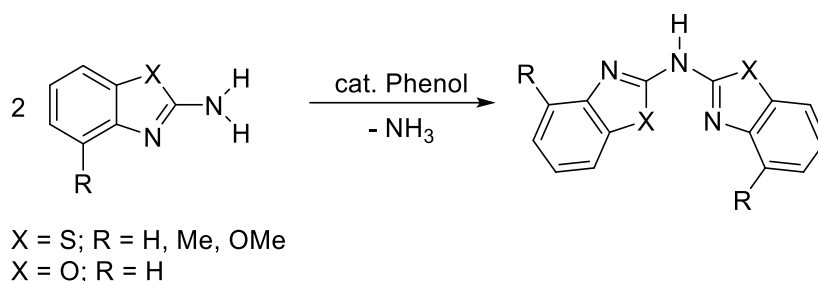


Figure 1-8. Comparison of the space-filling models of $[\text{AlMe}_2\{(4\text{-MeNCOC}_6\text{H}_3)_2\text{CH}\}]$ (top), $[\text{AlMe}_2\{\text{D}^{\text{ipp}}\text{NacNac}\}]$ (middle) and the reduced alumylene species $[\text{Al}\{\text{D}^{\text{ipp}}\text{NacNac}\}]$ (bottom) (left: side views; right: bottom views). Note, the top and the bottom structure, both show an in-plane arrangement of the metal fragment with respect to the chelating plane of the ligand molecule. Reprinted from reference ^[167]. Copyright 2016, The Royal Society of Chemistry.

the cation from the chelating C_3N_2 plane, assuring an enhanced orbital overlap. Thus, charge delocalization between a potentially low oxidation state metallylene and the ligand framework is facilitated (Figure 1-8). Moreover, the methyl substituents in proximity to the coordination pocket combine the best of two worlds. A sufficient shielding is supplied to the metal fragment, which still allows additional substitutions at the metal center.^[167]



Scheme 1-11. General procedure for the synthesis of different bis(benzoxazol-2-yl)- and bis(benzothiazol-2-yl)amine ligands. Adapted with permission from reference ^[173]. Copyright 2016, The Royal Society of Chemistry.

Regarding Group 15 bridged ligand scaffolds (**G** in Figure 1-7, *vide supra*), the respective NH bridged bis(heterocyclo)amines are accessed by reaction of two equivalents of 2-aminobenzothiazole or -oxazole accompanied by the addition of 1.4 equivalents of phenol and a release of ammonia (Scheme 1-11).^[173] Following this procedure, a couple of novel chelate ligands (4-RNCX- C_6H_3) $_2$ NH ($X = S, O; R = H, \text{ Me, OMe}$) carrying hydrogen-, methyl- or methoxy substituents at the 4-position adjacent to the coordination

pocket were obtained. Subsequently, an evaluation of their coordination behavior towards lithium and aluminum cations was performed. While in the case of aluminum structures similar to the aforementioned methanide ligand frameworks were obtained, a donor-base free lithiation of the parent amine scaffolds afforded tetrameric species like in $[Li\{(4\text{-MeNCSC}_6\text{H}_3)_2\text{N}\}]_4$ (Figure 1-9). These structures exhibit an exclusive *N*-coordination mode under incorporation of the bridging nitrogen atom. Interestingly, in contrast to stacked ring or ladder shaped structures, which are observed for related lithium amides, a strongly distorted Li_4 -tetrahedron is formed.^[174-177]

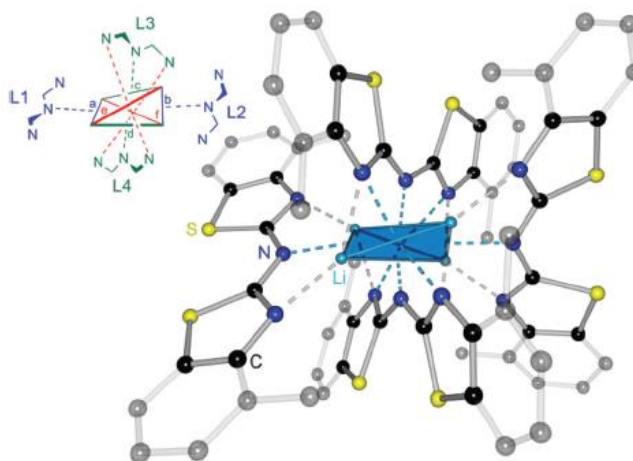


Figure 1-9. Isotropic solid-state structure of $[Li\{(4\text{-MeNCSC}_6\text{H}_3)_2\text{N}\}]_4$. The heterocyclic side arms are partially depicted in faded colors and the lattice solvent molecules as well as hydrogen atoms are omitted for clarity. To emphasize on the unique binding motif, the smaller figure shows a simplified representation of the coordinative situation. Reprinted with permission from reference ^[173]. Copyright 2016 The Royal Society of Chemistry.

The synthesis of the corresponding heavier group 15 bridged homologue bis(benzothiazol-2-yl)phosphane (NCSC₆H₄)₂PH (**G** in Figure 1-7, *vide supra*) is carried out just like for its 2-pyridyl substituted congener. The preparation of the tertiary phosphide (NCSC₆H₄)₃P is followed by abstraction of one of the heterocyclic side arms and subsequent hydrolysis, as developed in our group.^[178] The neutral ligand scaffold as well as its monoanionic phosphanide form offer many feasible coordination motifs, due to three different types of donor atoms (N, P and S) in the ligand periphery. Thus, an enhanced ability to address metal cations of different *Lewis* acidity and basicity according to the HSAB concept by *Pearson* is given.^[179-181] Moreover, the heteroaromaticity of this ligand scaffold was carefully examined by theoretical calculations and charge density studies.^[178, 182] The investigations unveil the formation of an NH tautomer to be energetically fostered in contrast to a hydrogen atom residing at the phosphorous atom in a respective PH tautomer. This is also reflected by the fact that the ligand in its NH tautomeric form is only stable when handled in diethyl ether. Dilution in any other solvent caused a hydrogen shift towards the PH tautomeric form, resulting in ligand scrambling and subsequent decomposition. Despite the sensitivity of this ligand platform, it was successfully used in the coordination of different main-group- (Li,^[183] Cs^[178]) and transition-metals (Fe,^[184] Mn,^[183] Cd,^[185] Zn^[185]), exhibiting a variety of different coordination motifs based on its unique set of N, P and S donor atoms.

1.5 Outline

In light of a successful and widespread implementation of the NacNac ligand scaffold, many efforts have been made to transfer the NacNacs steric and electronic features to other ligand systems in the last two decades. For example, the development of novel symmetrically and partly asymmetrically substituted bis(heterocyclo)methane, -amine and-phosphane ligand scaffolds mirror some advance within this process. These ligand systems were developed in our group by *Stey*^[6, 125, 178, 183, 184] and *Dauer*,^[166-168, 173] and offer additional N, O, S or P donor sites in the ligand periphery. In the course of this research, especially the bis(4-Me-benzoxazol-2-yl)methanide ligand system turned out to be a vital aspirant for the synthesis of low oxidation state main-group compounds.^[167] Continuing on these investigations, this thesis focuses on the development of novel bulky bis(benzoxazol-2-yl)methane derivatives and their application in s-block metal coordination (Figure 1-10).

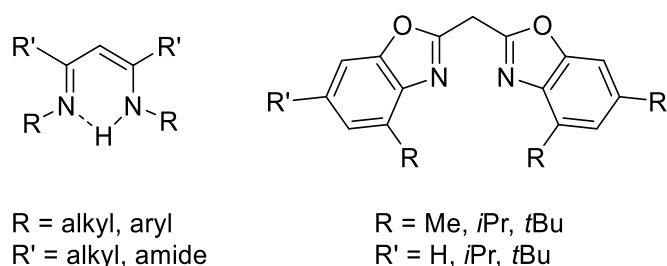


Figure 1-10. The β -diketiminato ligand system (left) in comparison to the bis(benzoxazol-2-yl)methane scaffolds used in this thesis (right).

In general, this ligand class is characterized by both, benzannulated as well as methylene bridged 1,3-azole moieties, mimicking the five-membered coordination pocket of the NacNac system. As an advance, the implementation of additional oxygen donor atoms and the simultaneous extension of the aromatic backbone leads to the formation of much more electron-rich ligand platforms. Furthermore, the presence of four donor sites gives access to several conceivable coordination motifs. Among others, these range from a NacNac-like N,N' chelation, over an O,O' to a mixed N,O coordination. Due to the synergy of the four heteroatoms, the adjacent methylene bridge can be readily deprotonated with organometallic reagents. So far, all developed benzannulated bis(heterocyclo)methane, -amine or -phosphane ligand scaffolds with H, Me or OMe substituents adjacent to the coordination pocket supply only limited steric shielding to a coordinated metal ion. Thus, to better mimic the shielding abilities provided by the mainly N -arylated NacNac ligand systems, new synthetic routes for the synthesis of benzannulated bis(benzoxazol-2-yl)methane ligand scaffolds featuring sterically demanding residues adjacent to the coordination pocket are presented. Hence, investigations embark on the synthesis and subsequent introduction of the three utilized ligand scaffolds bis(4-Me-benzoxazol-2-yl)- and bis(4,6-R-benzoxazol-2-yl)methanide ($R = iPr, tBu$) (see Figure 1-10) to group 1 and 2 metal coordination. The methods of choice are concerted deprotonation-metalation reactions with group 1 or 2 organometallics or salt metathesis reactions starting from group 1 precursor complexes and the corresponding alkaline-earth-metal halides. In light of ten years of low oxidation state magnesium(I) dimers reported by Jones et al.,^[81, 82] focus is put on the ability of the ligand scaffolds to stabilize heteroleptic alkaline-earth-metal halide and -amide precursor complexes for subsequent reduction. Finally, on the way to dimeric Ae^I-Ae^I bound species for small molecule activation and potential catalytic applications, first reduction attempts on magnesium(II) halide precursors are presented.

2 RESULTS AND DISCUSSION

Major parts of this chapter have been published in:

- [1] I. Koehne, R. Herbst-Irmer, D. Stalke, “Bis(4-methylbenzoxazol-2-yl)methanide in *s*-Block Metal Coordination”, *Eur. J. Inorg. Chem.* **2017**, 2017, 3322-3326.^[1]
- [2] I. Koehne, S. Bachmann, T. Niklas, R. Herbst-Irmer, D. Stalke, “A Novel Bulky Heteroaromatic-Substituted Methanide Mimicking NacNac: Bis(4,6-*tert*-butylbenzoxazol-2-yl)methanide in *s*-Block Metal Coordination”, *Chem. Eur. J.* **2017**, 23, 13141-13149.^[2]
- [3] I. Koehne, S. Bachmann, R. Herbst-Irmer, D. Stalke, “A Water-Containing Organopotassium Compound Based on Bis(4,6-*t*Bu-benzoxazol-2-yl)methanide and Its Unexpected Stability to Hydrolysis”, *Angew. Chem.* **2017**, 129, 15337-15342; *Angew. Chem. Int. Ed.* **2017**, 56, 15141-15145.^[3]
- [4] I. Koehne, N. Graw, T. Teuteberg, R. Herbst-Irmer, D. Stalke, “Introducing NacNac-Like Bis(4,6-isopropylbenzoxazol-2-yl)methanide in *s*-Block Metal Coordination”, *Inorg. Chem.* **2017**, 56, 14968-14978.^[4]

2.1 Important Structural Features

Besides the consideration of bond lengths and angles, some additional features are of importance for the discussion of the solid-state structures of the metal complexes in the following chapters of this thesis. The distinct dislocation from the chelating ligand plane displayed by each metal fragment is one of these features (Figure 2-1).

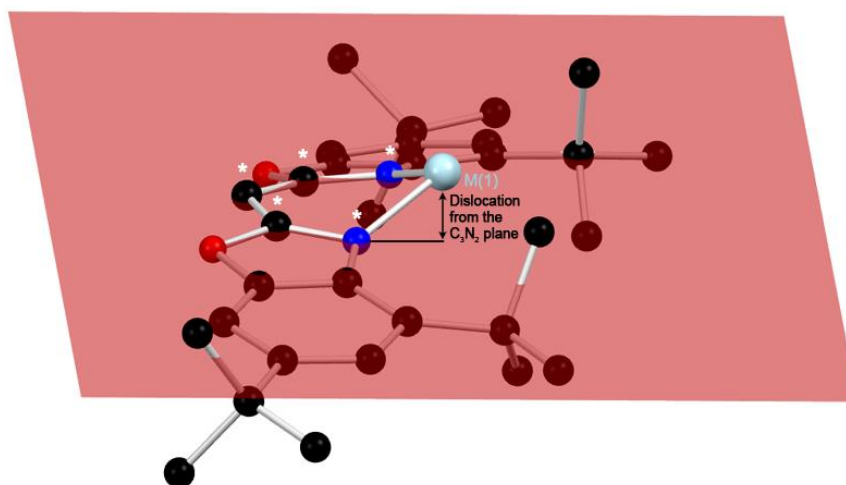


Figure 2-1. Determination of the metal fragments dislocation in the discussed methanide complexes.

In most cases, the imine nitrogen atoms coordinate to the utilized s-block metals. Thus, if not stated otherwise, the dislocation of the cation is calculated with respect to the chelating C_3N_2 plane. The red colored plane was put through the atoms marked with a white star. To determine its dislocation, the distance of the respective metal fragment to the aforementioned plane was calculated.

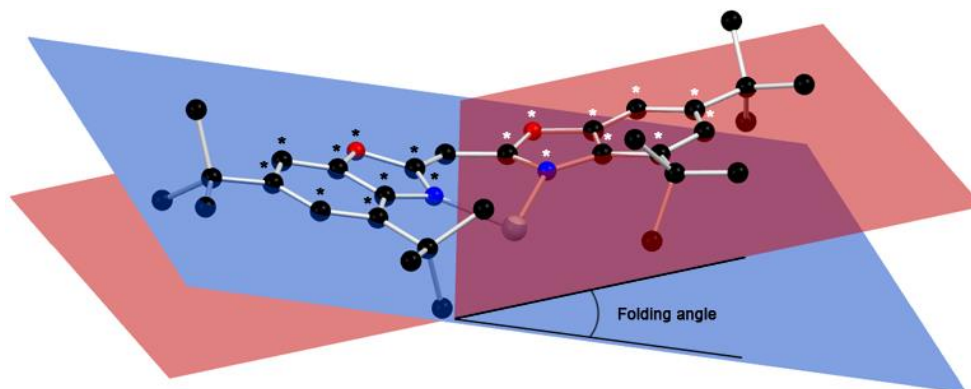


Figure 2-2. Determination of the butterfly-like folding angle between both heteroaromatic side arms in the discussed methanide complexes.

In addition to that, a plane can be spanned based on the ring atoms of each heteroaromatic side arm (Figure 2-2). The blue plane was spanned based on the atoms highlighted with a black star, while the red plane was fitted through the atoms marked with a white star. Both planes intersect at a specific angle. Upon deprotonation, the formation of a formally planar aromatic system delocalized about the whole ligand framework is expected. Hence, the butterfly-like folding angle reflects the deviation of the aromatic ligand scaffold from perfect planarity in consequence of the coordination of a metal cation.

2.2 Bis(4-Me-benzoxazol-2-yl)methanide (1) Based s-Block Complexes

Major parts of this chapter have been published in:

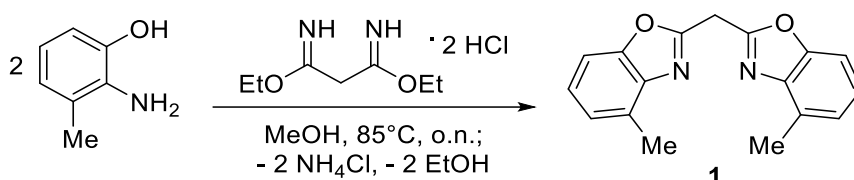
- [1] I. Koehne, R. Herbst-Irmer, D. Stalke, “Bis(4-methylbenzoxazol-2-yl)methanide in s-Block Metal Coordination”, *Eur. J. Inorg. Chem.* **2017**, 2017, 3322-3326.^[1]

2.2.1 Ligand Synthesis

In previous investigations by *Dauer*, especially the bis(4-Me-benzoxazol-2-yl)methane ligand system (**1**) has turned out to be most promising for the generation of low oxidation state main-group compounds. It was shown that upon metalation with group 13 organometallics its complexes exhibit the least deviation of the metal cation from the chelating ligand plane, indicating

the best charge distribution within the aromatic system. This is advantageous, for example for the stabilization of low oxidation state species obtained from subsequent reduction. Furthermore, the methyl substituents offer a certain amount of shielding to the metal cation while not hampering further substitution reactions at the metal center.^[167]

Continuing on these studies, synthesis was started on the preparation of **1** according to procedures by *Dauer* and *Ben Ammar* (Scheme 2-1).^[167, 186]



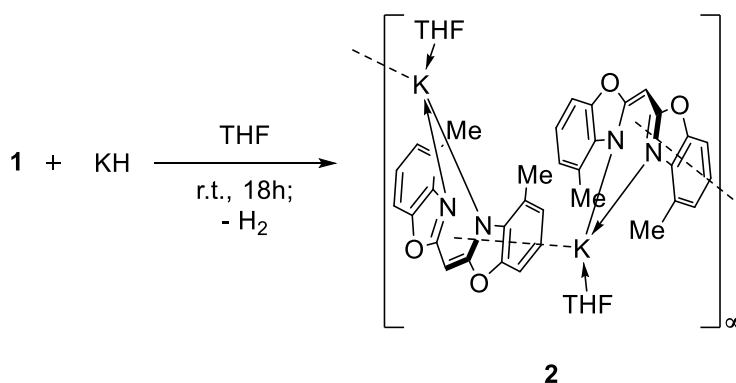
Scheme 2-1. Preparation of bis(4-Me-benzoxazol-2-yl)methane (**1**). Reprinted with permission from reference^[1]. Copyright 2017, John Wiley and Sons.

Initially, the bisimidate dihydrochloride linker had to be prepared from malonodinitrile. In this reaction, the addition of ethanol and hydrochloric acid dissolved in 1,4-dioxane to the starting material leads to the preliminary formation of a primary imine that is subsequently protonated to give the activated bisimidate dihydrochloride salt.^[167, 186] Subsequently, from the addition of two equivalents of 3-methyl-2-aminophenol to the C₃-linker unit, compound **1** was accessed *via* a two-fold cyclocondensation reaction under release of ammonium chloride and ethanol.^[167]

2.2.2 Group 1 Complexes

2.2.2.1 [K(THF){(4-Me-NCOC₆H₃)₂CH}]_∞ (**2**)

To obtain a starting material for subsequent salt metathesis reactions with group 2 halides, a potassium precursor complex was prepared (Scheme 2-2).



Scheme 2-2. Synthesis of [K(THF){(4-Me-NCOC₆H₃)₂CH}]_∞ (**2**). Reprinted with permission from reference^[1]. Copyright 2017, John Wiley and Sons.

The addition of **1** to a suspension of potassium hydride (KH) in THF led to the formation of a red solution under vigorous evolution of hydrogen gas. After removal of the solvent and washing with pentane, the corresponding potassium complex $[\text{K}(\text{THF})\{(4\text{-Me-NCOC}_6\text{H}_3)_2\text{CH}\}]_\infty$ (**2**) was obtained in a yield of 73%.

The ^1H NMR spectrum of **2** shows one set of signals for the methanide ligand and the additionally attached THF molecule, indicating that the two sides of the ligand framework are chemically and magnetically equivalent. The resonances in a range of 6.85 to 6.60 ppm can be assigned to the aromatic protons of the benzene perimeters. The signals at 4.65 and 2.41 ppm with integrals of one and six, respectively, can be ascribed to the bridging CH fragment and the methyl substituents. The coordinating THF molecule gives rise to resonances at 3.62 and 1.77 ppm with integrals of four in each case. In Figure 2-3, a comparative stack of the ^1H NMR spectra of **1** (bottom) and **2** (top) is given.

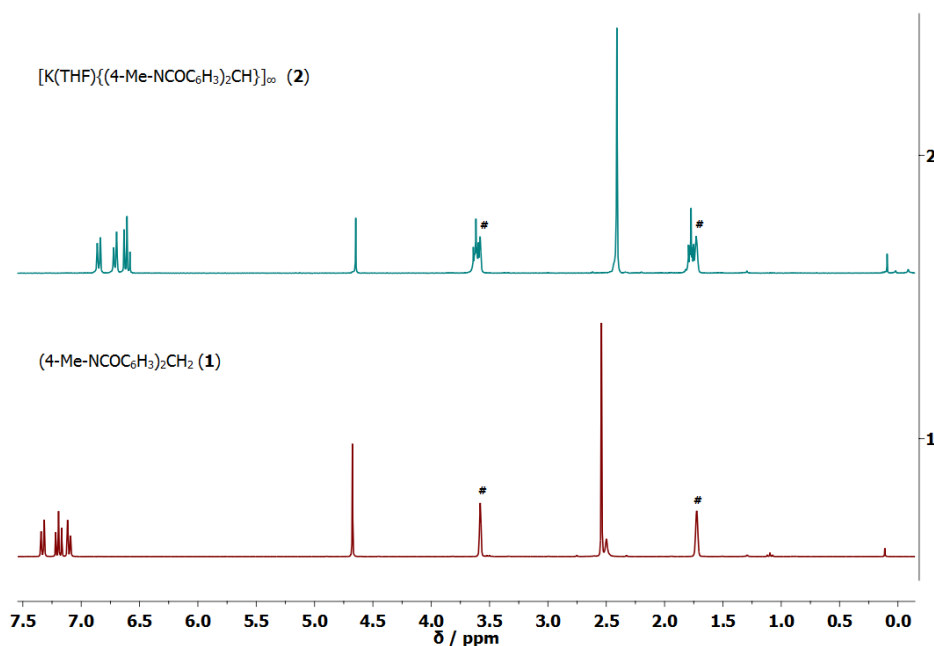


Figure 2-3. Stacked ^1H NMR spectra of the ligand system **1** (bottom) and the derived potassium complex **2** (top) in $[\text{D}_8]\text{THF}$. The residual proton resonances of the solvent are marked with #.

In comparison to the neutral ligand **1**, the resonances of complex **2** are shifted to higher field without exception (Figure 2-3). The coordination of an electron deficient cation usually causes an electronic deshielding of the ligand protons that is reflected by a stronger down-field shift of most of its proton resonances. This effect should be pronounced for the signal corresponding to the proton at the bridging methylene position, because this signal is most sensitive to changes in the electron density accumulated in the perpendicular p -orbital of the bridging carbon atom that is formed upon deprotonation and re-hybridization. The observations made for **2** are most likely a

feature of the additionally present η^5 -coordination of a second ligand molecule to the potassium ion that decreases the net electronic deshielding of the ligand protons.

Colorless needle-shaped crystals were obtained by gas-phase diffusion of pentane into a saturated solution of **2** in THF. The four-fold coordinated compound **2** crystallizes in the orthorhombic space group *Pbca*. It contains two molecules in the asymmetric unit that form infinite zigzag strands (Figure 2-4).

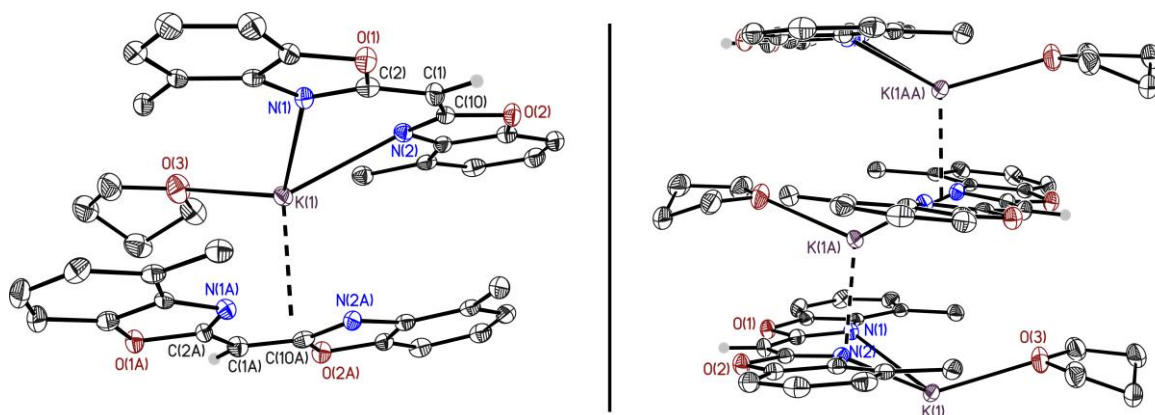


Figure 2-4. Excerpts of the polymeric solid-state structure of $[\text{K}(\text{THF})\{(4\text{-Me-NCOC}_6\text{H}_3)_2\text{CH}\}]_\infty$ (**2**). Left: Illustration of the four-fold coordination motif around the potassium cation. Right: Illustration of the formed infinite zigzag strands. Anisotropic displacement parameters are depicted at the 50% probability level. Hydrogen atoms are omitted for clarity, except for those at the bridging methylene positions. Reprinted with permission from reference^[1]. Copyright 2017, John Wiley and Sons.

The central potassium cation shows a distorted tetrahedral coordination by two ring nitrogen atoms of a monoanionic methanide ligand, a THF molecule and an additional η^5 -coordination to the central C_3N_2 plane of a second ligand molecule.

In comparison to the free uncharged ligand **1** (1.484(2) to 1.489(2) Å),^[167] the C(1)– C_{ipso} distances in **2** (1.386(3) to 1.398(3) Å) decrease (Table 2-1).

Table 2-1. Selected bond lengths [Å] and angles [°] of **2**.

K(1)–N(1)	2.770(2), 2.890(2)	N(1)–C(2)	1.331(2), 1.334(2)	K(1)– C_3N_2 dist.	1.28(3), 1.39(3)
K(1)–N(2)	2.795(2), 2.919(2)	N(2)–C(10)	1.329(2), 1.334(2)	N(1)–K(1)–N(2)	67.9(5), 67.4(5)
C(1)–C(2)	1.393(3), 1.386(3)	C(2)–O(1)	1.398(2), 1.395(2)	C(2)–C(1)–C(10)	125.1(2), 124.9(2)
C(1)–C(10)	1.398(3), 1.393(3)	C(10)–O(2)	1.392(2), 1.394(2)	Folding angle	4.56(3), 9.53(3)

The asymmetric unit contains two molecules. Hence, two values are given for each parameter. Symmetry transformations used to generate equivalent atoms: #1: $x+1/2, y, -z+1/2$; #2: $x-1/2, y, -z+1/2$; #3: $x+1/2, -y+1/2, -z+1$; #4: $x-1/2, -y+1/2, -z+1$.

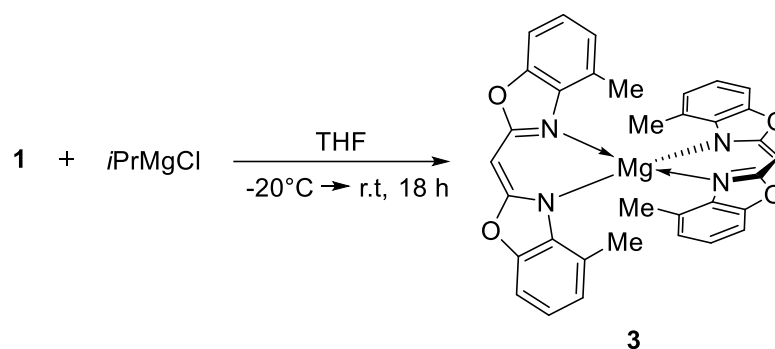
The opposite is true for the N– C_{ipso} distances. These range from 1.329(2) to 1.334(2) Å and are slightly elongated in comparison to **1** (1.290(2) to 1.292(2) Å). This is due to the formation of a conjugated π -system throughout the ligand and a change in hybridization of the bridging carbon

atom from sp^3 to sp^2 upon deprotonation. This re-hybridization is also reflected by the widening of the C(2)–C(1)–C(10) angle from $110.8(1)^\circ$ in **1** to an average of $125.0(2)^\circ$ in **2**, indicating a nearly trigonal-planar geometry adopted by the bridging carbon atom in the complex. As one can see from Table 2-1, the determined C(1)–C_{ipso} distances range between a characteristic C(sp^3)–C(sp^2) single- (1.51 \AA) and a C(sp^2)=C(sp^2) double bond (1.34 \AA), indicating effective charge delocalization. The same can be derived for the corresponding N–C_{ipso} bond lengths. Here, typical values for a N(sp^3)–C(sp^2) single- and a N(sp^2)=C(sp^2) double bond are 1.43 and 1.29 \AA , respectively.^[187, 188] To satisfy its coordination sphere and to facilitate the η^5 -coordination to a second ligand molecule, the potassium ion in **2** shows a strong dislocation ($1.28(3)$ to $1.39(3) \text{ \AA}$) from the κ^2 -N,N' chelating C₃N₂ plane. Despite that, with butterfly-like folding angles between $4.56(3)$ and $9.53(3)^\circ$, the methanide ligand exhibits only a minor deviation from ideal planarity. The K(1)–N distances range from $2.770(2)$ to $2.919(2) \text{ \AA}$ and are in good agreement with other potassium amides. For example, the η^6 -coordination of the potassium ion in the complex [K(THF)(PyCPh₂){PMDETA}] exhibits an averaged K–N distance of 2.809 \AA .^[189] Generally, the structural features of **2** also match quite well those of a related homoleptic β -diketiminato-based barium complex [Ba{DippNacNac}₂],^[190] that exhibits a similar averaged dislocation of 1.222 \AA to its chelating ligand planes. Additional structural parameters like an averaged Ba–N distance of 2.712 \AA and an averaged N–Ba–N bite angle of 68.9° are also in good agreement. These observations are not surprising in consideration of similar effective ionic radii of both cations (K⁺ = 137 pm to Ba²⁺ = 135 pm).^[191]

2.2.3 Group 2 Complexes

2.2.3.1 [Mg{(4-Me-NCOC₆H₃)₂CH}₂] (3)

As a first step, attempts to synthesize a magnesium halide complex of ligand system **1** were performed. Hence, treatment of **1** with a magnesium chloride *Grignard* reagent seemed to be best suited for this purpose. Contrary to expectations, adding ligand **1** to a solution of a slight excess of *i*PrMgCl in THF at -20°C did not give an intended heteroleptic magnesium chloride complex. Instead, the homoleptic species [Mg{(4-Me-NCOC₆H₃)₂CH}₂] (**3**) was obtained (Scheme 2-3).



Scheme 2-3. Synthesis of $[\text{Mg}\{(4\text{-Me-NCOC}_6\text{H}_3)_2\text{CH}\}_2]$ (**3**). Reprinted with permission from reference^[1]. Copyright 2017, John Wiley and Sons.

After removal of the solvent and extraction with toluene, crystalline **3** was isolated in a yield of 39% at room temperature.

The ^1H NMR spectrum of **3** in $[\text{D}_8]\text{THF}$ shows only one set of signals, which indicates the presence of chemically and magnetically equivalent heteroaromatic side arms as well as ligand molecules in the complex. The three resonances corresponding to the aromatic protons at the benzene perimeters are found in a range of 7.07 to 6.92 ppm. The methylene bridge protons show a signal at 5.05 ppm and the methyl substituents at the 4-positions give rise to a singlet at 2.69 ppm. In comparison to the protonated ligand **1**, which shows a methylene bridge signal at 4.68 ppm (Figure 2-3, *vide supra*),^[167] upon metalation, this signal experiences a shift to lower field in **3**. This effect is also observed for the resonance of the methyl substituents. In contrast to that, the three resonances caused by the benzene perimeter protons experience a pronounced shift to higher field, indicating a now enhanced charge accumulation at these positions.

A saturated solution of **3** in toluene afforded colorless prism-shaped crystals at room temperature. Compound **3** crystalizes in the monoclinic space group $P2_1/n$ that contains one molecule in the asymmetric unit. The central magnesium(II) cation adopts a slightly distorted tetrahedral coordination sphere, resulting in the two planar ligand molecules to exhibit an almost perfectly perpendicular arrangement with an twisting angle of $85.42(4)^\circ$ (Figure 2-5).

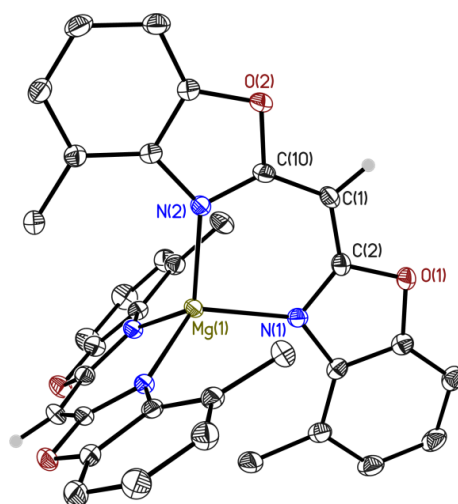


Figure 2-5. Solid-state structure of $[\text{Mg}\{(4\text{-Me-NCOC}_6\text{H}_3)_2\text{CH}\}_2]$ (**3**). Anisotropic displacement parameters are depicted at the 50% probability level. Hydrogen atoms are omitted for clarity, except for those at the bridging methylene positions. Reprinted with permission from reference ^[1]. Copyright 2017, John Wiley and Sons.

The magnesium cation shows dislocations of 0.021(2) and 0.124(2) Å from the chelating C_3N_2 planes giving a minor averaged dislocation of only 0.07(2) Å. On the one hand, the smaller dislocation is affiliated to N(1)–Mg(1)–N(2) and C(2)–C(1)–C(10) angles of 94.8(4) and 123.8(1)°, respectively. The folding angle in this particular ligand deviates with 4.24(3)° only marginally from perfect planarity (Table 2-2).

Table 2-2. Selected bond lengths [Å] and angles [°] of **3**.

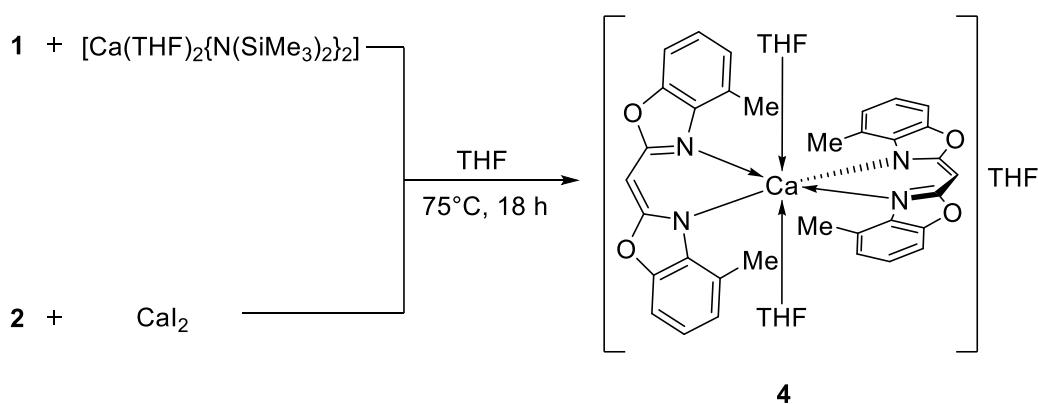
Mg(1)–N(1)	2.056(1), 2.053(1)	N(1)–C(2)	1.341(2), 1.334(2)	Mg(1)– C_3N_2 dist.	0.021(2), 0.124(2)
Mg(1)–N(2)	2.058(1), 2.060(1)	N(2)–C(10)	1.342(2), 1.346(2)	N(1)–Mg(1)–N(2)	94.8(4), 93.3(4)
C(1)–C(2)	1.393(2), 1.398(2)	C(2)–O(1)	1.374(2), 1.372(2)	C(2)–C(1)–C(10)	123.8(1), 122.7(1)
C(1)–C(10)	1.391(2), 1.385(2)	C(10)–O(2)	1.376(1), 1.382(1)	Folding angle	4.24(3), 16.16(5)

Two ligands coordinate to the magnesium cation. Hence, two values are given for each parameter.

On the other hand, the stronger dislocation of 0.124(2) Å produces slightly more acute N(1')–Mg(1')–N(2') and C(2')–C(1')–C(10') angles of 93.3(4) and 122.7(1)°, respectively. The folding of this ligand molecule exhibits with 16.16(5)° an about four times more pronounced butterfly-like arrangement than the other. Additionally, the folding is accompanied by a torsion of the two heteroaromatic side arms of 9.5(2)°. Both features can be ascribed to a reduction of steric strain around the cation. Again, the C(1)– C_{ipso} as well as the N– C_{ipso} distances range between the values of characteristic single- and double bonds, indicating an effective charge delocalization throughout the ligand framework. Comparing **3** to the related homoleptic compound $[\text{Mg}(\text{DippNacNac})_2]$,^[190] similar structural features like an averaged Mg–N distance of 2.111 Å and an averaged N–Mg–N bite angle of 93.0° are found for the NacNac-based structure. Interestingly, in the hexa-coordinated magnesium complex $[\text{Mg}\{(\text{pz}^*)_3\text{C}\}_2]$ ($\text{pz}^* = 3,5\text{-dimethylpyrazolyl}$), the mean Mg–N bond path of 2.197 Å is only slightly longer.^[192]

2.2.3.2 $[\text{Ca}(\text{THF})_2\{(\text{4-Me-NCOC}_6\text{H}_3)_2\text{CH}\}_2] \cdot \text{THF}$ (**4**)

Simultaneously to the intended generation of **1**-based magnesium halide complexes, the preparation of similar heteroleptic halide- or amide complexes of the heavier alkaline-earth-metal calcium was attempted. A ligand **1** supported calcium amide compound should be accessible in a concerted deprotonation-metalation reaction utilizing a suitable organometallic calcium reagent. For the generation of a corresponding calcium halide complex, a salt metathesis reaction between the potassium precursor complex **2** and a calcium halide was intended. In the first case, **1** was added to a suspension of the calcium-HMDS precursor complex $[\text{Ca}(\text{THF})_2\{\text{N}(\text{SiMe}_3)_2\}_2]$ (Scheme 2-4, top route), while for the latter a suspension of anhydrous calcium iodide beads and compound **2** was prepared (Scheme 2-4, bottom route).



Scheme 2-4. Two investigated synthesis routes which afforded the calcium complex $[\text{Ca}(\text{THF})_2\{(\text{4-Me-NCOC}_6\text{H}_3)_2\text{CH}\}_2] \cdot \text{THF}$ (**4**). Reprinted with permission from reference^[1]. Copyright 2017, John Wiley and Sons.

Recrystallizations by slow evaporation of pentane into saturated solutions of the crude products in THF were carried out at -30°C . The top procedure afforded crystals of calcium complex **4** in a yield of 66%, the bottom procedure in a yield of 84%. Also the ^1H NMR spectrum of **4** in $[\text{D}_8]\text{THF}$ exhibits only one set of signals for the two coordinating ligands. Again, this unequivocally indicates the heteroaromatic side arms as well as ligand molecules in the complex to be chemically and magnetically equivalent. The signals at 6.97, 6.73 and 6.55 ppm belong to the protons residing at the benzene perimeters, while the remaining hydrogen atom attached to each singly deprotonated methylene bridge shows a signal at 5.07 ppm. A resonance at 1.91 ppm with an integral of twelve can be assigned to the four methyl substituents. The signals observed at 3.62 and 1.77 ppm each showing an integral of eight correspond to the two additionally coordinating THF donor molecules.

Upon recrystallization, colorless prism-shaped crystals of **4** were obtained. The six-fold coordinated compound **4** crystallizes in the orthorhombic space group $Pbca$ and contains one molecule in the asymmetric unit (Figure 2-6).

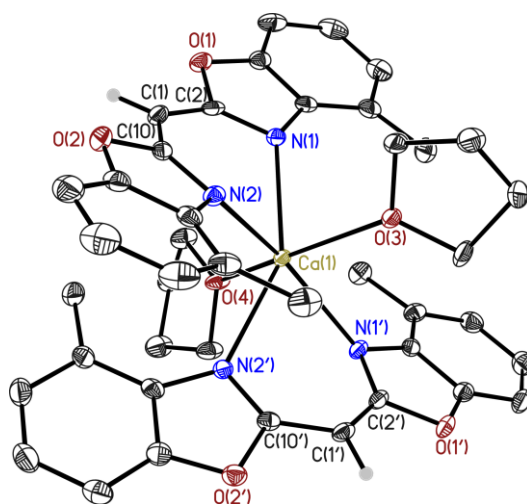


Figure 2-6. Solid-state structure of $[\text{Ca}(\text{THF})_2\{(4\text{-Me-NCOC}_6\text{H}_3)_2\text{CH}\}_2] \cdot \text{THF}$ (**4**). Anisotropic displacement parameters are depicted at the 50% probability level. A lattice THF molecule as well as the hydrogen atoms are omitted for clarity, except for those at the bridging methylene positions. Reprinted with permission from reference^[1]. Copyright 2017, John Wiley and Sons.

The central calcium cation shows a distorted octahedral coordination made up from the four nitrogen donor atoms of two methanide ligands and two additionally attached THF donor molecules. The two methanides show an almost perfect parallel arrangement with a twisting angle of only 7.25(9)°. Steric crowding causes the dication to adopt a similar dislocation of averaged 1.34 Å from both chelating C_3N_2 planes (Table 2-3).

Table 2-3. Selected bond lengths [Å] and angles [°] of **4**.

Ca(1)–N(1)	2.482(2), 2.470(2)	N(1)–C(2)	1.336(3), 1.338(3)	Ca(1)– C_3N_2 dist.	1.330(3), 1.348(3)
Ca(1)–N(2)	2.461(2), 2.475(2)	N(2)–C(10)	1.330(3), 1.327(3)	N(1)–Ca(1)–N(2)	78.8(6), 78.4(6)
C(1)–C(2)	1.386(3), 1.378(3)	C(2)–O(1)	1.391(2), 1.389(2)	C(2)–C(1)–C(10)	125.0(2), 124.8(2)
C(1)–C(10)	1.392(3), 1.397(3)	C(10)–O(2)	1.391(3), 1.389(3)	Folding angle	18.41(5), 20.42(5)

Two ligands coordinate to the calcium cation. Hence, two values are given for each parameter.

This is accompanied by almost identical N(1)–Ca(1)–N(2) bite angles (av. 78.6°) as well as C(2)–C(1)–C(10) angles (av. 124.9°) of the ligand backbone. The folding angle between the heteroaromatic side arms of the methanides ranges from 18.41(5) to 20.42(5)°, indicating a rather strong deviation from a planar arrangement than expected for an aromatic system. Each methanide is folded to the opposite direction of the second chelate ligand. Thus, this feature can be assigned to the avoidance of steric congestion around the calcium cation. The Ca(1)–N distances in **4** cover the range of 2.461(2) to 2.482(2) Å. In comparison to that, in the related homoleptic β -diketiminate compound $[\text{Ca}(\text{DippNacNac})_2]$ a considerably shorter averaged Ca(1)–N bond length of 2.379 Å is found.^[190] Associated with that, the NacNac-based structure features a smaller averaged dislocation of the calcium ion of 1.291 Å from its C_3N_2 planes as well as a widened mean N–Ca–N bite angle of 83.09°.

2.2.4 Comparison of Complexes 2-4 and Conclusions

With potassium compound **2** a promising precursor complex for subsequent transmetallation reactions was prepared. Moreover, two new homoleptic alkaline-earth-metal complexes **3** and **4** were obtained. Some general structural trends for **2-4** can be deduced from Table 2-4.

Table 2-4. Selected averaged bond lengths [\AA] and angles [$^\circ$] of **2-4**.

	M–N	N(1)–M–N(2)	C(2)–C(1)–C(10)	M–C ₃ N ₂ distance	Folding angle
3	2.057	94.1	122.6	0.07	4.24(3), 16.16(5)
4	2.472	78.6	124.9	1.34	18.41(5), 20.42(5)
2	2.844	67.7	125.0	1.34	4.56(3), 9.53(3)

An order of the complexes of **3**, **4**, **2** was chosen to emphasize on the trends caused by an increasing cation size from Mg²⁺ to K⁺. The folding angles are not averaged.

Just like for a set of related NacNac-based structures [M^{(Dipp)NacNac}]₂ (M = Mg, Ca, Ba),^[190] these features are predominantly caused by the increasing effective ionic radii of the cations from Mg²⁺ (72 pm) over Ca²⁺ (100 pm) to K⁺ (137 pm):

- i) The M–N distances increase with increasing cation size: Mg²⁺ < Ca²⁺ < K⁺
- ii) The N(1)–M–N(2) bite angles decrease with increasing cation size: Mg²⁺ > Ca²⁺ > K⁺
- iii) The C(2)–C(1)–C(10) angle increases with increasing cation size: Mg²⁺ < Ca²⁺ < K⁺

Due to changes in coordination modes, the M–C₃N₂ distances as well as the butterfly folding angles of the ligand molecules do not follow such trends. Nonetheless, in contrast to complexes **2** and **4**, the magnesium cation in **3** shares both C₃N₂ planes with a marginal average deviation of 0.07 \AA , thus fitting best into the offered coordination pocket of the methanide ligand. In consideration of the smaller folding angle of 4.24(3) $^\circ$ displayed by **3**, these values match well to those found in related group 13 (Al³⁺, Ga³⁺, In³⁺) complexes of the bis(4-Me-benzoxazol-2-yl)methanide system. Here, M–C₃N₂ distances and folding angles in a range of 0.005(2) to 0.154(3) \AA and 3.04(2) $^\circ$ to 6.23(3) $^\circ$, respectively were reported.^[167]

In conclusion, the intended syntheses of heteroleptic group 2 halide- or amide complexes for subsequent reduction attempts based on ligand system **1** failed. Instead, the homoleptic complexes **3** and **4** were obtained, which presumably formed upon *Schlenk* equilibrium ligand scrambling. Due to the limited steric shielding offered by the methyl substituents adjacent to the coordination pocket in **1**, such a ligand redistribution is assumed to be favored. Thus, to stabilize the intended heteroleptic group 2 compounds, the implementation of bis(benzoxazol-2-yl)methanides that carry more bulky substituents at the 4-position close to the coordination pocket seems to be mandatory.

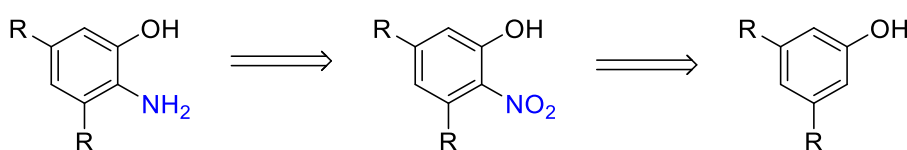
2.3 Syntheses of the Bis(4,6-*t*Bu-benzoxazol-2-yl)methane (7) Ligand and its *s*-Block Complexes

Major parts of this chapter have been published in:

- [2] I. Koehne, S. Bachmann, T. Niklas, R. Herbst-Irmer, D. Stalke, "A Novel Bulky Heteroaromatic-Substituted Methanide Mimicking NacNac: Bis(4,6-*tert*-butylbenzoxazol-2-yl)methanide in *s*-Block Metal Coordination", *Chem. Eur. J.* **2017**, 23, 13141-13149.^[2]
- [3] I. Koehne, S. Bachmann, R. Herbst-Irmer, D. Stalke, "A Water-Containing Organopotassium Compound Based on Bis(4,6-*t*Bu-benzoxazol-2-yl)methanide and Its Unexpected Stability to Hydrolysis", *Angew. Chem.* **2017**, 129, 15337-15342; *Angew. Chem. Int. Ed.* **2017**, 56, 15141-15145.^[3]

2.3.1 Ligand Synthesis

Building up on the knowledge obtained from the syntheses on ligand system **1** (see Subchapter 2.2.4), the search for a ligand scaffold was started that stronger mimics the steric shielding offered by the *N*-aryl substituents in the paragon NacNac system. To obtain a bis(benzoxazol-2-yl)methane derivative that provides sufficient steric demand adjacent to the five-membered coordination ring, a synthetic route to a corresponding bulky substituted 2-aminophenol derivative had to be established first. From a retrosynthetic point of view, it seemed to be most convenient to start from a symmetrically substituted phenol derivative. Then, an amino function at the 2-position of this compound should be successively introduced (Scheme 2-5).

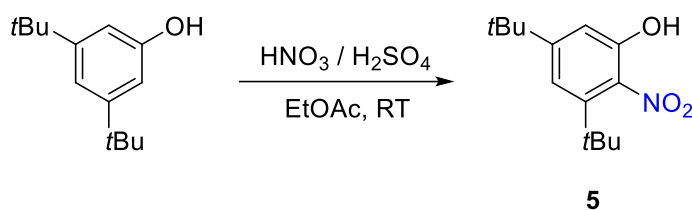


Scheme 2-5. Retrosynthetic approach to access bulky substituted 2-aminophenol compounds.

In the first step of this two-step procedure, a nitration reaction is carried out to generate a 2-nitrophenol derivative. From a subsequent hydrogenation reaction, the intended steric demanding 2-aminophenol compound is obtained. With such a molecule in hand, the desired ligand species would be easily accessible through a double cyclocondensation reaction with a suitable C₃-linker unit as already applied in the synthesis of **1**.^[167, 186]

2.3.1.1 3,5-di-*tert*-butyl-2-nitrophenol (5) & 3,5-di-*tert*-butyl-2-aminophenol (6)

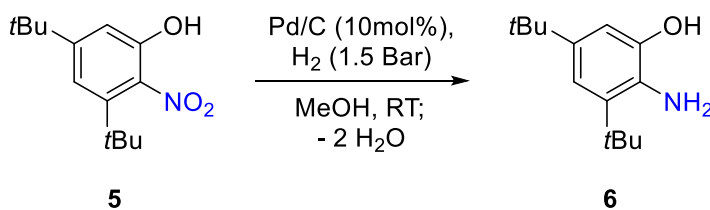
With this in mind, it was decided to start with the synthesis of a ligand system that carries *tert*-butyl substituents close to the coordination pocket. To cope with the unselective nature of the common nitration reaction at aromatic compounds with nitrating acid, synthesis commenced from the symmetrically substituted 3,5-di-*tert*-butylphenol. Advantageously, this compound features two equivalent *ortho* positions as well as a sterically hindered *para* position. As a result, upon slow addition of one equivalent of nitrating acid to the starting material in ethyl acetate, a yellow solution formed. Workup and removal of the solvent gave a reddish-orange solid, which was subsequently recrystallized from pentane. The corresponding mono *ortho*-nitrated derivative 3,5-di-*tert*-butyl-2-nitrophenol (5) was obtained as a yellow crystalline solid in an appreciable yield of 45% (Scheme 2-6).^[193]



Scheme 2-6. Synthesis of 3,5-di-*tert*-butyl-2-nitrophenol (5). Adapted with permission from reference ^[2]. Copyright 2017, John Wiley and Sons.

In the ¹H NMR spectrum of 5 in [D₆]acetone, a singlet at 9.12 ppm with an integral of one can be assigned to the present OH group. For the remaining two aromatic protons, doublets at 7.12 and 7.01 ppm can be reported. Singlets at 1.37 and 1.30 ppm are caused by the *tert*-butyl substituents at the 4- and 6-positions of 5. The observed characteristic signal pattern indicates the presence of an unsymmetrically substituted product, thus confirming the successful synthesis of the desired mono *ortho*-nitrated compound 5. Additionally, in the IR spectrum characteristic vibrational bands for the symmetric (1366 cm⁻¹) and asymmetric (1518 cm⁻¹) NO₂ stretching vibrations are found.

In the next step, a reduction of the NO₂ moiety in 5 with H₂ gas and a hydrogenation catalyst was carried out (Scheme 2-7).



Scheme 2-7. Synthesis of 3,5-di-*tert*-butyl-2-aminophenol (6). Adapted with permission from reference ^[2]. Copyright 2017, John Wiley and Sons.

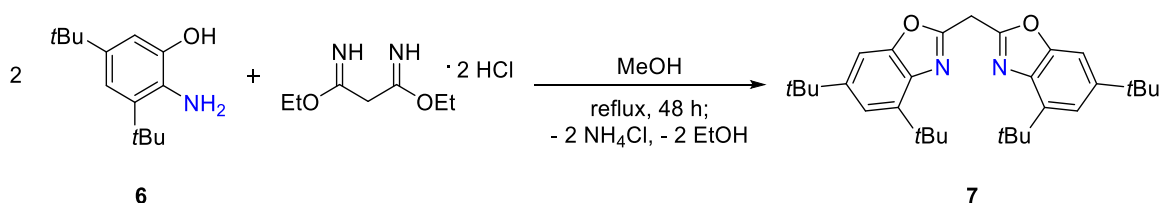
For this purpose, a suspension of **5** and palladium on charcoal (Pd/C) in MeOH was prepared in a pressure flask. Then, 1.5 bar of H₂ gas were applied to the mixture. When the reaction was completed, separation from the heterogeneous hydrogenation catalyst had to be performed under inert conditions to avoid the formation of a purple side product. A recrystallization of the crude product from chloroform gave 3,5-di-*tert*-butyl-2-aminophenol (**6**) as a white, fluffy solid in an excellent yield of 90%.

In comparison to the ¹H NMR spectrum of **5**, the resonances found for compound **6** in [D₆]acetone experience a shift to higher field. This is due to a switch from a -M-effect causing NO₂ substituent in **5**, to a +M-effect induced by the established NH₂ group in **6**. The resonances for the aromatic protons as well as for the two *t*Bu substituents are found in a typical range. A singlet at 7.86 ppm can be assigned to the OH group, while the NH₂ moiety exhibits a broad singlet at 4.02 ppm. Moreover, the IR spectrum of **6** exhibits characteristic vibrational bands for the symmetric (3316 cm⁻¹) and asymmetric (3415 cm⁻¹) NH₂ stretching vibrations.

2.3.1.2 Bis(4,6-*t*Bu-benzoxazol-2-yl)methane (**7**)

Finally, with the successful synthesis of the *tert*-butyl substituted 2-aminophenol derivative **6**, a preparation analog to the synthesis of **1** was carried out. Hence, two equivalents of **6** and one equivalent of ethyl-bisimidate dihydrochloride were dissolved in MeOH and heated for 48 hours (

Scheme 2-8).



Scheme 2-8. Synthesis of bis(4,6-*t*Bu-benzoxazol-2-yl)methane (**7**). Adapted with permission from reference ^[2]. Copyright 2017, John Wiley and Sons.

After removal of the solvent, the residue was extracted with pentane by sonication. The solid obtained from the extract was recrystallized from EtOH to give colorless crystals of bis(4,6-*t*Bu-benzoxazol-2-yl)methane^a (**7**) in a sufficient yield between 18 to 21%.

As expected, the ¹H NMR spectrum of **7** in [D₈]THF shows resonances with integrals in a ratio of 2:2:2:18:18. Doublets at 7.42 and 7.30 ppm can be assigned to the four aromatic protons at the 5-

^a In the following also abbreviated as: (4,6-*t*Bu-NCOC₆H₂)₂CH₂.

and 7-positions of the benzene perimeter. Those at the 7-positions are shifted the most to lower field. The protons at the bridging methylene moiety cause a singlet at 4.66 ppm, while the four *t*Bu groups at the 4- and 6-positions exhibit resonances at 1.54 and 1.35 ppm, respectively. Apparently, the protons of the *t*Bu substituents at the 4-positions experience a stronger electronic deshielding, resulting in a signal shifted 0.19 ppm more to lower field.

Compound **7** crystallizes in the monoclinic space group $P2_1/n$ and contains one molecule in the asymmetric unit (Figure 2-7 and Table 2-5).

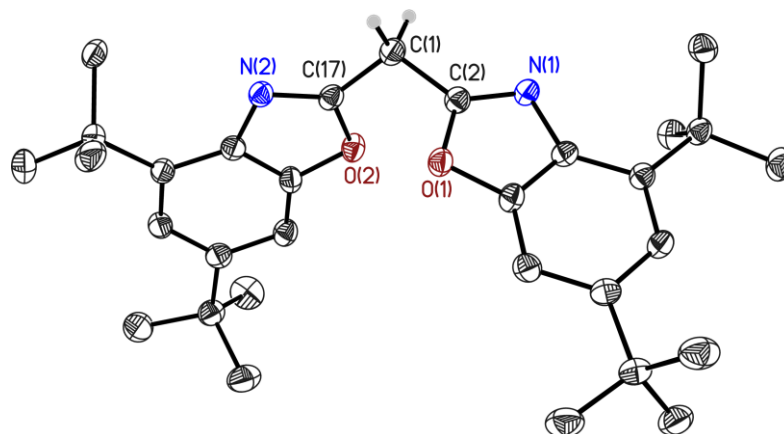


Figure 2-7. Solid-state structure of (4,6-*t*Bu-NCOC₆H₂)₂CH₂ (**7**). Anisotropic displacement parameters are depicted at the 50% probability level. Hydrogen atoms are omitted for clarity, except for those at the bridging methylene position. Reprinted with permission from reference. [2] Copyright 2017, John Wiley and Sons.

Table 2-5. Selected bond lengths [Å] and angles [°] of **7**.

C(1)–C(2)	1.495(2), 1.496(1)	N(2)–C(17)	1.288(2), 1.286(2)	C(2)–C(1)–C(17)	111.2(1), 114.5(1)
C(1)–C(17)	1.494(2), 1.511(1)	O(1)–C(2)	1.371(2), 1.369(2)	O(1)–C(2)–C(1)	115.5(1), 112.8(1)
N(1)–C(2)	1.290(2), 1.295(2)	O(2)–C(17)	1.369(2), 1.367(2)	O(2)–C(17)–C(1)	114.8(1), 111.8(1)

The whole molecule shows a positional disorder about two positions (see Figure 5-4). Hence, two values are given for each parameter.

In comparison to the related bis(benzoxazol-2-yl)methane derivatives (NCOC₆H₄)₂CH₂^[166] and (4-Me-NCOC₆H₃)₂CH₂ (**1**),^[167] some general trends can be derived. On the one hand, in all three compounds the corresponding averaged $C_{bridge}-C_{ipso}$ and $N-C_{ipso}$ distances are within the same range, showing no significant deviation upon increasing steric demand of the introduced substituents (Table 2-6).

Table 2-6. Selected angles and averaged bond lengths of (NCOC₆H₄)₂CH₂, **1** and **7**.

	$C_{bridge}-C_{ipso}$	$N-C_{ipso}$	$C_{ipso}-C_{bridge}-C_{ipso}$	Torsion angle: $N-C_{ipso}-C_{bridge}-C_{ipso}$
(NCOC ₆ H ₄) ₂ CH ₂	1.489	1.286	120.2(3)	15.4(2), 96.3(6)
(4-Me-NCOC ₆ H ₃) ₂ CH ₂ (1)	1.487	1.291	110.8(1)	15.3(2), 90.3(2)
(4,6- <i>t</i> Bu-NCOC ₆ H ₂) ₂ CH ₂ (7)	1.495	1.289	111.2(1)	130.1(2), 133.2(2)

On the other hand, the $C_{ipso}-C_{bridge}-C_{ipso}$ angle gets significantly narrowed from $120.2(3)^\circ$ in the non-substituted ligand to $110.8(1)^\circ$ in **1** upon introduction of a methyl group at the 4-positions. This strong deviation might also be caused by the formation of a 3D network of C–H...N hydrogen bonds in the solid-state of **1**. Regarding compound **7**, the parent $C_{ipso}-C_{bridge}-C_{ipso}$ angle is slightly increased to $111.2(1)^\circ$ if *tert*-butyl substituents are introduced at the 4- as well as the 6-positions. Due to a distorted tetrahedral coordination around the bridging carbon atom in the three considered molecules, the benzoxazol side arms display a twisted orientation (see Figure 2-7 and Figure 2-8).

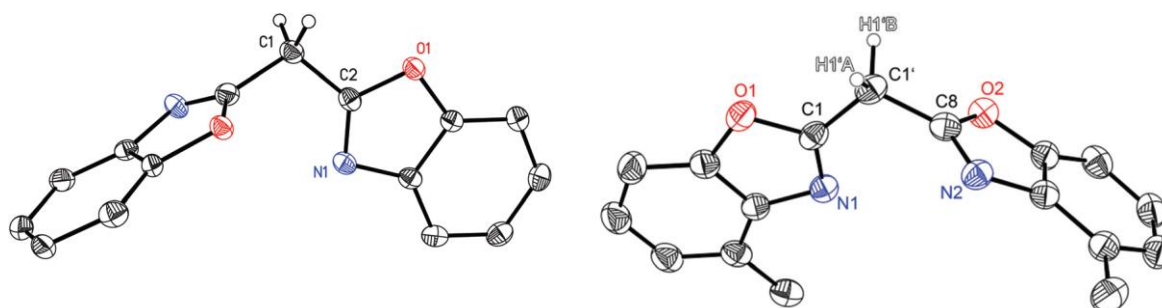


Figure 2-8. Solid-state structures of the to **7** related ligand scaffolds. Left: Non-substituted derivative. Right: ligand system **1**. The left structure was reprinted with permission from reference ^[166]. The right structure from reference ^[167]. Copyright 2014, 2016, The Royal Society of Chemistry.

As can be deduced from Table 2-6, in the non-substituted derivative as well as in ligand **1**, one of the heterocycles stays almost in plane with the C_3 -linker unit showing a torsion of only $15.4(2)$ and $15.3(2)^\circ$, respectively. The other shows a nearly perpendicular torsion with respect to this moiety ($96.3(6)^\circ$ in the non-substituted derivative and $90.3(2)^\circ$ in **1**). In contrast, **7** shows a notably stronger twisted orientation due to its greater steric demand. Here both $N-C_{ipso}-C_{bridge}-C_{ipso}$ angles show with an average of 131.6° a similar torsion out of the plane set up by the C_3 -linker unit. Noteworthy, while the coordination pocket in the solid-state of the non-substituted ligand and **1** is made up by the $C_{ipso}-C_{bridge}-C_{ipso}$ bridging moiety and the ring nitrogen atoms, the opposite is true for **7**. Here, the oxygen atoms are twisted inwards now occupying the position of the donor atoms. Only in this arrangement, minimal steric repulsion of neighboring *t*Bu groups is ensured and a 2D C–H...N hydrogen bond network is established (Figure 2-9, *vide infra*). Each methylene bridge hydrogen atom is coordinated by an imine nitrogen atom of a neighboring ligand, resulting in four moderate hydrogen bonds per ligand molecule to be formed. In moderate hydrogen bonds, the interactions are mostly of electrostatic nature.^[194] Two of these hydrogen bonds are more pronounced (H(1A)...N(2): 2.579 \AA), while the other two are energetically slightly less favored and thus elongated (H(1B)...N(1): 2.639 \AA).

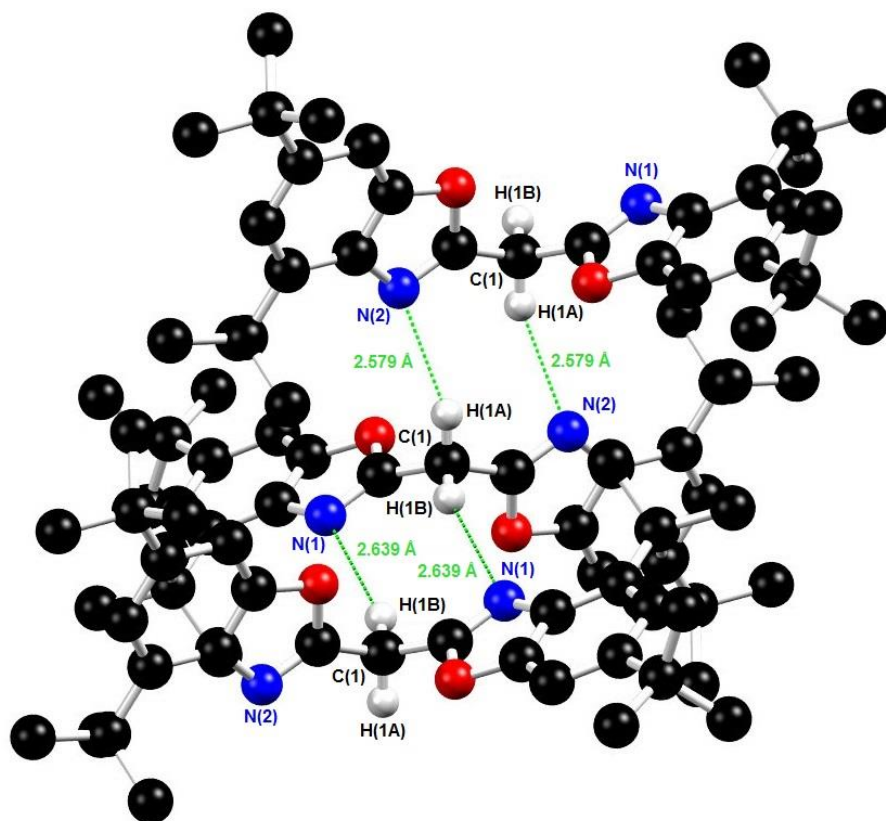
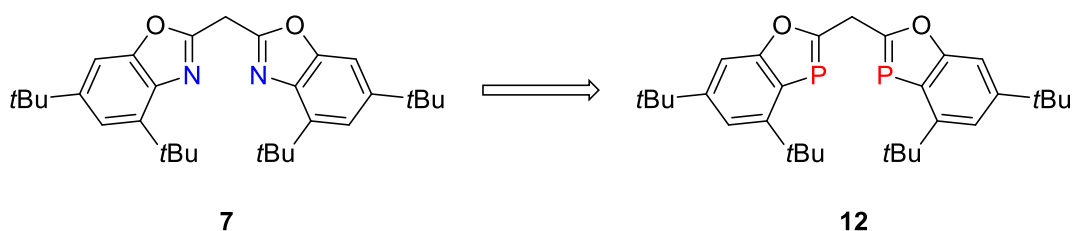


Figure 2-9. Isotropic solid-state structure of 7 with illustrated 2D hydrogen bond network.

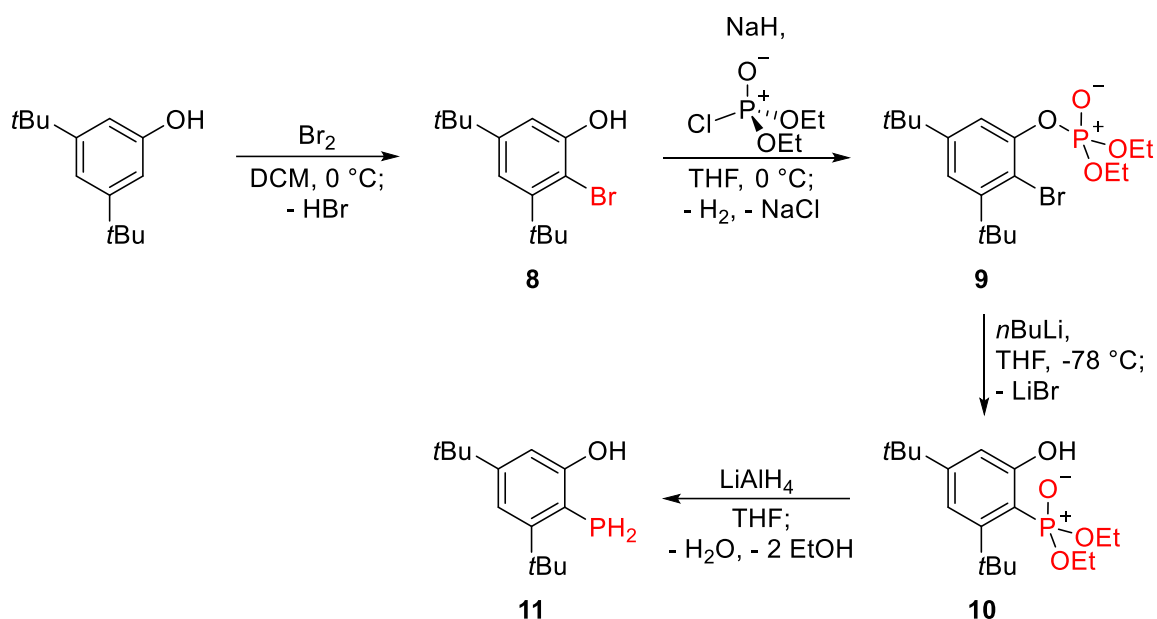
2.3.1.3 Excursus: Attempts for Bis(4,6-*t*Bu-benzoxaphosphol-2-yl)methane (12)

In this chapter, attempts to get access to the heavier phosphorous containing derivative of 7 are described. In such a species, phosphorous atoms formally replace the imine nitrogen atoms of the five-membered coordination pocket forming benzoxaphosphol side arms attached to the bridging methylene moiety (Scheme 2-9).



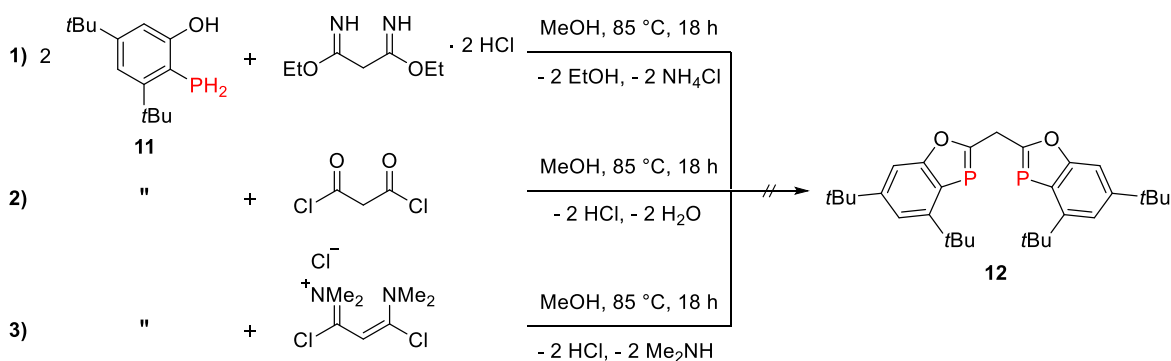
Scheme 2-9. Intended switch to the heavier phosphorous homologue bis(4,6-*t*Bu-benzoxaphosphol-2-yl)-methane (12).

Similar to the synthesis of ligand system 7, the respective 2-phosphinophenol derivative had to be prepared prior to subsequent cyclocondensation reactions. The desired 3,5-di-*tert*-butyl-2-phosphinophenol (11) is obtained in a four-step procedure in an overall yield of 39% (Scheme 2-10).

Scheme 2-10. Synthesis route for the preparation of 3,5-di-*tert*-butyl-2-phosphenol (**11**).^[195]

Starting from 3,5-di-*tert*-butylphenol, the corresponding 2-bromophenol **8** was quantitatively accessed by a reaction with bromine at 0°C .^[196] With **8** in hand, the 2-phosphenol **11** was prepared according to a procedure by *Wu* and co-workers.^[195] A deprotonation of the hydroxyl function with sodium hydride at 0°C followed by the addition of diethylchlorophosphate gave phosphate compound **9**. In an anionic *phospha-Fries* rearrangement,^[197, 198] the respective phosphonate **10** was obtained by addition of $n\text{BuLi}$ and subsequent workup with aqueous ammonium chloride. Finally, the desired 2-phosphenol **11**, with a phosphorous atom in the formal oxidation state of +III, is prepared by addition of LiAlH_4 under strict exclusion of air after aqueous work up.

Next, three different activated 1,3-dielectrophiles, based on malonic acid, were evaluated towards their ability to function as potential C_3 -linker compounds in the preparation of **12** (Scheme 2-11).

Scheme 2-11. Attempted cyclocondensation reactions for the synthesis of **12**.

In procedure **1**), due to an already successful application in the syntheses of **1** and **7**, ethyl-bisimidate dihydrochloride was used. In procedure **2**), malonyl dichloride was tested, while in procedure **3**) a highly 1,3-activated chloro-bis(dimethyl)imidate chloride linker was utilized. For a better comparability, the reaction conditions were not altered. The ^1H NMR spectra of the reaction crudes are depicted in combination with a *Lewis* structure of the utilized linker unit in Figure 2-10.

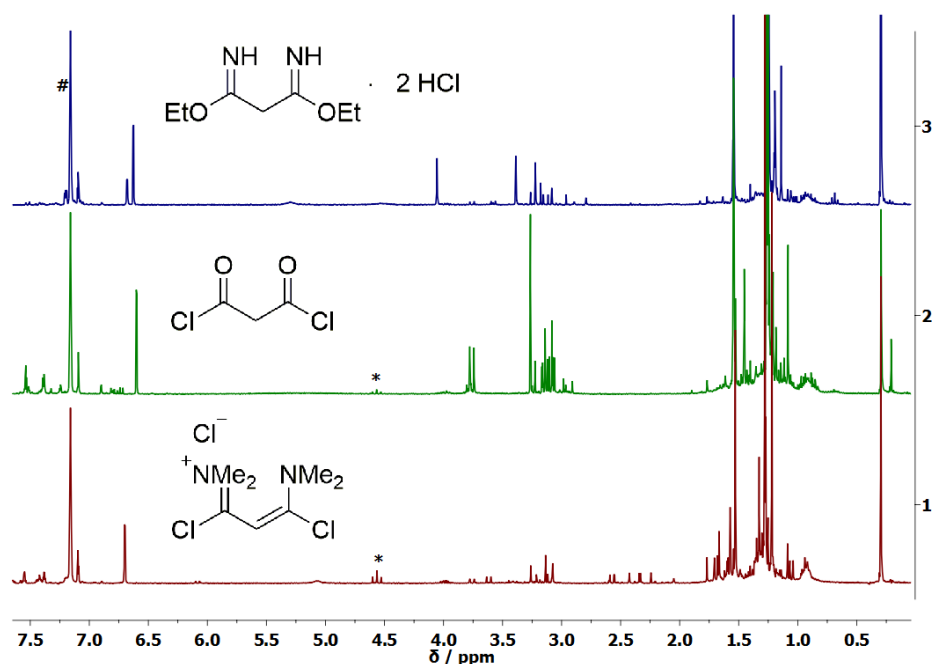


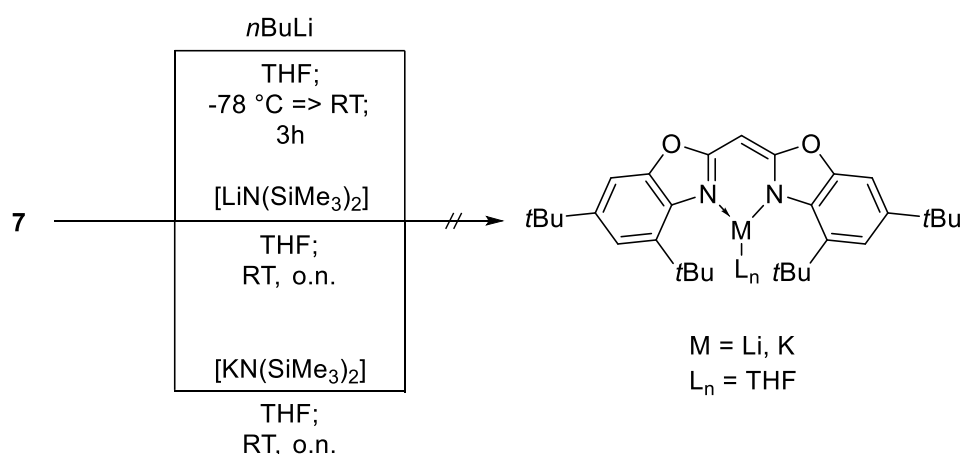
Figure 2-10. A stack of ^1H NMR spectra of the reaction crudes of the synthesis described in Scheme 2-11. The spectra apply to the usage of the corresponding linker units as follows: **1**: chloro-bis(dimethyl)imidate chloride; **2**: malonyl dichloride; **3**: ethyl-bisimidate dihydrochloride. The residual proton signal of C_6D_6 is marked with #. Signals indicative for a formation of **12** are marked with *.

The observation of a resonance with triplet structure is expected for the methylene bridge signal in the ^1H NMR spectrum of compound **12**. This is due to an expected coupling of the attached protons with the two chemically equivalent phosphorous atoms in this species. The related ligand scaffold **7** shows a methylene bridge resonance at 4.20 ppm in C_6D_6 , thus in **12** this signal is expected to appear in a similar range. As can be deduced from Figure 2-10, the reaction crude of a reaction of **11** with ethyl-bisimidate dihydrochloride as linker mainly shows signals of the starting materials and some unknown side products. However, a characteristic methylene bridge resonance indicating a formation of **12** is not observed. In contrast to that, in the spectrum of the reaction crude from a conversion of **11** with malonyl dichloride the observation of such a characteristic triplet at 4.57 ppm can be reported. With a coupling constant of 10.8 Hz this signal displays a typical $^3J_{\text{HP}}$ coupling.^[199] This signal becomes even stronger if the chloro-bis(dimethyl)imidate chloride spacer unit was used. For related benzoxaphospholes, $^{31}\text{P}\{^1\text{H}\}$ signals between 77.2 to 92.2 ppm are reported.^[195] Among other signals, the $^{31}\text{P}\{^1\text{H}\}$ spectra of the latter two reactions exhibit a resonance at 93.3 ppm, which is additionally affiliated to a successful formation of **12**.

Unfortunately, it was not possible to crystallize any product from the reaction crudes, yet. Attempts to obtain pure **12** *via* column chromatography led to the isolation of decomposition products. Hence, due to an aggravated workup and a relatively low spectroscopic yield, the intended synthesis of **12** was discarded.

2.3.2 Group 1 Complexes

With a successful synthesis of bis(4,6-*t*Bu-benzoxazol-2-yl)methane (**7**), preparation of group 1 precursor complexes for subsequent salt metathesis reactions with group 2 halides was started. At the beginning, finding a suitable metalation agent turned out to be rather difficult. Because of its steric demanding *tert*-butyl substituents, a deprotonation of **7** seemed to be kinetically hindered (Scheme 2-12).



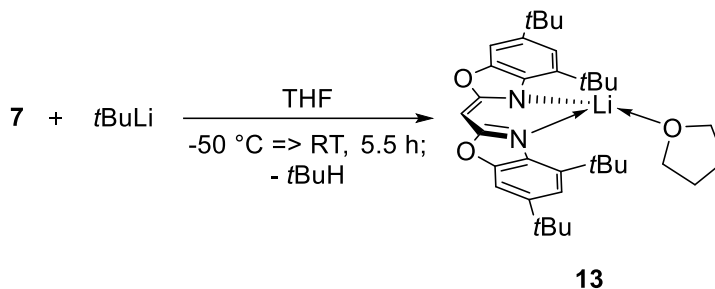
Scheme 2-12. Syntheses attempts on the way to group 1 complexes of **7**.

Neither a reaction with *n*BuLi, nor the use of lithium or potassium hexamethyldisilazane compounds afforded a group 1 complex of **7** at room temperature. NMR spectroscopic investigations of the reaction crude solely reveal the presence of signals that correspond to the starting materials in all three cases. To force a conversion, the reactions were repeated with heating and an extended reaction time. Again, NMR spectroscopic evaluation of the reaction crudes only indicates the presence of unreacted starting materials and no evidence of product formation. Hence, the application of these reagents to compound **7** in concerted deprotonation-metalation reactions was discarded.

2.3.2.1 [Li(THF){(4,6-*t*Bu-NCOC₆H₂)₂CH}] (**13**)

Treatment of **7** with *t*BuLi at -50 °C led to the formation of a yellow solution. After removal of the solvent, the residue was washed with ice-cold pentane. The three-fold coordinated lithium complex

[Li(THF){(4,6-*t*Bu-NCOC₆H₂)₂CH}] (**13**) was obtained as a pale-yellow solid in a yield of 74% (Scheme 2-13).



Scheme 2-13. Synthesis of [Li(THF){(4,6-*t*Bu-NCOC₆H₂)₂CH}] (**13**). Adapted with permission from reference ^[2]. Copyright 2017, John Wiley and Sons.

The ¹H NMR spectrum of **13** in C₆D₆ displays signals of the deprotonated ligand and a coordinating THF molecule. As expected, the ligand related resonances exhibit integrals in a ratio of 2:2:1:18:18, while the THF signals show an integral ratio of 4:4. In particular, doublets at 7.34 and 7.30 ppm with ⁴J_{HH} couplings of 1.8 Hz can be assigned to the aromatic protons H7 and H5 residing at the benzene perimeters. The bridging CH moiety exhibits a singlet resonance at 5.60 ppm and is shifted about 1.40 ppm to lower field in comparison to the free protonated ligand. For the *t*Bu substituents at the 4- and 6-positions, singlets at 1.58 as well as 1.34 ppm can be reported. A singlet at 2.76 ppm is found in the ⁷Li NMR spectrum of **13**. For the related lithium methanides [Li(THF)₂{(1-Me-NCNC₆H₄)₂CH}] and [Li(diox)₂{NCSC₆H₄}CH(1-Me-NCNC₆H₄)] stronger high-field shifted signals at 2.54 and 2.37 ppm, respectively are observed.^[168] With singlets at 1.61 ppm and 1.67 ppm, the corresponding NacNac-based structures [Li(L){^{Dipp}NacNac}] (L = Et₂O, THF) show ⁷Li resonances that are shifted even stronger to higher field.^[25]

Furthermore, in a collaboration with *Bachmann*, the structure of **13** in solution was evaluated by ¹H-DOSY-ECC-MW estimation.^a It was shown in previous studies that for most organometallic compounds the dissipated spheres and ellipsoids (DSE) calibration curve is the most suitable for an accurate estimation.^[200] Hence, only resulting values from the DSE and, for comparison, from the merge calibration curve are considered.^b The molecular weight of **13** in solution was estimated to be 575 g/mol (DSE) and 643 g/mol (merge). Within the error range, either these values fit to a three-fold (553 g/mol) or a four-fold (625 g/mol) coordinated species with one or two attached THF molecules, respectively. This finding indicates dynamical exchange processes to be present that are in tune with the THF signals exhibiting a diffusion coefficient that slightly differs from the

^a All ¹H-DOSY-ECC-MW estimations discussed in Chapter 2.3 were performed in collaboration with *Bachmann*.

^b This applies to all DOSY experiments discussed in Chapter 2.3.

remaining complex related signals. In comparison to the ^1H NMR spectrum of **13**, which shows one equivalent of THF to be attached to the complex, it is most likely that the three-fold coordination derived from the solid-state (*vide infra*) is also retained in solution. A superimposition of the ^1H - and ^7Li DOSY experiments of **13** reveals the ligand related signals as well as the ^7Li signal to show the same diffusion coefficient, indicating the presence of a strong contact ion pair (Figure 2-11).

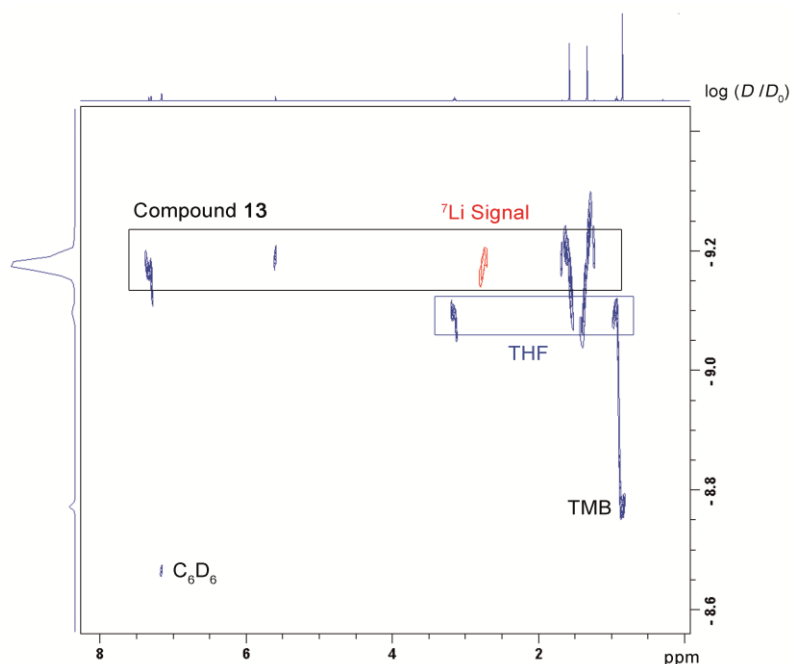


Figure 2-11. Superimposition of the ^1H - and ^7Li DOSY spectra of $[\text{Li}(\text{THF})\{(4,6\text{-}t\text{Bu-NCOC}_6\text{H}_2)_2\text{CH}\}]$ (**13**) in C_6D_6 . Internal reference: 2,2,3,3-Tetramethylbutane (TMB). Reprinted with permission from reference [2]. Copyright 2017, John Wiley and Sons.

Colorless crystals were obtained from a saturated solution of **13** in hexane at room temperature. Complex **13** crystallizes in the monoclinic space group $C2/c$ containing one molecule in the asymmetric unit (Figure 2-12, *vide infra*). The central lithium cation shows a trigonal-pyramidal coordination made up by two ring nitrogen atoms of the monoanionic methanide ligand and an oxygen donor atom of a THF molecule. Obviously, the hard lithium ion prefers to coordinate the nitrogen atoms despite the steric strain imposed by the cross-ligand *t*Bu substituents. Interestingly, the fourth coordination site at the Li^+ center is shielded by the *t*Bu substituents at the 4-positions of the ligand periphery. This prevents the cation from being tetrahedrally coordinated by another potential THF donor-base.

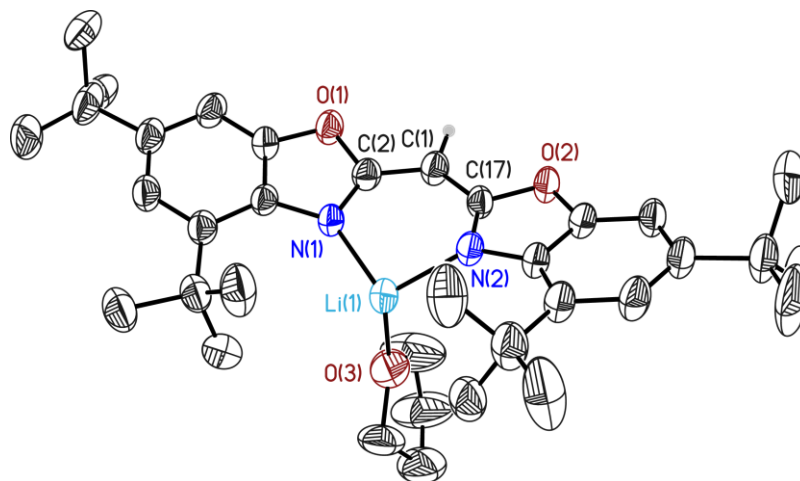


Figure 2-12. Solid-state structure of $[\text{Li}(\text{THF})\{(4,6\text{-}t\text{Bu-NCOc}_6\text{H}_2)_2\text{CH}\}]$ (**13**). Anisotropic displacement parameters are depicted at the 50% probability level. Hydrogen atoms are omitted for clarity, except for the one at the bridging methylene position. Reprinted with permission from reference ^[2]. Copyright 2017, John Wiley and Sons.

The metal ion is lifted 0.629(6) Å from the plane defined by N(1)–O(3)–N(2). Furthermore, the steric repulsion of the *t*Bu substituents forces the lithium cation 0.696(7) Å out of the plane of the chelating C₃N₂ ring (Table 2-7).

Table 2-7. Selected bond lengths [Å] and angles [°] of **13**.

Li(1)–N(1)	1.950(6)	N(1)–C(2)	1.327(4)	Li(1)–C ₃ N ₂ dist.	0.696(7)
Li(1)–N(2)	1.951(6)	N(2)–C(17)	1.324(4)	N(1)–Li(1)–N(2)	99.0(3)
C(1)–C(2)	1.399(4)	C(2)–O(1)	1.381(4)	C(2)–C(1)–C(17)	121.7(3)
C(1)–C(17)	1.393(4)	C(17)–O(2)	1.391(3)	Folding angle	23.1(1)

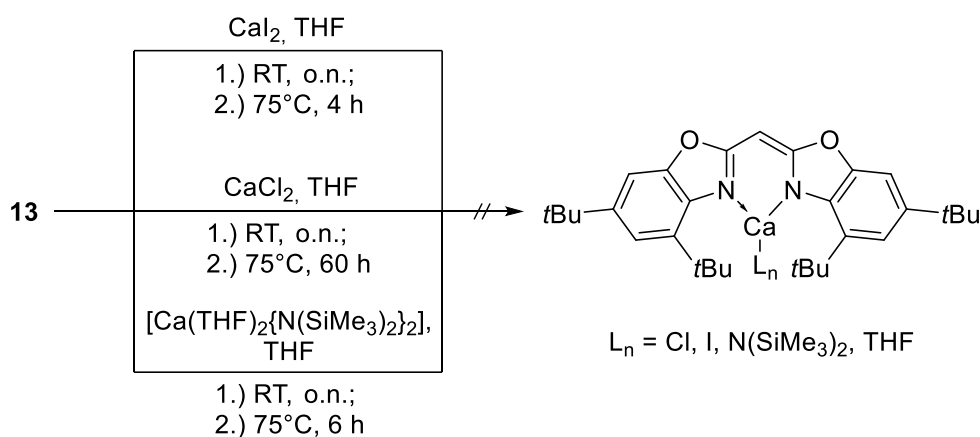
The ligand framework displays with 23.1(1)° a considerable folding and deviation from perfect planarity. Interestingly, the strongly related β -diketiminato structure $[\text{Li}(\text{THF})\{t\text{Bu-NacNac}\}]$ shows a similar trigonal-pyramidal coordination mode (see Figure 1-2, middle).^[50] Here, the fourth coordination site of the lithium ion is blocked as well by the present *t*Bu substituents. The dislocations of the cation from the N–O–N as well as the chelating C₃N₂ plane are with 0.600(1) and 0.622(1) Å, respectively in good agreement to those found in complex **13**. Moreover, the methanide complex **13** displays Li–N bond lengths of 1.950(6) and 1.951(6) Å, while these distances are slightly shortened in the NacNac-based structure (1.918(4) and 1.917(4) Å.) In contrast to 102.25° found in the NacNac-supported lithium compound, **13** shows a slightly more acute N(1)–Li(1)–N(2) angle of 99.0(3)°. The opposite is observed for the C_{ipso}–C(1)–C_{ipso} angles. In comparison to 121.7(3)° in **13**, this angle is strongly widened to 130.9(2)° in the β -diketiminato based structure.

Complex **13** is the first bis(benzoxazol-2-yl)methanide lithium complex displaying a trigonal-pyramidal coordination. In addition, it is reminiscent of the related three-fold coordinated trigonal-planar lithium compounds $[\text{Li}(\text{L})\{\text{Dipp}^{\text{NacNac}}\}]$ (L = Et₂O, THF).^[25] Their reported

averaged Li–N distances (1.915 and 1.958 Å) are in good agreement with the averaged distance of 1.951 Å found in **13**, fitting best the THF solvate. The same is true for the corresponding N–Li–N bite angles. Here, the 99.9(2)° displayed by the Et₂O solvate fit best the value of 99.0(3)° found in **13**. While the values for the C_{ipso}–C1–C_{ipso} angles in the ligand periphery of the reported structures are very similar (129.5(2)° and 128.6(3)°), in **13** this angle experiences a considerable reduction to 121.7(3)°. Even the related four-fold coordinated bis(pyridyl)methanide-based compound [Li(THF)₂{(2-NC₅H₄)₂CH}] and its higher homologue the bis(pyridyl)phosphide-based [Li(THF)₂{(2-NC₅H₄)₂P}] show comparable structural features to **13**.^[116, 122]

Reactivity of Complex **13**

To get access to 7-supported calcium compounds, the lithium precursor complex **13** was reacted with different calcium halides and the calcium-HMDS compound [Ca(THF)₂{N(SiMe₃)₂]₂] (Scheme 2-14).

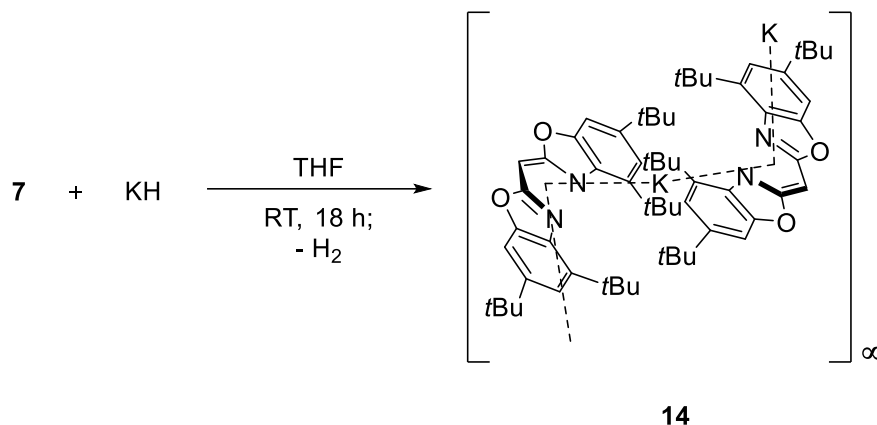


Scheme 2-14. Synthesis attempts on the way to calcium complexes starting from the lithium precursor **13**.

An attempted salt metathesis reaction with anhydrous CaI₂ beads did not afford the intended calcium complex under precipitation of the corresponding lithium halide at room temperature. As affirmed by ¹H NMR spectroscopy, only an isolation of the starting material **13** from the reaction crude can be reported. Thus, the reaction was repeated with heating but with the same negative result. To facilitate the formation of lithium halide, calcium iodide was replaced by CaCl₂. Due to the more favorable ratio of the ionic radii of both ions, the expected precipitation of the lithium halide was assumed to be fostered. Unfortunately, also from this reaction no desired calcium complex was obtained. Even if the reaction was carried out at elevated temperature and an extended reaction time of 60 h. A conversion of **13** with [Ca(THF)₂{N(SiMe₃)₂]₂] only led to the isolation of the starting materials at room- as well as at increased temperature. In this conversion, the reaction was assumed to proceed *via* formation of Li{N(SiMe₃)₂} as driving force.

2.3.2.2 $[K\{\eta^5-(4,6-tBu-NCOC_6H_2)_2CH\}]_\infty$ (**14**)

The addition of **7** to a suspension of potassium hydride (KH) in THF led to a visible evolution of hydrogen gas, indicating a successful deprotonation of the bulky ligand system. From this reaction, the corresponding potassium precursor compound **14** was obtained in an excellent yield of 80% overnight (Scheme 2-15).



Scheme 2-15. Synthesis of $[K\{\eta^5-(4,6-tBu-NCOC_6H_2)_2CH\}]_\infty$ (**14**). Adapted with permission from reference ^[2]. Copyright 2017, John Wiley and Sons.

The 1H NMR spectrum of **14** in $[D_8]THF$ exhibits one set of signals for the deprotonated ligand and no evidence for additionally coordinating THF molecules. The doublets corresponding to the aromatic protons H7 and H5 that reside at the benzene perimeters are found at 7.01 and 6.97 ppm, respectively. The bridging CH moiety resonates at 4.56 ppm. The singlets at 1.54 and 1.32 ppm can be assigned to the *t*Bu substituents at the 4- and 6-positions. Just like for the bis(4-Me-benzoxazol-2-yl)methanide based potassium compound **2**, all signals are shifted to higher field in comparison to the free protonated ligand. In an investigation of its structure in solution by 1H DOSY NMR experiments in C_6D_6 , the molecular weight of **14** was estimated to be 490 g/mol (DSE) and 620 g/mol (merge). This observation indicates the formation of monomeric structures with an additionally attached benzene molecule to satisfy the coordination sphere of the cation. This assumption is consistent with a theoretical molecular weight of 591 g/mol for such a species fitting best the estimated values.

The slow evaporation of pentane into a saturated solution of **14** in THF afforded small needle-shaped crystals. Complex **14** crystalizes in the triclinic space group $P\bar{1}$. The asymmetric unit contains one ligand molecule and two potassium cations lying on an inversion center (see Figure 5-6 in the appendix). Due to the formation of needle-shaped crystals with decreased scattering abilities causing low data resolution, the determined bond lengths and angles within this structure suffer from a certain unreliability. Hence, no detailed discussion concerning these parameters is attempted. Only the unambiguous data for the N(1)–K(1/2)–N(2) bite angles, the

dislocation of the potassium cations from the chelating C_3N_2 plane as well as the folding of the ligand backbone are discussed in the following paragraph (Table 2-8). The central potassium cation is sandwiched by η^5 -coordination to two C_3N_2 planes forming infinite linear strands (Figure 2-13).

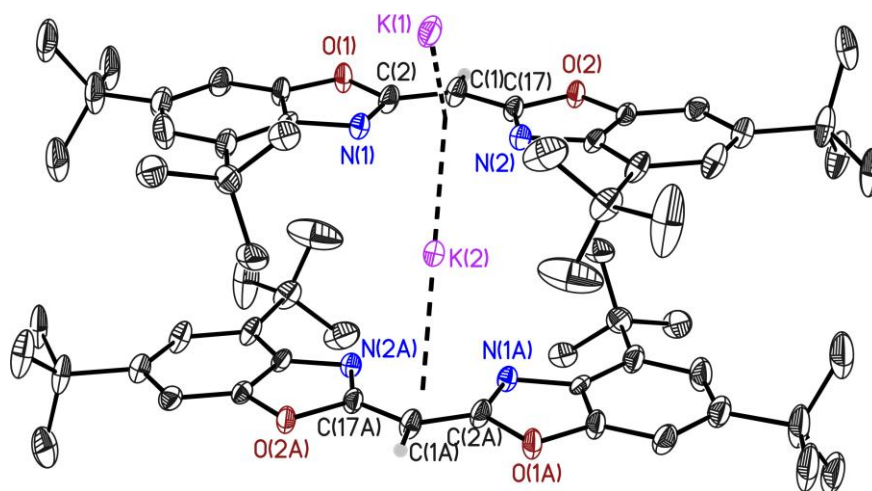


Figure 2-13. Excerpt from the solid-state structure of $[K\{\eta^5\text{-(4,6-}t\text{Bu-NCOC}_6\text{H}_2)_2\text{CH}\}]_\infty$ (**14**) forming infinite linear coordination polymer strands. Anisotropic displacement parameters are depicted at the 50% probability level. Hydrogen atoms are omitted for clarity, except for those at the bridging methylene positions. Reprinted with permission from reference [2]. Copyright 2017, John Wiley and Sons.

Table 2-8. Selected bond lengths [Å] and angles [°] of **14**.

K(1/2)–N(1)	2.850(6), 2.838(6)	N(1)–C(2)	1.325(8)	K(1/2)– C_3N_2 dist.	2.313(7), 2.308(7)
K(1/2)–N(2)	2.889(6), 2.857(6)	N(2)–C(17)	1.318(8)	N(1)–K(1/2)–N(2)	65.7(2), 66.3(2)
C(1)–C(2)	1.386(10)	C(2)–O(1)	1.390(8)	C(2)–C(1)–C(17)	125.5(6)
C(1)–C(17)	1.402(9)	C(17)–O(2)	1.394(8)	Folding angle	1.57(2)

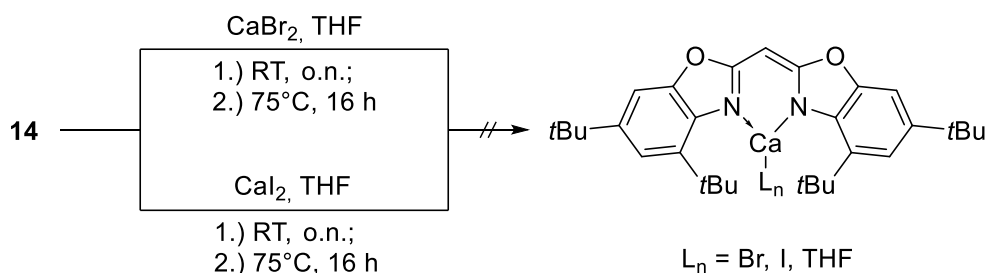
The asymmetric unit contains two K^+ ions with an occupancy of 0.5 (see Figure 5-6). Hence, two values are given for the K^+ related parameters. Symmetry transformations used to generate equivalent atoms: #1: $-x+1, -y+1, -z+1$; #2: $-x, -y+1, -z+1$.

Just like in the lithium congener **13**, the steric demand of the *t*Bu substituents inhibits the coordination of THF donor molecules to the metal ions within the polymer strands. Because of the K^+ ions residing on top and below the ligand molecules, the total ligand framework is only marginally folded by $1.57(2)^\circ$. To realize a favored η^5 -coordination of the soft potassium ion to the soft and undirected π -density of the deprotonated ligand molecules,^[179–181, 201] complex **14** shows an averaged N(1)–K(1/2)–N(2) bite angle of 66.0° . This fits well to a mean bite angle of 67.7° found in the related potassium structure **2**. Moreover, a dislocation of the metal ions from the C_3N_2 plane with on average 2.311 \AA and a mean N(1)–K(1/2)–N(2) bite angle of 66.0° are in good agreement with the values found in a related dimeric NacNac-based potassium complex.^[202] For this structure a C_3N_2 plane distance of averaged 2.29 \AA and a mean bite angle of 65.7° are reported. In contrast, the dislocation found in **14** falls at the short end of the range for other non-NacNac related compounds that display potassium- π -system interactions. For example, the η^6 - and η^5 -bound species $[K(\text{PMDETA})(\text{PhCH}_2)]_\infty$ ^[203] and $[K(\text{Py})_2(\text{C}_5\text{Me}_5)]_\infty$ ^[204] adopt a polymeric structure in the

solid-state as well, but show with 3.150(2) Å and 2.79(1) Å significantly longer K^+ - π -plane distances.

Reactivity of Complex 14

Just like **13**, potassium precursor **14** was evaluated in terms of its ability to undergo salt metathesis reactions with calcium halides (Scheme 2-16).



Scheme 2-16. Synthesis attempts on the way to calcium complexes starting from the potassium precursor **14**.

As can be deduced from Scheme 2-16, again no calcium halide complexes of ligand **7** were obtained from reactions of precursor **14** with calcium bromide or -iodide at room temperature or after heating at 75 °C for 16 h. The ^1H NMR spectra of the reaction crudes solely display signals of the starting material **14** or free protonated **7** which formed upon decomposition. Nonetheless, in an NMR tube containing a solution of the reaction crude from a reaction of **14** with CaBr_2 in $[\text{D}_8]\text{THF}$, crystals suitable for X-ray diffraction experiments grew after a few weeks. The crystal structure revealed that an oxidative C=C coupling between the bridging methylene moieties of two monoanionic ligands **7** had occurred (Figure 2-14).

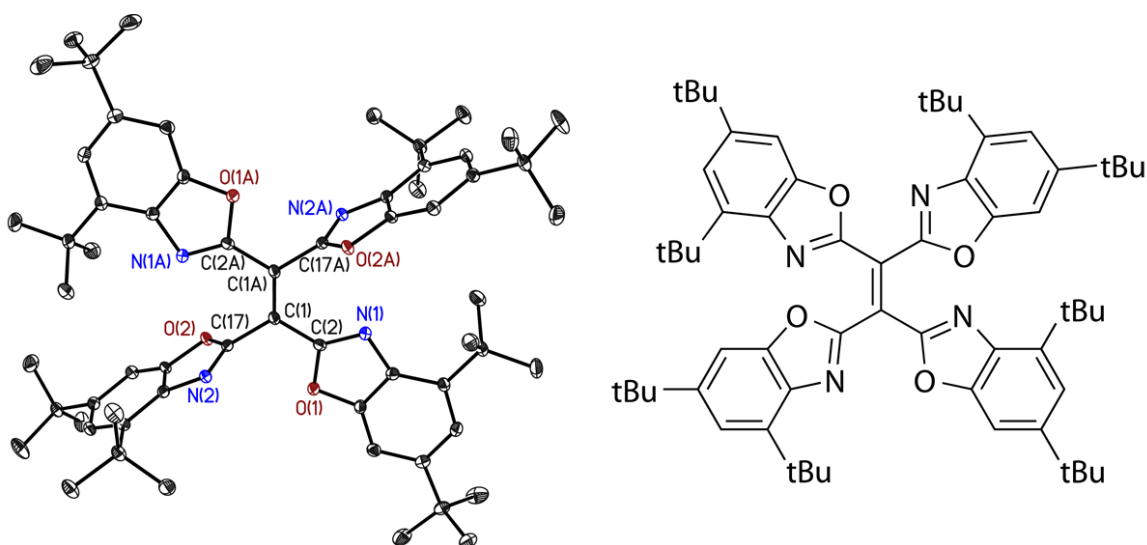


Figure 2-14. Left: Solid-state structure of 1,1,2,2-tetrakis(4,6-*t*Bu-benzoxazol-2-yl)ethane (**15**). Anisotropic displacement parameters are depicted at the 50% probability level. Hydrogen atoms are omitted for clarity. Right: *Lewis* structure of **15** to illustrate the present binding situation.

The newly formed tetra-dentate ligand system 1,1,2,2-tetrakis(4,6-*t*Bu-benzoxazol-2-yl)ethane (**15**) crystallizes in the monoclinic space group $P2_1/c$, containing half a molecule in the asymmetric unit. As sp^2 hybridized bridging carbon atoms, C(1) and C(1A) display a distorted trigonal planar environment. The C(1A)–C(1)–C(2/17) angles exhibit values of $122.3(1)^\circ$ and $121.6(1)^\circ$, respectively that match almost perfectly an ideal angle of 120° expected for a trigonal planar binding motif. However, the C(2)–C(1)–C(17) angle shows a slightly more acute arrangement ($115.95(8)^\circ$). This is most likely caused by steric strain induced by *t*Bu substituents of neighboring heteroaromatic side arms (Table 2-9).

Table 2-9. Selected bond lengths [Å] and angles [$^\circ$] of **15**.

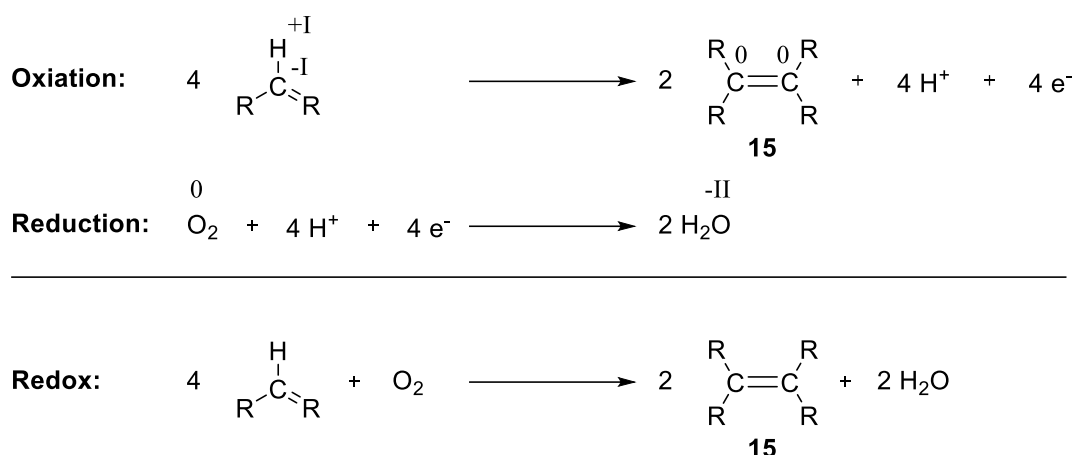
C(1)–C(2)	1.460(1)	C(2)–O(1)	1.378(1)	C(1A)–C(1)–C(2)	122.3(1)
C(1)–C(17)	1.491(1)	C(17)–O(2)	1.373(1)	C(1A)–C(1)–C(17)	121.6(1)
N(1)–C(2)	1.295(1)	C(1)–C(1A)	1.356(2)	O(1)–C(2)–C(1)–C(17)	8.6(1)
N(2)–C(17)	1.283(1)	C(2)–C(1)–C(17)	115.95(8)	O(2)–C(17)–C(1)–C(2)	94.4(1)

Symmetry transformations used to generate equivalent atoms: $-x+1, -y+1, -z+1$.

The determined C(1)–C(1A) distance of $1.356(2)$ Å being only slightly longer than a characteristic $C(sp^2)=C(sp^2)$ double bond (1.34 Å) is also in tune with this observation.^[187, 188] To avoid steric congestion, one of the heteroaromatic side arms in each ligand molecule stays almost in plane with the bridging moiety (O(1)–C(2)–C(1)–C(17) torsion angle of only $8.6(1)^\circ$), while the other is perpendicularly arranged (O(2)–C(17)–C(1)–C(2) torsion angle of $94.4(1)^\circ$). Other structural features do not differ much from those found in the monomeric ligand molecule **7**.

On the one hand, the formation of **15** can be rationalized by a catalytic C=C double bond formation mediated by the presence of the *Lewis*-acid CaBr_2 . In former studies on bis(heterocydo)methanes, reactions with M(II)acetates (M = Mn, Fe, Pb) led to the observation of similar *Lewis* acid catalyzed coupling and oxidation products.^[157] Here, ligand dimers bridged either by C–C single- or by C=C double bonds were isolated. It was stated that present *Brønstedt* bases like the aforementioned acetate anion or the monoanionic ligand itself might additionally promote such dimerization reactions.^[205, 206] Moreover, the ability of β -diketiminato supported alkali salts to function as one-electron reducing agents was observed.^[207] In this case, ligand dimerization was reported to be mediated by the generation of a ligand centered, π -delocalized radical species upon Ag(I) salt reduction, and subsequent radical C–C coupling.

On the other hand, a formation of **15** promoted by direct oxidation with oxygen from leaked in air is feasible (Scheme 2-17).

Scheme 2-17. Proposed redox reaction between monoanionic **7** and oxygen yielding **15** and water.

Due to a storage of the reaction crude in an NMR tube and the elongated reaction time, the presence of leaked in air is reasonable. The oxygen promotes the oxidation of monoanionic ligand molecules of complex **14** to yield **15** with an unknown standard potential in ([D₈])THF. In combination with the released protons the oxygen molecules are reduced under formation of water. This particular reaction proceeds in water with a standard potential of $E^0(\text{red}) = 1.229 \text{ V}$.^[208] Because of the missing standard potentials of the reactions in ([D₈])THF, a ΔE^0 value cannot be calculated *via* the equation $\Delta E^0 = E_{(\text{red})} - E_{(\text{ox})}$. In assumption of the reduction of oxygen to exhibit a standard potential in ([D₈])THF in a similar positive range as in water, the redox reaction in total should be favored to show a positive ΔE^0 value. In connection with the so-called free *Gibbs* energy $\Delta G^0 = -z \cdot F \cdot \Delta E^0$ (z = number of transferred electrons, F = *Faradays* constant), a negative ΔG^0 value would be received. In such a case, the redox reaction depicted in Scheme 2-17 would proceed spontaneously.

Interestingly, in related β -diketiminato-based lanthanide complexes, a direct oxidation and ligand dimerization under aerobic conditions was postulated to proceed *via* formation of a radical residing at the bridging carbon of the ligand backbone and subsequent radical coupling.^[209] Due to the NacNacs preference to show an NH tautomerism of the bridging protons, only dimers with C–C single bonds were observed so far.^[9]

In general, with compound **15** an interesting novel ligand scaffold was accessed. In future studies, an application as neutral tetra-dentate ligand platform, for example, in the preparation of homo- as well as heterobimetallic complexes is conceivable.

2.3.2.3 [K(18-crown-6){(4,6-*t*Bu-OCNC₆H₂)₂CH}·(H₂O)_{0.35}]}·(THF)₂ (16)

Introduction

Modern chemical synthesis is not conceivable without organometallic compounds. In particular, *Grignard* as well as organolithium reagents are cornerstones in organic and life science product syntheses. Unfortunately, these reagents are prone to hydrolysis while bearing a highly polarized metal-carbon (M-C) or metal-hydrogen bond (M-H) in the case of potassium hydride. Thus, handling in anhydrous inert organic solvents and under strict exclusion of water to avoid fast degradation is mandatory to date.^[210] In contrast, it was shown that in the presence of stoichiometric amounts of water in conventional solvents the reactivity and outcome of an organometallic transformation can be influenced in several ways. Examples are the modification of the stereochemistry within a synthetic pathway or the enhancement of a reaction rate.^[211, 212]

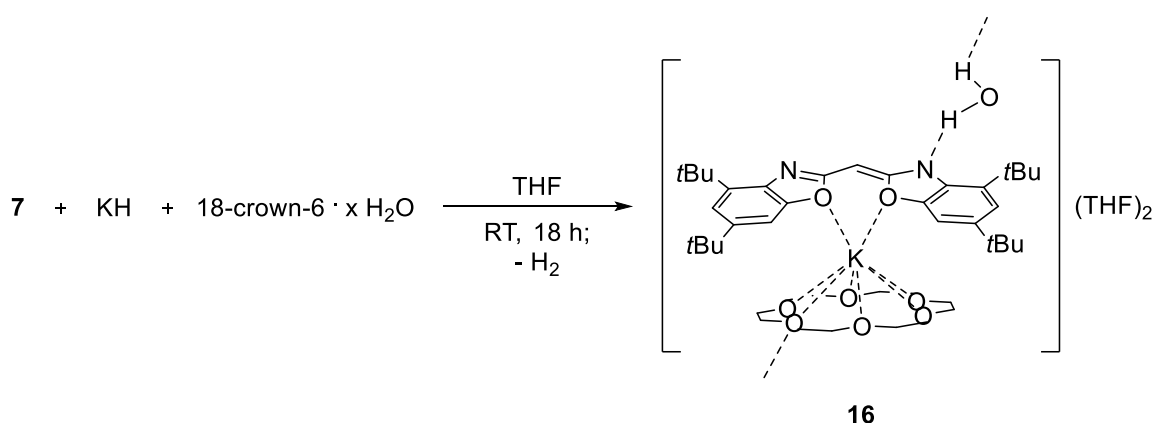
Taylor et al. reported one of the first examples that mention the unexpected influence of present water on the outcome of a reaction in 1975. They could show that the direct addition of *n*BuLi to a mixture of a bromoarene in T₂O wetted sodium-dried Et₂O is the most suitable procedure on the way to tritium labelled aromatic compounds. These findings displayed that the parent lithium/bromide exchange has at least to be as fast as and potentially even faster than the competitive decomposition reaction between the organometallic reagent and the tritiated water to form BuT and LiOT.^[213] An example for a comparable so-called water effect on the enantioselectivity of a reaction is the asymmetric lithium-*diisopropylamide* (LDA) mediated synthesis of the anticancer drug *Lonafarnib*. Here, the addition of water in the key alkylation step with an LDA·THF complex gave the highest yields and enantiomeric excesses (*ee*) (both 95%) for this particular reaction. In contrast, attempts without the addition of water led to significant lower yields and *ees*.^[214] *Wipf* and co-workers reported the strong influence of stoichiometric amounts of water on the reaction rate in the carboalumination of alkynes in 1993. In the methylalumination of 1-hexyne in the presence of 1.5 equivalents of water full turnover was achieved within minutes even at -70 °C.^[215] As a landmark, [Li(TMEDA)(H₂O){C₆H₄OCSN}] as the unprecedented example of an organolithium compound coordinated by a water molecule even as polar ligand was introduced by *Wright et al.* in 1990.^[216] This breakthrough fired the synthetic efforts on further aqua ligands containing organometallic species.^[217, 218] Two years later, *Schleyer et al.* presented the formation of the first water containing lithium complex bearing an organic residue with a C-H acidic moiety. Upon addition of TMEDA and water to lithiated malonodinitrile the polymeric structure [Li(TMEDA)(H₂O){CH(CN)₂}]_∞ is formed. Its solid-state structure revealed a unique three-dimensional hydrogen bonded pattern build up on water molecules. This emphasizes the ability of water molecules to function simultaneously as both, a donor as well as an acceptor molecule.^[219]

However, many open questions remain about the striking effect of water on the outcome of organometallic transformations. A recent article by *Capriati et al.* emphasizing on organolithiums

underscores some of these topical aspects: Under which conditions can water act as a polar ligand?; How reactive is “coordinated water” in comparison to “free water”?; Is the transfer of a water molecule to the carbanion mediated by a preliminary coordination of this molecule to the corresponding Li^+ center?^[220] In this context, also DESs (deep eutectic solvent) have emerged as alternative and versatile green solvent class in the field of sustainable organometallic transformations like addition reactions, the ring opening or synthesis of tetrahydrofuran’s and even in organo- and transition-metal catalysis. Thus, in the last years the groups of *Hevia*^[221, 222] and *Capriati*^[223–227] significantly contributed to this topic and showed that s-block element chemistry in bio-renewable protic DES is indeed feasible. Furthermore, DES’s have found widespread application as effective electrolyte solution in dye-sensitized solar cells,^[228] in bio-catalysis,^[229] and as medium for photosynthetic reaction centers in energy technology.^[230] Astonishingly, even the use of neat water as the only reaction medium for nucleophilic addition reactions of *Grignard*- as well as organolithium reagents on imines, nitriles and carbonyl compounds has been reported only very recently.^[231]

Synthesis and Characterization

To facilitate the release of the potassium ion from the deprotonated ligand in later salt metathesis reactions, preparation of **14** was repeated under addition of 18-crown-6 ether. Hence, a treatment of **7** with potassium hydride in the presence of 18-crown-6 ether that contained traces of water was performed in vigorously dried THF. Subsequent workup afforded a pale-yellow solid that was recrystallized *via* gas-phase diffusion of pentane into a saturated solution of this residue in THF. From the solution pale-yellow needle-shaped crystals of the remarkable potassium complex $[\text{K}(18\text{-crown-6})\{(4,6\text{-}t\text{Bu-OCNC}_6\text{H}_2)_2\text{CH}\}\cdot(\text{H}_2\text{O})_{0.35}]\cdot(\text{THF})_2$ (**16**) were obtained in a yield of 83% (Scheme 2-18).



Scheme 2-18. Synthesis of $[\text{K}(18\text{-crown-6})\{(4,6\text{-}t\text{Bu-OCNC}_6\text{H}_2)_2\text{CH}\}\cdot(\text{H}_2\text{O})_{0.35}]\cdot(\text{THF})_2$ (**16**). Adapted with permission from reference^[3]. Copyright 2017, John Wiley and Sons.

Complex **16** crystallizes in the monoclinic space group $P2_1/c$. The asymmetric unit contains one molecule of the potassium complex, 0.35 equivalents of co-crystallized water and two lattice THF

molecules. Its solid-state structure shows several remarkable features: Despite the bulky *t*Bu substituents in the periphery of monoanionic **7**, a contact-ion-pair is formed. Moreover, eight oxygen atoms exclusively coordinate the potassium ion. These originate from two heteroaromatic ring atoms of **7** and from six oxygen donor atoms of a 18-crown-6 ether molecule (Figure 2-15).

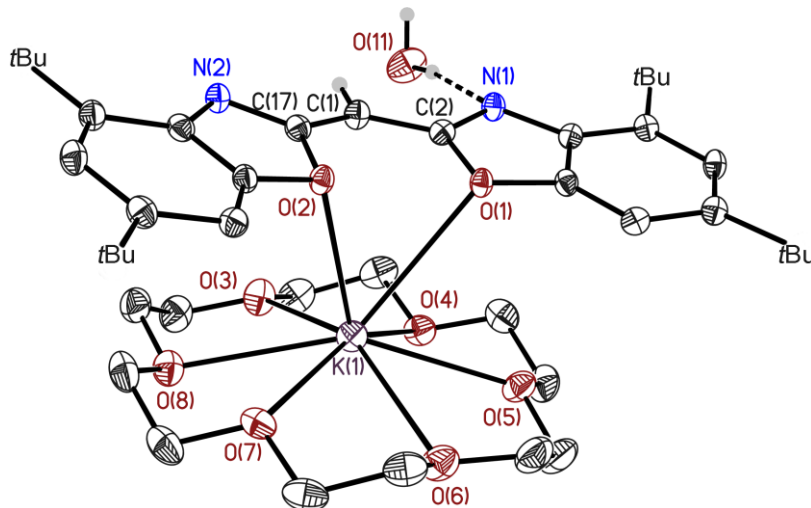


Figure 2-15. Solid-state structure of $[\text{K}(18\text{-crown-6})\{(\text{4,6-}t\text{Bu-OCNC}_6\text{H}_2)_2\text{CH}\} \cdot (\text{H}_2\text{O})_{0.35}] \cdot (\text{THF})_2$ (**16**). Anisotropic displacement parameters are depicted at the 50% probability level. Co-crystallized lattice THF molecules and hydrogen atoms are omitted for clarity, except for those at the bridging methylene position and the water molecule. Reprinted with permission from reference^[3]. Copyright 2017, John Wiley and Sons.

Most likely, the preferred solely *N*-coordination by the heteroaromatic rings is prevented by the increased steric repulsion from the *t*Bu substituents at the 4-position blocking that coordination pocket. So far, **16** represents the first example of a bis(benzoxazol-2-yl)-, bis(oxazol-2-yl)methane or –methanide displaying a solely oxygen coordination to any metal ion. The main electron density in these ligand systems is located at the ring nitrogen atoms,^[157, 158, 232] and multitudes of solely *N*-bound structures are present in the literature.^[139, 144, 166–168, 173, 233–235] Despite that, in **16** an *O*-coordination to the electron deficient metal ion is favored. A further remarkable feature of **16** is the presence of a water molecule with a site occupation factor estimated to 35%. This results in the formation of a two-dimensional hydrogen bonded network between the outwards tilted accessible ring nitrogen atom of a monoanionic ligand and the crown-ether molecule of a second equivalent of **16**. These hydrogen bonds are only facilitated by the unique all-*O*-coordination of the ligand. The $\text{N}(1) \cdots \text{O}(11)$ and $\text{O}(11) \cdots \text{O}(8_{\text{\$3}})$ distances are 2.929(4) and 3.060(5) Å, respectively.^[194] There are two maxima present in the electron density distribution along the $\text{N}_{\text{ligand}} \cdots \text{O}_{\text{water}}$ vector indicating a double potential hydrogen bond. One maximum was refined to give 21% occupation, the second 14%. This results in 14% of the molecular units being *N*-protonated to give neutral **7** with the negative charge residing at the resulting hydroxide anion in $[\text{K}(18\text{-crown-6})\{(\text{4,6-}t\text{Bu-OCN}(\text{H})\text{-C}_6\text{H}_2)_2\text{CH}(\text{4,6-}t\text{Bu-OCNC}_6\text{H}_2)\} \cdot \text{OH}]$, whereas 21% contain complexed intact water molecules in $[\text{K}(18\text{-crown-6})\{(\text{4,6-}t\text{Bu-OCNC}_6\text{H}_2)_2\text{CH}\} \cdot \text{H}_2\text{O}]$. The remaining 65% of the molecular units

contain no water and consist of $[K(18\text{-crown-6})\{(4,6\text{-}t\text{Bu-OCNC}_6\text{H}_2)_2\text{CH}\}]$. These findings underline, on the one hand, the amphoteric ability of water, but on the other hand, indicate an enhanced stability of **16** against hydrolysis. Noteworthy, in a phenylene-1,4-bis(trifluoroborate) dipotassium salt, presumed to be prone to hydrolysis, a co-crystallized water molecule was reported to contribute through $K\cdots O$ and $OH\cdots\pi$ interactions to its ability to self-assemble in the solid-state.^[236] To facilitate the formation of a contact ion pair, the potassium ion in **16** shows a dislocation of 0.689(7) Å from the plane made up by the six oxygen atoms of the crown ether molecule. Additionally, a dislocation of 2.729(2) Å from the C_3O_2 plane of the monoanionic chelate ligand is found (Table 2-10).

Table 2-10. Selected bond lengths [Å] and angles [°] of **16**.

K(1)–O(1)	3.177(1)	O(2)–C(17)	1.403(2)	K(1)–18-crown-6 dist.	0.689(7)
K(1)–O(2)	2.954(1)	C(2)–N(1)	1.323(2)	K(1)– C_3O_2 dist.	2.729(2)
C(1)–C(2)	1.394(2)	C(17)–N(2)	1.320(2)	O(1)–K(1)–O(2)	52.64(3)
C(1)–C(17)	1.395(2)	N(1)···O(11)	2.929(4)	C(2)–C(1)–C(17)	128.83(2)
O(1)–C(2)	1.402(2)	O(11)···O(8_3)	3.060(5)	Folding angle	14.12(5)

Symmetry operation to generate 3: $-x+1, y+1/2, -z+1/2$.

The averaged $C(1)–C_{ipso}$ and $N–C_{ipso}$ distances of 1.395 and 1.322 Å, respectively, indicate a significant double-bond character.^[187,208] This observation is consistent with a distinct conjugation of the methylene bridge to the adjacent heteroaromatic side arms. The $K(1)–O_{18\text{-crown-6}}$ distances in a range from 2.7881(1) to 2.9346(1) Å are in good agreement with the mean value of 2.84(8) Å displayed by related structural fragments found in the Cambridge Structural Data Base (1061 structures with $R \leq 0.075$).^[237]

As expected, the 1H NMR spectrum of **16** in $[D_8]THF$ shows one set of signals for the deprotonated monoanionic ligand **7** and a singlet at 3.45 ppm that can be assigned to the coordinating crown-ether molecule. A broad singlet at 6.98 ppm and a doublet at 6.85 ppm can be assigned to the aromatic protons residing at the benzene perimeters, with H5 being shifted most to lower field. The signal broadening indicates that H5 is subject to unknown dynamical processes within the structure. Additionally, a singlet at 4.55 ppm caused by the methylene bridge moiety and two doublets at 1.50 and 1.32 ppm arising from the *t*Bu substituents are observed. Unfortunately, neither a water, nor a NH signal resulting from protonation can be reported. In the light of an occupancy of only 35% of the water molecule, this becomes less surprising.

A 1H -DOSY-ECC-MW estimation was applied to further examine the structure of **16** in solution. Its molecular weight was estimated to be 870 g/mol (DSE) and 967 g/mol (merge), excluding larger polymeric structures to be retained in solution. The fact that all complex-related signals show the same diffusion coefficient unequivocally indicates the CIP to be maintained in solution. Monomeric structures with one or two additionally attached THF molecules are most likely formed.

Within the error range, this hypothesis is consistent with theoretical molecular weights of 849 and 921 g/mol for such species, which deviate by only 2% and 6%, respectively, from the estimated DOSY molecular weights (DSE). Furthermore, this assumption is in tune with the solid-state structure of **16**. Here, one of the two co-crystallized and disordered lattice THF molecules in one of the positions also tends to *O*-coordinate to the central potassium cation (see Figure 5-8).

Reactivity of Complex **16**

A ^1H NMR water titration experiment was carried out with **16** to shed light on its stability to hydrolysis. Utilizing an electronically supported microliter syringe, a well-defined amount of water was added to a single NMR sample. The effect of the successively increasing water content was monitored by ^1H NMR spectroscopy (Figure 2-16).

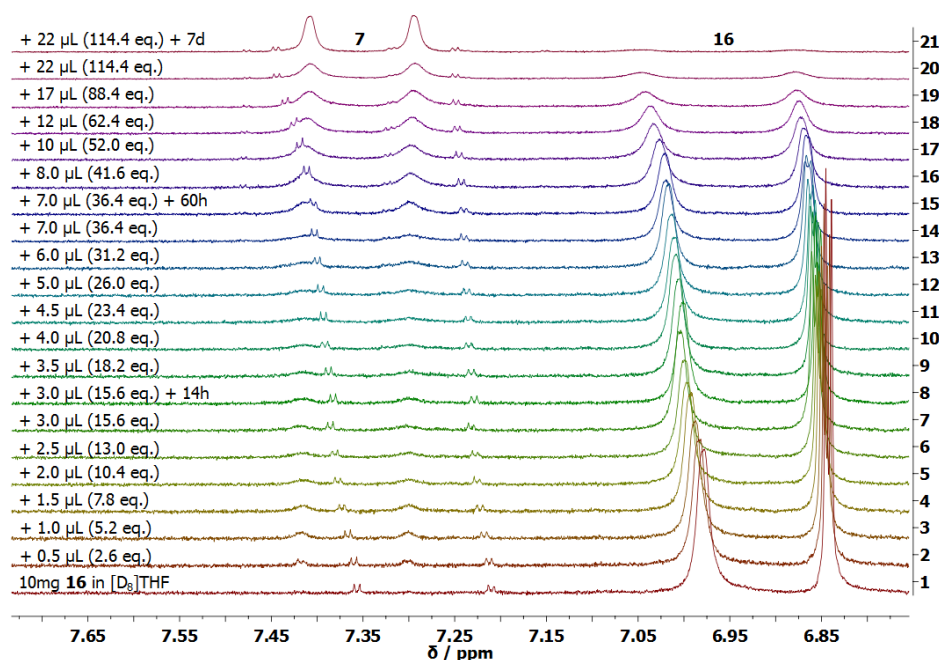


Figure 2-16. Excerpt from the stacked ^1H NMR spectra of a water titration experiment of **16** in $[\text{D}_8]\text{THF}$. For clarity, only the aromatic region is displayed. Spectrum 1 shows the two aromatic resonances of **16** before the first addition of water. Spectra 2 to 20 display the slow decomposition process of **16** to protonated **7**. Finally, spectrum 21 solely exhibits the two aromatic resonances of **7**. A full spectrum is included in the appendix (see Figure 5-16). Adapted with permission from reference^[3]. Copyright 2017, John Wiley and Sons.

Unexpectedly for an organopotassium compound, the titration experiment revealed **16** to be remarkably stable towards hydrolysis. As obvious from Figure 2-16, the aromatic signals of free protonated **7** only emerge very slowly upon gradual addition of water to the sample. Even after addition of 15.6 equivalents and an extended reaction time of 14 hours, only a small amount of **7** is detected. The signals for **2** are slightly but constantly shifted to lower field. The same trend continues until 36.4 equivalents of water are added and the reaction time is extended by additional 60 hours. Finally, full protonation of **16** is achieved after the addition of a huge excess of water (114.4 eq.) and an additional reaction time of seven days.

A recent combined MS and DFT study on a 3-aminopyrrolidine lithium salt by *Gimbert et al.* exhibited a certain protection of the lithium amide against hydrolysis only if additionally aggregated with lithium halides.^[238] In the light of these findings, the role played by the 18-crown-6 ether molecule either to act as a bystander or to contribute actively to the hydrolysis resistant character of **16** was further examined. Thus, a similar water titration experiment was carried out on the related potassium compound $[\text{K}\{\eta^5\text{-}(4,6\text{-}t\text{Bu-NCO}_6\text{H}_2)_2\text{CH}\}]_\infty$ (**14**) to estimate its hydrolysis stability in comparison to complex **16**. The experiment revealed this complex to show a certain, but definitely not as astonishing stability against hydrolysis as compound **16** (Figure 2-17).

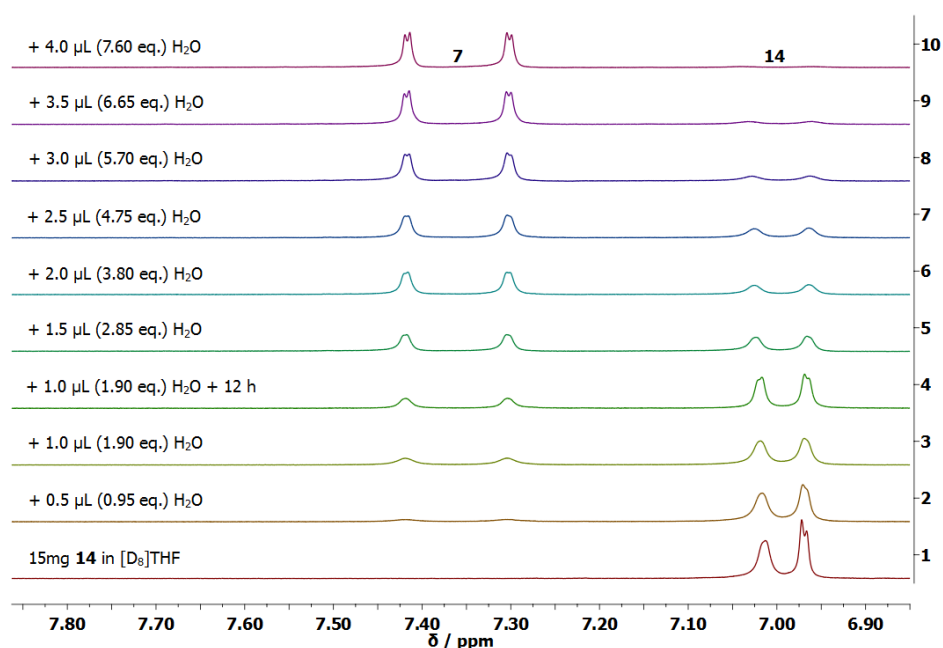
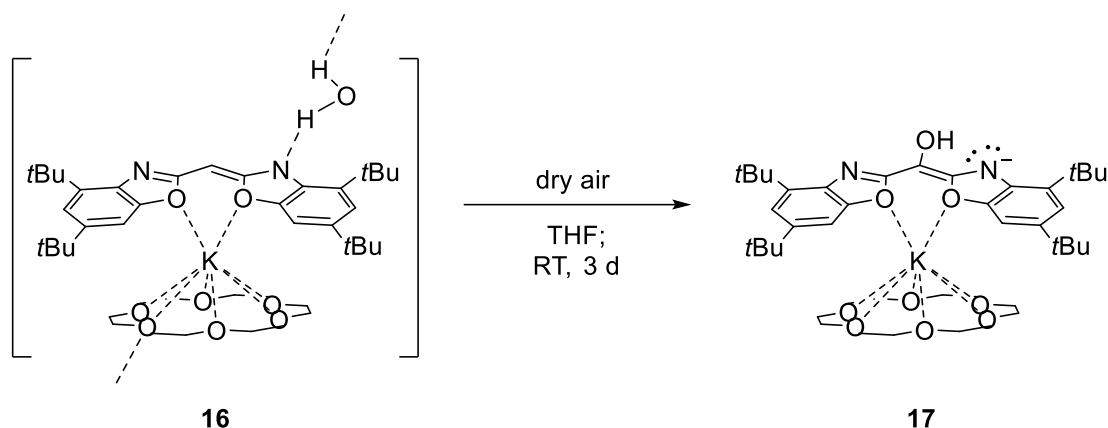


Figure 2-17. Excerpt from the stacked ¹H NMR spectra of a water titration experiment of $[\text{K}\{\eta^5\text{-}(4,6\text{-}t\text{Bu-NCO}_6\text{H}_2)_2\text{CH}\}]_\infty$ (**14**) in $[\text{D}_8]\text{THF}$. For clarity, only the aromatic region is displayed. Spectrum 1 shows the two aromatic resonances of **14** before the first addition of water. Spectra 2 to 9 display the slow decomposition process of **14** to protonated **7**. Finally, spectrum 10 solely exhibits the two aromatic resonances of **7**. A full spectrum is included in the appendix (see Figure 5-17). Adapted with permission from reference^[3]. Copyright 2017, John Wiley and Sons.

A significant amount of **7** can be detected even after the addition of only 1.90 equivalents of water, which did not increase after an extended reaction time of 12 hours. Full protonation is achieved after addition of 7.60 equivalents of water and a total reaction time of approximately 24 hours. To conclude, the comparative water titration experiment revealed compound **14** to have a strongly diminished stability to hydrolysis compared to complex **16**. This finding certifies the 18-crown-6 ether molecule to play an active role in the water resistance of **16** by forcing the methanide ligand to adopt a solely *O*-coordination to the potassium ion. The unique binding motif established is accompanied by the ability of the nitrogen atoms in the ligand periphery to function preferably as hydrogen bond acceptors, thus preventing the methylene bridge from quick protonation.

Furthermore, the air-stability of compound **16** was elucidated by exposing it to air which had been dried for several days over P_4O_{10} prior to use. Hence, a solution of **16** in THF was exposed to dry air at room temperature for three days. The experiment revealed the ligand backbone to be prone to oxidation leading to the formation of the new complex $[K(18\text{-crown-}6)\{(4,6\text{-}t\text{Bu-OCNC}_6\text{H}_2)_2\text{C(OH)}\}]$ (**17**) (Scheme 2-19).



Scheme 2-19. Synthesis of $[K(18\text{-crown-}6)\{(4,6\text{-}t\text{Bu-OCNC}_6\text{H}_2)_2\text{C(OH)}\}]$ (**17**). Adapted with permission from reference^[3]. Copyright 2017, John Wiley and Sons.

An extraction of the reaction crude with THF afforded a white residue and a pale-yellow filtrate. The white residue was insoluble in common organic solvents and can most likely be ascribed to the formation of an inorganic potassium salt. From the filtrate, complex **17** was obtained as a pale-yellow solid in a yield of 46% and was characterized by ^1H -, ^{13}C NMR spectroscopy and ESI mass spectrometry.

The ^1H NMR spectrum of **17** in $[D_8]\text{THF}$ exhibits a distinct signal pattern with the absence of any resonance for a bridging methylene moiety. Despite that, the presence of a singlet at 8.20 ppm in a typical range of an OH group attached to an aromatic system,^[199] can only be rationalized by the bridging carbon atom now carrying a hydroxyl function. Thus, the formation of the new complex $[K(18\text{-crown-}6)\{(4,6\text{-}t\text{Bu-OCNC}_6\text{H}_2)_2\text{C(OH)}\}]$ (**17**) which exhibits an oxidized ligand scaffold is plausible (Figure 2-18, *vide infra*). The doublets found for the aromatic protons H5 and H7 at 7.48 and 7.33 ppm are shifted both about 0.5 ppm to lower field in comparison to the starting material **16**. The 18-crown-6 ether molecule shows a singlet resonance at 3.64 ppm that is shifted about 0.2 ppm to lower field in comparison to the starting complex. Singlets at 1.54 and 1.38 ppm can be assigned to the *t*Bu substituents at the 6- and 4-positions, respectively.

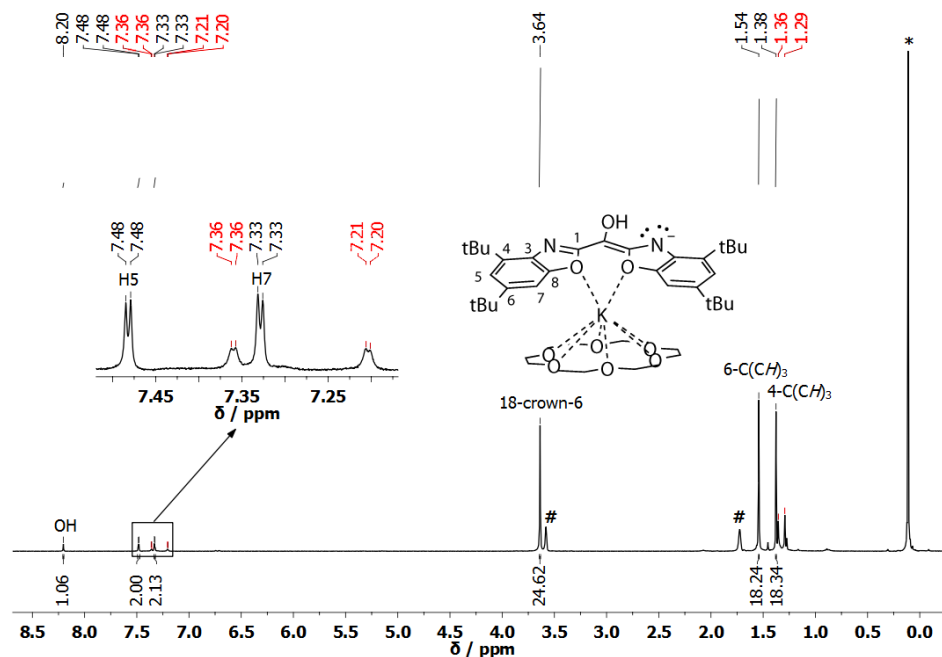
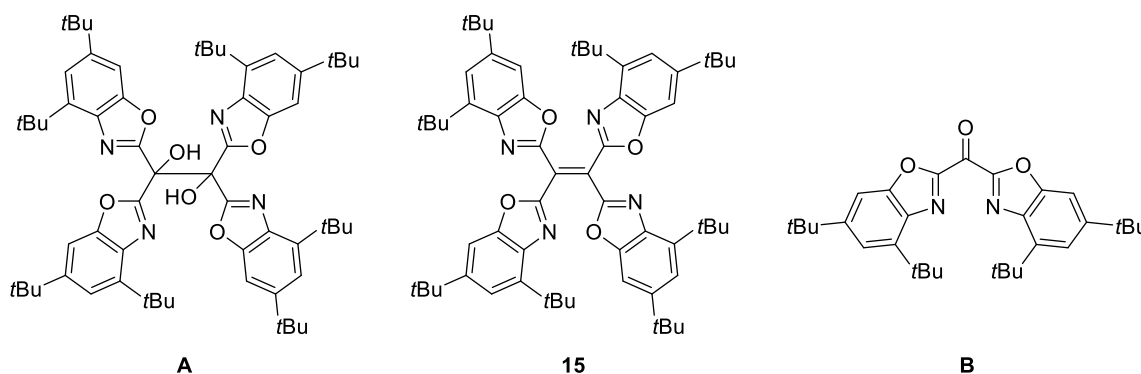


Figure 2-18. ^1H NMR spectrum of **17** in $[\text{D}_8]\text{THF}$. Residual solvent signals are marked with #. Grease is marked with *. Resonances marked in red correspond to a minor contamination with a side product. Reprinted with permission from reference^[3]. Copyright 2017, John Wiley and Sons.

In the light of these findings, the formation of a structure **A** can be ruled out (Scheme 2-20). The presence of this compound would result in the same signal pattern but with doubled integral intensities. In particular, the OH groups in **A** are no longer attached to an aromatic system, thus the observation of a stronger high-field shifted resonance between 4–6 ppm for these substituents would be expected.^[199]

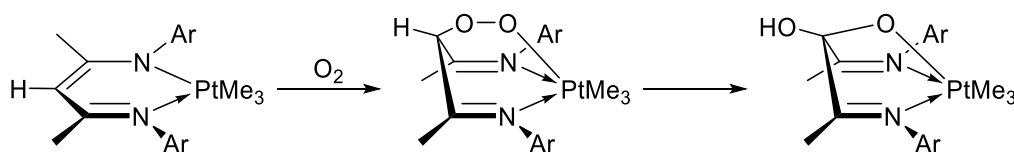


Scheme 2-20. Additional feasible oxidation products from a direct oxygen oxidation of complex **16**. Adapted with permission from reference^[3]. Copyright 2017, John Wiley and Sons.

Compounds **15** and **B** represent additional feasible oxidation products. The formation of these structures would be in tune with the resonances marked in red in Figure 2-18. As already mentioned before, similar oxidation products were observed for other heteroaromatic substituted methanide^[157] as well as NacNac^[9] ligand systems. Moreover, the successful formation of complex

17 is supported by ESI mass spectrometry. A peak observed at $m/z = 791.4$ can be assigned to the molecule radical cation $[M]^+$ of **17**. Furthermore, a peak at $m/z = 880.4$ corresponds to the radical cation $[M + C_4H_9O_2]^+$. The fragment $C_4H_9O_2^+$ with $m/z = 89$ is a typical fragmentation product of an 18-crown-6 ether molecule due to the ionization process. Until the end of the work, no further spectroscopic investigations could be carried out. Crystals of **17** remain to be obtained and to be subjected to X-ray diffraction experiments in the future. Furthermore, an estimation of the structure of **17** in solution by 1H -DOSY-ECC-MW experiments has to be carried out.

Complex **17** is formed upon an oxygenative oxidation of the ligand backbone. Unfortunately, it was not possible to elucidate the exact mechanism of this reaction until the end of this work. Nonetheless, similar oxygenations of the ligand backbone in transition-metal complexes based on β -diketiminato and related ligands can be found in the literature.^[239, 240] In this context, a reaction by *Goldberg* and co-worker that was reported in 2010 is particularly interesting (Scheme 2-21).^[241]

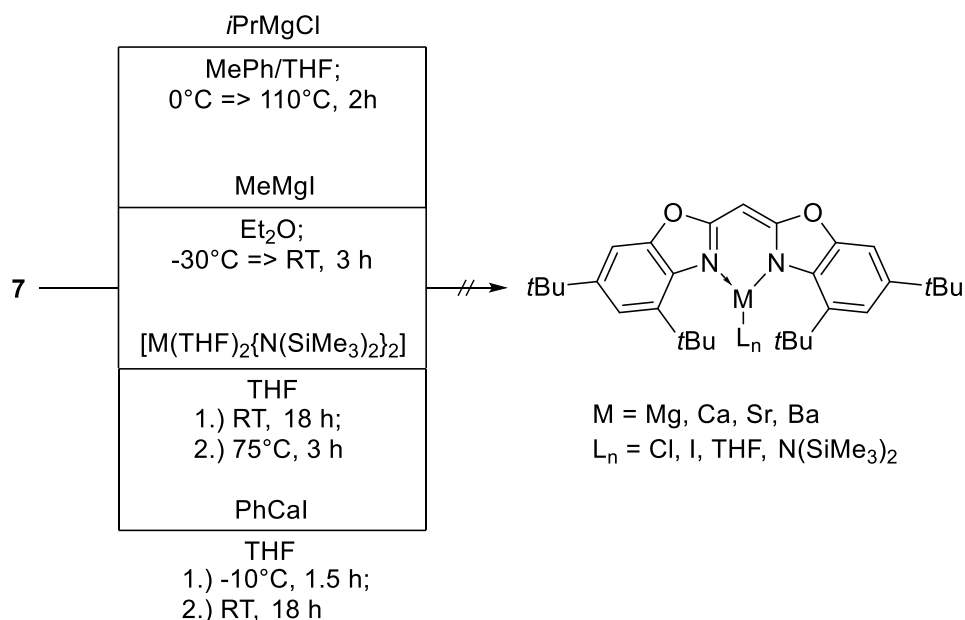


Scheme 2-21. Reaction of a NacNac-based platinum(IV) complex with oxygen. Ar = 4-*tert*-butyl-2,6-dimethylphenyl.

The reaction of a β -diketiminato supported platinum(IV) complex $[PtMe_3\{Ar\}NacNac]$ (Ar = 4-*tert*-butyl-2,6-dimethylphenyl) with dry oxygen led to the rapid formation of a Pt(IV)peroxo-complex (Scheme 2-21, middle). As confirmed by X-ray diffraction analysis, in the formed compound one of the oxygen atoms is bound to the bridging γ -carbon atom of the NacNac ligand, while the other is bound to the platinum ion. Within a few days, this complex rearranged to another platinum(IV) complex with a cleaved oxygen–oxygen bond (Scheme 2-21, right). Its solid-state structure revealed the bridging moiety to carry a hydroxyl function as well as an oxygen atom that binds to the platinum center. Unfortunately, no abstraction of the bridging oxygen was observed, which would have led to the formation of a platinum complex reminiscent of compound **17**. Still, it is feasible that the formation of **17** proceeded *via* a metal-ligand cooperative mechanism similar to that observed by *Goldberg* et al.

2.3.3 Group 2 Complexes

Simultaneously to the attempts to obtain group 2 complexes *via* salt metathesis reactions, concerted deprotonation-metalation reactions with alkaline-earth-metal organometallics were carried out with ligand **7** (Scheme 2-22).

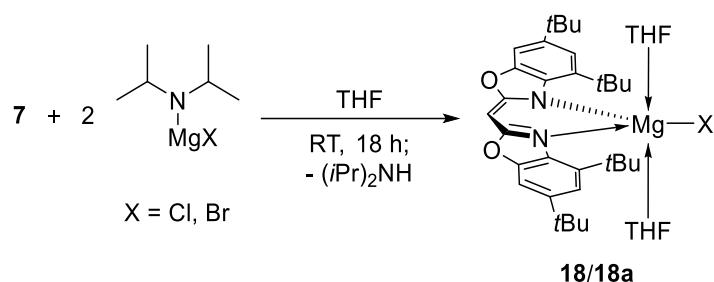


Scheme 2-22. Synthesis attempts on the way to group 2 complexes starting from **7**.

Unfortunately, no reaction was observed between ligand **7** and common group 2 metal sources, like different magnesium *Grignard* reagents or alkaline-earth-metal hexamethyldisilazanes. ^1H NMR spectra of the reaction crudes solely exhibit signals of the starting materials in all cases. Even at elevated temperatures, no product formation could be observed. In addition, a conversion of **7** with a freshly prepared PhCaI *Grignard* compound, obtained from a reaction with activated calcium metal and iodobenzene was carried out. Again, NMR spectroscopic investigation of the reaction crude showed no evidence of a successful complex formation, but resonances of the starting materials.

2.3.3.1 $[\text{MgX}(\text{THF})_2\{(4,6\text{-}t\text{Bu-NCOC}_6\text{H}_2)_2\text{CH}\}]$ ($\text{X} = \text{Cl, Br}$: **18/18a**)

Finally, from reactions of ligand system **7** with the *Hauser* type bases $(i\text{Pr})_2\text{NMgX}$ ($\text{X} = \text{Cl, Br}$) in THF, the heteroleptic magnesium halide complexes $[\text{MgX}(\text{THF})_2\{(4,6\text{-}t\text{Bu-NCOC}_6\text{H}_2)_2\text{CH}\}]$ ($\text{X} = \text{Cl, Br}$: **18/18a**) were obtained (Scheme 2-23).



Scheme 2-23. Synthesis of $[\text{MgX}(\text{THF})_2\{(4,6\text{-}t\text{Bu-NCOCH}_2)_2\text{CH}\}]$ ($\text{X} = \text{Cl, Br}$: **18/18a**). Adapted with permission from reference^[2]. Copyright 2017, John Wiley and Sons.

The chloride-substituted complex **18** was isolated as colorless plate-shaped crystals in a yield of 48%. Due to its high solubility, even in unpolar solvents like hexane, no crystals of the bromide congener **18a** have formed at lower temperatures, yet. Thus, **18a** was obtained as an amorphous, almost pure orange solid in a yield of 68%. To generate a magnesium complex with an even better leaving group for subsequent reduction attempts, preparation of the corresponding iodide *Hauser* base was attempted. Unfortunately, the procedure by *Neufeld* that worked for the respective chloride and bromide congeners did not afford the iodide substituted base.^[242] In contrast to its lighter halide homologues that were obtained as white solids, the white residue obtained from reactions of diisopropylamine and a slight excess of MeMgI did not react with **7**.

In Figure 2-19 (*vide infra*), the stacked ¹H NMR spectra of **7** and the derived complexes **18** and **18a** are shown. The ¹H NMR spectra of **18** and **18a** exhibit signals of the methanide ligand as well as for the coordinating THF molecules with an integral ratio from left to right of 2:2:1:8:18:18:8. The spectra of the two complexes deviate only marginally. The biggest differences can be found for the methylene bridge resonances (5.62 ppm in **18** and 5.56 ppm in **18a**) and the high-field signal of the THF donor ligands (1.07 ppm in **18** and 1.16 ppm in **18a**). In comparison to the protonated ligand **7**, upon metalation, the signal of the methylene bridge experiences the strongest shift of averaged 1.39 ppm to lower field in the magnesium halide complexes.

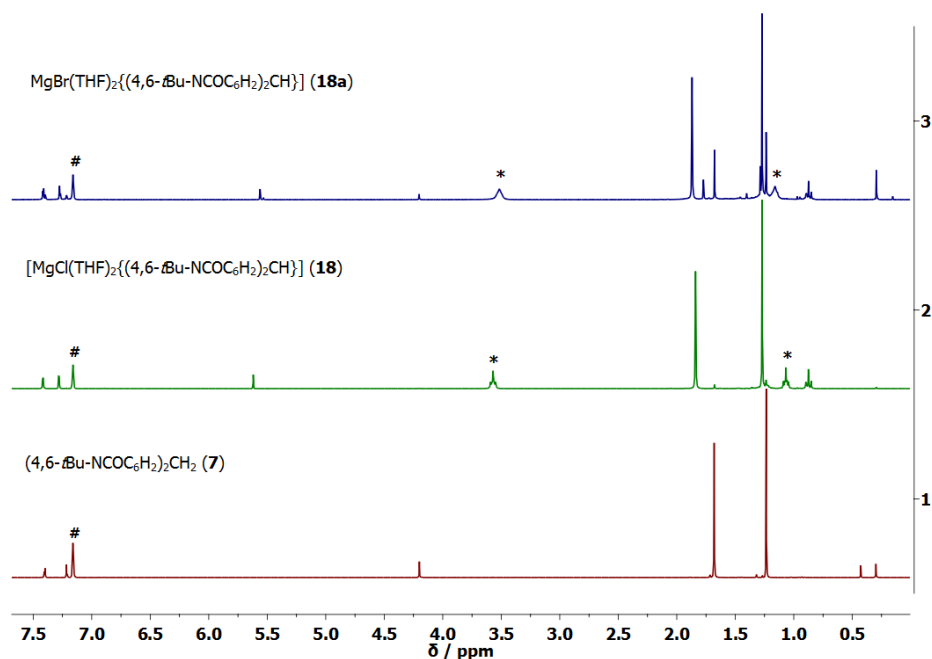


Figure 2-19. Stacked ¹H NMR spectra of ligand **7** and the complexes **18** and **18a** in C₆D₆. The residual solvent signal is marked with #. The signals of coordinating THF molecules are marked with *. Note that there is a slight contamination of **7** in the spectra of complexes **18** and **18a**.

Regarding the structures of both complexes in solution, their molecular weights were estimated by DOSY experiments to be 609 g/mol (**18**) / 634 g/mol (**18a**) (DSE) and 685 g/mol (**18**) / 715 g/mol (**18a**) (merge). Within the error range, the experimental molecular weights of the structures fit to theoretical values of either a four-fold or a five-fold coordination with one or two attached THF molecules, respectively. Again, these findings show the THF donor ligands to be subject to rapid dynamical exchange processes exacerbating a reliable conclusion on the molecular shape of **18/18a** in solution.

Complex **18** crystallizes in the monoclinic space group $P2_1/n$. The asymmetric unit contains one molecule of the complex as well as a lattice pentane molecule. An Addison parameter of $\tau_5 = 0.74$ undoubtedly indicates a five-fold trigonal-bipyramidal coordination around the central magnesium(II) ion.^[243] Two chelating ring nitrogen atoms of the methanide ligand and a chloride substituent form the equatorial plane, while two THF donor molecules reside at the apical positions of the coordination polyhedron (Figure 2-20).

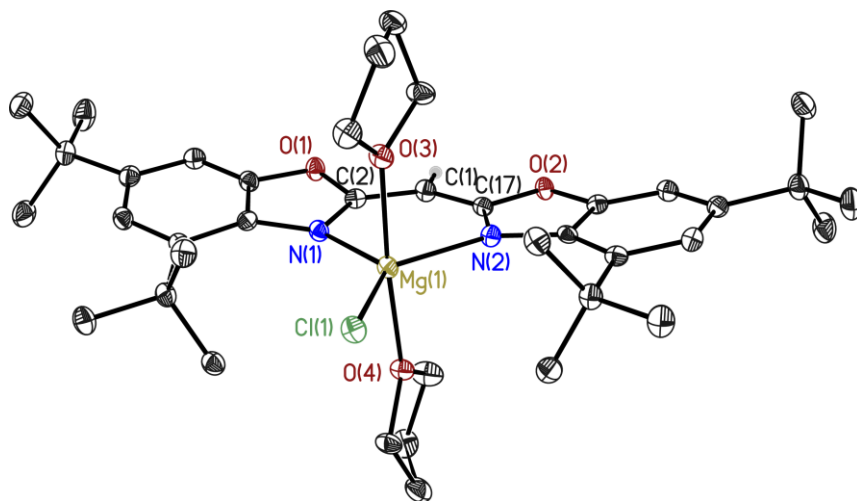


Figure 2-20. Solid-state structure of $[\text{MgCl}(\text{THF})_2\{(4,6\text{-}t\text{Bu-NCOC}_6\text{H}_2)_2\text{CH}\}]\cdot\text{pentane}$ (**18**). Anisotropic displacement parameters are depicted at the 50% probability level. A co-crystallized pentane molecule as well as hydrogen atoms are omitted for clarity, except for the one at the bridging methylene position. *Reprinted with permission from reference* ^[2]. Copyright 2017, John Wiley and Sons.

With a dislocation of only 0.010(2) Å the Mg^{2+} cation shows an in-planar arrangement to the chelating C_3N_2 moiety fitting perfectly into the offered coordination pocket. Interestingly, this feature is still accompanied by a folding of the ligand framework by 10.16(3)° (Table 2-11).

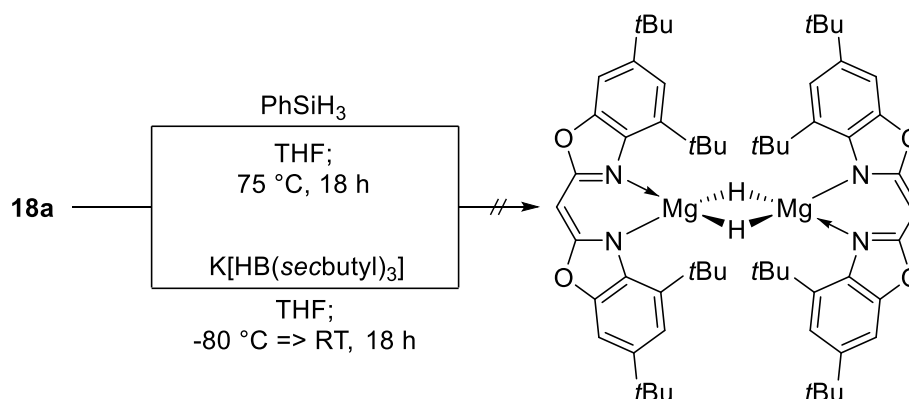
Table 2-11. Selected bond lengths [Å] and angles [°] of **18**.

Mg(1)–N(1)	2.179(2)	C(1)–C(2)	1.399(2)	C(17)–O(2)	1.379(2)
Mg(1)–N(2)	2.160(2)	C(1)–C(17)	1.391(2)	Mg(1)– C_3N_2 dist.	0.010(2)
Mg(1)–Cl(1)	2.343(8)	N(1)–C(2)	1.342(2)	N(1)–Mg(1)–N(2)	99.83(6)
Mg(1)–O(3)	2.172(2)	N(2)–C(17)	1.344(2)	C(2)–C(1)–C(17)	128.9(2)
Mg(1)–O(4)	2.139(1)	C(2)–O(1)	1.375(2)	Folding angle	10.16(3)

In comparison to the lithium complex **13**, the N(1)–Mg(1)–N(1) bite angle in **18** experiences no significant change upon cation change. In contrast to that, the corresponding N–M distances (2.179(2) and 2.160(2) Å to av. 1.951(6) Å in **13**) and the $\text{C}_{\text{ipso}}\text{–Cl–C}_{\text{ipso}}$ angle (128.9(2)° to 121.7(3)° in **13**) increase, which is in good agreement with the elevated ionic radius of the Mg^{2+} cation. Complex **18** is the first example of a NacNac-like bis(benzoxazol-2-yl)methanide magnesium complex with a trigonal-bipyramidal coordination geometry. Comparable five-fold coordinated NacNac-based magnesium species are the di-nuclear $[\text{Mg}_2\text{Br}_2(\text{THF})_4\{(\text{N}(\text{SiMe}_3)\text{C}(t\text{Bu})\text{C}(\text{H}))_2\text{C}_4\text{H}_2\text{N}_2\}]^{[202]}$ and the tripodal species $[\text{Mg}(\mu\text{-I})_2\{\kappa^3\text{-N,N',O-}(\text{DippN}(\text{CMe})_2(\text{OCCPh}_2)\text{CH})\}]^{[84]}$ and $[\{\text{Mg}\{\kappa^3\text{-N,N',O-}(\text{DippN}(\text{CMe})_2(\text{OCCPh}_2)\text{CH})\}]_2(\mu\text{-}\kappa^2\text{:}\kappa^2\text{-S}_2\text{O}_4)]^{[84]}$. Those exhibit with values in a range from 2.155 to 2.132 Å slightly shorter averaged Mg–N bonds than found in compound **18**.

Reactivity of Complex 18a

To get access to magnesium hydride species, reactions with different hydride sources were carried out with complex **18a** that carries with bromide a better leaving group than **18** (Scheme 2-24).

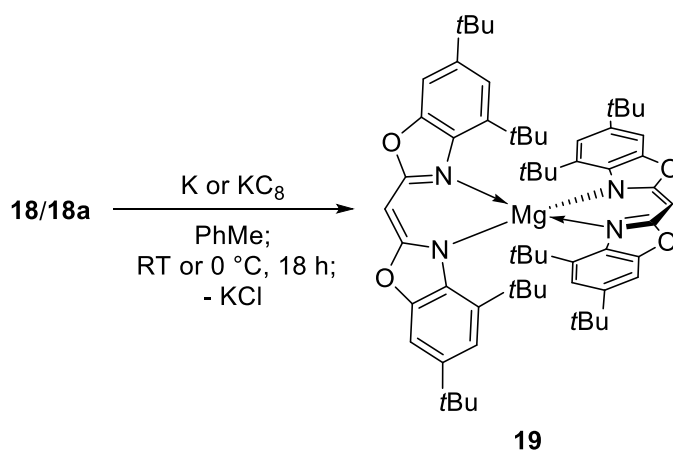


Scheme 2-24. Synthesis attempts on the way to a potentially dimeric magnesium hydride complex starting from **18a**.

In the synthesis of related NacNac-supported magnesium hydride complexes, phenylsilane was successfully utilized as a hydride source.^[53] Thus, in first attempts, this hydride donor was applied to **18a** as well. In addition to that, the hydride-transfer reagent potassium tri-*sec*-butylborohydride, also known as *K-Selectride*[®], was evaluated as potential alternative to phenylsilane. Starting from this hydride donor, the formation of the magnesium hydride complex would proceed *via* the release of a potassium halide and volatile tri-*sec*-butylborane as side products. For NacNac-based magnesium hydride compounds like, for example, $[\text{Mg}(\mu\text{-H})\{\text{DippNacNac}\}]_2$ ^[68] and $[\text{MgH}(\text{DMAP})\{\text{DippNacNac}(\beta\text{-C}(t\text{Bu}))\}]$,^[53] hydride resonances between 3.83 ppm and 4.65 ppm are reported from ¹H NMR data. Hence, hydride signals for 7-based magnesium hydride compounds are expected to occur within a similar region. So far, neither reactions of **18a** with phenylsilane, nor with *K-Selectride*[®] led to the formation and isolation of such a magnesium hydride complex. ¹H NMR spectroscopic investigations of the reaction crudes only afforded spectra that indicate a decomposition of the starting complex as well as the methanide ligand. Until the end of this work, attempts to isolate distinct species from the reaction crudes by crystallization have been unsuccessful. Hence, repetition of the reactions with complex **18** as starting material was discarded.

2.3.3.2 [Mg{(4,6-*t*Bu-NCOC₆H₂)₂CH₂}]₂ (19**)**

With 7-based magnesium halides **18** and **18a** in hand, reductions to obtain a potentially dimeric, low oxidation state Mg(I)–Mg(I) complex were attempted. In analogy to the synthesis of related NacNac-supported magnesium(I) dimers, both complexes were reacted with potassium metal in toluene at room temperature. Moreover, these reactions were repeated with potassium graphite as reducing agent (Scheme 2-25).



Scheme 2-25. Synthesis of $[\text{Mg}\{(4,6\text{-}t\text{Bu-NCOCH}_2\text{C}_6\text{H}_4)_2\text{CH}\}_2]$ (**19**). Adapted with permission from reference^[2]. Copyright 2017, John Wiley and Sons.

Unfortunately, from all attempts, the homoleptic Mg(II) complex $[\text{Mg}\{(4,6\text{-}t\text{Bu-NCOCH}_2\text{C}_6\text{H}_4)_2\text{CH}\}_2]$ (**19**) was isolated as sole product in a yield between 76-80%. As a result, and to avoid a possible over-reduction of the starting material, the reaction was attenuated by repetition at 0 °C, but with the same outcome. Because of a high solubility of the product, even at reduced temperatures, no single-crystals suitable for X-ray diffraction experiments could be obtained so far.

Nevertheless, formation of homoleptic compound **19** was indicated by LIFDI experiments. The molecule radical cation peak $[M]^+$ at $m/z = 970.7$ undoubtedly displays the isotopic pattern and mass of an Mg(II) ion chelated by two methanide ligand molecules. Despite that, it is also feasible that this species might have formed upon the ionization process from a previously present Mg(I) complex.

In $^1\text{H-DOSY-ECC-MW}$ experiments, the molecular weight of the obtained product in solution was estimated to be 857 g/mol (DSE) and 993 g/mol (merge). Within the error range of 9%, especially the latter estimate would fit to both, complex **19** as well as an only 24.3 g/mol heavier dimeric, low oxidation state $\text{Mg}^{\text{I}}\text{-Mg}^{\text{I}}$ species. Because of the lack of a solid-state structure, and in light of more evidence for the formation of a homoleptic magnesium(II) compound, in the following it is assumed that structure **19** represents the obtained product. In particular, formation of **19** might be the result of a *Schlenk* equilibrium redistribution of a heteroleptic complex towards its homoleptic equivalent, or due to a transient Mg(I) complex that is prone to disproportionation yielding Mg(0) and Mg(II) and an excess of negatively charged ligand molecules. Jones and co-workers made similar observations when carrying out reduction attempts with sodium or potassium metal on the related NacNac precursor complex $[\text{MgI}(\text{Et}_2\text{O})\{\text{PhNacNac}\}]$.^[53]

In a $^1\text{H NMR}$ spectrum of **19** in C_6D_6 , the complex related resonances are partly obscured by the residual solvent signal, thus the measurements were repeated in $[\text{D}_{12}]$ cyclohexane as another non-donating solvent. Here, doublets at 7.05 ppm and 7.01 ppm with $^4J_{\text{HH}}$ couplings of 2.0 Hz are

found for the aromatic protons H7 and H5 of the methanide ligands. A singlet at 5.38 ppm can be assigned to the proton at the bridging methylene positions. The *t*Bu substituents residing at the 4- and 6-positions exhibit resonances at 1.25 ppm and 1.15 ppm, respectively. The presence of *N*- and *O*-donor sites within the deprotonated bis(4,6-*t*Bu-benzoxazol-2-yl)methanide ligand results in two feasible symmetrical coordination modes: An exclusively *N*-bound (**19**) and a solely *O*-bound species (**19a**) (Figure 2-21).

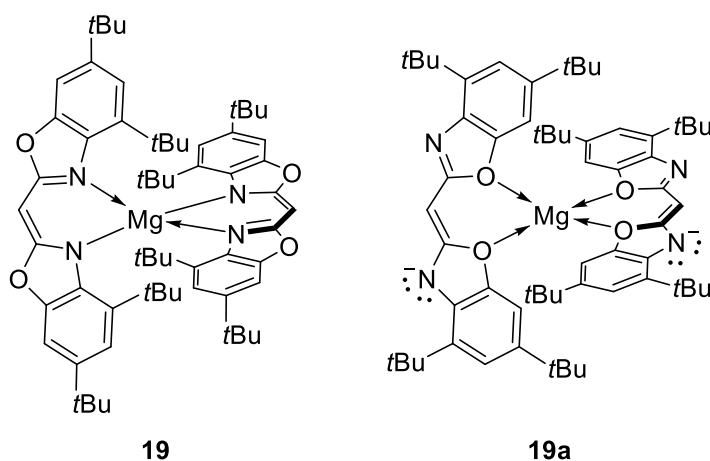


Figure 2-21. Comparison of exclusively *N*-bound (**19**) and solely *O*-bound (**19a**) coordination motifs. Adapted with permission from reference^[2]. Copyright 2017, John Wiley and Sons.

Due to the presence of only one set of signals in the ¹H NMR spectrum of **19**, a third feasible coordination motif that comprises one *N*- and one *O*-bound ligand can be directly ruled out. From the coordination chemist's point of view, a solely *N*-bound complex should be less favored. This is due to steric crowding around the Mg(II) ion caused by the *t*Bu groups at the 4-positions of the methanides. Hence, for a correct determination of the coordination mode advanced NMR techniques were applied.

First, the *N*-binding motif of deprotonated **7** to the Mg(II) cation in solution was evaluated by considering the ¹⁵N NMR chemical shift as determined from ¹⁵N-¹H HMBC spectroscopy. For complex **19**, a resonance at -213 ppm is found. This shift is close to the signal at -217 ppm displayed by **18**, which exhibits an *N*-binding mode, as determined from single-crystal X-ray diffraction. The exclusively *O*-coordinated **7** exhibits a less high-field shifted ¹⁵N resonance at -184 ppm.

In a collaboration with Niklas, this motif was further corroborated by ¹H NOESY experiments. The cross-peak between the *t*Bu substituents at the 4-position of an attached ligand and the methylene bridging moiety of the second one is much stronger than between the *t*Bu groups at the corresponding 6-position and the bridging motif (Figure 2-22, *vide infra*). Thus, the correlated proximity in space can only be rationalized by the *N*-binding mode present in **19** (also see structural models as included in the appendix: Figure 5-18).

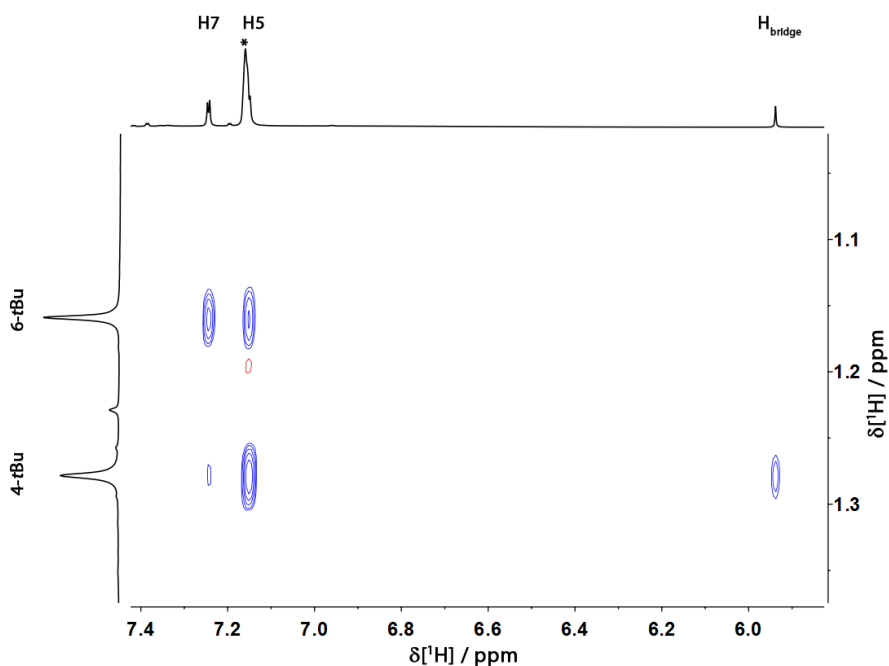


Figure 2-22. Excerpt from the ^1H NOESY spectrum of **19** in C_6D_6 (*). For clarity, only relevant cross-peaks are shown. Reprinted with permission from reference ^[2]. Copyright 2017, John Wiley and Sons.

Moreover, the observation of a cross-peak between 4-*t*Bu and H_{bridge} is indicative for the formation of **19** instead of a $\text{Mg}^{\text{I}}\text{-Mg}^{\text{I}}$ complex. Due to a missing proximity in space of the considered structural fragments in the latter, the absence of such a cross-peak would be expected.

In a further collaboration with *Niklas*, a preliminary study on one-bond residual dipolar couplings (RDCs) between C and H was performed and revealed that this technique can also be applied to shed light on this stereochemical problem. A detailed introduction on the theoretical background of RDCs and the utilized alignment tensor concept would go beyond the scope of this thesis. Thus, for a comprehensive overview on this issue it is highly recommended to consult reference ^[244].

A D_{4d} symmetric compound such as **19** exhibits a uniaxial alignment tensor with its principal components aligned along the C_2 symmetry axes. Thereby, a single one-bond RDC is sufficient to determine the alignment tensor (Table 2-12).

Table 2-12. Experimental one-bond scalar couplings $^1J_{\text{CH}}$, sums of scalar couplings and residual dipolar couplings $^1T_{\text{CH}}$ and resulting residual dipolar coupling $^1D_{\text{CH}}$ in Hz. Adapted with permission from reference ^[2]. Copyright 2017, John Wiley and Sons.

	$^1J_{\text{CH}}$	$^1T_{\text{CH}}$	$^1D_{\text{CH}}$
C- H_{bridge}	162.5 ± 0.2	169.6 ± 1.2	7.1 ± 1.2
C5-H5	153.4 ± 0.2	154.6 ± 0.8	1.2 ± 0.8
C7-H7	160.8 ± 0.2	171.3 ± 1.8	10.5 ± 1.8

Practically, compound **19** was set into a coordinate system by aligning its C–H_{bridge} vector along z. Furthermore, the ring planes were embedded within the y-z plane. Polar angles ϑ were then determined between the z-axis and the respective C–H bond vector (Figure 2-23).

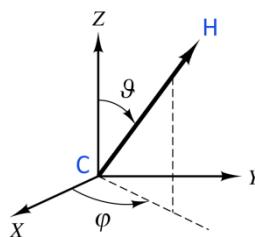


Figure 2-23. Polar angle ϑ and azimuthal angle φ for an arbitrary C–H bond vector. Reprinted with permission from reference [2]. Copyright 2017, John Wiley and Sons.

The parallel arrangement between the ring and the y-z plane leads to $\varphi = 90^\circ$ for all bonds. Angles are summarized in Table 2-13 (*vide infra*). The Equations (1) to (3) are fundamental and more thoroughly explained in reference [244] which can be employed to derive the alignment tensor elements from the RDC of C–H_{bridge}.

$$D = k(A_{\bar{x}}\sin^2\vartheta\cos^2\varphi + A_{\bar{y}}\sin^2\vartheta\sin^2\varphi + A_{\bar{z}}\cos^2\vartheta) \quad (1)$$

$$A_{\bar{x}} = A_{\bar{y}} \quad (2)$$

$$A_{\bar{x}} + A_{\bar{y}} + A_{\bar{z}} = 0 \quad (3)$$

The constant k is derived from the vacuum permeability, the gyromagnetic ratios of ^{13}C and ^1H , the Planck's constant, numerical factors and the distance between the coupling nuclei. The latter is 1.09 Å and thereby gives $k = -69959.8$ Hz.

Finally, $D = 7.1$ Hz yields the following results for A_x and A_z :

- i) $A_x = A_y = (5.1 \pm 0.9) \cdot 10^{-5}$ and
- ii) $A_z = (10.1 \pm 1.7) \cdot 10^{-5}$.

Subsequently, 3D structure proposals of the two possible binding motifs were obtained from simple force-field optimization (see Figure 5-18). Note that state-of-the-art structure analysis *via* RDCs usually employs DFT derived geometries, but low-level theoretical means have proven to yield sufficiently accurate results as well.

Table 2-13. Polar angles ϑ between C–H_{bridge} and C5–H5 and C–H_{bridge} and C7–H7 as determined from simple force-field optimized *N*-bound and *O*-bound structures. Resulting back-calculated RDCs D_{calc} and experimental RDCs D_{exp} . Adapted with permission from reference [2]. Copyright 2017, John Wiley and Sons.

	$\vartheta(\text{C5-H5}) [^\circ]$	$\vartheta(\text{C7-H7}) [^\circ]$	$D_{\text{calc}} [\text{Hz}]$	$D_{\text{exp}} [\text{Hz}]$
<i>N</i> -bound	9.8	131.5	6.8 ± 1.2 1.1 ± 0.6	10.5 ± 1.8 1.2 ± 0.8
<i>O</i> -bound	149.3	87.9	4.3 ± 0.9 -3.5 ± 0.6	10.5 ± 1.8 1.2 ± 0.8

This allows the determination of angles between the vectors C–H_{bridge}/C5–H5 and C–H_{bridge}/C7–H7 which correspond to the polar angles ϑ . Back-calculation through equation (1) utilizing the estimated tensor elements A_x , A_y and A_z yields theoretical RDCs D_{calc} as summarized in Table 2-13 (*vide supra*). These values can be compared with the actual experimental RDCs D_{exp} .

The agreement between back-calculated and experimental RDC is better in the case of *N*-bound as can be immediately recognized. This can additionally be quantified by *e.g.* the *Q*-factor which should be low for the correct structure (equation (4)).^[245]

$$Q = \sqrt{\frac{\sum (D_{\text{calc},i} - D_{\text{exp},i})^2}{\sum D_{\text{exp},i}}} \quad (4)$$

This gives:

- i) $Q = 1.1$ for the *N*-bound structure and
- ii) $Q = 2.3$ for the *O*-bound structure.

In summary, the *N*-binding mode in **19** is supported by i) the ¹⁵N NMR chemical shift, ii) NOE contacts and iii) analysis of experimental and back-calculated RDCs.

2.4 Syntheses of the Bis(4,6-*i*Pr-benzoxazol-2-yl)methane (26) Ligand and its *s*-Block Complexes

Major parts of this chapter have been published in:

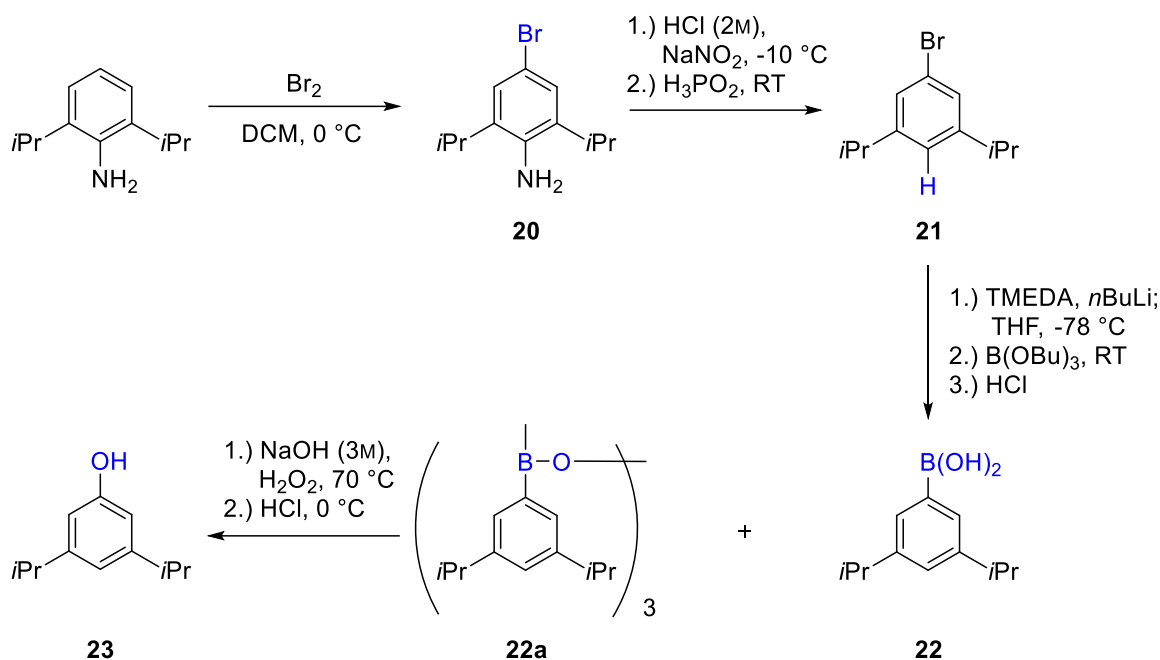
- [4] I. Koehne, N. Graw, T. Teuteberg R. Herbst-Irmer, D. Stalke, “Introducing NacNac-Like Bis(4,6-isopropylbenzoxazol-2-yl)methanide in *s*-Block Metal Coordination”, *Inorg. Chem.* **2017**, 56, 14968-14978.^[4]

2.4.1 Ligand Synthesis

To exceed the group of bis(benzoxazol-2-yl)methane ligands that carry sterically demanding substituents in close proximity to the coordination pocket, synthesis of the 4,6-*i*Pr-substituted derivative of **7** was started. In contrast to **7** and due to its smaller alkyl substituents, this ligand system is assumed to exhibit a diminished kinetic hindrance towards concerted deprotonation-metalation reactions with organometallic reagents. The symmetrically substituted 3,5-diisopropylphenol (**23**) is ten times as expensive as its corresponding *t*Bu-substituted derivative. Thus, this compound was self-made for a fraction of the cost, prior to the successive introduction of an amino function at its 2-position. The latter proceeds according to the retrosynthetic approach already depicted in Scheme 2-5 in Chapter 2.3.1.

2.4.1.1 3,5-diisopropylphenol (**23**)

Starting from commercially available 2,6-diisopropylaniline, **23** was prepared in a four-step procedure following a protocol by *Diemer* and co-workers, which was modified and improved (Scheme 2-26, *vide infra*).^[246] In the first step, a bromine substituent was introduced at the para position of the aniline starting material forming 4-bromo-2,6-diisopropylaniline (**20**) in a quantitative yield of 99%.^[247] A subsequent diazotization with *in situ* generated nitrous acid followed by the addition of hypophosphorous acid as reducing agent readily gave 1-bromo-3,5-diisopropylbenzene (**21**) in a high yield of 93%. In contrast to the procedure proposed by *Diemer*, a less elaborate purification method was acquired: A simple extraction of the reaction crude with 0.5 M sodium hydroxide solution and water. In the next step, a borylation with tributylborate of *in situ* generated (3,5-diisopropylphenyl)lithium, obtained from a reaction of **21** with *n*BuLi, gave a mixture of boronic acid **22** (14%) and cyclo-triboroxane **22a** (86%) in a yield of 60%. Notably, the assignment of the ¹H NMR spectroscopic resonances of compounds **22** and **22a** in CDCl₃ were mistakenly interchanged by *Diemer* and co-workers. Additionally, a singlet at 4.56 ppm (CDCl₃) with an integral of two, also missing in reference ^[246], could be assigned to the corresponding B(OH)₂ group of product **22**.

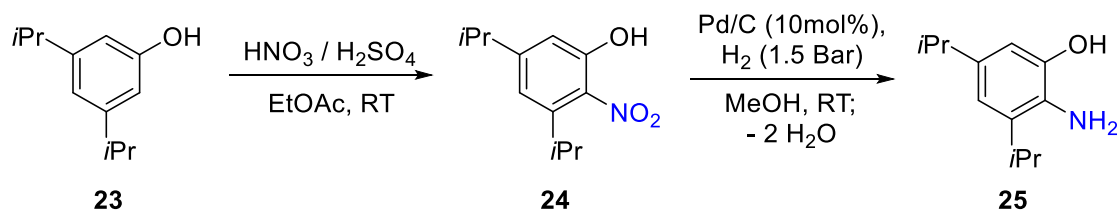


Scheme 2-26. Four-step synthesis route for the preparation of 3,5-diisopropylphenol (**23**). Adapted with permission from reference^[4]. Copyright 2017, American Chemical Society.

Finally, anion oxidation was carried out through addition of H_2O_2 to a solution of **22/22a** in aqueous sodium hydroxide. To facilitate the formation of reactive hydroperoxide anions, reaction was carried out in an alkaline instead of the suggested neat concentrated hydrogen peroxide medium.^[248] After protonation of the formed phenolate with aqueous HCl and subsequent workup, 3,5-diisopropylphenol (**23**) was obtained in an almost quantitative yield of 95%. Simultaneously, a time-consuming workup *via* column chromatography suggested by *Diemer* and co-workers was avoided. In conclusion, the overall yield of the four-step synthesis of **23** could be improved from 46% to 52%. This is accompanied by the implementation of less elaborate workup methods like simple washing/extraction of the products with solutions of different pH-values.

2.4.1.2 3,5-diisopropyl-2-nitrophenol (**24**) & 3,5-diisopropyl-2-aminophenol (**25**)

Finally, with a sufficient amount of **23** in hand and analogous to the preparation of compound **6**, successive introduction of an amino function at the 2-position of **23** was started (Scheme 2-27).



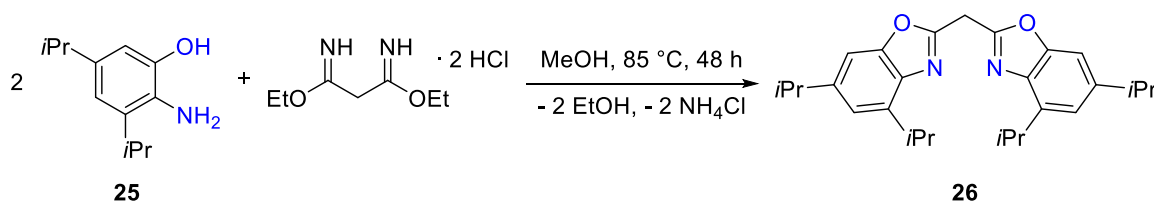
Scheme 2-27. Syntheses of 3,5-Diisopropyl-2-nitrophenol (**24**) and 3,5-Diisopropyl-2-aminophenol (**25**). Adapted with permission from reference^[4]. Copyright 2017, American Chemical Society.

Just like for the corresponding *t*Bu-substituted derivative,^[2] the first step consisted of adding one equivalent of nitrating acid to compound **23**. Subsequent fractional distillation of the reaction crude, gave the parent mono ortho-substituted 3,5-diisopropyl-2-nitrophenol (**24**) as a yellowish-orange oil in an appreciable yield of 46%. Besides resonances of the *i*Pr substituents and the OH group in the ¹H NMR spectrum of **24** in acetone-*d*₆, an additional doublet at 6.89 ppm and a doublet of doublets at 6.83 ppm with an integral of one for each of the aromatic protons are observed. This indicates the formation of an asymmetric product and thus, a successful mono ortho-nitration. Furthermore, the IR spectrum of **24** displays characteristic vibrational bands for the symmetric ($\tilde{\nu} = 1365 \text{ cm}^{-1}$) and asymmetric ($\tilde{\nu} = 1525 \text{ cm}^{-1}$) NO₂ stretching vibrations which are in good agreement with the values of 1366 cm⁻¹ and 1518 cm⁻¹ found for the *t*Bu-substituted derivative **5**.

Proceeding with the synthetic protocol depicted in Scheme 2-27, reduction of the parent nitro function in **24** was performed by applying the already approved method used in the preparation of compound **6**. Subsequent recrystallization of the reaction crude from CHCl₃ readily gave the desired 3,5-diisopropyl-2-aminophenol (**25**) in a yield of 90%. In the ¹H NMR spectrum of **25** in [D₈]THF, a characteristic broad singlet at 3.82 ppm with an integral of two can be assigned to the introduced NH₂ group. Again, distinctive vibrational bands at 3307 cm⁻¹ and 3376 cm⁻¹, arising from the symmetric and asymmetric NH₂ stretching vibrations, are in tune with wave numbers of 3316 cm⁻¹ and 3415 cm⁻¹ found for **5**.

2.4.1.3 Bis(4,6-*i*Pr-benzoxazol-2-yl)methane (**26**)

As a last step and to ultimately generate the desired ligand system bis(4,6-*i*Pr-benzoxazol-2-yl)methane (**26**),^a a two-fold cyclocondensation reaction between two equivalents of **25** and the well-established ethyl-bisimidate dihydrochloride C₃-linker unit was carried out (Scheme 2-28).



Scheme 2-28. Synthesis of bis(4,6-*i*Pr-benzoxazol-2-yl)methane (**26**). Adapted with permission from reference ^[4]. Copyright 2017, American Chemical Society.

Practically pure **26** was obtained as an orange oil in a yield of 43% by simple extraction of the reaction crude with pentane and sonication. For analysis, the product was additionally purified by

^a In the following also abbreviated as: (4,6-*i*Pr-NCOC₆H₂)₂CH₂.

column chromatography. In the ^1H NMR spectrum of **26** in $[\text{D}_8]\text{THF}$, ligand signals with an integral ratio of 2:2:2:2:2:12:12 are observed (Figure 2-24).

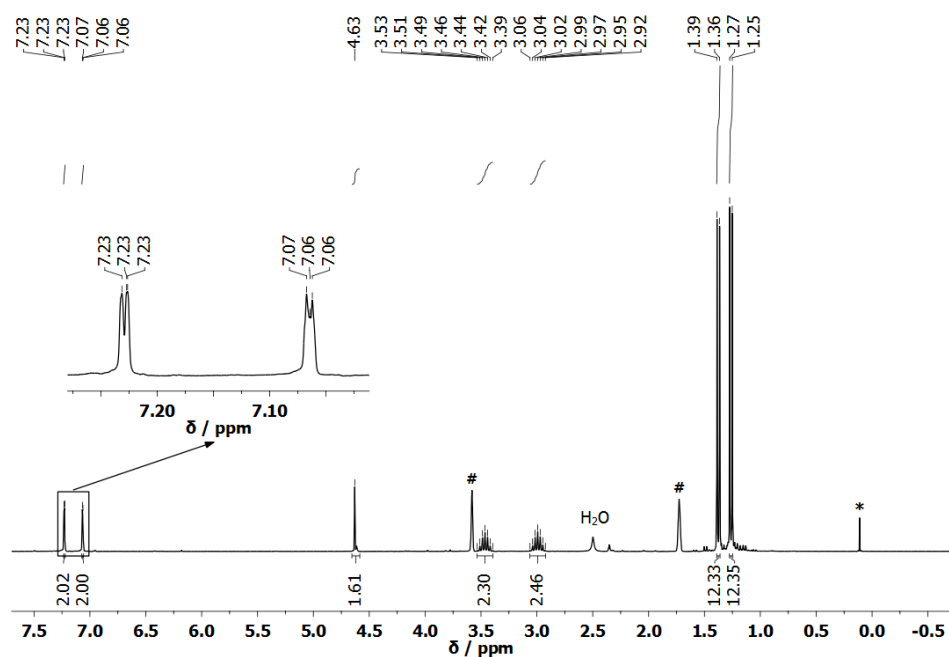


Figure 2-24. ^1H NMR spectrum of compound **26** in $[\text{D}_8]\text{THF}$. Residual solvent signals are marked with #. Grease is marked with *. Adapted with permission from reference^[4]. Copyright 2017, American Chemical Society.

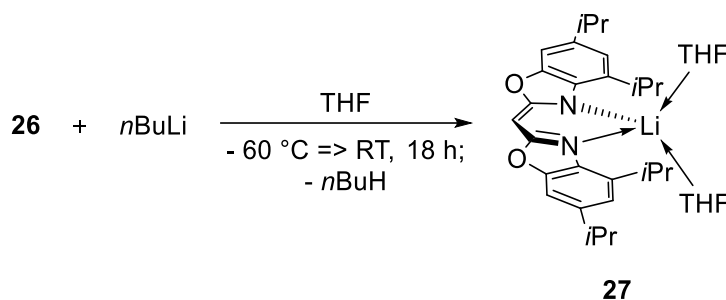
Besides resonances at 7.23 and 7.07 ppm for the benzene perimeter protons H7 and H5, the spectrum additionally shows a distinct singlet at 4.63 ppm caused by the methylene bridge protons. Furthermore, a characteristic pattern of septets at 3.46 and 2.99 ppm as well as doublets at 1.38 and 1.26 ppm is observed, which exhibit $^3J_{\text{HH}}$ couplings of 7.0 Hz. This can be assigned to the chemically inequivalent *i*Pr substituents at the corresponding 4- and 6-positions. Interestingly, despite bearing four methyl groups less than its *t*Bu-substituted congener **7**, and being accompanied by a supposedly decreased +I effect, the ^1H NMR signals of **26** are less down-field shifted. Thus, an enhanced electron density residing at these positions is indicated. Additionally, a C=N stretching vibration observed at 1609 cm^{-1} is in good agreement with a value of 1601 cm^{-1} found for **7**.

2.4.2 Group 1 Complexes

For ligand system bis(4,6-*i*Pr-benzoxazol-2-yl)methane (**26**), complex syntheses also commenced with the preparation of group 1 precursors for the later implementation in salt metathesis reactions with group 2 halides.

2.4.2.1 [Li(THF)₂{(4,6-*i*Pr-NCOC₆H₂)₂CH}] (27)

To evaluate a lessened kinetic hindrance of **26** in comparison to its *t*Bu-substituted congener **7**, the compound was lithiated with *n*BuLi. In contrast to the behavior of **7** (see Chapter 2.3.2), the addition of *n*BuLi to a solution of **26** in THF at -60 °C gave the corresponding four-fold coordinated lithium precursor complex [Li(THF)₂{(4,6-*i*Pr-NCOC₆H₂)₂CH}] (**27**) in a yield of 69% overnight (Scheme 2-29).



Scheme 2-29. Synthesis of [Li(THF)₂{(4,6-*i*Pr-NCOC₆H₂)₂CH}] (**27**). Adapted with permission from reference^[4]. Copyright 2017, American Chemical Society.

Upon lithiation of **26**, the resonances intrinsic to the aromatic protons at the benzene perimeters experience a significant up-field shift. Now, signals at 6.84 ppm and 6.82 ppm are found in the ¹H NMR spectrum of **27** in [D₈]THF. This observation is in tune with an increased electron density at these positions, due to a successful charge delocalization from the C₃N₂ moiety towards the C₆ perimeters in the ligand periphery. This is also accompanied by a deshielding and simultaneous downfield shift of the corresponding methylene bridge signal to 4.72 ppm. In addition, complex **27** shows a ⁷Li NMR signal at 2.07 ppm that is shifted about 0.69 ppm to higher field than the resonance exhibited by its congener **13**.

Moreover, **27** crystallizes in the non-centrosymmetric monoclinic space group *Cc* comprising one molecule in the asymmetric unit. The solid-state structure reveals an only slightly distorted tetrahedral coordination around the central lithium ion (Figure 2-25).

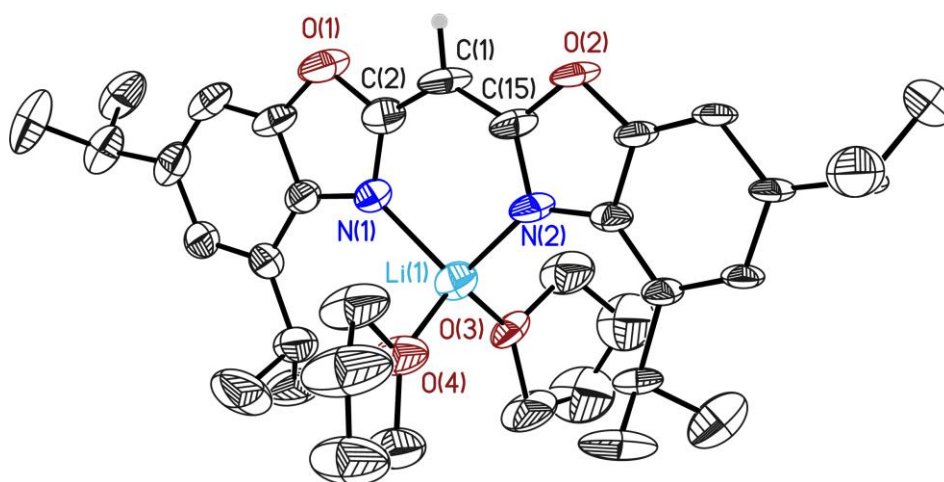


Figure 2-25. Solid-state structure of $[\text{Li}(\text{THF})_2\{(4,6\text{-}i\text{Pr-NCOC}_6\text{H}_2)_2\text{CH}\}]$ (**27**). Anisotropic displacement parameters are depicted at the 50% probability level. Hydrogen atoms are omitted for clarity, except for the one at the bridging methylene position. Reprinted with permission from reference^[4]. Copyright 2017, American Chemical Society.

The coordination sphere is made up by two ring nitrogen atoms of deprotonated monoanionic **26** and additionally by the oxygen atoms of two attached THF donor molecules. With a dislocation between 0.00(3) and 0.07(5) Å, the lithium ion is almost ideally placed within the chelating C_3N_2 plane. Moreover, a butterfly-like folding angle in a range of only 2.2(10)° to 2.3(6)° between the two benzoxazol side arms indicates an almost planar ligand framework (Table 2-14).

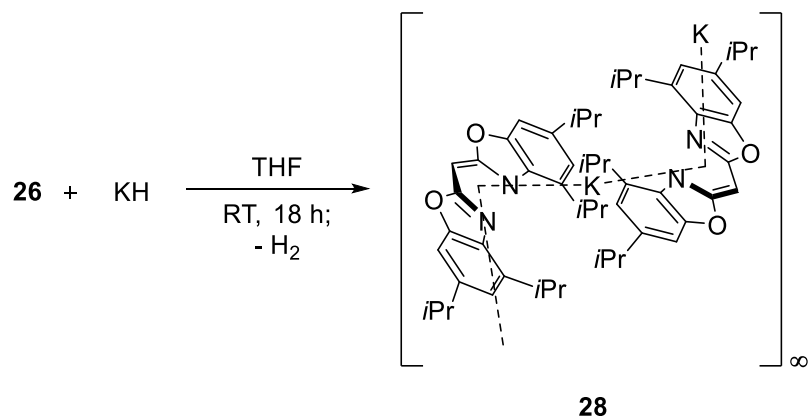
Table 2-14. Selected bond lengths [Å] and angles [°] of **27**.

Li(1)–N(1)	2.03(1)	N(1)–C(2)	1.331(8)	Li(1)– C_3N_2 dist.	0.00(3), 0.07(5)
Li(1)–N(2)	1.96(2), 2.11(2)	N(2)–C(15)	1.33(1), 1.32(2)	N(1)–Li(1)–N(2)	99.7(6), 91.7(8)
C(1)–C(2)	1.41(1), 1.39(2)	C(2)–O(1)	1.400(8)	C(2)–C(1)–C(15)	126.8(1), 119(2)
C(1)–C(15)	1.39(1), 1.37(2)	C(15)–O(2)	1.41(1)	Folding angle	2.2(10), 2.3(6)

The N–M distances in **27** between 1.96(2) to 2.03(1) Å are elongated in comparison to the closely related complex $[\text{Li}(\text{THF})\{(4,6\text{-}t\text{Bu-NCOC}_6\text{H}_2)_2\text{CH}\}]$ (**13**). An electronically more depleted ligand periphery and an increased coordination number of four, due to an additional THF donor, most likely causes this feature. The same trend can be derived for the corresponding N–M–N bite angle between 91.7(8)° and 99.7(6)° and a considerable widening of the $\text{C}_{\text{ipso}}\text{--C}_1\text{--C}_{\text{ipso}}$ angle from 121.7(3)° in **13** to 119(2)° – 126.8(1)° in **27**. Another related lithium complex $[\text{Li}(\text{THF})_2\{(1\text{-Me-NCN-}\text{C}_6\text{H}_4)_2\text{CH}\}]$ ^[168] exhibits comparable N–M bond lengths (1.979(3) and 1.974(3) Å) to **27**, but reduced N–M–N and $\text{C}_{\text{ipso}}\text{--C}_1\text{--C}_{\text{ipso}}$ angles of 96.85(1)° and 124.28(2)°, respectively. Furthermore, the general structural features of **27** are also in good agreement with those for comparable β -diketiminato-based lithium compounds from literature.^[49, 249]

2.4.2.2 $[K\{\eta^5-(4,6-iPr-NCOC_6H_2)_2CH\}]_\infty$ (**28**)

The addition of compound **26** to a suspension of potassium hydride in THF led to the formation of a novel potassium species in a yield of 71% overnight (Scheme 2-30).



Scheme 2-30. Synthesis of $[K\{\eta^5-(4,6-iPr-NCOC_6H_2)_2CH\}]_\infty$ (**28**). Adapted with permission from reference^[4]. Copyright 2017, American Chemical Society.

Recrystallization from gas-phase diffusion of pentane into a saturated solution of **28** in THF only afforded small needle-shaped crystals unsuitable for single-crystal X-ray diffraction experiments. Nevertheless, in light of the structural motifs of other bis(benzoxazol-2-yl)methanide based potassium compounds, it is most likely that $[K\{\eta^5-(4,6-iPr-NCOC_6H_2)_2CH\}]_\infty$ (**28**) was obtained as product. For example, the complexes $[K(THF)\{(4-MeNCOC_6H_3)_2CH\}]_\infty$ (**2**) and $[K\{\eta^5-(4,6-tBu-NCOC_6H_2)_2CH\}]_\infty$ (**14**) form polymeric strands in the solid-state, thus this coordination polymer is assumed for **28** as well. Because the 1H NMR spectrum of **28** in $[D_8]THF$ solely exhibits resonances of the monoanionic ligand **26** and no additionally attached THF molecules, a donor-base free polymeric structure like in the aforementioned and closely related **14** is most likely (Figure 2-26, *vide infra*). In comparison to **14**, the signals for the protons H7 and H5 residing at the benzene perimeters experience a stronger upfield shift (6.78 and 6.73 ppm versus 7.01 and 6.97 ppm in **14**) in the 1H NMR spectrum of **28**. In contrast, the resonance for the bridging CH moiety (4.61 ppm compared to 4.56 ppm in **14**) is shifted slightly more downfield, again indicating an enhanced charge redistribution towards the benzene perimeter than in its *t*Bu-substituted congener.

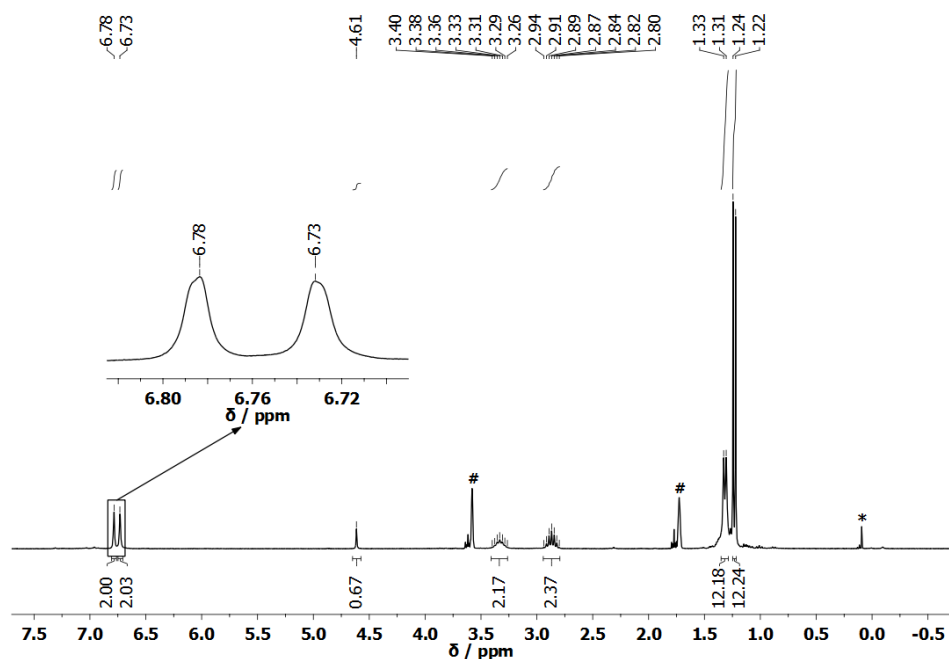
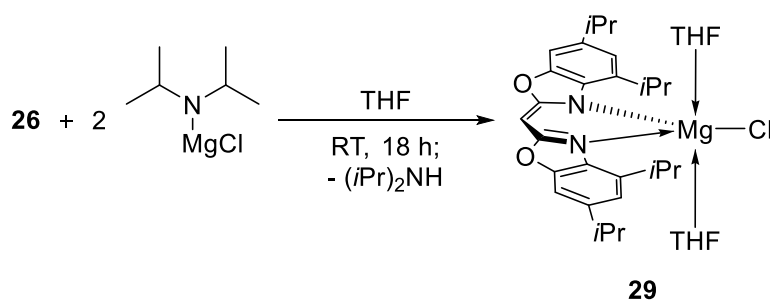


Figure 2-26. ^1H NMR spectrum of compound $[\text{K}\{\eta^5\text{-}(4,6\text{-}i\text{Pr-NCOC}_6\text{H}_2)_2\text{CH}\}]_\infty$ (**28**) in $[\text{D}_8]\text{THF}$. Residual solvent signals are marked with #. Grease is marked with *. Adapted with permission from reference^[4]. Copyright 2017, American Chemical Society.

2.4.3 Group 2 Complexes

2.4.3.1 $[\text{MgCl}(\text{THF})_2\{(4,6\text{-}i\text{Pr-NCOC}_6\text{H}_2)_2\text{CH}\}]\cdot\text{hexane}$ (**29**)

To maximize the formation of a heteroleptic complex, compound **26** was added very slowly to a solution of two equivalents of the well-established *Hauser* base $(i\text{Pr})_2\text{NMgCl}$.^[242] As a result, the derived magnesium halide compound $[\text{MgCl}(\text{THF})_2\{(4,6\text{-}i\text{Pr-NCOC}_6\text{H}_2)_2\text{CH}\}]\cdot\text{hexane}$ (**29**) was isolated in form of colorless crystals in a yield of 56% (Scheme 2-31).



Scheme 2-31. Synthesis of $[\text{MgCl}(\text{THF})_2\{(4,6\text{-}i\text{Pr-NCOC}_6\text{H}_2)_2\text{CH}\}]\cdot\text{hexane}$ (**29**). Adapted with permission from reference^[4]. Copyright 2017, American Chemical Society.

Again, the deprotonated ligand system **26** shows an enhanced dislocation of the negative charge throughout the ligand framework, which is reflected in the chemical shifts found in the ^1H NMR spectrum of **29** in C_6D_6 . In detail, the two resonances for the aromatic protons at the benzene

perimeters (7.11 and 7.03 ppm versus 7.42 and 7.28 ppm in **18**) and the signal arising from the bridging CH fragment (5.59 ppm relative to 5.62 ppm in **18**), experience a stronger electronic shielding effect expressed by a more pronounced upfield shift.

Moreover, complex **29** crystallizes in the triclinic space-group $P\bar{1}$ and was refined as a four-fold non-merohedral twin. The asymmetric unit contains four equivalents of non-crystallographic C_{2v} symmetric **29** and four lattice hexane molecules (see Figure 5-11 in the appendix). The central magnesium dication displays a five-fold trigonal-bipyramidal coordination (*Addison* parameter $\tau_5 = 0.77$).^[243] Like in **18**, the equatorial plane is spanned by a chloride substituent and two imine nitrogen atoms of the chelating monoanionic ligand **26**, while two THF donor molecules reside at the apical positions (Figure 2-27).

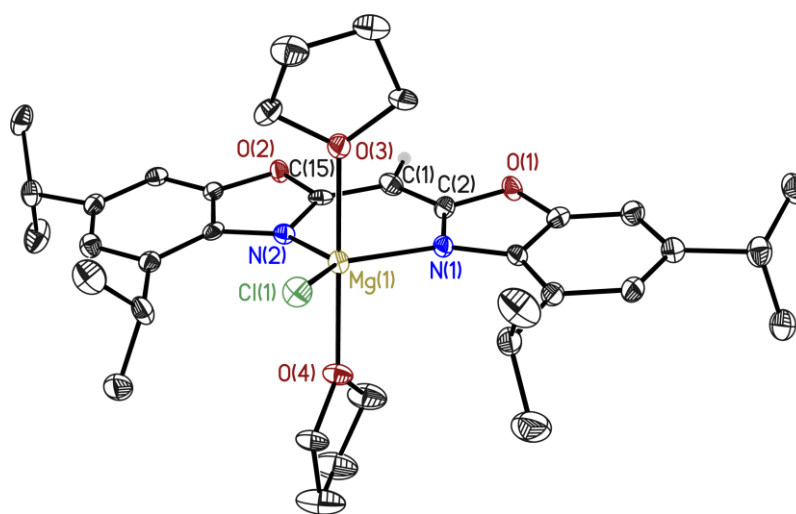


Figure 2-27. Solid-state structure of $[\text{MgCl}(\text{THF})_2\{(4,6\text{-}i\text{Pr-NCOC}_6\text{H}_2)_2\text{CH}\}]\cdot\text{hexane}$ (**29**). Anisotropic displacement parameters are depicted at the 50% probability level. Hydrogen atoms are omitted for clarity, except for the one at the bridging methylene position. Three additional molecules of **29** as well as four lattice hexane molecules present in the asymmetric unit are omitted as well. Reprinted with permission from reference^[4]. Copyright 2017, American Chemical Society.

Concerning the ligand framework of the four molecules present in the asymmetric unit, the butterfly-like folding angle between the heteroaromatic side arms ranges from $1.99(9)^\circ$ in the least bend structure to $15.72(6)^\circ$ in the most folded one. As can be seen from Table 2-15 and the superposition plot in Figure 2-28 (*vide infra*), the Mg(II) ion in **18** (blue) shows an in-planar arrangement with respect to the chelating C_3N_2 plane. In contrast, the cation in **29** (red) exhibits a significant dislocation of $0.412(5)$ to $0.547(4)$ Å from this moiety in contrast to the vanishingly low $0.010(2)$ Å in **18**. Most likely, this can be ascribed to the reduced steric demand of the *i*Pr substituents in **29**, diminishing the kinetic barrier for the magnesium dication to leave an in-planar arrangement.

Table 2-15. Selected bond lengths [\AA] and angles [$^\circ$] of **29**.

Mg(1)–N(1)	2.114(3), 2.098(3), 2.100(3), 2.100(3)	C(1)–C(2)	1.397(5), 1.392(5), 1.392(5), 1.390(5)	C(15)–O(2)	1.383(4), 1.377(4), 1.379(4), 1.389(4)
Mg(1)–N(2)	2.109(3), 2.106(3), 2.098(3), 2.101(3)	C(1)–C(15)	1.389(5), 1.391(5), 1.383(5), 1.397(4)	Mg(1)–C ₃ N ₂ dist.	0.435(4), 0.547(4), 0.412(5), 0.437(4)
Mg(1)–Cl(1)	2.336(2), 2.318(2), 2.332(2), 2.339(2)	N(1)–C(2)	1.325(5), 1.336(5), 1.335(5), 1.332(5)	N(1)–Mg(1)–N(2)	94.1(1), 94.4(1), 93.8(1), 94.2(1)
Mg(1)–O(3)	2.114(3), 2.103(3), 2.112(3), 2.106(3)	N(2)–C(15)	1.341(5), 1.341(4), 1.336(5), 1.330(4)	C(2)–C(1)–C(15)	124.8(3), 125.2(3), 125.0(3), 124.0(3)
Mg(1)–O(4)	2.102(3), 2.116(3), 2.127(3), 2.107(3)	C(2)–O(1)	1.384(4), 1.379(4), 1.383(4), 1.384(4)	Folding angle	1.99(9), 15.72(6), 4.27(8), 13.35(5)

The asymmetric unit contains four equivalents of complex **29**. Hence, four values are given for each parameter.

Symmetry transformations used to generate equivalent atoms: #1: $-x+2, -y+1, -z+1$; #2: $-x, -y+1, -z$.

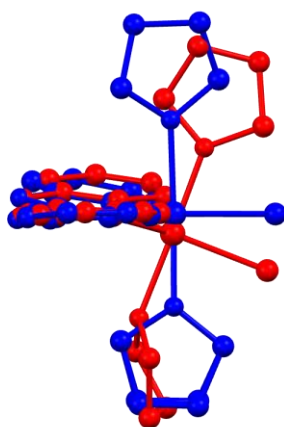


Figure 2-28. Superimposition of the molecular structures of **29** (red) and **18** (blue). Hydrogen atoms and the corresponding *i*Pr/*t*Bu substituents are omitted for clarity. Reprinted with permission from reference^[4]. Copyright 2017, American Chemical Society.

In the case of **18**, the cation is locked between the inwardly pointing methyl groups of the *t*Bu substituents bound at the 4-positions (also see Figure 2-29, *vide infra*). The observed N–C_{ipso} distances within the six-membered metalla-heterocycle span the narrow range from 1.325(5) to 1.341(5) \AA , consistent with efficient delocalized bonding.^[187, 188] Because of a decreased steric repulsion, the N–M distances in **29** cover the narrow array of 2.098(3) to 2.114(3) \AA and are considerably shortened with respect to the corresponding values of 2.1786(2) and 2.1602(2) \AA found in **18**. The same trend can be derived for the correlating N–Mg–N and C_{ipso}–C(1)–C_{ipso} angles. In **29** they range from 93.84(1) $^\circ$ to 94.38(1) $^\circ$ and 124.0(3) $^\circ$ to 125.2(3) $^\circ$, respectively, while being significantly widened in **18** (99.83(6) $^\circ$ and 128.9(2) $^\circ$).

2.4.3.2 Excursus: Percent Buried Volume (%V_{bur}) Calculations

The next step was to gain a firm estimation of the steric demand and the offered shielding capabilities of each ligand system towards the coordinated magnesium dication. For this purpose, percent buried volume (%V_{bur}) and topographic steric map calculations were carried out for the

monoanionic ligand platforms in compounds **29**, the closely related **18**, as well as bis(oxazol-2-yl)methanide derived species $[\text{ZnMe}\{\text{tBuBOX}\}]$ (**A**).^[250] Because of the lack of metal complexes comprising the monoanionic *i*PrBOX, this ligand system is not considered. For comparison, the closely related *i*Pr- and *t*Bu-substituted NacNac ligands in $[\text{Mg}\{\text{R}^{\text{NacNac}}\}_2]$ ^[251] (**B**, R = *i*Pr) and (**C**, R = *t*Bu) and the popular Dipp-substituted congener in $[\text{MgCl}(\text{THF})\{\text{Dipp}^{\text{NacNac}}\}]$ ^[252] (**D**) are also considered (Figure 2-29). For computational details, see Subchapter 4.1.5.

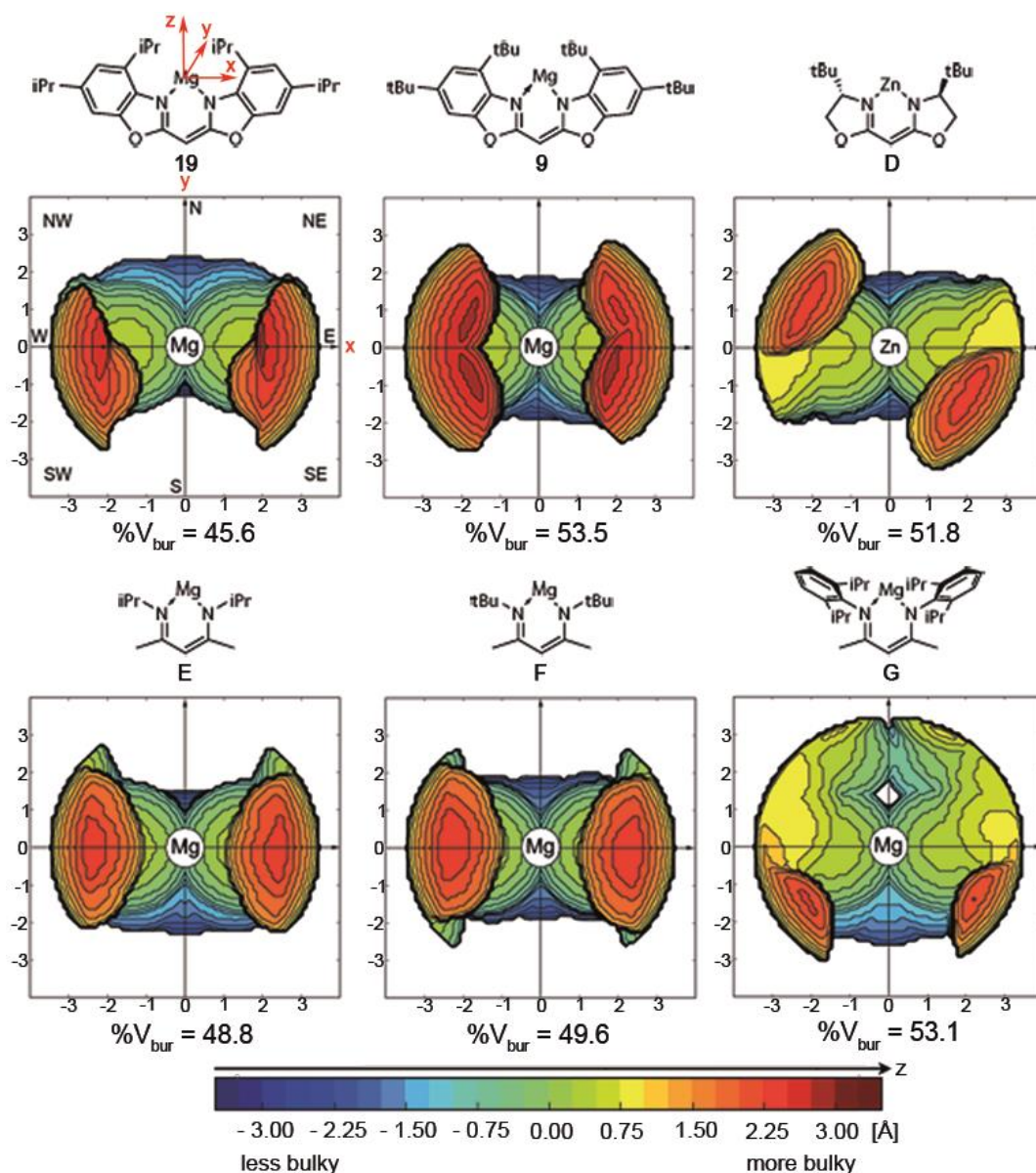


Figure 2-29. Percent buried volumes ($\%V_{\text{bur}}$) and topographic steric maps of compounds **18**, **29** and **A-D**. For clarity, only the relevant metal ion and the considered dicoordinate ligand are depicted. The orientation of the ligand as well as the notation of quadrants as NE (northeast), SE (southeast), SW (southwest) and NW (northwest) for **29** is valid for all systems and steric maps. For structures that show several molecules in the asymmetric unit or more than one molecule of the considered ligand attached to the metal ion, averaged $\%V_{\text{bur}}$ values are given. Adapted with permission from reference^[4]. Copyright 2017, American Chemical Society.

The steric map of **29** reveals good shielding properties ($\%V_{\text{bur}} = 45.6$) of the coordination pocket within this system (Figure 2-29: top, left). An additional feature responsible for the dislocation of the metal from the chelating plane is revealed when taking a closer look at the CH hydrogen atoms of the C4 *iPr* groups pointing in toward the coordination pocket (red bulges in SW and SE quadrants). Because they already claim an in-planar arrangement to the C_3N_2 scaffold, the Mg(II) ion is forced to leave this plane to evade steric congestion, resulting in an upwardly aligned MgCl bond and a dislocation of the metal ion. Proceeding with structure **18**, the steric map of this complex reveals a sufficient shielding of the MgCl unit, which is almost perfectly positioned between the four inwardly pointing methyl groups visualized by the red bulges in all four quadrants (Figure 2-29: top, middle). In this arrangement, an enhanced charge delocalization between the metal ion and the ligand framework is assured. Additionally, the *tBu* substituents offer a fair shielding on top and underneath *via* wrapping around the MgCl moiety, resulting in the highest $\%V_{\text{bur}}$ value of 53.5% of all of the considered structures. Despite that the coordination pocket of the chiral BOX ligand in **A** is characterized by a SW and NE groove (Figure 2-29: top, right), the *tBu* substituents, which correlate with the red bulges that protrude into the NW and SE, provide sufficient shielding in these directions. This results in a $\%V_{\text{bur}}$ of 51.8% that is only slightly smaller than in **29**.

Interestingly, the *iPr*- and *tBu*-substituted NacNac ligands in **B** and **C** give rise to almost identical topographic steric maps and $\%V_{\text{bur}}$ values of 48.8% and 49.6%, respectively. These values lie between those of the bis(benzoxazol-2-yl)methanide ligand systems in **29** and **18** (Figure 2-29: bottom, left and middle). The molecular structures of **D**, containing the popular ^{Dipp}NacNac ligand, and complex **29** share some common structural features: Despite the different tetrahedral coordination, the metal in **D** shows a similar dislocation of 0.534 Å from the chelating C_3N_2 plane as well as a comparable N–Mg–N bite angle and N–Mg distances. **D** exhibits a coordination pocket that almost covers the entire area. With angles of 73.3° and 69.9°, the parent Dipp substituents are considerably twisted away from a perpendicular alignment with respect to the chelating C_3N_2 plane. This is visualized by the strong bulges in the SW and SE and rather depleted NW and NE regions in the steric map of this structure (Figure 2-29: bottom, right). The $\%V_{\text{bur}}$ value was calculated to be 53.1%, which is only slightly smaller than that in the methanide supported **18**.

In light of the substituents bending away from the coordination pocket, the shielding abilities of the *iPr*-substituted bis(benzoxazol-2-yl)methanide in **29** ($\%V_{\text{bur}}$ of 45.6%) are still good and comparable to those of the *iPr*- and *tBu*-substituted NacNac systems in complexes **B** and **C**. The *tBu*-substituted bis(benzoxazol-2-yl)methanide in **18** and the Dipp-substituted NacNac ligand in **D** exhibit $\%V_{\text{bur}}$ values of 53.5% and 53.1%, respectively. These are the best shielding capabilities within the considered series, being most pronounced in the methanide **18**. Nevertheless, both bis(benzoxazol-2-yl)methanides provide sufficient shielding to the cation, preventing the

complexes from aggregation. Regarding the coordination pockets in the MgCl complexes, the size offered by the *t*Bu-substituted methanide seems to be the most suitable. Here, the magnesium ion exhibits the least dislocation from the chelating C₃N₂ ligand plane.

2.4.3.3 Excursus: Electronic Structure Analyses

In order to gain some insight into the electronic structure and the related donating properties of the examined ligand systems, electronic structure analyses were carried out in collaboration with *Teuteberg* from the *Mata* group. For computational details, see Subchapter 4.1.4. In a related study, this tool was already successfully applied to clarify the structural description of 2-picoyllithium,^[253] that turned out to be best described as a lithium amide, rather than by lithium-carbanion interactions. Hence, the lithium complexes **13** and **27** as well as [Li(THF){*t*BuNacNac}] (**E**),^[50] [Li(THF){DippNacNac}]^[25] (**F**) and amide-functionalized [Li(Et₂O){*N*-DippNacNac}]^[28] (**G**) were taken into account. The latter is based on an electron-rich so-called *N*-NacNac ligand system, which bears NMe₂ groups at the β -carbons and was reported only very recently. For these systems, NPA charges were calculated and NBO as well as NRT analyses were carried out. All calculations were performed at the BP86-D3/def2-TZVP level of theory. Some calculations were repeated at the B3LYP-D3/def2-TZVP level of theory to ensure consistency of the results and only minor differences could be observed.

The NPA only reveals minor differences between the systems. As expected, all systems show an almost entirely ionic lithium and both, the coordinating nitrogen atoms *N* and *N'* as well as the bridging γ -C atom are assigned with significant negative charges. The two bis(benzoxazol-2-yl)methanide systems **27** and **13** show only slightly different charge distributions, therefore exhibiting similar donating properties (Figure 2-30).

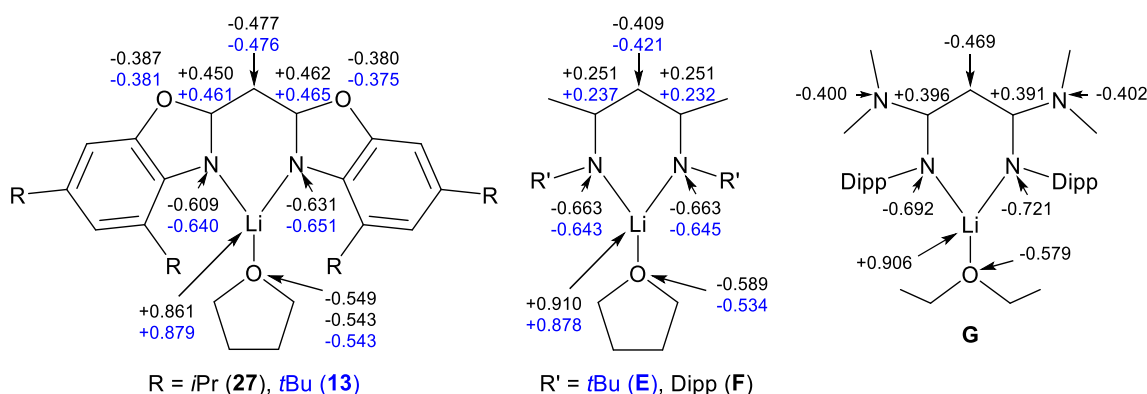


Figure 2-30. Calculated NPA charges for selected lithium compounds **27**, **13** and **E-G** at the BP86-D3/def2-TZVP level. Adapted with permission from reference^[4]. Copyright 2017, American Chemical Society.

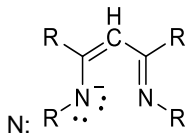
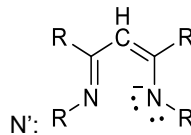
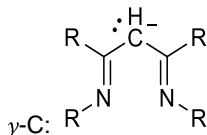
Still, a stronger asymmetric charge distribution, e.g., at the coordinating nitrogen atoms, in **27** (-0.609 e and -0.631 e to -0.640 e and -0.651 e in **13**) is found. Accompanied by considerably

deviating Li-N and N-C_{ipso} distances in **27** (see Table 2-14), these features indicate a slightly less pronounced delocalized imino-enamide ligand description than in **13** or the highly symmetric NacNac species **E** and **F**. Interestingly, a comparable asymmetric charge distribution was calculated for the N-NacNac-based species **G**. In addition, an averaged charge of -0.401 e residing at the nitrogen atoms in its ligand periphery fits quite well to averaged values of -0.384 e and -0.378 e calculated for the oxygen atoms in **27** and **13**, indicating an enhanced conjugation throughout the oxygen atoms in the methanides. In general, slightly larger charges of average -0.64 e (**E**), -0.66 e (**F**) and -0.71 e (**G**) at the coordinating nitrogen atoms indicate slightly enhanced donating properties for the NacNac systems.

Standard NBO analysis for all systems results in a carbanionic diimino structure as the reference *Lewis* representation. In all cases, however, the lone pair on the bridging γ -C atom is assigned an occupation number of only about 1.3 electrons, and second-order perturbation theory indicates strong delocalization towards the N/N'-C_{ipso} anti bonds. Thus, the electronic structure is strongly delocalized, somewhere between a carbanionic diimino and an imino-enamide structure. While, in principle, the perturbation interaction energies provide useful insight into the donating properties, interpretation based on a single *Lewis* representation is not meaningful in this case.

Because the single carbanionic structure does not represent the calculated electronic structure very well, NRT analyses were performed to estimate the influence of other resonance structures. Although the carbanionic diimino structure is found to have the largest contribution for all five systems, it only contributes to a small extent for the NacNac-based structures **E** (21.5%), **F** (12.3%) and **G** (9.2%) and even less for **13** and **27** (8.3% and 7.7%, respectively). Hence, a large number of small contributions from several resonance structures have to be taken into account. Summation and renormalization of contributions for all structures featuring a lone pair at γ -C or one of the coordinating nitrogen atoms N and N' leads to much more comparable results (Table 2-16).

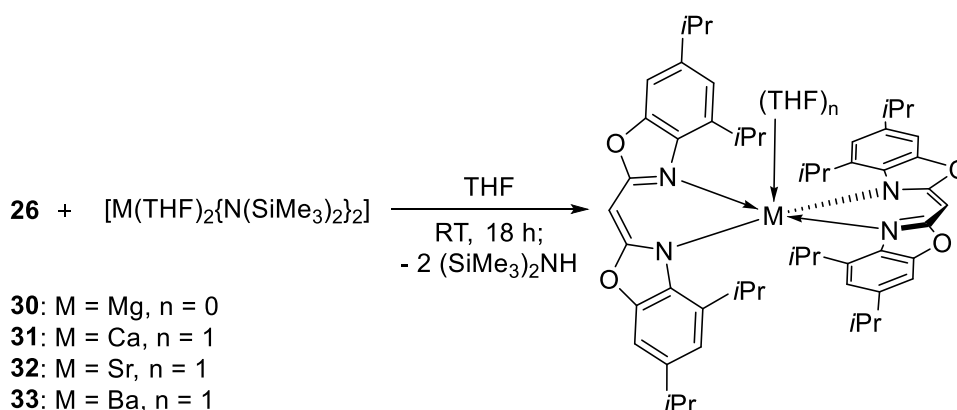
Table 2-16. Fraction of NRT resonance structures exhibiting a carbanionic diimino (lone pair at the bridging γ -carbon) or an imino-enamide (two lone pairs at N or N') structure for **27**, **13** and **E-G**. Adapted with permission from reference [4]. Copyright 2017, American Chemical Society.

			
27	37.3	39.7	17.9
13	36.6	39.5	17.2
E	34.0	34.2	24.6
F	36.0	36.0	19.6
G	39.9	35.0	17.4

The NacNac-based compounds **E** and **F** show more contribution from carbanionic structures (24.6% and 19.6%, respectively) than the electron-rich *N*-DippNacNac-derived **G** (17.4%) and the bis(benzoxazol-2-yl)methanide systems **27** and **13** (17.9% and 17.2%, respectively) and slightly less from amidic structures. While the summation revealed all five systems to be significantly more amidic than carbanionic, it seems reasonable to assign the electron-rich systems **G**, **27** and **13** a somewhat more amidic character compared to **E** and **F**. This also indicates that the electron-rich bis(benzoxazol-2-yl)methanide systems could act as better donor systems than the “normal” NacNac ones and even than the electron-rich *N*-DippNacNac systems.

2.4.3.4 [M(THF)_n{(4,6-*i*Pr-NCOC₆H₂)₂CH₂}₂] (**30-33**) (M = Mg, Ca, Sr, Ba; n = 0-1)

To obtain heteroleptic amide complexes of **26**, group 2-HMDS compounds were applied again as reagents in concerted deprotonation-metalation reactions. Unfortunately, a treatment of **26** with [M(THF)₂{N(SiMe₃)₂}₂] (M = Mg, Ca, Sr and Ba) gave the corresponding homoleptic compounds [M(THF)_n{(4,6-*i*Pr-NCOC₆H₂)₂CH₂}₂] (M = Mg, n = 0 (**11**); M = Ca, n = 1 (**12**); M = Sr, n = 1 (**13**); M = Ba, n = 1 (**14**)) in yields of 40-71% at room temperature (Scheme 2-32).



Scheme 2-32. Syntheses of [M(THF)_n{(4,6-*i*Pr-NCOC₆H₂)₂CH₂}₂] (**30-33**) (M = Mg, Ca, Sr, Ba; n = 0-1). Adapted with permission from reference [4]. Copyright 2017, American Chemical Society.

Complex **30** displays a four-fold distorted tetrahedral MgN₄ arrangement made up by four ring nitrogen atoms of two monoanionic ligands **26**. The higher homologues **31-33** all show an isotype five-fold coordination with one additional THF donor molecule to saturate the coordination sphere. With τ_5 parameters of 0.46 (**31**), 0.48 (**32**) and 0.37 (**33**), all three structures adopt a distorted square-pyramidal-based coordination of the dication, being most pronounced in the barium derivative. Against all expectations, the ionic radius of 1.35 Å for the barium(II) ion still is not large enough to accommodate a second THF donor molecule.^[191] All four compounds show an exclusive κ^2 -coordination by the imine ring nitrogen atoms and a similar puckering of the six-membered metalla-heterocycle (Figure 2-31).

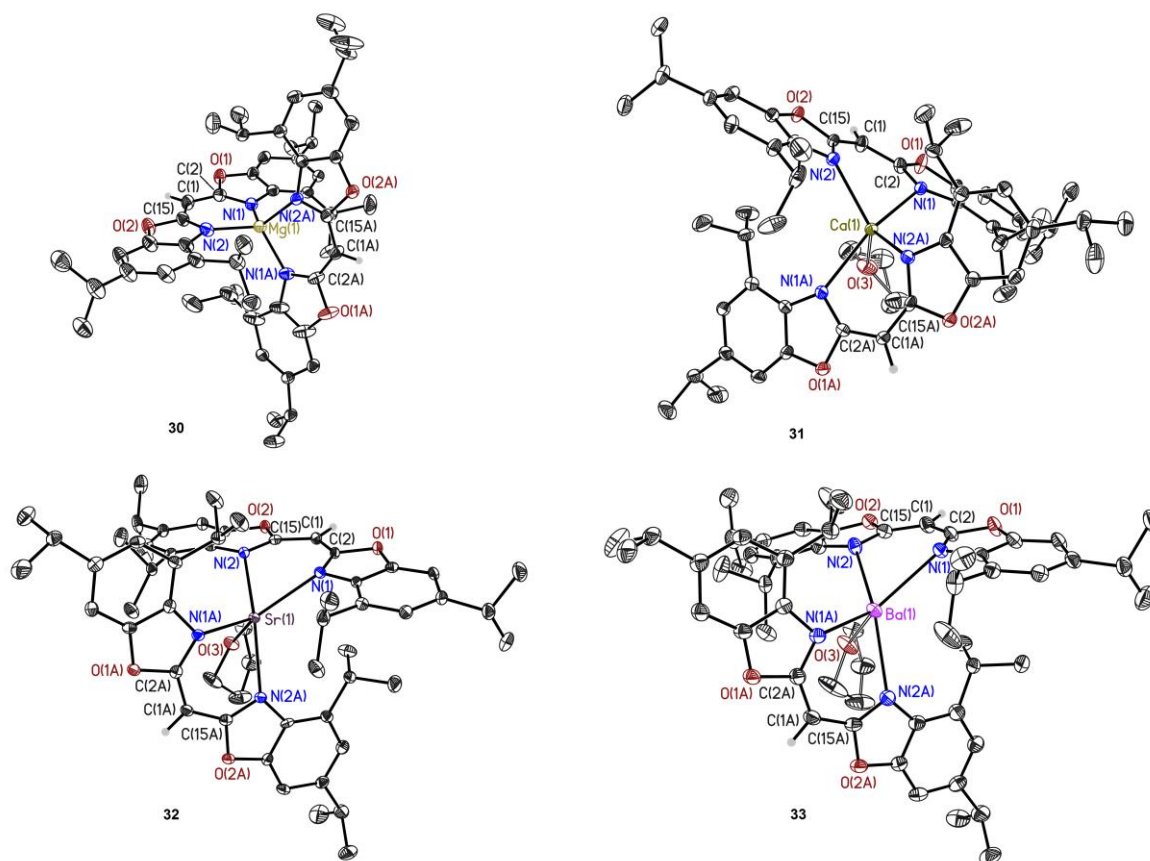


Figure 2-31. Solid-state structures of complexes **30-33**. Anisotropic displacement parameters are depicted at the 50% probability level. Hydrogen atoms are omitted for clarity, except for those at the bridging methylene positions. A lattice hexane molecule present in the asymmetric unit of **30** is omitted as well. *Adapted with permission from reference* ^[4]. Copyright 2017, American Chemical Society.

With butterfly-like folding angles between $10.76(3)^\circ$ and $13.34(3)^\circ$, this feature is most prominent in the tetrahedral structure **30**. The square-pyramidal-based species **31-33** exhibit angles between $1.98(5)^\circ$ and $8.24(4)^\circ$ and show enhanced planarity due to the present change in geometry. The latter is accompanied by a decrease in steric crowding. The opposite trend is observed for metal dislocation from the chelating C_3N_2 plane. Here, the distances gradually increases along the line Mg ($0.018(2)/0.072(2) \text{ \AA}$) < Ca ($1.182(3) \text{ \AA}$) < Sr ($1.247(4)/1.130(4) \text{ \AA}$) < Ba ($1.281(2) \text{ \AA}$). The C_3N_2 moiety provides both, σ - as well as π -electron density. Because polarizability and softness of the dications rise with increasing ionic radius from Mg^{2+} to Ba^{2+} , the increasing out-of-plane arrangement also indicates a more and more pronounced metal- π interaction of the cations to the non-directed π -density of the delocalized aromatic system. Furthermore, in **30-33** the N-M distances also increase along the row Mg < Ca < Sr < Ba (average values: Mg 2.045 \AA , Ca 2.424 \AA , Sr 2.569 \AA , Ba 2.733 \AA), while the corresponding N-M-N bite angles decrease with cation size: Mg > Ca > Sr > Ba (average values: Mg 95.0° , Ca 80.81° , Sr 75.2° , Ba 70.83°). These observations are in tune with increasing ionic radii from Mg^{2+} (0.66 \AA) over Ca^{2+} (1.00 \AA) to Sr^{2+} (1.18 \AA) and Ba^{2+} (1.35 \AA).^[191]

Table 2-17. Selected bond lengths [Å] and angles [°] of **30-33**.

	30 (M = Mg)	31 (M = Ca)	32 (M = Sr)	33 (M = Ba)
M(1)–N(1)	2.046(1), 2.041(1)	2.440(2)	2.579(2), 2.550(2)	2.726(1)
M(1)–N(2)	2.048(1), 2.046(1)	2.409(2)	2.569(2), 2.578(2)	2.740(1)
C(1)–C(2)	1.391(2), 1.386(2)	1.399(3)	1.388(4), 1.390(4)	1.399(2)
C(1)–C(15)	1.386(2), 1.389(2)	1.385(3)	1.397(4), 1.393(4)	1.398(2)
N(1)–C(2)	1.340(2), 1.336(2)	1.323(3)	1.336(3), 1.332(3)	1.332(2)
N(2)–C(15)	1.341(2), 1.339(2)	1.334(3)	1.328(3), 1.329(3)	1.325(2)
C(2)–O(1)	1.373(2), 1.376(2)	1.392(3)	1.391(3), 1.390(3)	1.396(2)
C(15)–O(2)	1.374(2), 1.373(2)	1.394(3)	1.390(3), 1.393(3)	1.400(2)
M(1)–C ₃ N ₂ dist.	0.018(2), 0.072(2)	1.182(3)	1.247(4), 1.130(4)	1.281(2)
N(1)–M(1)–N(2)	95.17(5), 94.83(5)	80.81(6)	74.88(7), 75.60(7)	70.83(4)
C(2)–C(1)–C(15)	123.8(1), 123.4(1)	125.5(2)	125.4(2), 125.7(2)	125.5(1)
Folding angle	13.34(3), 12.09(4), 10.76(3)	3.90(3)	1.98(5), 8.24(4)	8.01(6)

In complexes **31** and **33**, the second methanide molecule is symmetry-generated. Hence, only one value is given for each parameter. Symmetry transformations used to generate equivalent atoms: **31**: $-y+1, -x+1, -z+1/2$; **33**: $-x+1, y, -z+3/2$.

In comparison to the magnesium complex, an elongation of 0.69 Å of the M–N distance in the barium complex fits quite well to the 0.69 Å difference regarding their ionic radii.

Moreover, a cross-validation for a given set of bis(4-Me-benzoxazol-2-yl)methanide-based complexes [Mg{(4-MeNCOC₆H₃)₂CH₂}₂] (**3**) and [Ca(THF)₂{(4-MeNCOC₆H₃)₂CH₂}₂] (**4**), and related NacNac-derived structures [M^{Dipp}NacNac]₂ (M = Sr, Ba),^[190] reveals the same trends with increasing cation radii for the N–M distances and N–M–N bite angles. Here, even the dislocation of the cations from the chelating C₃N₂ plane follows a similar tendency, emphasizing on the close relationship between both ligand platforms. The same is valid among the related *i*Pr- and *t*Bu-substituted homoleptic β-diketiminato complexes [M^{*i*Pr/*t*Bu}NacNac]₂ (M = Mg, Ca, Sr, Ba).^[37, 251] While **30-33** solely exhibit κ²-N,N'-coordinations to the metal ions, different motifs are reported for the related NacNac structures. The magnesium complexes in both ^RNacNac (R = *i*Pr, *t*Bu) structures show a κ²-coordination as well. In contrast, in association with the *t*Bu-substituted NacNac ligand, the heavier alkaline-earth-metals (Ca, Sr and Ba) preferably adopt η⁵-binding modes consistent with the preference of those cations for non-directed π-density. In the *i*Pr-substituted systems, the Ca compound maintains a κ²-N,N'- and the Sr complex a η⁵-coordination, due to decreased steric crowding. Only the barium species does not fit the trend, now exhibiting an unprecedented mixed coordination pattern to two Ba²⁺ cations.

The structurally characterized less bulky solvated group 2 aminoiminophosphoranates [M(THF)_n-{(NSiMe₃)₂PPh₂}₂]^[254] (M = Be to Ba; n = 0-2) and benzamidinates [ML_n{(NSiMe₃)₂CPh}₂]^[255-258]

(M = Mg to Ba; L_n = THF, benzonitrile, 1,2-dimethoxyethane), show the same trends for metal dislocation with increasing cation size like in **30-33**, despite exhibiting a less pronounced out-of-plane arrangement. In the phosphoranates it increases gradually from 0.098 Å for Be²⁺ to 0.557 Å for Ba²⁺, while for the latter, values between 0.054 Å for Mg²⁺ and 0.816 Å for Ba²⁺ are reported. These dislocations indicate a less populated and therefore less attractive π-density in both ligand systems. The aforementioned comparable influences on N-M distances and N-M-N bite angles are observed as well. In comparison to **30-33**, considerable elongated N-M distances are reported as steric demand increases within the narrowed N-P-N and N-C-N coordination pockets. Interestingly, the group 2 diazasulfonates [M(THF)₂{(NSiMe₃)₂SPh}₂]^[259] (M = Ca to Ba), which bear an electron-withdrawing phenyl substituent at the ligand backbone, show no metal dislocation from the chelating plane. An increasing dislocation of the metal with increasing ionic radius is observed with an electron-donating substituent at this position like in the corresponding triazasulfites [M(THF)_n{(NSiMe₃)₂SN(SiMe₃)₂]^[259] (M = Mg, Sr, n = 0-1).

In addition, structures **30-33** were studied by ¹H- and ¹³C{¹H} NMR spectroscopy. All recorded spectra show a distinctive pattern of chemical shifts arising from the monoanionic ligand scaffold and, in **31-33**, from an additionally attached THF donor molecule. Regarding the ¹H NMR spectra of the discussed complexes, the resonances arising from the ligand molecules show a ratio of 4:4:2:4:4:24:24 for the aromatic protons at the benzene perimeters (4:4), the bridging CH moiety (2) and the corresponding CH (4:4) and CH₃ (24:24) moieties of the *i*Pr substituents at the 4- and 6-positions, respectively. This observation indicates that all four compounds adopt a C_{2v} symmetric geometry in solution, resulting in one set of chemically and magnetically equivalent heteroaromatic side arms as well as ligand molecules in each structure. As summarized in Figure 2-32 (*vide infra*), some general trends within the Mg²⁺ to Ba²⁺ series can be derived from the NMR data: The ¹H NMR shifts for the C-H bridging position exhibit a continuous decline along the line Mg (5.39 ppm) > Ca (5.08 ppm) > Sr (5.02 ppm) > Ba (4.85 ppm). Because this resonance is highly indicative for the corresponding electron density accumulated in the perpendicular p-orbital being part of the aromatic system, a stronger down-field shift descending from Mg²⁺ to Ba²⁺ directly correlates with an enhanced negative charge at this position. The same trend can be deduced for the aromatic proton at the C7 position. In contrast, all remaining protons in the ligand periphery, even the *i*Pr methyl groups, exhibit a small but steady upfield shift. The carbon atoms involved in the six-membered metalla-heterocycle show a comparable tendency like the proton at the bridging moiety (Mg (59.7 ppm) > Ca (58.8 ppm) > Sr (58.1 ppm) > Ba (56.9 ppm)). As was also stated in a related study on homoleptic alkaline-earth-metal NacNac complexes, a steady decrease in chemical shifts in the row Mg > Ca > Sr > Ba is related to an increasing ionicity accompanied by an enhanced charge delocalization through the ligand system.^[190] Concerning the ligand backbone, only the chemical shifts of the quaternary C4 and C6 ring carbon atoms seem to be affected by a cation change.

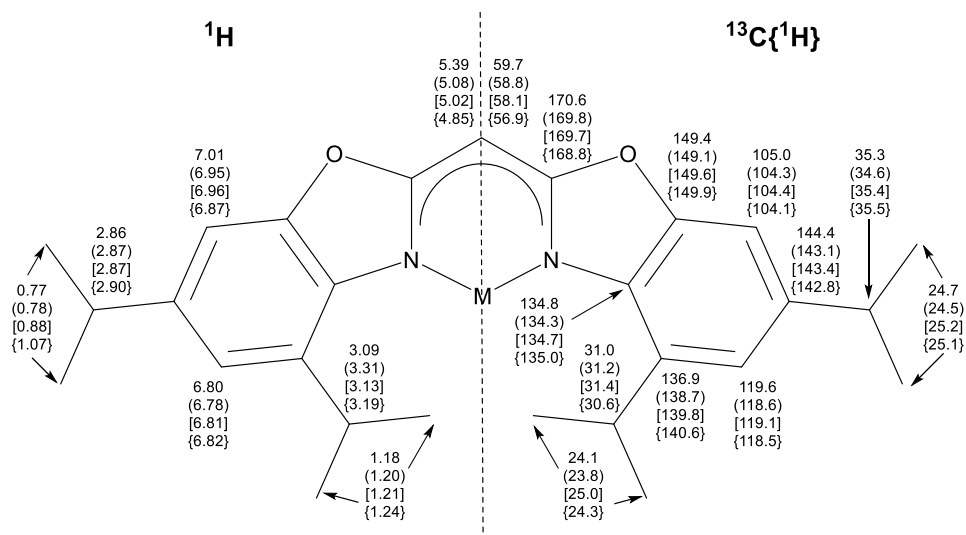


Figure 2-32. ^1H - (left) and $^{13}\text{C}\{^1\text{H}\}$ NMR shifts (right) of the complexes: $[\text{M}(\text{THF})_n\{(4,6\text{-}i\text{Pr}\text{-NCO}\text{C}_6\text{H}_2\text{-CH})_2]$ ($\text{M} = \text{Mg}$, $n = 0$ (**30**); $\text{M} = \text{Ca}$, $n = 1$ (**31**); $\text{M} = \text{Sr}$, $n = 1$ (**32**); $\text{M} = \text{Ba}$, $n = 1$ (**33**)). Measurements were performed in $[\text{D}_8]\text{THF}$, except for the $^{13}\text{C}\{^1\text{H}\}$ (C_6D_6) of **31**, due to a poor solubility of pure crystalline **31** in $[\text{D}_8]\text{THF}$. The stacks of numbers represent the values for the corresponding Mg, (Ca), [Sr] and {Ba} compounds. Reprinted with permission from reference ^[4]. Copyright 2017, American Chemical Society.

On the one hand, for the C6 carbon, again a decreasing chemical shift on the way from Mg (144.4 ppm) to Ba (142.8 ppm) can be reported. On the other hand, for the corresponding C4 carbon, the opposite trend is observed (Mg 136.9 ppm to Ba 140.6 ppm). Because the charge accumulation increases with an increasing ionic character along the array $\text{Mg}^{2+} < \text{Ca}^{2+} < \text{Sr}^{2+} < \text{Ba}^{2+}$, this observation is in tune with the negative charge being more and more pushed into the benzene perimeter and obviously preferably accumulated at the C6 position. The unique tendencies in NMR shifts observed within the series of the discussed homoleptic compounds **30-33** emphasize this method to be indicative to charge distribution analysis.

3 SUMMARY & OUTLOOK

This thesis focused on the development and synthesis of novel sterically demanding bis(benzoxazol-2-yl)methane ligand systems and their introduction to group 1 and 2 metal coordination. In addition, special focus was put on the preparation of alkaline-earth-metal halide and -amide complexes for subsequent reduction attempts on the way to reduced Ae^I-Ae^I dimers. In the three parts of this work, it was finally possible to exceed the family of bis(benzoxazol-2-yl)methane ligand scaffolds to bulkier representatives carrying *i*Pr and *t*Bu substituents adjacent to the coordination pocket (Figure 3-1). As a result, first steps to mimic better the shielding abilities of the paragon NacNac ligand were made. Thereupon, varieties of new group 1 and 2 complexes were accessed and first reduction attempts were carried out.

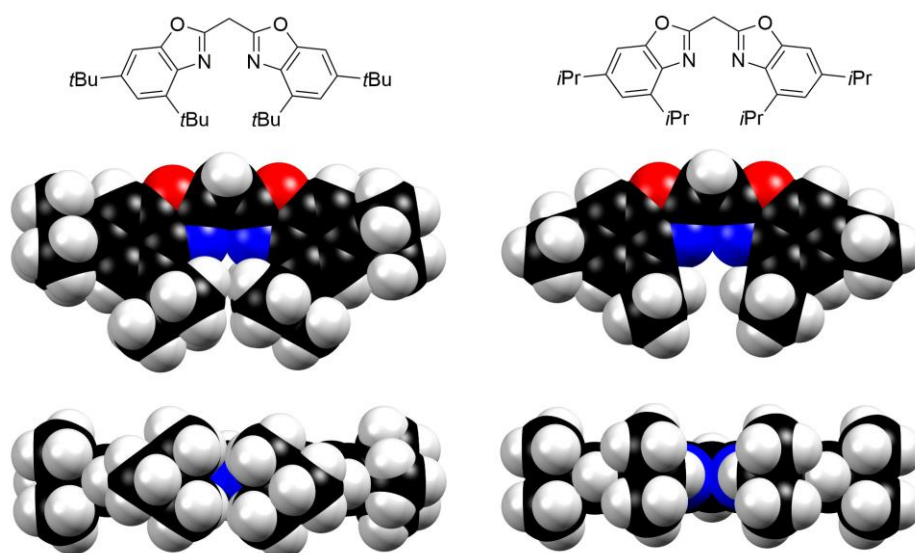


Figure 3-1. Space-filling models of the prepared bulky methane ligand systems: Left: (4,6-*t*Bu-NCO-C₆H₂)₂CH₂) (7); Right: (4,6-*i*Pr-NCOC₆H₂)₂CH₂) (26).

In the first part of this thesis, research focused on the less bulky bis(4-Me-benzoxazol-2-yl)methane (**1**) ligand system, because my predecessor *Dauer* successfully introduced this ligand to group 13 coordination. In light of a bulk of prepared heteroleptic group 13 alky- and halide complexes, start of an extension to early main-group elements on this ligand scaffold was compelling. Subsequently, the successful preparation and characterization of a potassium precursor complex **2** for subsequent salt metathesis reactions can be reported. Furthermore, the homoleptic alkaline-earth-metal compounds **3** and **4** were accessed *via* salt metathesis of **2** and/or conversion of **1** with a suitable group 2 organometallic reagent. From the solid-state structures of **2-4**, general trends caused by increasing ionic radii could be derived.

To conclude, the intended syntheses of monoanionic **1**-supported heteroleptic group 2 halide- or amide complexes for subsequent reduction were unsuccessful. Formation of the homoleptic complexes **3** and **4** is assumed to proceed *via Schlenk* equilibrium-like ligand scrambling, promoted by the limited steric shielding offered by the methyl substituents adjacent to the coordination pocket. To stabilize the desired heteroleptic group 2 compounds, implementation of bis(benzoxazol-2-yl)methanides that carry substituents with enhanced bulkiness at the 4-positions close to the coordination pocket seemed to be obligatory. As a result, the preparation of more bulky ligands that meet those requirements was pursued.

In the second part of this thesis, the sterically demanding ligand system bis(4,6-*t*Bu-benzoxazol-2-yl)methane (**7**) was successfully prepared in a straight-forward three-step synthesis starting from 3,5-di-*tert*-butylphenol. Concerted deprotonation-metalation reactions with group 1 reagents like *t*BuLi or KH were carried out, yielding the respective precursor complexes **13**, **14** and **16**. Furthermore, from reactions with the *Hauser* bases (*i*Pr)₂NMgX (X = Cl, Br) the related five-fold coordinated magnesium halide species **18/18a** were accessed. For the prepared complexes, several different coordination motifs adopted by the methanide ligand **7** can be reported. Especially potassium complex [K(18-crown-6){(4,6-*t*Bu-OCNC₆H₂)₂CH}·(H₂O)_{0.35}]·(THF)₂ (**16**) should be mentioned as highlight. Compound **16** is a rare example of a water-containing organopotassium species that proved that organometallic syntheses and the presence of protic solvents like water do not automatically have to exclude each other (Figure 3-2).

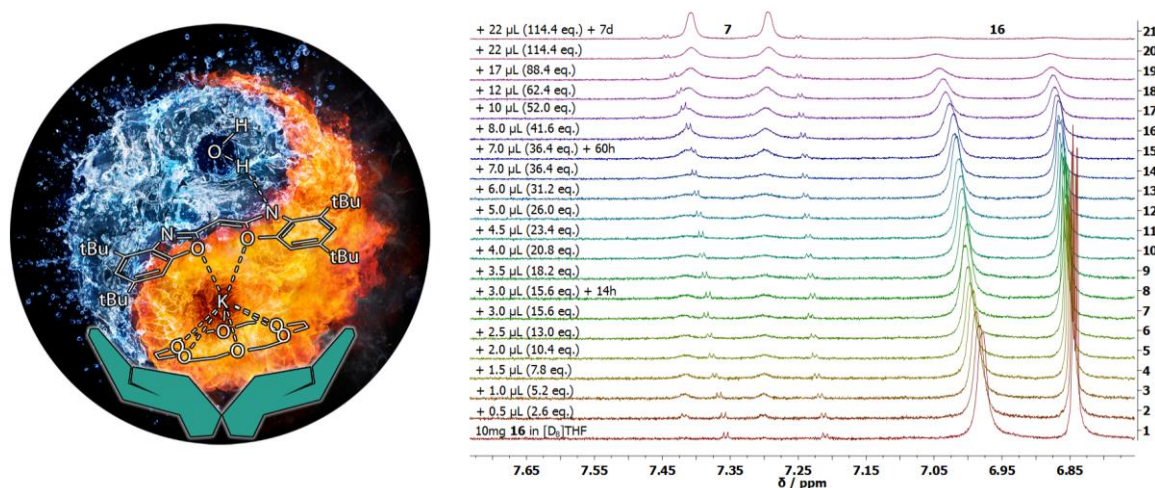


Figure 3-2. Left: Artistic illustration of the unique solid-state structure of **16** that figuratively unifies fire and water in one compound. Right: Excerpt from the water titration experiment carried out with **16**, which revealed a pronounced water resistant character of the complex. Figures reprinted/adapted with permission from reference^[3]. Copyright 2017, John Wiley and Sons.

Complex **16** exhibits several remarkable features in the solid-state as well as in solution that were extensively studied by X-ray diffraction and DOSY NMR experiments, which are discussed in detail. For example, the methanide ligand shows an unprecedented all-O-coordination to the

potassium cation. In addition, ^1H NMR water titration experiments confirmed a high resistance of **16** against hydrolysis. In comparative water titration experiments with the related potassium complex **14**, the 18-crown-6 ether molecule was certified to play a crucial role for the water resistant character of **16**. A reaction of **16** with dry air led to the formation of potassium complex **17** that comprises an oxidized ligand backbone. Instead of a hydrogen atom, the bridging methylene position now carries a hydroxyl function. The Oxygen activation is assumed to proceed in a metal-ligand cooperative fashion.

On the way to low oxidation state $\text{Mg}^{\text{I}}\text{-Mg}^{\text{I}}$ dimers, first reduction attempts were performed with magnesium halide compounds **18/18a** utilizing potassium metal or KC_8 as reducing agents. From these reactions and in spite of the steric bulk provided by the *t*Bu substituents, the homoleptic magnesium(II) complex **19** was obtained as the sole product. An X-ray structure of **19** could not be obtained. The formation of **19** as well as the correct *N*-coordination motif were affirmed by applying LIFDI mass spectrometry and advanced NMR techniques (DOSY, NOESY, clean-inphase HSQC). In particular, a formation of **19** is assumed to proceed *via Schlenk* equilibrium ligand redistribution or disproportionation processes of an intermediate magnesium(I) species.

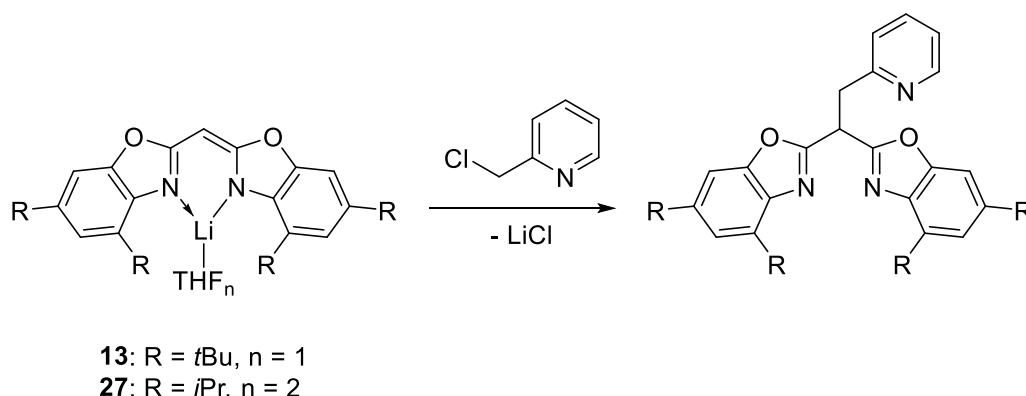
In the third part of this thesis, the bulky *iPr*-substituted bis(4,6-*iPr*-benzoxazol-2-yl)methane (**26**) ligand system was accessed *via* a seven-step procedure. For later salt metathesis reactions, lithium (**27**) and potassium (**28**) precursor compounds were prepared in a first step. Utilizing the aforementioned and well-established MgCl *Hauser* base, a synthesis of the **26**-supported magnesium chloride complex **29** for future reduction attempts was provided. In comparison to **7**, ligand system **26** shows no kinetic hindrance in concerted deprotonation-metalation reactions with *s*-block organometallics. Thus, organometallic reagents that showed no reactivity towards **7** yielded related metal complexes in combination with **26**. Subsequent conversions of **26** with group 2 HMDS compounds gave the corresponding homoleptic compounds **30-33** (Mg-Ba). Here, distinct structural trends were observed in the solid-state, which are induced by an increasing cation size within the Mg^{2+} to Ba^{2+} series. In addition, certain trends in charge distribution were derived from a comparative analysis of the ^1H - and ^{13}C NMR data of **30-33**. This indicated an increasing ionic character of the complexes as well as a pronounced charge delocalization throughout the ligand framework going from Mg^{2+} to Ba^{2+} .

Additionally, the shielding abilities offered to a coordinate metal ion by monoanionic **7** and **26** were evaluated. For this purpose, percent buried volume ($\%V_{\text{bur}}$) calculations were carried out on magnesium complexes **18** and **29** in comparison to related oxazolinato- and β -diketiminato-supported compounds. Within the set of considered complexes, calculations revealed the herein presented bulky bis(benzoxazol-2-yl)methanides **7** and **26** to show shielding capabilities that are indeed comparable to other *iPr*-, *t*Bu- or Dipp-substituted oxazolinato as well as β -diketiminato

platforms. In detail, the *t*Bu-substituted monoanionic **7** exhibits the highest % V_{bur} value of 53.5%. Even a related $\text{Dipp}^-\text{NacNac}$ -based magnesium compound shows with 53.1% an inferior value.

In comparison to related NacNac platforms, an electronic structure analysis of monoanionic **7** and **26** was carried out to shed light on their electronic structure and related donating properties. For calculation, compounds **13** and **27** as well as ${}^t\text{BuNacNac}^-$, $\text{Dipp}^-\text{NacNac}^-$ and $N\text{-Dipp}^-\text{NacNac}$ -based lithium complexes were taken into account. From NPA, only marginal differences between the considered systems could be reported. Similar charge distributions and thus donating properties were found for the bis(benzoxazol-2-yl)methanides in **13** and **27** as well as in comparison to their NacNac-supported congeners. Summation and renormalization of the results from a NRT analysis revealed especially the electron-rich methanides and the $N\text{-Dipp}^-\text{NacNac}$ structure to exhibit a more amidic than carbanionic character. In particular, the methanides in **13** and **27** exhibited the most contributions from amidic resonance structures. Still, the binding situation in all systems is best described by effectively delocalized imino-enamide and carbanionic diimino resonance structures.

In conclusion, especially the % V_{bur} calculations as well as the electronic structure analysis underscored the NacNac-like character of the prepared bulky ligand systems **7** and **26**. Nonetheless, the offered shielding abilities in the third dimension, above and underneath a formed metal heterocycle, are still not as embracing as in the case of their NacNac congeners. In future studies, special focus has to be put on the synthesis of bis(heterocylco)methane systems carrying even bulkier substituents adjacent to the coordination pocket, that supply sufficient shielding in all three dimensions (*e.g.* Dipp). As a result, a *Schlenk* equilibrium ligand scrambling yielding homoleptic species should be less favored and a successful formation of reduced $\text{Ae}^{\text{I}}\text{-Ae}^{\text{I}}$ dimers more likely. A further method to enhance the shielding abilities of the existing ligand platforms **7** and **26** might be the introduction of a third donor arm at the ligand backbone (Scheme 3-1).



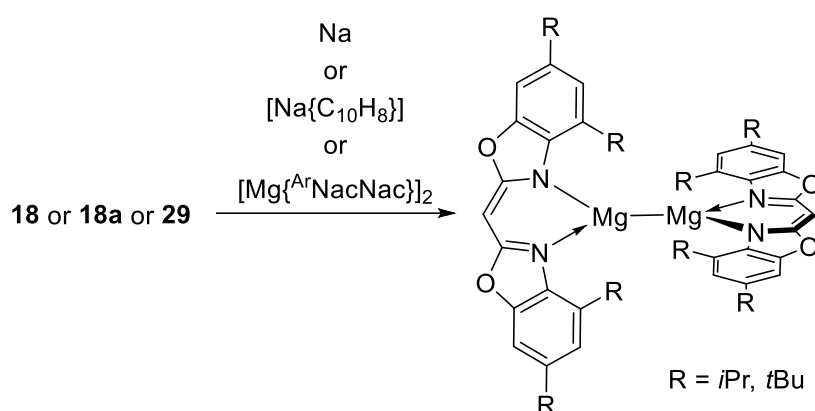
Scheme 3-1. Feasible exemplary preparation of tri-dentate scorpionate ligands starting from bis(4,6-*R*-benzoxazol-2-yl)methanide (R = *i*Pr, *t*Bu)-based lithium compounds **13** and **27**.

From reactions of the lithium salts **13** and **27** with suitable electrophiles like 2-(chloromethyl)pyridine, the formation of derived scorpionate ligand systems is feasible. This method was already

successfully applied to related bis(oxazoline) systems.^[260] By addition of a second equivalent of an alky-lithium reagent as well as of the electrophile, the corresponding *ter*-dentate ligand scaffolds might be accessed as well.

In future projects, the group 1-precursor complexes **16**, **17** and **27**, **28** still have to be evaluated in terms of their ability to undergo salt metathesis reactions with group 2 halides. Due to its enhanced hydrolysis resistance, the ability of potassium complex **16** to function as an organometallic synthon in sustainable deep-eutectic as well as protic solvents should be further investigated.

Regarding future reduction attempts on the magnesium halides **18/18a** and **29**, an application of milder reducing agents should be favored to avoid potential over reduction (Scheme 3-2).



Scheme 3-2. Alternative preparation methods on the way to 7- and **26**-supported magnesium(I) dimers applying different sodium- as well as magnesium-based reducing agents.

Reduction reactions should be repeated utilizing sodium metal, sodium naphthalene or readily accessible NacNac-based $\text{Mg}^{\text{I}}\text{-Mg}^{\text{I}}$ dimers as stoichiometrically controllable one- or two-electron sources. The latter were already successfully applied to access other reduced group 2-^[105] and group 14^[261] element dimers. In addition, these reactions could be accompanied by cyclic voltammetric measurements. From these experiments, an insight on structural changes as well as the stability of the complexes upon oxidation state variation can be gained. Moreover, determination of the corresponding redox potentials should simplify the process of finding a suitable reducing agent and if the reduction process is reversible.

Due to an increasing cation size and ionicity from Mg^{2+} to Ba^{2+} , the **26**-based complexes **30-33** show distinctive trends in the solid-state as well as in solution. For related NacNac-based compounds, an implementation to CVD film growth processes was suggested.^[37, 262] An application as precursor compounds for the preparation of heteroleptic species exhibiting catalytic activity was discussed as well.^[190, 263] Thus, in future projects, **30-33** should be evaluated in terms of their sublimation behavior as well as their ability to undergo further substitution reactions.

4 EXPERIMENTAL PART

Major parts of this chapter have been published in:

- [1] I. Koehne, R. Herbst-Irmer, D. Stalke, “Bis(4-methylbenzoxazol-2-yl)methanide in *s*-Block Metal Coordination”, *Eur. J. Inorg. Chem.* **2017**, 2017, 3322-3326.^[1]
- [2] I. Koehne, S. Bachmann, T. Niklas, R. Herbst-Irmer, D. Stalke, “A Novel Bulky Heteroaromatic-Substituted Methanide Mimicking NacNac: Bis(4,6-*tert*-butylbenzoxazol-2-yl)methanide in *s*-Block Metal Coordination”, *Chem. Eur. J.* **2017**, 23, 13141-13149.^[2]
- [3] I. Koehne, S. Bachmann, R. Herbst-Irmer, D. Stalke, “A Water-Containing Organopotassium Compound Based on Bis(4,6-*t*Bu-benzoxazol-2-yl)methanide and Its Unexpected Stability to Hydrolysis”, *Angew. Chem.* **2017**, 129, 15337-15342; *Angew. Chem. Int. Ed.* **2017**, 56, 15141-15145.^[3]
- [4] I. Koehne, N. Graw, T. Teuteberg, R. Herbst-Irmer, D. Stalke, “Introducing NacNac-Like Bis(4,6-isopropylbenzoxazol-2-yl)methanide in *s*-Block Metal Coordination”, *Inorg. Chem.* **2017**, 56, 14968-14978.^[4]

4.1 Work Techniques and Experimental Setups

4.1.1 Handling of Air- and Moisture-Sensitive Compounds

All manipulations involving air- and moisture sensitive compounds were carried out under an argon atmosphere using *Schlenk* techniques^[264–266] or handled in an argon glove box. All solvents used for metalation reactions and subsequent manipulations were distilled from sodium or potassium, or sodium-potassium alloy before use. Filtering of moisture sensitive compounds was carried out with the aid of self-made filter-cannulas assembled from *Whatman* fiberglass filters (GF/B, 25 mm), which were applied with Teflon[®] tape to Teflon[®] cannulas.

4.1.2 Preparation and Workup of Starting Materials

Starting materials were purchased commercially and were used as received if not stated otherwise. The bis(4-Me-benzoxazol-2-yl)methane (**1**) ligand and the C₃ linker unit ethyl-bisimidate dihydrochloride were prepared according to procedures by *Dauer*^[167] and *Ben Ammar*.^[186] 3,5-di-*tert*-butyl-2-nitrophenol (**5**) was synthesized based on a procedure by *Elder*, which was modified.^[193] *Hauser* type bases (*i*Pr)₂NMgX (X = Cl, Br, I) were prepared following a protocol by

Neufeld.^[242] Group 2 hexamethyldisilazanes $[M(\text{THF})_2\{\text{N}(\text{SiMe}_3)_2\}_2]$ ($M = \text{Ca}, \text{Sr}$ and Ba) and the calcium *Grignard* compound PhCaI were synthesized according to procedures by *Westerhausen*^[267] and *Fischer*,^[268] respectively. The metals $\text{Ca}, \text{Sr}, \text{Ba}$ were activated by dissolving in liquid ammonia under inert conditions to obtain a fine and highly reactive metal powder after evaporation of the solvent.^[269, 270] The Mg-HMDS compound was prepared in a reaction of $\text{Mg}(n\text{Bu})_2$ with HHMDS . Compounds **8-11** and the chloro-bis(dimethyl)imidate chloride linker were synthesized according to protocols by *Zhang*,^[196] *Wu*^[195] and *Viehe*,^[29] respectively. 2,6-diisopropylaniline was freshly distilled prior to use. Compounds **20-23** were synthesized based on modified and improved protocols by *Diemer*^[246] and *Basauri-Molina*.^[247] KC_8 was prepared following a procedure by *Uhlig*.^[92] The organometallic reagents $n\text{BuLi}$, as well as $t\text{BuLi}$ were percolated through *Celite*[®] (frit, P4) before use to separate formed lithium hydroxide, followed by the determination of the concentration according to a procedure by *Burchat*.^[271] Deuterated solvents for NMR spectroscopic investigations of organometallic compounds were dried over activated molecular sieves (3 Å) and were additionally stored in an argon dry box.

4.1.1 Elemental Analyses

Elemental analyses (C, H, N) were performed on an *Elementar* Vario EL3 machine at the Micro-analytics Laboratory, Department of Inorganic Chemistry, University of Göttingen. Deviations between the calculated and measured mass fractions are due to the loss of lattice solvent molecules or minor impurities.

4.1.2 Mass Spectrometry

The mass spectra were recorded at the Central Analytics Department, Department of Organic Chemistry, University of Göttingen. EI-MS^[272] spectra (70 eV) were recorded with a *Thermo Finnigan* DSQ, ESI-MS^[273] spectra with a *Bruker* MicroTOF and LIFDI-MS^[274, 275] spectra with a *Jeol* AccuTOF spectrometer. The isotopic pattern of molecule ion and fragment ion peaks are correlated to their isotopes with the highest natural abundancies (e.g. $^1\text{H}, ^7\text{Li}, ^{13}\text{C}, ^{14}\text{N}, ^{16}\text{O}, ^{24}\text{Mg}, ^{31}\text{P}, ^{35}\text{Cl}/^{37}\text{Cl}, ^{39}\text{K}, ^{40}\text{Ca}, ^{79}\text{Br}/^{81}\text{Br}, ^{88}\text{Sr}, ^{138}\text{Ba}$).

4.1.3 NMR Techniques and Experiments

The NMR spectroscopic data were recorded with either a *Bruker* Avance III 300 MHz or 400 MHz spectrometer. All measurements were conducted at ambient temperature with samples prepared in 1-10% solutions of deuterated solvents. All spectra were processed with *MestReNova* 6.02. The chemical shifts (δ) are given in ppm relative to TMS, using the residual solvent signals as internal standards.^[276, 277] Coupling constants (J) are reported in Hz and standard abbreviations indicating

multiplicity are used as follows: s = singlet, d = doublet, t = triplet, m = multiplet, br = broad. Combined abbreviations are derived from their components (e.g. dd = doublet of doublets). A correct signal assignment was ascertained by applying 2D ^1H , ^{13}C -HSQC^[278] and ^1H , ^{13}C -HMBC^[279] NMR techniques. ^1H , ^1H -NOESY^[280] spectra were recorded using a relaxation delay of 1.5 s and 0.5 s mixing time. 2048×512 data points were sampled over a spectral width of 12 ppm. Number of scans was 4. ^1H , ^{15}N -HMBC spectra were recorded using a relaxation delay of 2 s. 2048×256 data points were sampled over a spectral width of 12 ppm in F2 and 200 ppm in F1. Number of scans was 2. The DOSY NMR experiments were recorded on two spectrometers. A *Bruker* Avance 400 spectrometer equipped with an observe broadband probe with z-axis gradient coil with a maximum gradient strength of 57 G cm⁻¹ and a *Bruker* Avance III HD 400 spectrometer equipped with an inverse broadband probe with z-axis gradient coil with a maximum gradient strength of 51 G cm⁻¹.

4.1.3.1 ^1H -DOSY-ECC-MW Estimation: Sample Preparation and Measuring Parameters

^1H -DOSY-ECC-MW measurements and calculations were carried out in collaboration with *Dr. Sebastian Bachmann* from the group of *Prof. Dr. Dietmar Stalke*. All samples for a ^1H -DOSY-ECC-MW^[281–283] estimation were prepared by the addition of an equimolar amount of 2,2,3,3-tetramethylbutane (TMB) as internal reference to a solution of the analyte in C_6D_6 or $[\text{D}_8]\text{THF}$. The ECC-parameters for DOSY measurements in these solvents are given in Table 5-16. It was shown in previous studies that for most organometallic compounds the DSE calibration curve is the most suitable for an accurate estimation.^[200] Thus, only resulting values from the DSE and for comparison from the merge calibration curve are considered in the discussion of the DOSY NMR results in Chapter 2.3. For measurements, sample spinning was deactivated and the temperature was set and kept at 298 K. The experiments were performed using the *dstebpgp3s* pulse sequence.^[284, 285] The diffusion time was $\Delta = 0.1$ s. The duration of the magnetic field pulse gradients $\delta/2$ was adjusted for every compound in a range of 400–3500 μs . After Fourier transformation, processing with a line broadening of 2 Hz and baseline correction, the diffusion dimension was processed with the Topspin 3.1 software. Diffusion coefficients were calculated by *Gaussian* fits with the T1/T2 software in Topspin. For MW calculation details, see Table 5-17 ff.

4.1.3.2 Clean-Inphase HSQC Measurements for Residual Dipolar Coupling Calculations

Clean-inphase HSQC measurements and calculations were carried out in collaboration with *Dr. Thomas Niklas* from the group of *Prof. Dr. Dietmar Stalke*. One-bond scalar couplings between C and H ($^1J_{\text{CH}}$) were measured by clean-inphase HSQC^[286] of compound **19** in isotropic C_6D_6 . Measurements were performed on a *Bruker* Avance III 400 spectrometer using an INEPT delay of $1/(4J)$ with $J = 145$ Hz. In the F1 dimension, 256 data points were sampled over a spectral width of 150 ppm. In F2, 4096 data points were recorded with a spectral width of 12 ppm. Number of scans

was 4. A sum of scalar couplings and residual dipolar couplings (${}^1T_{\text{CH}} = {}^1J_{\text{CH}} + {}^1D_{\text{CH}}$) is obtained by a further clean-in-phase HSQC measurement in anisotropic media. Therefore, a polystyrene stick^[287] (2 cm, cross-linked by 0.4 vol% divinylbenzene) was swollen in a solution of compound **19** and C_6D_6 . In this measurement, in the F1 dimension 512 data points were sampled over a spectral width of 150 ppm. In F2, 4096 data points were recorded with a spectral width of 12 ppm. Number of scans was 16. The RDCs (${}^1D_{\text{CH}}$) then were obtained by simple subtraction.

4.1.3.3 ${}^1\text{H}$ NMR Water Titration Experiments

The samples were prepared in *Young* NMR tubes using 10 mg (**14**) or 15 mg (**16**) analyte dissolved in 0.5 mL of $[\text{D}_8]\text{THF}$. The water was added with an electronically assisted *SGE Analytic Science* “*eVol*” syringe (0.5 μL per step). Measurements were carried out with a *Bruker* Avance III 300 MHz spectrometer.

4.1.4 Computational Details of Electronic Structure Analyses

The electronic structure analyses were carried out in collaboration with *M.Sc. Thorsten Teuteberg* from the group of *Prof. Dr. Ricardo Mata*. Electronic structure calculations were performed using the *ORCA* 3.0.3 program package,^[288] the following NPA,^[289] NBO^[290] and NRT^[291, 292] analyses of the wave function were carried out using the *GenNBO* 5.9^[293] program. For NRT analysis three reference-bonding structures were defined manually, locating the negative charge on the bridging γ -C carbon atom or at one of the coordinating N atoms. The molecular structure was taken from the crystallographic data and hydrogen positions were relaxed. The BP86^[294] and B3LYP^[295] DFT functionals were used together with the def2-TZVP^[296] basis set. DFT-D3^[297] dispersion corrections with *Becke-Johnson*^[298–300] damping were included for all calculations. For all calculations the RIJ^[301, 302] approximation, for B3LYP together with the COSX^[303] approximation, was applied.

4.1.5 Percent Buried Volume (% V_{bur}) calculations

The percent buried volume calculations were performed with the *SambVca 2* web tool.^[304, 305] Based on crystallographic data, topographic steric maps were created by orienting the complexes in a *Cartesian* coordinate system. The metal ion was positioned at the origin. The midpoint of the two nitrogen donor atoms was aligned along the negative direction of the z -axis. One of the nitrogen atoms was placed in the xy -plane. For calculation, all unneeded atoms were removed. The H atoms were included. The default parameters recommended by the web application were applied to all % V_{bur} computations: Sphere radius of 3.5 Å; mesh of 0.1; *Bondi* radii scaled by 1.17. For detailed data, see the supporting information of reference^[4].

4.1.6 Single Crystal X-ray Diffraction Experiments

The selection of air- and moisture sensitive crystals from *Schlenk* flasks was carried out under an argon inert gas flow followed by the quick transfer of the crystal to a microscope slide covered in perfluorinated polyether oil. The crystals were immediately shock cooled using the *X-TEMP2* device.^[306–308] A suitable single crystal was selected with the help of a microscope equipped with a polarizing filter. The crystal then was mounted either on a *MiTeGEN*[®] *MicroMount* loop or on the tip of a glass fiber and was instantly transferred to the X-ray diffractometer where it was shock-cooled by the machines cooling device.

The data were collected with an *Incoatec* Mo I μ S microfocus source^[309] or with a Bruker TXS-Mo rotating anode, both supplying MoK α radiation ($\lambda = 0.71073 \text{ \AA}$). Measurements were carried out applying ω -scans with a step width of 0.5 degree per frame and fixed Φ angles at a temperature of 100(2) K if not stated otherwise. The diffractometers were equipped with mirror optics, an *APEX II* CCD detector and a D8 goniometer head.

The determination of the unit cells and their refinement as well as the data collection strategy calculations were performed with the help of *APEX2*.^[310] All data were integrated with *SAINT*.^[311] For multi-scan absorption correction the *SADABS*^[312] or in the case of non-merohedral twinning the *TWINABS*^[313] programs were applied. If necessary, an additional 3λ correction of the data was carried out.^[314] The space group determinations were performed with the program *XPREP*^[315] and the structures were solved by direct methods (*SHELXT*)^[316] and refined on F^2 using the full-matrix least-squares methods of *SHELXL*^[317] within the *shelXle* GUI.^[318]

4.2 Syntheses and Characterizations

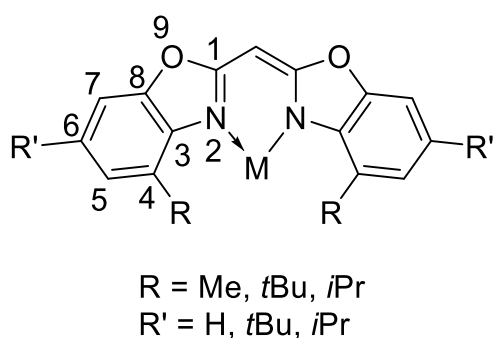


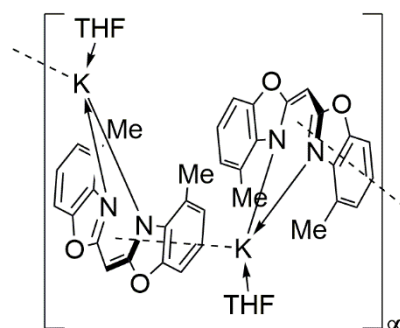
Figure 4-1. General ligand numbering for NMR spectroscopic data assignment.

4.2.1 Syntheses of Bis(4-Me-benzoxazol-2-yl)methane based s-Block Complexes

4.2.1.1 $[K(THF)\{(4-Me-NCOC_6H_3)_2CH\}]_\infty$ (**2**)

KH (48.0 mg, 1.19 mmol, 1.10 eq.) was suspended in THF (10 mL) and compound **1** (300 mg, 1.08 mmol, 1.00 eq.) dissolved in THF (10 mL) was slowly added drop wise. A red suspension forms upon gas evolution. The mixture was stirred at RT overnight. The resulting brownish-orange suspension was filtered *via* cannula and the solvent of the filtrate was evaporated. The residue was washed with pentane (3 x 10 mL) and dried under reduced pressure. For analysis, the residue was recrystallized by slow evaporation of pentane into a saturated solution of **2** in THF at RT to give colorless needle-shaped crystals.

Chemical Formula:	$C_{21}H_{21}KN_2O_3$
Molecular weight:	388.50 g/mol
Yield:	306 mg, 788 μ mol, 73%



1H NMR

(300 MHz, $[D_8]THF$): δ = 6.85 (m, 2 H, H7), 6.71 (m, 2 H, H5), 6.60 (m, 2 H, H6), 4.65 (s, 1 H, H_{bridge}), 3.62 (m, 4 H, OCH_2CH_2), 2.41 (s, 6 H, CH_3), 1.77 (m, 4 H, OCH_2CH_2) ppm.

$^{13}C\{^1H\}$ NMR

(75 MHz, $[D_8]THF$): δ = 170.3 (2 C, C2), 149.9 (2 C, C8), 146.5 (2 C, C3), 123.9 (2 C, C5), 122.5 (2 C, C4), 118.5 (2 C, C6), 105.6 (2 C, C7), 68.4 (2 C, OCH_2CH_2), 57.0 (1 C, C_{bridge}), 26.5 (2 C, OCH_2CH_2), 17.5 (2 C, CH_3) ppm.

MS (LIFDI)

m/z (%): 671.1 (12) $[2(M - 2THF) + K^+]^+$, 632.1 (40) $2[M - 2THF]^+$, 316.1 (100) $[M - 2THF]^+$.

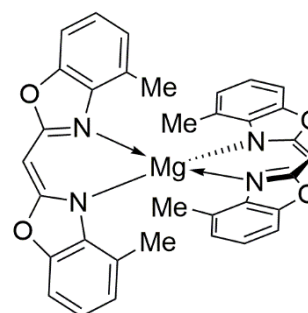
Elemental analysis

in % (calculated): $C_{21}H_{21}KN_2O_3$ (388.51 g/mol): C 64.71 (64.92), H 5.31 (5.45), N 7.38 (7.21).

4.2.1.2 [Mg{(4-Me-NCOC₆H₃)₂CH}₂] (3)

*i*PrMgCl (2M in THF, 1.00 mL, 1.98 mmol, 1.11 eq.) was diluted in THF (10 mL) and cooled to -20 °C. Then, compound **1** (500 mg, 1.80 mmol, 1.00 eq.) dissolved in THF (10 mL) was slowly added drop wise. After completed addition, the cooling-bath was removed and the mixture was stirred at RT overnight. The solvent was removed under reduced pressure and the residue was extracted with toluene (3 x 10 mL) and filtered *via* cannula. The volume of the toluene extract was reduced to a minimum and gentle heating again dissolved a formed precipitate. From this solution colorless prism-shaped crystals of **3** were obtained at RT.

Chemical Formula:	C ₃₄ H ₂₆ MgN ₄ O ₄
Molecular weight:	578.90 g/mol
Yield:	405 mg, 700 μmol, 78%



¹H NMR

(300 MHz, [D ₈]THF):	δ = 7.07 (m, 4 H, H7), 6.92 (m, 8 H, H5 + H6), 5.05 (s, 2 H, H _{bridge}), 2.69 (s, 12 H, CH ₃) ppm.
----------------------------------	---

¹³C{¹H} NMR

(75 MHz, [D ₈]THF):	δ = 169.9 (4 C, C2), 149.1 (4 C, C8), 140.8 (4 C, C3), 125.6 (4 C, C5), 124.6 (4 C, C4), 121.6 (4 C, C6), 108.6 (4 C, C7), 60.4 (2 C, C _{bridge}), 19.2 (4 C, CH ₃) ppm.
---------------------------------	--

MS (LIFDI)

<i>m/z</i> (%):	578.1 (100) [M] ⁺ , 278.1 (20) [(4-Me-NCOC ₆ H ₃) ₂ CH] ⁺ .
-----------------	---

Elemental analysis

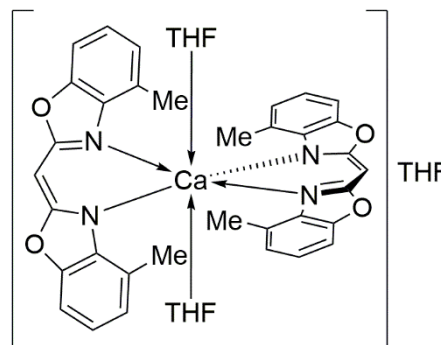
in % (calculated)	C ₃₄ H ₂₆ MgN ₄ O ₄ (578.91 g/mol): C 69.95 (70.54), H 4.31 (4.53), N 9.29 (9.68).
-------------------	--

4.2.1.3 [Ca(THF)₂{(4-Me-NCOC₆H₃)₂CH}₂]·THF (4)

Method A: Complex **2** (290 mg, 747 μmol, 1.00 eq.) and anhydrous CaI₂ beads (241 mg, 821 μmol, 1.10 eq.) were suspended in THF (15 mL). The suspension was heated under reflux at 75 °C overnight. The mixture was cooled to RT and the solvent was removed under reduced pressure. The residue was washed with pentane (2 x 10 mL), and then extracted with toluene (3 x 10 mL) and filtered. The solvent of the toluene filtrate was evaporated and the crude product was recrystallized by slow evaporation of pentane into a saturated solution of **4** in THF at -30 °C. From this solution, colorless prism-shaped crystals were obtained.

Method B: $[\text{Ca}(\text{THF})_2\{\text{N}(\text{SiMe}_3)_2\}_2]$ (200 mg, 396 μmol , 1.00 eq.) was suspended in THF (10 mL). Then **1** (110 mg, 396 μmol , 1.00 eq.) dissolved in THF (5 mL) was added drop wise. The mixture was stirred at RT for 2 h, and was heated under reflux at 75 °C overnight. The formed suspension was filtered *via* cannula and the solvent was evaporated under reduced pressure. Recrystallization following the above-mentioned procedure afforded colorless prism-shaped crystals.

Chemical Formula: $\text{C}_{46}\text{H}_{50}\text{CaN}_4\text{O}_7$
Molecular weight: 810.98 g/mol
Yield (Method A): 255 mg, 314 μmol , 84%
Yield (Method B): 212 mg, 261 μmol , 66%



^1H NMR

(300 MHz, $[\text{D}_8]\text{THF}$): δ = 6.97 (m, 4 H, H7), 6.73 (t, $^3J_{\text{HH}} = 7.8$ Hz, 4 H, H6), 6.55 (m, 4 H, H5), 5.07 (s, 2 H, H_{bridge}), 3.62 (m, 8 H, OCH_2CH_2), 1.91 (s, 12 H, CH_3), 1.77 (m, 8 H, OCH_2CH_2) ppm.

$^{13}\text{C}\{^1\text{H}\}$ NMR

(75 MHz, $[\text{D}_8]\text{THF}$): δ = 170.2 (4 C, C2), 149.6 (4 C, C8), 142.8 (4 C, C3), 125.4 (4 C, C5), 124.8 (4 C, C4), 121.3 (4 C, C6), 106.3 (4 C, C7), 68.4 (4 C, OCH_2CH_2), 59.0 (2 C, C_{bridge}), 26.6 (4 C, OCH_2CH_2), 17.1 (4 C, CH_3) ppm.

MS (LIFDI)

m/z (%): 594.1 (100) $[\text{M} - 3\text{THF}]^+$.

Elemental analysis

in % (calculated) $\text{C}_{42}\text{H}_{42}\text{CaN}_4\text{O}_6$ (738.90 g/mol): C 67.73 (68.27), H 5.51 (5.73), N 7.69 (7.58).

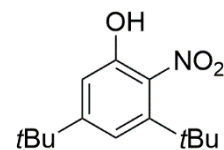
4.2.2 Syntheses of the Bis(4,6-*t*Bu-benzoxazol-2-yl)methane Ligand and its s-Block Complexes

4.2.2.1 3,5-di-*tert*-butyl-2-nitrophenol (**5**)

3,5-di-*tert*-butylphenol (10.0 g, 48.5 mmol, 1.00 eq.) was dissolved in ethyl acetate (800 mL). Under vigorous stirring, nitrating acid (1:2 $\text{HNO}_3/\text{H}_2\text{SO}_4$, 9.32 mL, 48.5 mmol, 1.00 eq.) was slowly added portion wise (0.20 mL/min). After complete addition, the mixture was stirred for an additional 15 minutes, then transferred to a separation funnel. The organic phase was washed with H_2O and brine until an almost pH neutral reaction of the aqueous phase. The organic phase was separated,

dried over MgSO₄, and the solvent was removed under reduced pressure. The reddish-orange residue was recrystallized several times from pentane to give **5** as a yellow crystalline solid.

Chemical Formula: C₁₄H₂₁NO₃
Molecular weight: 251.33 g/mol
Yield: 5.44 g, 21.6 mmol, 45%



¹H NMR

(300 MHz, [D₆]acetone): δ = 9.12 (s, 1 H, OH), 7.12 (d, ⁴J_{HH} = 1.9 Hz, 1 H, H4), 7.01 (d, ⁴J_{HH} = 1.9 Hz, 1 H, H6), 1.37 (s, 9 H, 3-C(CH₃)₃), 1.30 (s, 9 H, 5-C(CH₃)₃) ppm.

¹³C{¹H} NMR

(75 MHz, [D₆]acetone): δ = 154.3 (1 C, C5), 149.6 (1 C, C1), 141.7 (1 C, C3), 138.9 (1 C, C2), 116.6 (1 C, C4), 112.8 (1 C, C6), 36.6 (1 C, 3-C(CH₃)₃), 35.8 (1 C, 5-C(CH₃)₃), 31.5 (1 C, 3-C(CH₃)₃), 31.2 (1 C, 5-C(CH₃)₃) ppm.

IR

(ATR) $\tilde{\nu}$ = 3423, 2956, 2908, 2872, 1592, 1518 ($\tilde{\nu}_{\text{NO}_2}^{\text{asym.}}$), 1366 ($\tilde{\nu}_{\text{NO}_2}^{\text{sym.}}$), 1291, 978, 860, 666 cm⁻¹.

MS (EI, 70 eV)

m/z (%): 251.3 (30) [M]⁺, 236.2 (100) [M - OH + H]⁺.

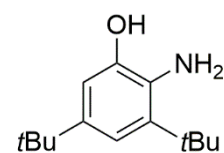
Elemental analysis

in % (calculated) C₁₄H₂₁NO₃ (251.33 g/mol): C 65.67 (66.91), H 8.37 (8.42), N 5.39 (5.57).

4.2.2.2 3,5-di-tert-butyl-2-aminophenol (**6**)

In a 100 mL pressure flask with screw cap and *Young* valve **5** (4.00 g, 15.9 mmol, 1.00 eq.) was dissolved in MeOH (20 mL) and Pd/C (10%) (180 mg, 1.59 mmol, 0.10 eq.) was added under cooling. The resulting suspension was degassed *via* three “freeze-pump-thaw” cycles, and then an H₂-atmosphere (1.5 bar) was established above the frozen suspension and the mixture was stirred at RT for 24 h. All solid material was removed by filtration *via* cannula under an argon atmosphere and then the solvent was removed under reduced pressure. The crude product was purified by recrystallization from CHCl₃ to give **6** as a white fluffy solid.

Chemical Formula: C₁₄H₂₃NO
Molecular weight: 221.34 g/mol
Yield: 3.17 g, 14.3 mmol, 90%



¹H NMR

(300 MHz, [D₆]acetone): δ = 7.86 (s, 1 H, OH), 6.81 (d, $^4J_{\text{HH}} = 2.2$ Hz, 1 H, H4), 6.74 (d, $^4J_{\text{HH}} = 2.2$ Hz, 1 H, H6), 4.02 (s, 2 H, NH₂), 1.41 (s, 9 H, 3-C(CH₃)₃), 1.22 (s, 9 H, 5-C(CH₃)₃) ppm.

¹³C{¹H} NMR

(75 MHz, [D₆]acetone): δ = 152.9 (1 C, C5), 145.2 (1 C, C1), 135.4 (1 C, C3), 133.4 (1 C, C2), 114.8 (1 C, C4), 104.5 (1 C, C6), 35.3 (1 C, 3-C(CH₃)₃), 35.2 (1 C, 5-C(CH₃)₃), 32.2 (1 C, 3-C(CH₃)₃), 30.0 (1 C, 5-C(CH₃)₃) ppm.

IR

(ATR) $\tilde{\nu}$ = 3415 ($\tilde{\nu}_{\text{NH}_2}^{\text{asym.}}$), 3316 ($\tilde{\nu}_{\text{NH}_2}^{\text{sym.}}$), 2954, 1580, 1418, 1301, 1171, 957, 860, 789 cm⁻¹.

MS (EI, 70 eV)

m/z (%): 221.3 (25) [M]⁺, 206.3 (100) [M - NH₂]⁺.

Elemental analysis

in % (calculated) C₁₄H₂₃NO (221.34 g/mol): C 74.08 (75.97), H 10.12 (10.47), N 6.14 (6.33).

4.2.2.3 Bis(4,6-*t*Bu-benzoxazol-2-yl)methane (7)

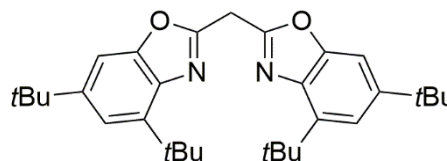
Compound **6** (8.00 g, 36.1 mmol, 2.00 eq.) and ethylbisimidate dihydrochloride (4.17 g, 18.1 mmol, 1.00 eq.) were dissolved in MeOH (60 mL) and heated at 85 °C for 48 h. The mixture was cooled to RT and the solvent was removed under reduced pressure. The residue was extracted with pentane (3 x 30 mL) utilizing a supersonic bath, and then filtered. The solvent of the filtrate was evaporated under reduced pressure and the crude product was recrystallized from EtOH to give **7** as a white crystalline solid suitable for X-ray diffraction analysis.

Chemical Formula:C₃₁H₄₂N₂O₂**Molecular weight:**

474.32 g/mol

Yield:

1.55 g, 3.27 mmol, 18%

**¹H NMR**

(300 MHz, CDCl₃): δ = 7.35 (d, $^4J_{\text{HH}} = 1.7$ Hz, 2 H, H5), 7.28 (d, $^4J_{\text{HH}} = 1.7$ Hz, 2 H, H7), 4.61 (s, 2 H, CH₂), 1.55 (s, 18 H, 4-C(CH₃)₃), 1.36 (s, 18 H, 6-C(CH₃)₃) ppm.

¹³C{¹H} NMR

(75 MHz, CDCl₃): δ = 157.7 (2 C, C1), 152.0 (2 C, C8), 148.5 (2 C, C6), 142.6 (2 C, C4), 137.2 (2 C, C3), 118.2 (2 C, C5), 105.2 (2 C, C7), 35.6 (2 C, 4-C(CH₃)₃), 35.4 (2 C, 6-C(CH₃)₃), 31.9 (6 C, 4-C(CH₃)₃), 30.5 (6 C, 6-C(CH₃)₃), 29.8 (1 C, C_{bridge}) ppm.

¹H NMR

(300 MHz, C₆D₆): δ = 7.40 (d, $^4J_{\text{HH}} = 1.7$ Hz, 2 H, H5), 7.21 (d, $^4J_{\text{HH}} = 1.7$ Hz, 2 H, H7), 4.20 (s, 2 H, CH₂), 1.68 (s, 18 H, 4-C(CH₃)₃), 1.23 (s, 18 H, 6-C(CH₃)₃) ppm.

¹³C{¹H} NMR

(75 MHz, C₆D₆): δ = 158.3 (2 C, C1), 152.6 (2 C, C8), 148.6 (2 C, C6), 142.9 (2 C, C4), 137.8 (2 C, C3), 118.2 (2 C, C5), 105.6 (2 C, C7), 35.9 (2 C, 4-C(CH₃)₃), 35.3 (2 C, 6-C(CH₃)₃), 31.8 (6 C, 4-C(CH₃)₃), 30.6 (6 C, 6-C(CH₃)₃), 29.5 (1 C, C_{bridge}) ppm.

¹H NMR

(300 MHz, [D₈]THF): δ = 7.42 (d, $^4J_{\text{HH}} = 1.7$ Hz, 2 H, H5), 7.30 (d, $^4J_{\text{HH}} = 1.7$ Hz, 2 H, H7), 4.66 (s, 2 H, CH₂), 1.54 (s, 18 H, 4-C(CH₃)₃), 1.35 (s, 18 H, 6-C(CH₃)₃) ppm.

IR

(ATR) $\tilde{\nu}$ = 2956, 1601 ($\tilde{\nu}_{\text{C=N}}$), 1396, 1243, 1153, 993, 853, 777.

MS (EI, 70 eV)

m/z (%): 474.3 (40) [M]⁺, 459.3 (100) [M - CH₃]⁺.

Elemental analysis

in % (calculated) C₃₁H₄₁N₂O₂ (474.23 g/mol): C 77.45 (78.44), H 8.55 (8.92), N 5.84 (5.90).

4.2.2.4 [Li(THF){(4,6-*t*Bu-NCOC₆H₂)₂CH}] (13)

Compound 7 (300 mg, 632 μmol , 1.00 eq.) was dissolved in THF (15 mL) and cooled to -50 °C. Under stirring, *t*BuLi (2.05 M in hexane, 0.32 mL, 656 μmol , 1.04 eq.) was slowly added dropwise. After complete addition, the mixture was stirred at -50 °C for an additional 15 min. The cooling-bath was removed and the solution was stirred at RT for 5 h. The solvent was removed under reduced pressure, then the residue was washed with ice cold pentane (3 x 10 mL), filtered *via* cannula, and dried under reduced pressure to give **13** as a pale-yellow solid (259 mg, 74%). Crystals suitable for X-ray diffraction analysis were obtained from a saturated solution of **13** in hexane at RT.

Chemical Formula:

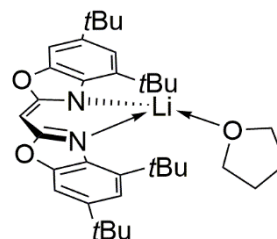
C₃₅H₄₉LiN₂O₃

Molecular weight:

552.72 g/mol

Yield:

259 mg, 469 μmol , 74%



¹H NMR

(300 MHz, C₆D₆): δ = 7.34 (d, ⁴J_{HH} = 1.8 Hz, 2 H, H7), 7.30 (d, ⁴J_{HH} = 1.8 Hz, 2 H, H5), 5.60 (s, 1 H, H_{bridge}), 3.15 (m, 4 H, OCH₂CH₂), 1.58 (s, 18 H, 4-C(CH₃)₃), 1.34 (s, 18 H, 6-C(CH₃)₃), 0.93 (m, 4 H, OCH₂CH₂) ppm.

¹³C{¹H} NMR

(75 MHz, C₆D₆): δ = 169.9 (2 C, C1), 150.8 (2 C, C8), 143.1 (2 C, C6), 139.0 (2 C, C4), 134.1 (2 C, C3), 117.5 (2 C, C5), 104.4 (2 C, C7), 68.6 (2 C, OCH₂CH₂), 57.3 (1 C, C_{bridge}), 35.1 (2 C, 6-C(CH₃)₃), 35.0 (2 C, 4-C(CH₃)₃), 32.1 (6 C, 6-C(CH₃)₃), 31.1 (6 C, 4-C(CH₃)₃), 25.1 (2 C, OCH₂CH₂) ppm.

⁷Li NMR

(116 MHz, C₆D₆): δ = 2.76 (s) ppm.

MS (LIFDI)

m/z (%): 480.2 (20) [*M* – THF]⁺, 474.3 (100) [4,6-*t*Bu-NCO(C₆H₂)₂CH₂]⁺.

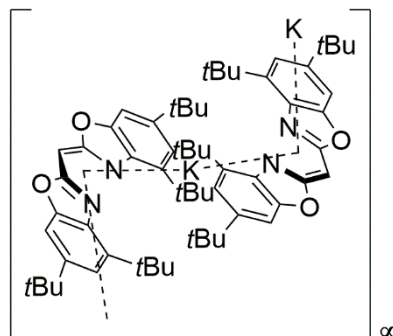
Elemental analysis

in % (calculated) C₃₅H₄₉LiN₂O₃ (552.72 g/mol): C 75.18 (76.06), H 8.86 (8.94), N 5.36 (5.07).

4.2.2.5 [K{ η^5 -(4,6-*t*Bu-NCO(C₆H₂)₂CH)}]_∞ (14)

KH (33.0 mg, 696 μmol, 1.10 eq.) was suspended in THF (10 mL) and **7** (300 mg, 633 μmol, 1.00 eq.) dissolved in THF (5 mL) was added drop wise *via* syringe. The mixture was stirred at RT for 18 h. The suspension was filtered *via* cannula, and the solvent of the filtrate was evaporated under reduced pressure. The residue was washed with pentane (3 x 10 mL), filtered, and dried under reduced pressure to give **14** as a white solid (296 mg, 80%). Recrystallization by evaporation of pentane into a saturated solution of **14** in THF at RT gave colorless needle-shaped crystals suitable for X-ray diffraction analysis.

Chemical Formula: C₃₁H₄₁KN₂O₂
Molecular weight: 512.77 g/mol
Yield: 296 mg, 577 μmol, 83%



¹H NMR

(300 MHz, [D₈]THF): δ = 7.01 (d, $^4J_{\text{HH}} = 1.7$ Hz, 2 H, H7), 6.97 (d, $^4J_{\text{HH}} = 1.8$ Hz, 2 H, H5), 4.56 (s, 1 H, H_{bridge}), 1.54 (s, 18 H, 4-C(CH₃)₃), 1.32 (s, 18 H, 6-C(CH₃)₃) ppm.

¹³C{¹H} NMR

(75 MHz, [D₈]THF): δ = 169.0 (2 C, C1), 151.2 (2 C, C8), 142.7 (2 C, C6), 141.3 (2 C, C4), 135.4 (2 C, C3), 116.1 (2 C, C5), 103.2 (2 C, C7), 55.3 (1 C, C_{bridge}), 35.9 (2 C, 6-C(CH₃)₃), 35.5 (2 C, 4-C(CH₃)₃), 32.6 (6 C, 6-C(CH₃)₃), 30.9 (6 C, 4-C(CH₃)₃) ppm.

MS (LIFDI)

m/z (%): 551.1 (33) [*M* + K⁺]⁺, 512.2 (100) [*M*]⁺, 474.2 (42) [4,6-*t*Bu-NCOC₆H₂)₂CH₂]⁺.

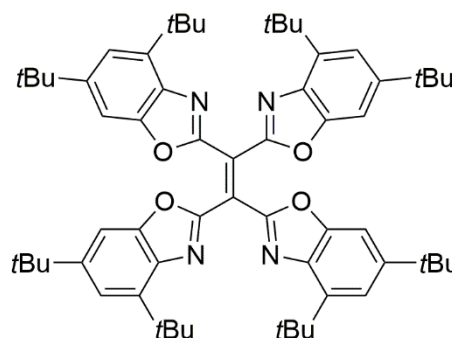
Elemental analysis

in % (calculated) C₃₁H₄₁KN₂O₂ (512.77 g/mol): C 70.34 (72.61), H 8.12 (8.06), N 5.25 (5.46).

4.2.2.6 1,1,2,2-tetrakis(4,6-*t*Bu-benzoxazol-2-yl)ethene (15)

Freshly prepared **14** (246 mg, 480 μ mol, 1.00 eq.) was suspended with CaBr₂ (93.0 mg, 463 μ mol, 0.97 eq.) in THF (10 mL). The mixture was heated at 75 °C for 18 h. The suspension was cooled to RT, and was subsequently filtered *via* cannula. The filtrate was evaporated under reduced pressure. Within a few weeks, some crystals of **15** formed in an almost completely dried out NMR sample of the residue in [D₈]THF.

Chemical Formula: C₆₂H₈₀N₄O₄
Molecular weight: 945.35 g/mol
Yield: few crystals

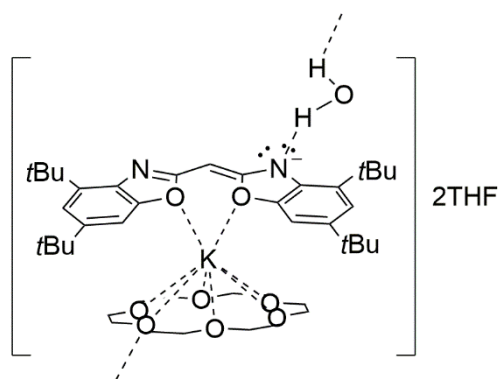
**4.2.2.7 [K(18-crown-6)]{(4,6-*t*Bu-OCNC₆H₂)₂CH}·(H₂O)_{0.35}·(THF)₂ (16)**

Compound **7** (300 mg, 633 μ mol, 1.00 eq.), KH (33.0 mg, 696 μ mol, 1.10 eq.) and 18-crown-6 ether (167 mg, 633 μ mol, 1.00 eq.) were dissolved in THF (15 mL) and stirred at RT for 18 h. The solvent was removed under reduced pressure. The residue was washed with pentane (3 x 10 mL) and dried *in vacuo*. Recrystallization through evaporation of pentane into a saturated solution of **16** in THF at RT yielded pale-yellow needle-shaped crystals suitable for X-ray diffraction analysis.

Chemical Formula: $C_{43}H_{65}KN_2O_8 \cdot (H_2O)_{0.35} \cdot (THF)_2$

Molecular weight: 927.58 g/mol

Yield: 484 mg, 522 μ mol, 83%

 **1H NMR**

(300 MHz, $[D_8]$ THF): $\delta = 6.98$ (s, 2 H, H5), 6.85 (d, $^4J_{HH} = 1.9$ Hz, 2 H, H7), 4.55 (s, 1 H, H_{bridge}), 3.45 (s, 24 H, 18-crown-6), 1.50 (s, 18 H, 6- $C(CH_3)_3$), 1.32 (s, 18 H, 4- $C(CH_3)_3$) ppm.

 $^{13}C\{^1H\}$ NMR

(75 MHz, $[D_8]$ THF): $\delta = 169.5$ (2 C, C1), 152.1 (2 C, C3), 146.3 (2 C, C4), 138.6 (2 C, C6), 134.4 (2 C, C8), 115.2 (2 C, C5), 102.8 (2 C, C7), 71.2 (12 C, 18-crown-6), 68.4 (1 C, C_{bridge}), 36.0 (2 C, 6- $C(CH_3)_3$), 35.4 (2 C, 4- $C(CH_3)_3$), 32.9 (6 C, 6- $C(CH_3)_3$), 30.8 (6 C, 4- $C(CH_3)_3$) ppm.

 ^{15}N NMR

(50 MHz, $[D_8]$ THF): $\delta = -184$ (s) ppm.

MS (LIFDI)

m/z (%): 1591.8 (10) $[2M - 2H_2O + K^+]^+$, 1552.9 (5) $[2M - 2H_2O]^+$, 1079.5 (5) $[M - H_2O + \{K(18-crown-6)\}]^+$, 551.1 (80) $[M - H_2O - 18-crown-6 + K^+]^+$, 512.2 (100) $[M - H_2O - 18-crown-6]^+$, 474.3 (50) $[4,6-tBu-NCOC_6H_2)_2C(OH)]^+$.

Elemental analysis

in % (calculated) $C_{51}H_{81}KN_2O_{10}$ (921.31 g/mol): C 66.16 (66.49), H 8.64 (8.86), N 3.31 (3.04). (For simplicity, the calculation of the elemental composition was performed assuming a non-occupied water molecule. The deviation is due to the loss of lattice THF molecules in the drying process.)

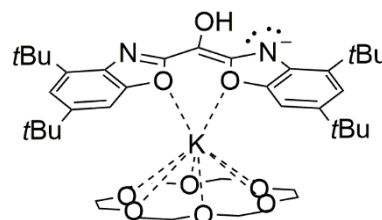
4.2.2.8 $[K(18-crown-6)\{(4,6-tBu-OCNC_6H_2)_2C(OH)\}]$ (17)

In a 500 mL *Schlenk* flask, air was dried over P_4O_{10} for several days prior to use.

Complex **16** (15 mg, 16.2 μ mol) was dissolved in dry THF (10 mL) in a 100 mL *Schlenk* flask. The solution was degassed through three “freeze-pump-thaw” cycles. Then, an atmosphere of dry air was established above the frozen solution. The mixture was allowed to react at RT for 3 days. The

solvent was removed under reduced pressure to give a white to pale-yellow solid. Extraction with dry THF and subsequent filtration *via* cannula afforded a pale-yellow filtrate and a white solid residue. The residue did not redissolve in common organic solvents hampering further investigations. The solvent from the filtrate was evaporated under reduced pressure to give **17** as a pale-yellow solid.

Chemical Formula: $C_{43}H_{65}KN_2O_9$
Molecular weight: 793.10 g/mol
Yield: 6.00 mg, 7.56 μ mol, 46%



^1H NMR

(300 MHz, $[D_8]$ THF): δ = 8.20 (s, 1 H, OH), 7.48 (d, $^4J_{\text{HH}} = 1.7$ Hz 2 H, H5), 7.33 (d, $^4J_{\text{HH}} = 1.7$ Hz, 2 H, H7), 3.64 (s, 24 H, 18-crown-6), 1.54 (s, 18 H, 6- $C(\text{CH}_3)_3$), 1.38 (s, 18 H, 4- $C(\text{CH}_3)_3$) ppm.

$^{13}\text{C}\{^1\text{H}\}$ NMR

(75 MHz, $[D_8]$ THF): δ = 167.5 (2 C, C1), 152.0 (2 C, C3), 144.8 (2 C, C4), 138.9 (2 C, C6), 137.3 (2 C, C8), 118.9 (2 C, C5), 106.2 (2 C, C7), 71.2 (12 C, 18-crown-6), 51.6 (1 C, C_{bridge}), 36.4 (2 C, 6- $C(\text{CH}_3)_3$), 36.1 (2 C, 4- $C(\text{CH}_3)_3$), 32.2 (6 C, 6- $C(\text{CH}_3)_3$), 30.9 (6 C, 4- $C(\text{CH}_3)_3$) ppm.

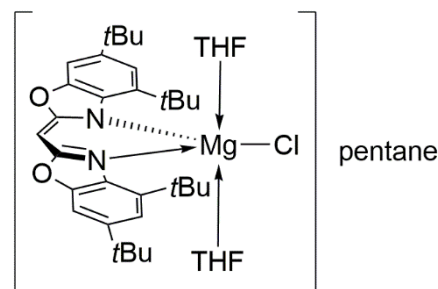
MS (ESI(+))

m/z (%): 880.4 (12) $[M + C_4H_9O_2]^+$, 791.4 (2) $[M]^+$, 303.1 (100) $[K\{18\text{-crown-6}\}]^+$.

4.2.2.9 $[\text{MgCl}(\text{THF})_2\{(\text{4,6-}t\text{Bu-NCOC}_6\text{H}_2)_2\text{CH}\}]\cdot\text{pentane}$ (**18**)

Compound **7** (300 mg, 633 μ mol, 1.00 eq.) and $(i\text{Pr}_2\text{N})\text{MgCl} \cdot (\text{THF})_{0.65}$ (283 mg, 1.39 mmol, 2.20 eq.) were suspended in THF (15 mL) and stirred at RT for 18 h. The solvent was removed under reduced pressure and the residue was extracted with pentane (3 x 10 mL) then filtered *via* cannula. The filtrate was concentrated to two thirds of its original volume, and then stored at -28 $^\circ\text{C}$ to afford **18** as colorless plate-shaped crystals suitable for X-ray diffraction analysis.

Chemical Formula: $C_{44}H_{69}ClMgN_2O_4$
Molecular weight: 749.80 g/mol
Yield: 228 mg, 304 μ mol, 48%



¹H NMR

(300 MHz, C₆D₆): δ = 7.42 (d, $^4J_{\text{HH}} = 2.0$ Hz, 2 H, H7), 7.28 (d, $^4J_{\text{HH}} = 2.0$ Hz, 2 H, H5), 5.62 (s, 1 H, H_{bridge}), 3.57 (m, 8 H, OCH₂CH₂), 1.84 (s, 18 H, 4-C(CH₃)₃), 1.27 (s, 18 H, 6-C(CH₃)₃), 1.07 (m, 8 H, OCH₂CH₂) ppm.

¹³C{¹H} NMR

(75 MHz, C₆D₆): δ = 168.3 (2 C, C1), 149.7 (2 C, C8), 145.3 (2 C, C6), 138.6 (2 C, C4), 136.5 (2 C, C3), 118.1 (2 C, C5), 104.2 (2 C, C7), 69.1 (4 C, OCH₂CH₂), 58.6 (1 C, C_{bridge}), 35.5 (2 C, 6-C(CH₃)₃), 34.7 (2 C, 4-C(CH₃)₃), 32.0 (2 C, 6-C(CH₃)₃), 31.6 (2 C, 4-C(CH₃)₃), 25.1 (4 C, OCH₂CH₂) ppm.

¹⁵N NMR

(30 MHz, C₆D₆): δ = -217 (s) ppm.

MS (LIFDI)

m/z (%): 532.2 (40) [*M* - 2THF - C₅H₁₂]⁺, 474.3 (100) [4,6-*t*Bu-NCO(C₆H₂)₂CH₂]^{v+}.

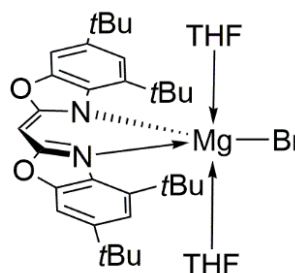
Elemental analysis

in % (calculated) C₄₄H₆₉MgN₂O₄ (749.79 g/mol): C 69.30 (70.48), H 8.72 (9.28), N 3.81 (3.74). (The deviation is due to the loss of lattice pentane molecules in the drying process.)

4.2.2.10 [MgBr(THF)₂{(4,6-*t*Bu-NCO(C₆H₂)₂CH)}] (18a)

Compound **7** (200 mg, 421 μ mol, 1.00 eq.) and (*i*Pr₂N)MgBr · (THF)₂ (293 mg, 842 μ mol, 2.00 eq.) were suspended in THF (15 mL) and stirred at RT for 18 h. The solvent was removed under reduced pressure and the residue was extracted with pentane (3 x 10 mL) then filtered *via* cannula. The filtrate was evaporated under reduced pressure to give **18a** as an orange solid. Due to a high solubility of the compound in common organic solvents even at low temperature, no pure crystalline material for analysis and X-ray diffraction experiments could be obtained.

Chemical Formula: C₃₉H₅₇BrMgN₂O₄
Molecular weight: 722.10 g/mol
Yield: 210 mg, 290 μ mol, 69%



¹H NMR

(300 MHz, C₆D₆): δ = 7.42 (d, ⁴J_{HH} = 2.0 Hz, 2 H, H7), 7.27 (d, ⁴J_{HH} = 2.0 Hz, 2 H, H5), 5.56 (s, 1 H, H_{bridge}), 3.52 (m, 8 H, OCH₂CH₂), 1.87 (s, 18 H, 4-C(CH₃)₃), 1.27 (s, 18 H, 6-C(CH₃)₃), 1.16 (m, 8 H, OCH₂CH₂) ppm.

¹³C{¹H} NMR

(75 MHz, C₆D₆): δ = 169.2 (2 C, C1), 149.9 (2 C, C8), 145.6 (2 C, C6), 138.5 (2 C, C4), 136.2 (2 C, C3), 118.8 (2 C, C5), 104.4 (2 C, C7), 69.3 (4 C, OCH₂CH₂), 59.1 (1 C, C_{bridge}), 36.0 (2 C, 6-C(CH₃)₃), 34.9 (2 C, 4-C(CH₃)₃), 32.7 (2 C, 6-C(CH₃)₃), 31.8 (2 C, 4-C(CH₃)₃), 25.3 (4 C, OCH₂CH₂) ppm.

MS (LIFDI)

m/z (%): 578.2 (25) [*M* – 2THF + H⁺]⁺, 474.3 (100) [4,6-*t*Bu-NCOC₆H₂)₂CH₂]⁺.

Elemental analysis

in % (calculated) C₃₉H₅₇BrMgN₂O₄ (722.10 g/mol): C 63.96 (64.87), H 9.01 (7.96), N 4.00 (3.88). (The deviation is due to a minor contamination with side product.)

4.2.2.11 [Mg{(4,6-*t*Bu-NCOC₆H₂)₂CH}₂] (19)**Method a:**

Complex **18/18a** (304 μ mol, 1.00 eq.) and KC₈ (41.0 mg, 304 μ mol, 1.00 eq.) were suspended in toluene (15 mL) and stirred at RT for 72 h. The suspension was filtered *via* cannula and the solvent of the filtrate was removed under reduced pressure to give **19** as a reddish-orange solid.

Method b:

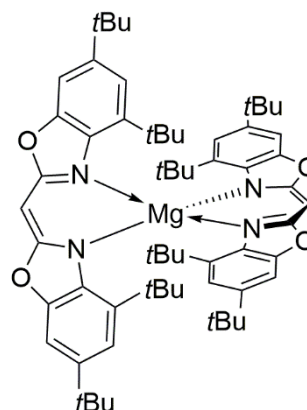
Complex **18/18a** and KC₈ were suspended in toluene (15 mL) at 0 ° and the mixture was stirred for 72 h, during which time the cooling-bath was allowed to slowly warm to RT. The suspension was filtered *via* cannula and the solvent of the filtrate was removed under reduced pressure to give **19** as a reddish-orange solid.

Method c:

Complex **18/18a** (412 μ mol, 1.00 eq.) was dissolved in toluene, and then stirred over a potassium mirror (56.0 mg, 412 μ mol, 1.00 eq.) at RT for 72 h. The suspension was filtered *via* cannula and the solvent of the filtrate was removed under reduced pressure to give **19** as a reddish-orange solid.

Due to a high solubility of the compound in common organic solvents even at low temperature, no crystalline material for X-ray diffraction analysis could be obtained.

Chemical Formula:	$C_{62}H_{82}MgN_4O_4$
Molecular weight:	971.67 g/mol
Yield:	118 – 152 mg, 121 – 156 μ mol, 76 – 80%



1H NMR

(400 MHz, $[D_{12}]$ cyclohexane): δ = 7.05 (d, $^4J_{HH} = 2.0$ Hz, 2 H, H7), 7.01 (d, $^4J_{HH} = 2.0$ Hz, 2 H, H5), 5.38 (s, 1 H, H_{bridge}), 1.25 (s, 36 H, 4- $C(CH_3)_3$), 1.15 (s, 36 H, 6- $C(CH_3)_3$) ppm.

$^{13}C\{^1H\}$ NMR

(100 MHz, $[D_{12}]$ cyclohexane): δ = 168.5 (4 C, C1), 150.1 (4 C, C8), 145.3 (4 C, C6), 138.7 (4 C, C4), 136.2 (4 C, C3), 118.6 (4 C, C5), 104.3 (4 C, C7), 60.9 (2 C, C_{bridge}), 35.2 (4 C, 6- $C(CH_3)_3$), 35.2 (4 C, 4- $C(CH_3)_3$), 31.9 (12 C, 6- $C(CH_3)_3$), 30.9 (12 C, 4- $C(CH_3)_3$) ppm.

^{15}N NMR

(30 MHz, C_6D_6): δ = -213 (s) ppm.

MS (LIFDI)

m/z (%): 970.7 (100) $[M]^+$.

Elemental analysis

in % (calculated) $C_{62}H_{82}MgN_4O_4$ (971.67 g/mol): An interpretable elemental analysis could not be obtained, presumably due to magnesium nitride formation.

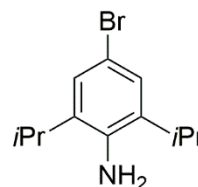
4.2.3 Syntheses of the Bis(4,6-*i*Pr-benzoxazol-2-yl)methane Ligand and its s-Block Complexes

4.2.3.1 4-Bromo-2,6-diisopropylaniline (20)

Br_2 (9.50 mL, 186 mmol, 1.00 eq.) dissolved in DCM (70 mL) was slowly added dropwise at 0 °C to a solution of 2,6-diisopropylaniline (35 mL, 186 mmol, 1.00 eq.) in DCM (1.00 L). After completed addition, the reaction mixture was stirred at RT for an additional 30 min. Then, a saturated solution of $Na_2S_2O_3$ (100 mL) was added and the mixture was stirred for an additional 15 min. The organic layer was separated, concentrated to half of its original volume and extracted with NaOH

(0.5M, 2 x 100 mL) and brine (2 x 100 mL). The organic layer was dried over MgSO₄ and concentrated under reduced pressure. Compound **20** was obtained as a pale-yellow oil (47.3 g, 99%) pure enough to be used without further purification.

Chemical Formula: C₁₂H₁₈BrN
Molecular weight: 256.19 g/mol
Yield: 47.3 g, 185 mmol, 99%

**¹H NMR**

(300 MHz, CDCl₃): δ = 7.11 (s, 2 H, H3 + H4), 3.70 (s_{br}, 2 H, NH₂), 2.88 (sept, ³J_{HH} = 6.8 Hz, 2 H, CH(CH₃)₂), 1.26 (d, ³J_{HH} = 6.8 Hz, 12 H, CH(CH₃)₂) ppm.

¹³C{¹H} NMR

(75 MHz, CDCl₃): δ = 139.4 (1 C, C1), 134.7 (2 C, C3 + C5), 125.8 (2 C, C2 + C6), 111.2 (1 C, C4), 28.1 (2 C, CH(CH₃)₂), 22.4 (4 C, CH(CH₃)₂) ppm.

MS (ESI(+))

m/z (%): 256.07 (100) [M + H]⁺.

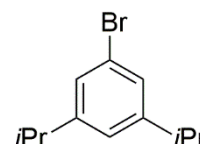
HR-MS (ESI(+))

m/z: calcd. for [M + H]⁺: 256.0695; found: 256.0697.

4.2.3.2 1-Bromo-3,5-diisopropylbenzene (21)

Sodium nitrite (47.1 g, 683 mmol, 2.50 eq.) dissolved in water (150 mL) was added dropwise to a precooled suspension (-10 °C) of **20** (70.0 g, 273 mmol, 1.00 eq.) in HCl (2M, 700 mL). The reaction was allowed to react at -10 °C for an additional 10 min., and then H₃PO₂ (50 w%, 283 mL, 2.73 mol, 10.0 eq.) was added. The reaction mixture was stirred for 48 h during which time the cooling-bath was allowed to slowly warm to RT. The mixture was transferred to a separation-funnel and the aqueous layer was extracted with Et₂O (3 x 150 mL). The combined organic layers were extracted with NaOH (0.5M, 4 x 100 mL) and H₂O (2 x 150 mL), then dried over MgSO₄ and concentrated under reduced pressure. Compound **21** was obtained as a brownish-orange oil pure enough to be used without further purification.

Chemical Formula: C₁₂H₁₇Br
Molecular weight: 241.17 g/mol
Yield: 61.1 g, 253 mmol, 93%

**¹H NMR**

(300 MHz, CDCl₃): δ = 7.18 (m, 2 H, H2 + H6), 6.99 (tt, ⁴J_{HH} = 1.6, 0.5 Hz, 1 H, H4) 2.86 (sept, ³J_{HH} = 6.9 Hz, 2 H, CH(CH₃)₂), 1.24 (d, ³J_{HH} = 6.9 Hz, 12 H, CH(CH₃)₂) ppm.

$^{13}\text{C}\{^1\text{H}\}$ NMR

(75 MHz, CDCl_3): $\delta = 151.2$ (2 C, C3 + C5), 127.0 (2 C, C2 + C6), 123.8 (1 C, C4), 122.5 (1 C, C1), 34.2 (2 C, $\text{CH}(\text{CH}_3)_2$), 24.0 (4 C, $\text{CH}(\text{CH}_3)_2$) ppm.

MS (EI, 70 eV)

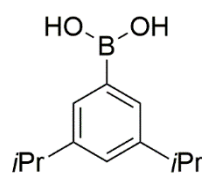
m/z (%): 240.05 (42) $[M]^+$, 225.1 (100) $[M - \text{CH}_3]^+$, 197.0 (60) $[M - i\text{Pr}]^+$, 161.2 (30) $[M - \text{Br}]^+$.

4.2.3.3 (3,5-Diisopropylphenyl)boronic acid (22) / 2,4,6-Tris(3,5-diisopropylphenyl)cyclotriboroxane (22a)

To a precooled solution ($-78\text{ }^\circ\text{C}$) of **21** (9.70 g, 40.2 mmol, 1.00 eq.) in dry Et_2O (40 mL), TMEDA (6.20 mL, 40.2 mmol, 1.00 eq.) was introduced. Subsequently, $n\text{BuLi}$ (2.4M, 16.8 mL, 40.2 mmol, 1.00 eq.) was added dropwise over a period of 30 min. and the mixture was stirred at $-78\text{ }^\circ\text{C}$ for an additional 30 min. The cooling-bath was removed, $\text{B}(\text{O}i\text{Bu})_3$ (13.0 mL, 48.2 mmol, 1.20 eq.) was introduced and the solution was stirred at RT for 10 h. HCl (1M, 80 mL) and additionally concentrated aqueous HCl (8 mL) were added and the resulting layers were separated. The aqueous layer was washed with Et_2O (2 x 80 mL) and the combined organic layers were extracted with NaOH (1M, 4×150 mL). Under stirring, the combined aqueous layers were acidified with concentrated aqueous HCl . Upon addition, a beige solid precipitated which was recovered by filtration (frit, P3), and then washed with H_2O (3 x 100 mL). The solid was redissolved in Et_2O , the remaining aqueous phase was separated and the organic phase was dried over MgSO_4 . Removal of the solvent under reduced pressure yielded a beige solid in an overall yield of 60% as a mixture of **22** (16%) and **22a** (84%), which was used without further purification.

22:

Chemical Formula: $\text{C}_{12}\text{H}_{19}\text{BO}_2$
Molecular weight: 206.09 g/mol
Yield: 4.97 g, 185 mmol, 60%

 **^1H NMR**

(400 MHz, CDCl_3): $\delta = 7.41$ (d, $^4J_{\text{HH}} = 1.8$ Hz, 2 H, H2 + H6), 7.21 (t, $^4J_{\text{HH}} = 1.8$ Hz, 1 H, H4), 4.56 (s, 2 H, $\text{B}(\text{OH})_2$), 2.93 (sept, $^3J_{\text{HH}} = 7.0$ Hz, 2 H, $\text{CH}(\text{CH}_3)_2$), 1.27 (d, $^3J_{\text{HH}} = 7.0$ Hz, 12 H, $\text{CH}(\text{CH}_3)_2$) ppm.

 $^{13}\text{C}\{^1\text{H}\}$ NMR

(100 MHz, CDCl_3): $\delta = 148.7$ (2 C, C3 + C5), 129.1 (2 C, C2 + C6), 128.1 (1 C, C4), 34.4 (2 C, $\text{CH}(\text{CH}_3)_2$), 24.2 (4 C, $\text{CH}(\text{CH}_3)_2$) ppm.

¹H NMR

(400 MHz, [D₆]DMSO): δ = 7.90 (s, 2 H, B(OH)₂), 7.49 (d, ⁴J_{HH} = 1.8 Hz, 2 H, H2 + H6), 7.11 (t, ⁴J_{HH} = 1.8 Hz, 1 H, H4), 2.84 (sept, ³J_{HH} = 6.9 Hz, 2 H, CH(CH₃)₂), 1.20 (d, ³J_{HH} = 6.9 Hz, 12 H, CH(CH₃)₂) ppm.

MS (ESI(+))

m/z (%): 257.2 (93) [ArB(OCH₃)₂ + Na⁺]⁺, 243.2 (100) [ArB(OH)(OCH₃) + Na⁺]⁺, 229.2 (34) [M + Na⁺]⁺.

HR-MS (ESI(+))

m/z: calcd. for [M + Na⁺]⁺: 229.1372, found: 229.1377.

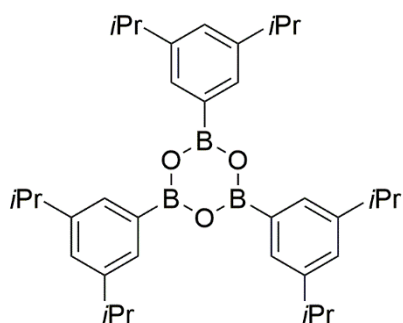
22a:

Chemical Formula:

C₃₆H₅₁B₃O₃

Molecular weight:

564.23 g/mol

**¹H NMR**

(400 MHz, CDCl₃): δ = 7.93 (d, ⁴J_{HH} = 1.9 Hz, 6 H, H2 + H6), 7.33 (t, ⁴J_{HH} = 1.9 Hz, 3 H, H4), 3.03 (sept, ³J_{HH} = 6.9 Hz, 6 H, CH(CH₃)₂), 1.35 (d, ³J_{HH} = 6.9 Hz, 36 H, CH(CH₃)₂) ppm.

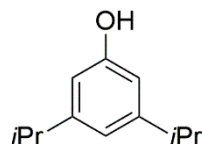
¹³C{¹H} NMR

(100 MHz, CDCl₃): δ = 148.5 (6 C, C3 + C5), 131.3 (6 C, C2 + C6), 129.3 (3 C, C4), 34.3 (6 C, CH(CH₃)₂), 24.3 (12 C, CH(CH₃)₂) ppm.

4.2.3.4 3,5-diisopropylphenol (23)

A mixture of **22** and **22a** (9.00 g, 43.7 mmol, 1.00 eq.) was dissolved in NaOH (3M, 200 mL) and warmed to 30 °C. Then H₂O₂ (35 w%, 4.51 mL, 52.4 mmol, 1.20 eq.) was added portion wise. After addition, the reaction mixture was heated at 70 °C for 1 h. Completion of the reaction was verified using potassium iodide-starch test strips. When there were peroxides left in the reaction mixture heating was continued at 70 °C for an additional 30 min. After a finished reaction, the mixture was cooled in an ice-bath and concentrated aqueous HCl was added to obtain a pH of 1. The mixture was transferred to a separation-funnel, and then extracted with Et₂O (3 x 200 mL). The combined organic layers were washed with H₂O, then dried over MgSO₄ and concentrated under reduced pressure. Compound **23** was obtained as a pale-yellow oil which became a white solid after a while that was used without further purification.

Chemical Formula: C₁₂H₁₈O
Molecular weight: 178.28 g/mol
Yield: 7.40 g, 41.5 mmol, 95%

**¹H NMR**

(300 MHz, CDCl₃): δ = 6.67 (tt, ⁴J_{HH} = 1.5, 0.5 Hz, 1 H, H4), 6.53 (m, 2 H, H2 + H6), 4.60 (s_{br}, 1 H, OH), 2.97 (sept, ³J_{HH} = 6.9 Hz, 2 H, CH(CH₃)₂), 1.23 (d, ³J_{HH} = 6.9 Hz, 12 H, CH(CH₃)₂) ppm.

¹³C{¹H} NMR

(75 MHz, CDCl₃): δ = 156.6 (1 C, C1), 150.9 (2 C, C3 + C5), 117.7 (1 C, C4), 110.8 (2 C, C2 + C6), 34.2 (2 C, CH(CH₃)₂), 24.1 (4 C, CH(CH₃)₂) ppm.

MS (EI, 70 eV)

m/z (%): 178.1 (53) [M]⁺, 163.1 (100) [M - CH₃]⁺, 135.1 (49) [M - iPr]⁺, 121.0 (45) [C₈H₉O]⁺, 107.0 (30) [C₇H₇O]⁺.

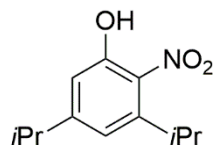
HR-MS (EI, 70 eV)

m/z: calcd. for [M]⁺: 178.1358; found: 178.1354.

4.2.3.5 3,5-diisopropyl-2-nitrophenol (24)

Compound **23** (5.00 g, 28.1 mmol, 1.00 eq) was dissolved in EtOAc (500 mL). Under vigorous stirring, nitrating acid (1:2 HNO₃/H₂SO₄, 5.50 mL, 28.1 mmol, 1.00 eq) was slowly added portion wise (0.25 mL/min) at RT. After complete addition, the mixture was stirred for an additional 15 min. Then H₂O (50 mL) was added and the mixture was transferred to a separation-funnel. The organic phase was separated and washed with H₂O and brine until an almost pH neutral reaction of the aqueous phase. The organic phase was dried over MgSO₄ and the solvent was removed under reduced pressure. The crude product was purified by fractional distillation under reduced pressure (150 °C oil bath) yielding **24** as a yellowish-orange oil.

Chemical Formula: C₁₂H₁₇NO₃
Molecular weight: 223.27 g/mol
Yield: 2.54 g, 11.4 mmol, 46%

**¹H NMR**

(300 MHz, [D₆]acetone): δ = 9.29 (s, 1 H, OH), 6.89 (d, ⁴J_{HH} = 1.7 Hz, 1 H, H6), 6.83 (dd, ⁴J_{HH} = 1.7, 0.4 Hz, 1 H, H4), 2.88 (m, 2 H, 3- + 5-CH(CH₃)₂), 1.25 (d, ³J_{HH} = 6.8 Hz, 6 H, 3-CH(CH₃)₂), 1.22 (d, ³J_{HH} = 6.9 Hz, 6 H, 5-CH(CH₃)₂) ppm.

$^{13}\text{C}\{^1\text{H}\}$ NMR

(75 MHz, $[\text{D}_6]$ acetone): $\delta = 154.4$ (1 C, C5), 149.2 (1 C, C1), 141.9 (1 C, C3), 130.3 (1 C, C2), 116.1 (1 C, C4), 113.1 (1 C, C6), 34.9 (2 C, 3- + 5- $\text{CH}(\text{CH}_3)_2$), 23.9 (2 C, 3- $\text{CH}(\text{CH}_3)_2$), 23.7 (2 C, 5- $\text{CH}(\text{CH}_3)_2$) ppm.

IR

(ATR) $\tilde{\nu} = 2965, 2934, 2873, 1612, 1579, 1524$ ($\tilde{\nu}_{\text{NO}_2}^{\text{asym.}}$), 1431, 1343 ($\tilde{\nu}_{\text{NO}_2}^{\text{sym.}}$), 1269, 1183, 994, 864, 712 cm^{-1} .

MS (ESI(-))

m/z (%): 222.1 (100) $[M - \text{H}]^-$.

HR-MS (ESI(-))

m/z : calcd. for $[M - \text{H}]^-$: 222.1136; found: 222.1134

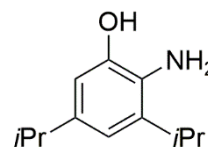
Elemental analysis

in % (calculated) $\text{C}_{12}\text{H}_{19}\text{NO}_3$ (223.27 g/mol): C 64.36 (64.55), H 7.55 (7.67), N 6.18 (6.27).

4.2.3.6 3,5-diisopropyl-2-aminophenol (25)

In a 100 mL flask with screw cap and Young valve **24** (5.12 g, 22.9 mmol, 1.00 eq) was dissolved in MeOH (25 mL) and Pd/C (10%) (240 mg, 2.29 mmol, 0.10 eq) was added under cooling. The resulting suspension was degassed *via* three “freeze-pump-thaw” cycles, and then an H_2 -atmosphere (1.5 bar) was established above the frozen suspension and the mixture was stirred at RT for 18 h. All solid material was removed by filtration *via* cannula under an argon atmosphere and the filtrate was evaporated under reduced pressure. The crude product was purified by recrystallization from CHCl_3 to give **25** as a white fluffy solid.

Chemical Formula: $\text{C}_{12}\text{H}_{19}\text{NO}$
Molecular weight: 193.29 g/mol
Yield: 3.98 g, 20.6 mmol, 90%

 **^1H NMR**

(300 MHz, $[\text{D}_8]$ THF): $\delta = 7.78$ (s_{br} , 1 H, OH), 6.46 (d, $^4J_{\text{HH}} = 2.0$ Hz, 1 H, H4), 6.36 (d, $^4J_{\text{HH}} = 2.0$ Hz, 1 H, H6), 3.82 (s_{br} , 2 H, NH_2), 2.95 (sept, $^3J_{\text{HH}} = 6.9$ Hz, 1 H, 3- $\text{CH}(\text{CH}_3)_2$), 2.68 (sept, $^3J_{\text{HH}} = 6.9$ Hz, 1 H, 5- $\text{CH}(\text{CH}_3)_2$), 1.19 (d, $^3J_{\text{HH}} = 6.9$ Hz, 6 H, 3- $\text{CH}(\text{CH}_3)_2$), 1.15 (d, $^3J_{\text{HH}} = 6.9$ Hz, 6H, 5- $\text{CH}(\text{CH}_3)_2$) ppm.

 $^{13}\text{C}\{^1\text{H}\}$ NMR

(75 MHz, $[\text{D}_8]$ THF): $\delta = 145.6$ (1 C, C1), 138.3 (1 C, C5), 133.6 (1 C, C3), 131.8 (1 C, C2), 114.9 (1 C, C4), 110.4 (1 C, C6), 34.9 (1 C, 3- $\text{CH}(\text{CH}_3)_2$), 28.7

(1 C, 5-CH(CH₃)₂), 25.1 (2 C, 3-CH(CH₃)₂), 23.0 (2 C, 5-CH(CH₃)₂) ppm.

IR

(ATR) $\tilde{\nu} = 3376$ ($\tilde{\nu}_{\text{NH}_2}^{\text{asym}}$), 3307 ($\tilde{\nu}_{\text{NH}_2}^{\text{sym}}$), 2961, 2868, 1560, 1435, 1324, 1190, 975, 854, 739 cm⁻¹.

MS (EI, 70 eV)

m/z (%): 193.1 (25) [M]⁺, 178.1 (100) [M - CH₃]⁺, 91.0 (24) [C₇H₇]⁺, 77.0 (19) [C₆H₅]⁺.

HR-MS (EI, 70 eV)

m/z: calcd. for [M]⁺: 193.1466, found: 193.1475.

Elemental analysis

in % (calculated) C₁₂H₁₉NO (193.29 g/mol): C 73.55 (74.57), H 9.77 (9.91), N 7.04 (7.25).

4.2.3.7 Bis(4,6-*i*Pr-benzoxazol-2-yl)methane (26)

Compound **25** (7.70 g, 39.8 mmol, 2.00 eq.) and ethylbisimidate dihydrochloride (3.15 g, 19.9 mmol, 1.00 eq.) were dissolved in MeOH (80 mL) and heated at 85 °C for 48 h. The mixture was cooled to RT and the solvent was removed under reduced pressure. The residue was extracted with pentane (3 x 50 mL) utilizing an ultrasonic bath and subsequently filtered. The combined organic phases were dried over MgSO₄, and then the solvent was removed under reduced pressure to give **26** as an orange oil, which was used without further purification. For analysis, the product was additionally purified *via* column chromatography (silica; DCM, neat). The product can be marked with an aqueous solution of vanillin and sulfuric acid.

Chemical Formula:

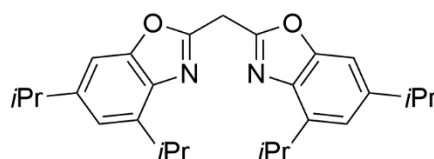
C₂₇H₃₄N₂O₂

Molecular weight:

418.58 g/mol

Yield:

3.60 g, 8.60 mmol, 43%

**¹H NMR**

(300 MHz, [D₆]acetone): $\delta = 7.30$ (dd, ⁴J_{HH} = 1.5, 0.4 Hz, 2 H, H7), 7.15 (m, 2H, H 5), 4.71 (s, 2 H, CH₂), 3.47 (sept, ³J_{HH} = 6.9 Hz, 2 H, 4-CH(CH₃)₂), 3.04 (sept, ³J_{HH} = 6.9 Hz, 2 H, 6-CH(CH₃)₂), 1.37 (d, ³J_{HH} = 6.9 Hz, 12 H, 4-CH(CH₃)₂), 1.28 (d, ³J_{HH} = 6.9 Hz, 12 H, 6-CH(CH₃)₂) ppm.

¹³C{¹H} NMR

(75 MHz, CDCl₃): $\delta = 158.7$ (2 C, C1), 151.6 (2 C, C8), 147.0 (2 C, C6), 140.8 (2 C, C4), 137.5 (2 C, C3) 119.9 (2 C, C5), 105.4 (2 C, C7), 34.7 (2 C, 6-CH(CH₃)₂), 29.8 (2 C, 4-CH(CH₃)₂), 29.8 (1 C, C_{bridge}), 24.5 (4C, 6-CH(CH₃)₂), 23.3 (4 C, 4-CH(CH₃)₂) ppm.

¹H NMR

(300 MHz, [D₈]THF): δ = 7.23 (d, $^4J_{\text{HH}} = 1.5$ Hz, 2 H, H7), 7.07 (m, 2 H, H5), 4.62 (s, 2 H, CH₂), 3.46 (sept, $^3J_{\text{HH}} = 6.9$ Hz, 2 H, 4-CH(CH₃)₂), 2.99 (sept, $^3J_{\text{HH}} = 6.9$ Hz, 2 H, 6-CH(CH₃)₂), 1.38 (d, $^3J_{\text{HH}} = 6.9$ Hz, 12 H, 4-CH(CH₃)₂), 1.26 (d, $^3J_{\text{HH}} = 6.9$ Hz, 12 H, 6-CH(CH₃)₂) ppm.

¹³C{¹H} NMR

(75 MHz, [D₈]THF): δ = 160.1 (2 C, C1), 152.8 (2 C, C8), 147.6 (2 C, C6), 141.5 (2 C, C4), 138.8 (2 C, C3) 120.9 (2 C, C5), 106.2 (2 C, C7), 35.7 (2 C, 6-CH(CH₃)₂), 31.5 (2 C, 4-CH(CH₃)₂), 29.9 (1 C, C_{bridge}), 24.9 (4 C, 6-CH(CH₃)₂), 23.5 (4 C, 4-CH(CH₃)₂) ppm.

¹H NMR

(300 MHz, C₆D₆): δ = 7.02 (m, 2 H, H7), 6.99 (m, 2 H, H5), 4.21 (s, 2 H, CH₂), 3.60 (sept, $^3J_{\text{HH}} = 6.9$ Hz, 2 H, 4-CH(CH₃)₂), 2.76 (sept, $^3J_{\text{HH}} = 6.9$ Hz, 2 H, 6-CH(CH₃)₂), 1.43 (d, $^3J_{\text{HH}} = 6.9$ Hz, 12 H, 4-CH(CH₃)₂), 1.13 (d, $^3J_{\text{HH}} = 6.9$ Hz, 12 H, 6-CH(CH₃)₂) ppm.

¹³C{¹H} NMR

(75 MHz, C₆D₆): δ = 159.1 (2 C, C1), 152.2 (2 C, C8), 146.9 (2 C, C6), 141.2 (2 C, C4), 138.4 (2 C, C3) 120.4 (2 C, C5), 105.7 (2 C, C7), 34.9 (2 C, 6-CH(CH₃)₂), 30.9 (2 C, 4-CH(CH₃)₂), 29.5 (1 C, C_{bridge}), 24.5 (4 C, 6-CH(CH₃)₂), 23.3 (4 C, 4-CH(CH₃)₂) ppm.

IR

(ATR) $\tilde{\nu}$ = 2959, 2930, 2870, 1609 ($\tilde{\nu}_{\text{C=N}}$), 1459, 1417, 1007, 848, 776 cm⁻¹.

MS (ESI(+))

m/z (%): 859.5 (67) [2*M* + Na⁺]⁺, 441.3 (36) [*M* + Na⁺]⁺, 419.3 (100) [*M* + H⁺]⁺.

HR-MS (ESI(+))

m/z: calcd. for [*M* + H⁺]⁺: 419.2693, found: 419.2695

Elemental analysis

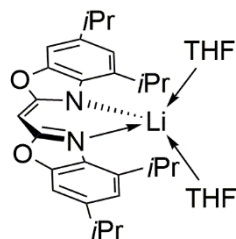
in % (calculated) C₂₇H₃₄N₂O₂ (418.58 g/mol): C 76.08 (77.48), H 8.38 (8.19), N 6.35 (6.69).

4.2.3.8 [Li(THF)₂{(4,6-*i*Pr-NCOC₆H₂)₂CH}] (27)

A solution of compound **26** (0.335M in THF, 1.43 mL, 478 μ mol, 1.00 eq.) was additionally diluted in THF (15 mL) and cooled to -60 °C. Under stirring, *n*BuLi (2.40M in hexane, 0.25 mL, 526 μ mol, 1.10 eq.) was slowly added dropwise. After complete addition, stirring was continued for an additional 15 min. The cooling-bath was removed and the mixture was stirred at RT for 18 h. The

solvent was removed under reduced pressure; the residue was washed with hexane (3 x 10 ml), then filtered *via* cannula and dried *in vacuo*. Recrystallization of the crude product from evaporation of pentane into a saturated solution of **27** in THF at RT gave colorless plate-shaped crystals suitable for X-ray diffraction analysis (188 mg, 69%).

Chemical Formula: C₃₅H₄₉LiN₂O₄
Molecular weight: 568.73 g/mol
Yield: 188 mg, 331 μmol, 69%



¹H NMR

(300 MHz, [D₈]THF): δ = 6.84 (dd, ⁴J_{HH} = 1.6, 0.4 Hz, 2 H, H7), 6.82 (m, 2 H, H5), 4.72 (s, 1 H, H_{bridge}), 3.62 (m, 8 H, OCH₂CH₂), 3.51 (sept, ³J_{HH} = 6.9 Hz, 2 H, 4-CH(CH₃)₂), 2.89 (sept, ³J_{HH} = 6.9 Hz, 2 H, 6-CH(CH₃)₂), 1.77 (m, 8 H, OCH₂CH₂), 1.29 (d, ³J_{HH} = 6.9 Hz, 12 H, 4-CH(CH₃)₂), 1.24 (d, ³J_{HH} = 6.9 Hz, 12 H, 6-CH(CH₃)₂) ppm.

¹³C{¹H} NMR

(75 MHz, [D₈]THF): δ = 170.5 (2 C, C1), 150.2 (2 C, C8), 141.2 (4 C, C6 + C4), 134.1 (2 C, C3), 117.8 (2 C, C5), 103.6 (2 C, C7), 68.4 (4 C, OCH₂CH₂), 56.9 (1 C, C_{bridge}), 35.5 (2 C, 6-CH(CH₃)₂), 28.4 (2 C, 4-CH(CH₃)₂), 26.6 (4 C, OCH₂CH₂), 25.2 (4 C, 6-CH(CH₃)₂), 24.9 (4 C, 4-CH(CH₃)₂) ppm.

⁷Li NMR

(116 MHz, [D₈]THF): δ = 2.07 (s) ppm.

MS (LIFDI)

m/z (%): 424.2 (100) [M - 2(THF)]⁺, 417.2 (20) [(4,6-*i*Pr-NCOC₆H₂)₂CH₂ - H]⁺.

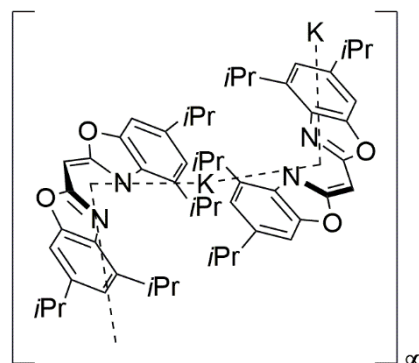
Elemental analysis

in % (calculated) C₃₅H₄₉LiN₂O₄ (568.73 g/mol): C 73.19 (73.92), H 8.80 (8.68), N 4.90 (4.93).

4.2.3.9 [K{η⁵-(4,6-*i*Pr-NCOC₆H₂)₂CH}]_∞ (**28**)

KH (25.0 mg, 623 μmol, 1.30 eq.) was suspended in THF (15 mL) and a solution of **26** (0.335M in THF, 1.43 mL, 478 μmol, 1.00 eq.) was slowly added dropwise. The mixture was stirred at RT for 18 h. The solvent from the green solution was removed under reduced pressure. The residue was washed with hexane (3 x 10 mL) and subsequently dried to give an off-white solid. Recrystallization from the evaporation of pentane into a saturated solution of **28** in THF at RT yielded tiny colorless needle-shaped crystals not suitable for X-ray diffraction analysis (155 mg, 71%).

Chemical Formula:	$C_{27}H_{33}KN_2O_2$
Molecular weight:	456.67 g/mol
Yield:	155 mg, 339 μ mol, 71%



1H NMR

(300 MHz, $[D_8]$ THF):	$\delta = 6.78$ (m, 2 H, H7), 6.73 (m, 2 H, H5), 4.61 (s, 1 H, H _{bridge}), 3.33 (sept, $^3J_{HH} = 6.9$ Hz, 2 H, 4-CH(CH ₃) ₂), 2.87 (sept, $^3J_{HH} = 6.9$ Hz, 2 H, 6-CH(CH ₃) ₂), 1.32 (d, $^3J_{HH} = 6.9$ Hz, 6 H, 4-CH(CH ₃) ₂), 1.23 (d, $^3J_{HH} = 6.9$ Hz, 6 H, 6-CH(CH ₃) ₂) ppm.
-------------------------	---

$^{13}C\{^1H\}$ NMR

(75 MHz, $[D_8]$ THF):	$\delta = 170.0$ (2 C, C1), 150.3 (2 C, C8), 143.3 (2 C, C3), 140.0 (2 C, C6), 132.9 (2 C, C4), 116.9 (2 C, C5), 103.3 (2 C, C7), 56.6 (1 C, C _{bridge}), 35.5 (2 C, 6-CH(CH ₃) ₂), 29.7 (2 C, 4-CH(CH ₃) ₂), 25.3 (4 C, 6-CH(CH ₃) ₂), 23.7 (4 C, 4-CH(CH ₃) ₂) ppm.
------------------------	---

MS (LIFDI)

m/z (%):	495.1 (35) $[M + K]^+$, 456.1 (100) $[M]^+$, 417.2 (20) $[(4,6-iPr-NCOC_6H_2)_2CH_2 - H]^+$.
------------	---

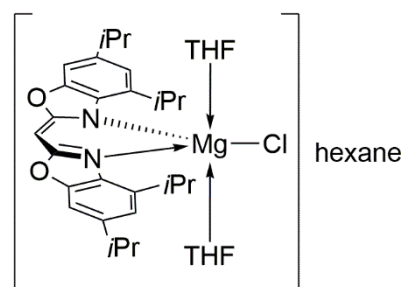
Elemental analysis

in % (calculated)	$C_{27}H_{33}KN_2O_2$ (456.67 g/mol): C 68.76 (71.01), H 7.37 (7.28), N 6.09 (6.13).
-------------------	--

4.2.3.10 $[MgCl(THF)_2\{(4,6-iPr-NCOC_6H_2)_2CH\}] \cdot \text{hexane}$ (**29**)

$(iPr)_2NMgCl \cdot (THF)_{0.65}$ (195 mg, 959 μ mol, 2.01 eq.) was dissolved in THF (15 mL). Then, a solution of **26** (0.335M in THF, 1.43 mL, 478 μ mol, 1.00 eq.) was very slowly added dropwise to maximize the formation of the heteroleptic compound. The mixture was stirred at RT for 18 h. The solvent was removed under reduced pressure; the residue was extracted with hexane (3 x 10 mL), and then filtered *via* cannula. The yellow filtrate was stored at $-28^\circ C$ to give colorless crystals of **29** suitable for X-ray diffraction analysis.

Chemical Formula:	$C_{41}H_{63}ClMgN_2O_4$
Molecular weight:	707.72 g/mol
Yield:	166 mg, 235 μ mol, 49%



¹H NMR

(300 MHz, C₆D₆): δ = 7.11 (d, $^4J_{\text{HH}} = 1.6$ Hz, 2 H, H7), 7.02 (d, $^4J_{\text{HH}} = 1.6$ Hz, 2 H, H5), 5.59 (s, 1 H, H_{bridge}), 4.15 (sept, $^3J_{\text{HH}} = 6.9$ Hz, 2 H, 4-CH(CH₃)₂), 3.59 (m, 8 H, OCH₂CH₂), 2.82 (sept, $^3J_{\text{HH}} = 6.9$ Hz, 2 H, 6-CH(CH₃)₂), 1.51 (d, $^3J_{\text{HH}} = 6.9$ Hz, 12 H, 4-CH(CH₃)₂), 1.19 (d, $^3J_{\text{HH}} = 6.9$ Hz, 12 H, 6-CH(CH₃)₂), 1.11 (m, 8 H, OCH₂CH₂) ppm.

¹³C{¹H} NMR

(75 MHz, C₆D₆): δ = 169.6 (2 C, C1), 149.2 (2 C, C8) 143.6 (4 C, C6 + C4), 135.1 (2 C, C3), 119.1 (2 C, C5) 104.4 (2 C, C7), 69.1 (4 C, OCH₂CH₂), 59.1 (1 C, C_{bridge}), 34.7 (2 C, 6-CH(CH₃)₂), 29.4 (2 C, 4-CH(CH₃)₂) 25.4 (4 C, OCH₂CH₂) 24.7 (4 C, 6-CH(CH₃)₂) 24.6 (4 C, 4-CH(CH₃)₂) ppm.

MS (LIFDI)

m/z (%): 858.5 (89) [*M* - Cl - 2(THF) + (4,6-*i*Pr-NCOC₆H₂)₂CH]⁺, 429.2 (50) [*M* - Cl - 2(THF) + 2((4,6-*i*Pr-NCOC₆H₂)₂CH₂)]²⁺, 418.3 (100) [(4,6-*i*Pr-NCOC₆H₂)₂CH₂]⁺.

Elemental analysis

in % (calculated) C₄₁H₆₃ClMgN₂O₄ (707.72 g/mol): C 67.85 (69.58), H 8.02 (8.97), N 4.66 (3.96). (The deviation is due to the loss of lattice hexane molecules in the drying process.)

4.2.3.11 [M(THF)_n{(4,6-*i*Pr-NCOC₆H₂)₂CH]₂] (30-33) (M = Mg, Ca, Sr, Ba; n = 0-1)

[M(THF)₂{N(SiMe₃)₂}]₂ (M = Mg, Ca, Sr, Ba, 526 μmol, 1.10 eq.) was dissolved in THF (15 mL). Then, a solution of **26** (0.335M in THF, 1.43 mL, 478 μmol, 1.00 eq.) was added dropwise and the mixture was stirred at RT for 18 h. The solvent was removed under reduced pressure. Recrystallization of crude **30** from a saturated hexane solution as well as from evaporation of pentane into saturated solutions of crude **31**, **32** or **33** in THF at RT yielded crystals suitable for X-ray diffraction analysis in each case.

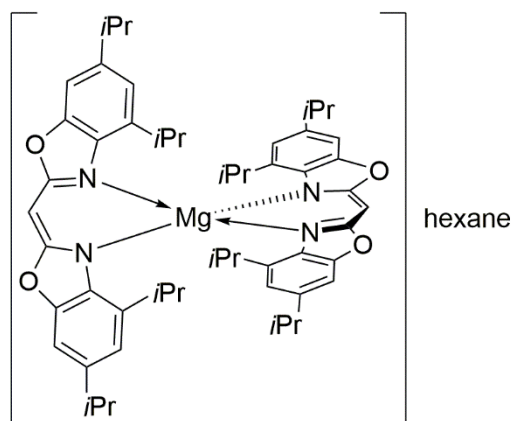
30 · hexane:**Chemical Formula:**C₆₀H₈₀MgN₄O₄**Molecular weight:**

945.63 g/mol

Yield:

134 mg, 142 μmol,

59%



¹H NMR

(300 MHz, [D₈]THF): δ = 7.01 (d, $^4J_{\text{HH}} = 1.6$ Hz, 4 H, H7), 6.80 (d, $^4J_{\text{HH}} = 1.6$ Hz, 4 H, H5), 5.39 (s, 2 H, H_{bridge}), 3.09 (sept, $^3J_{\text{HH}} = 6.9$ Hz, 4 H, 4-CH(CH₃)₂), 2.86 (sept, $^3J_{\text{HH}} = 6.9$ Hz, 4 H, 6-CH(CH₃)₂), 1.18 (d, $^3J_{\text{HH}} = 6.9$ Hz, 24 H, 4-CH(CH₃)₂), 0.77 (d, $^3J_{\text{HH}} = 6.8$ Hz, 24 H, 6-CH(CH₃)₂) ppm.

¹³C{¹H} NMR

(75 MHz, [D₈]THF): δ = 170.6 (4 C, C1), 149.4 (4 C, C8), 144.4 (4 C, C6), 136.9 (4 C, C3), 134.8 (4 C, C4), 119.6 (4 C, C5) 105.0 (4 C, C7), 59.7 (2 C, C_{bridge}), 35.3 (4 C, 6-CH(CH₃)₂), 31.0 (4 C, 4-CH(CH₃)₂), 24.7 (8 C, 6-CH(CH₃)₂), 24.1 (8 C, 4-CH(CH₃)₂) ppm.

MS (LIFDI)

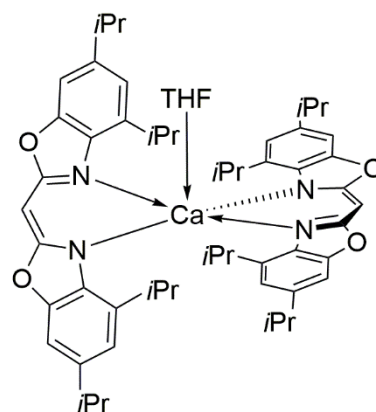
m/z (%): 858.5 (70) [*M* - C₆H₁₄]⁺, 729.4 (100) [*M* - (4,6-*i*Pr-NCOC₆H₂) - C₆H₁₄ + THF]⁺.

Elemental analysis

in % (calculated) C₆₀H₈₀MgN₄O₄ (945.63 g/mol): C 75.26 (76.21), H 7.93 (8.53), N 6.65 (5.92). (The deviation is due to the loss of lattice hexane molecules in the drying process.)

31:**Chemical Formula:**C₅₈H₇₄CaN₄O₅**Molecular weight:**

947.33 g/mol

Yield:97.0 mg, 102 μ mol, 43%**¹H NMR**

(300 MHz, [D₈]THF): δ = 6.95 (d, $^4J_{\text{HH}} = 1.6$ Hz, 4 H, H7), 6.78 (d, $^4J_{\text{HH}} = 1.6$ Hz, 4 H, H5), 5.08 (s, 2 H, H_{bridge}), 3.62 (m, 4 H, OCH₂CH₂), 3.31 (sept, $^3J_{\text{HH}} = 6.9$ Hz, 4 H, 4-CH(CH₃)₂), 2.87 (sept, $^3J_{\text{HH}} = 6.9$ Hz, 4 H, 6-CH(CH₃)₂), 1.78 (m, 4 H, OCH₂CH₂), 1.20 (d, $^3J_{\text{HH}} = 6.9$ Hz, 24 H, 4-CH(CH₃)₂), 0.78 (d, $^3J_{\text{HH}} = 6.9$ Hz, 24 H, 6-CH(CH₃)₂) ppm.

(400 MHz, C₆D₆):

δ = 7.01 (dd, $^4J_{\text{HH}} = 1.6, 0.4$ Hz, 4 H, H7), 6.80 (d, $^4J_{\text{HH}} = 1.6$ Hz, 4 H, H5), 5.78 (s, 2 H, H_{bridge}), 3.49 (sept, $^3J_{\text{HH}} = 6.9$ Hz, 4 H, 4-CH(CH₃)₂), 3.13 (m, 4 H, OCH₂CH₂), 2.71 (sept, $^3J_{\text{HH}} = 6.8$ Hz, 4 H, 6-CH(CH₃)₂), 1.10 (d, $^3J_{\text{HH}} = 6.9$ Hz, 24 H, 4-CH(CH₃)₂), 0.98

(d, $^3J_{\text{HH}} = 6.9$ Hz, 24 H, 6-CH(CH₃)₂), 0.84 (m, 4 H, OCH₂CH₂) ppm.

¹³C{¹H} NMR

(100 MHz, C₆D₆):

$\delta = 169.8$ (4 C, C1), 149.1 (4 C, C8), 143.1 (4 C, C6) 138.7 (4 C, C4), 134.3 (4 C, C3), 118.6 (4 C, C5), 104.3 (4 C, C7), 68.5 (2 C, OCH₂CH₂), 58.8 (2 C, C_{bridge}), 34.6 (4 C, 6-CH(CH₃)₂), 31.2 (4 C, 4-CH(CH₃)₂), 25.0 (2 C, OCH₂CH₂), 24.5 (8 C, 6-CH(CH₃)₂), 23.8 (8 C, 4-CH(CH₃)₂) ppm.

MS (LIFDI)

m/z (%):

874.5 (100) [*M* – THF]⁺.

Elemental analysis

in % (calculated)

C₅₈H₇₄SrN₄O₅ (947.33 g/mol): C 73.48 (73.54), H 7.91 (7.87), N 6.39 (5.91). (The deviation is due to partial loss of THF in the drying process.)

32:

Chemical Formula:

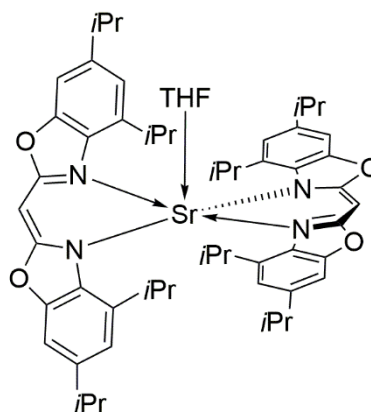
C₅₈H₇₄SrN₄O₅

Molecular weight:

994.87 g/mol

Yield:

169 mg, 170 μmol , 71%

**¹H NMR**

(300 MHz, [D₈]THF):

$\delta = 6.96$ (d, $^4J_{\text{HH}} = 1.6$ Hz, 4 H, H7), 6.81 (d, $^4J_{\text{HH}} = 1.6$ Hz, 4 H, H5), 5.02 (s, 2 H, H_{bridge}), 3.62 (m, 4 H, OCH₂CH₂), 3.13 (sept, $^3J_{\text{HH}} = 6.9$ Hz, 4 H, 4-CH(CH₃)₂), 2.87 (sept, $^3J_{\text{HH}} = 6.9$ Hz, 4 H, 6-CH(CH₃)₂), 1.78 (m, 4 H, OCH₂CH₂), 1.21 (d, $^3J_{\text{HH}} = 6.9$ Hz, 24 H, 4-CH(CH₃)₂), 0.88 (d, $^3J_{\text{HH}} = 6.9$ Hz, 24 H, 6-CH(CH₃)₂) ppm.

¹³C{¹H} NMR

(75 MHz, [D₈]THF):

$\delta = 169.7$ (4 C, C1), 149.6 (4 C, C8), 143.4 (4 C, C6), 139.8 (4 C, C4), 134.7 (4 C, C3), 119.1 (4 C, C5), 104.4 (4 C, C7), 68.4 (2 C, OCH₂CH₂), 58.1 (2 C, C_{bridge}), 35.4 (4 C, 6-CH(CH₃)₂), 31.4 (4 C, 4-CH(CH₃)₂), 26.6 (2 C, OCH₂CH₂), 25.2 (8 C, 6-CH(CH₃)₂), 25.0 (8 C, 4-CH(CH₃)₂) ppm.

MS (LIFDI)

m/z (%):

922.4 (100) [*M* – THF]⁺.

Elemental analysis

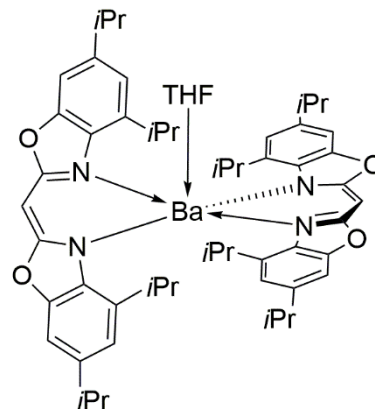
in % (calculated)

$C_{58}H_{74}SrN_4O_5$ (994.87 g/mol): C 69.31 (70.02), H 7.20 (7.50), N 5.92 (5.63). (The deviation is due to partial loss of THF in the drying process and a minor contamination with **26**.)

33:

Chemical Formula: $C_{58}H_{74}BaN_4O_5$ **Molecular weight:**

1044.58 g/mol

Yield:100 mg, 95.7 μ mol, 40% **1H NMR**(300 MHz, $[D_8]$ THF):

δ = 6.87 (d, $^4J_{HH}$ = 1.6 Hz, 4 H, H7), 6.82 (d, $^4J_{HH}$ = 1.6 Hz, 4 H, H5), 4.85 (s, 2 H, H_{bridge}), 3.62 (m, 4 H, OCH_2CH_2), 3.19 (sept, $^3J_{HH}$ = 6.9 Hz, 4 H, 4- $CH(CH_3)_2$), 2.90 (sept, $^3J_{HH}$ = 6.9 Hz, 4 H, 6- $CH(CH_3)_2$), 1.77 (m, 4 H, OCH_2CH_2), 1.24 (d, $^3J_{HH}$ = 6.9 Hz, 24 H, 4- $CH(CH_3)_2$), 1.07 (d, $^3J_{HH}$ = 6.9 Hz, 24 H, 6- $CH(CH_3)_2$) ppm.

 $^{13}C\{^1H\}$ NMR(75 MHz, $[D_8]$ THF):

δ = 168.8 (4 C, C1), 149.9 (4 C, C8), 142.8 (4 C, C6), 140.6 (4 C, C4), 135.0 (4 C, C3), 118.5 (4 C, C5), 104.1 (4 C, C7), 68.4 (2 C, OCH_2CH_2), 56.9 (2 C, C_{bridge}), 35.5 (4 C, 6- $CH(CH_3)_2$), 30.6 (4 C, 4- $CH(CH_3)_2$), 26.6 (2 C, OCH_2CH_2), 25.1 (8 C, 6- $CH(CH_3)_2$), 24.3 (8 C, 4- $CH(CH_3)_2$) ppm.

MS (LIFDI) m/z (%):972.4 (100) $[M - THF]^+$.**Elemental analysis**

in % (calculated)

$C_{58}H_{74}BaN_4O_5$ (1044.58 g/mol): C 66.52 (66.69), H 7.21 (7.14), N 5.70 (5.36). (The deviation is due to partial loss of THF in the drying process and a minor contamination with **26**.)

5 APPENDIX

Major parts of this chapter have been published in:

- [1] **I. Koehne**, R. Herbst-Irmer, D. Stalke, “*Bis(4-methylbenzoxazol-2-yl)methanide in s-Block Metal Coordination*”, *Eur. J. Inorg. Chem.* **2017**, 2017, 3322-3326.^[1]
- [2] **I. Koehne**, S. Bachmann, T. Niklas, R. Herbst-Irmer, D. Stalke, “*A Novel Bulky Heteroaromatic-Substituted Methanide Mimicking NacNac: Bis(4,6-tert-butylbenzoxazol-2-yl)methanide in s-Block Metal Coordination*”, *Chem. Eur. J.* **2017**, 23, 13141-13149.^[2]
- [3] **I. Koehne**, S. Bachmann, R. Herbst-Irmer, D. Stalke, “*A Water-Containing Organopotassium Compound Based on Bis(4,6-tBu-benzoxazol-2-yl)methanide and Its Unexpected Stability to Hydrolysis*”, *Angew. Chem.* **2017**, 129, 15337-15342; *Angew. Chem. Int. Ed.* **2017**, 56, 15141-15145.^[3]
- [4] **I. Koehne**, N. Graw, T. Teuteberg, R. Herbst-Irmer, D. Stalke, “*Introducing NacNac-Like Bis(4,6-isopropylbenzoxazol-2-yl)methanide in s-Block Metal Coordination*”, *Inorg. Chem.* **2017**, 56, 14968-14978.^[4]

5.1 Crystallographic Data

5.1.1 [K(THF){(4-Me-NCOC₆H₃)₂CH}]_∞ (2)

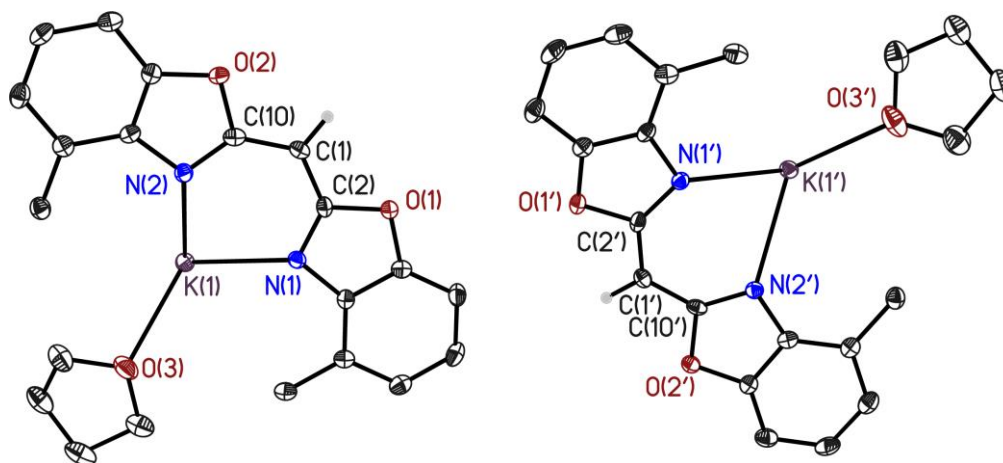


Figure 5-1. Asymmetric unit of **2** containing two molecules. Anisotropic displacement parameters are depicted at the 50% probability level. Hydrogen atoms are omitted for clarity, except for those at the bridging methylene positions. Reprinted with permission from reference ^[1]. Copyright 2017, John Wiley and Sons.

Table 5-1. Crystallographic data for **2**.

Structure code	IDK_069	CCDC no.	1536931	
Empirical formula	C ₂₁ H ₂₁ KN ₂ O ₃	μ [mm ⁻¹]	0.299	
Formula weight [g · mol ⁻¹]	388.50	$F(000)$	3264	
Temperature [K]	100(2)	Crystal size [mm]	0.405 x 0.097 x 0.030	
Wavelength [Å]	0.71073	θ range [°]	1.070 to 25.352	
Crystal system	Orthorhombic	Reflections collected	61122	
Space group	<i>Pbca</i>	Unique Reflections	7074	
Unit cell parameters		R_{int}	0.0659	
	a [Å]	7.103(2)	Completeness to θ_{max} [%]	100.0
	b [Å]	28.522(2)	Restraints / parameters	0 / 492
	c [Å]	38.061(3)	Goodness-of-fit on F^2	1.035
	α [°]	90	$R1$ [$I > 2\sigma(I)$]	0.0366
	β [°]	90	$wR2$ (all data)	0.0891
	γ [°]	90	Max. diff. peak / hole [$e \cdot \text{\AA}^{-3}$]	0.234 / -0.263
Volume [Å ³]	7711(2)	Absolute structure	--	
Z	16	Extinction coefficient	--	
$\rho_{calcd.}$ [Mg · m ⁻³]	1.339			

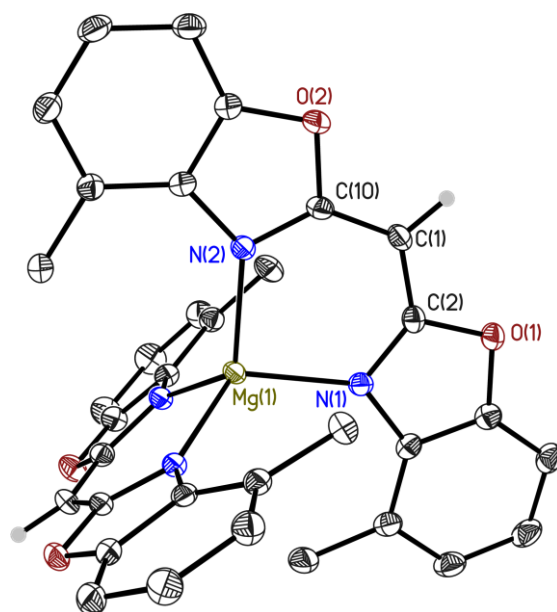
5.1.2 [Mg{(4-Me-NCOC₆H₃)₂CH₂}]₂ (3)

Figure 5-2. Asymmetric unit of **3**. Anisotropic displacement parameters are depicted at the 50% probability level. Hydrogen atoms are omitted for clarity, except for those at the bridging methylene positions. *Reprinted with permission from reference [1]. Copyright 2017, John Wiley and Sons.*

Table 5-2. Crystallographic data for **3**.

Structure code	IDK_067	CCDC no.	1536929
Empirical formula	C ₃₄ H ₂₆ MgN ₄ O ₄	μ [mm ⁻¹]	0.110
Formula weight [g · mol ⁻¹]	578.90	<i>F</i> (000)	1208
Temperature [K]	100(2)	Crystal size [mm]	0.218 x 0.142 x 0.128
Wavelength [Å]	0.71073	θ range [°]	1.822 to 30.042
Crystal system	Monoclinic	Reflections collected	58293
Space group	<i>P</i> 2 ₁ / <i>n</i>	Unique Reflections	8328
Unit cell parameters		<i>R</i> _{int}	0.0466
<i>a</i> [Å]	11.336(2)	Completeness to θ_{\max} [%]	100.0
<i>b</i> [Å]	15.002(2)	Restraints / parameters	0 / 392
<i>c</i> [Å]	16.777(2)	Goodness-of-fit on <i>F</i> ²	1.039
α [°]	90	<i>R</i> 1 [<i>I</i> >2 σ (<i>I</i>)]	0.0398
β [°]	93.10(2)	w <i>R</i> 2 (all data)	0.1034
γ [°]	90	Max. diff. peak / hole [e · Å ⁻³]	0.416 / -0.301
Volume [Å ³]	2849.0(7)	Absolute structure	--
<i>Z</i>	4	Extinction coefficient	--
$\rho_{\text{calcd.}}$ [Mg · m ⁻³]	1.350		

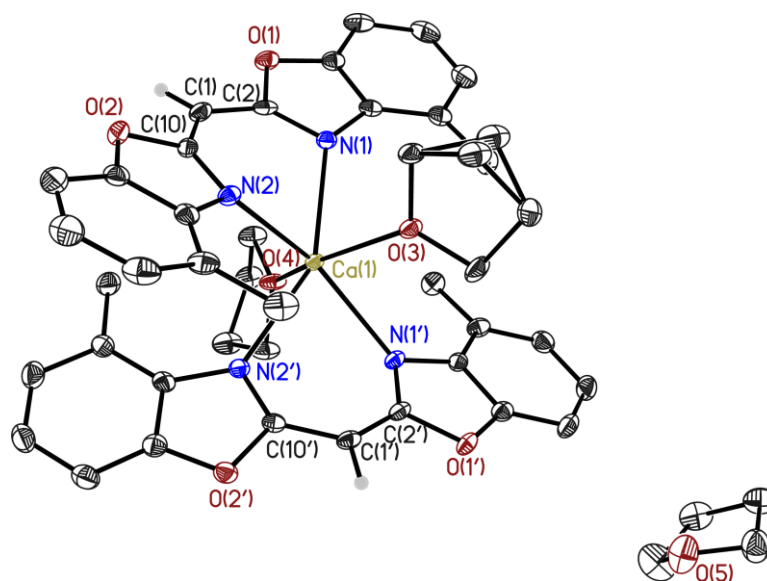
5.1.3 [Ca(THF)₂{(4-Me-NCOC₆H₃)₂CH₂}₂·THF (4)

Figure 5-3. Asymmetric unit of **4** also containing a co-crystallized lattice THF molecule. Anisotropic displacement parameters are depicted at the 50% probability level. Hydrogen atoms are omitted for clarity, except for those at the bridging methylene positions. One carbon atom and the corresponding hydrogen atoms of a coordinating THF molecule are disordered about two positions. They are refined with distance restraints and the anisotropic displacement parameters are constrained to be the same. The occupancy of the minor position refined to 0.061(7). Reprinted with permission from reference ^[1]. Copyright 2017, John Wiley and Sons.

Table 5-3. Crystallographic data for **4**.

Structure code	IDK_071	CCDC no.	1536930	
Empirical formula	C ₄₆ H ₅₀ CaN ₄ O ₇	μ [mm ⁻¹]	0.214	
Formula weight [g · mol ⁻¹]	810.98	$F(000)$	3440	
Temperature [K]	100(2)	Crystal size [mm]	0.219 x 0.165 x 0.043	
Wavelength [Å]	0.71073	θ range [°]	1.481 to 26.369	
Crystal system	Orthorhombic	Reflections collected	50606	
Space group	<i>Pbca</i>	Unique Reflections	8215	
Unit cell parameters		R_{int}	0.0634	
	a [Å]	18.297(2)	Completeness to θ_{max} [%]	100.0
	b [Å]	15.994(2)	Restraints / parameters	11 / 531
	c [Å]	27.504(3)	Goodness-of-fit on F^2	1.006
	α [°]	90	$R1$ [$I > 2\sigma(I)$]	0.0441
	β [°]	90	$wR2$ (all data)	0.1230
	γ [°]	90	Max. diff. peak / hole [$e \cdot \text{Å}^{-3}$]	0.599 / -0.280
Volume [Å ³]	8048.8(16)	Absolute structure	--	
Z	8	Extinction coefficient	--	
$\rho_{calcd.}$ [Mg · m ⁻³]	1.338			

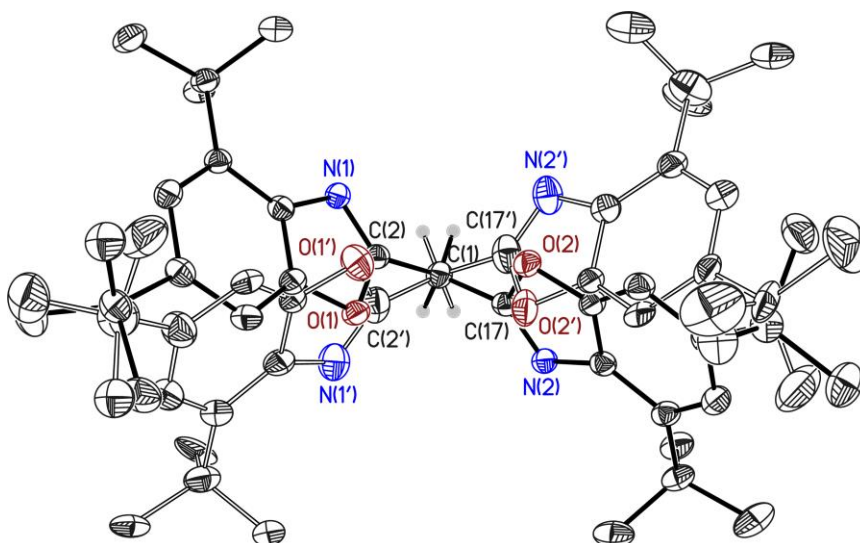
5.1.4 Bis(4,6-*t*Bu-benzoxazol-2-yl)methane (7)

Figure 5-4. Asymmetric unit of 7 containing one molecule. Anisotropic displacement parameters are depicted at the 50% probability level. Hydrogen atoms are omitted for clarity, except for those at the bridging methylene position. The whole molecule (except of C1) is disordered about two positions. It is refined with distance restraints and some of the anisotropic displacement parameters are constrained to be the same. The occupancy of the minor position refined to 0.062(1). Reprinted with permission from reference ^[2]. Copyright 2017, John Wiley and Sons.

Table 5-4. Crystallographic data for 7.

Structure code	IDK_035	CCDC no.	1551829
Empirical formula	C ₃₁ H ₄₂ N ₂ O ₂	μ [mm ⁻¹]	0.069
Formula weight [g · mol ⁻¹]	474.66	<i>F</i> (000)	1032
Temperature [K]	100(2)	Crystal size [mm]	0.274 x 0.215 x 0.070
Wavelength [Å]	0.71073	θ range [°]	1.400 to 26.062
Crystal system	Monoclinic	Reflections collected	50265
Space group	<i>P</i> 2 ₁ / <i>n</i>	Unique Reflections	5570
Unit cell parameters		<i>R</i> _{int}	0.0564
	<i>a</i> [Å] 18.068(2)	Completeness to θ_{\max} [%]	100.0
	<i>b</i> [Å] 7.992(2)	Restraints / parameters	1781 / 606
	<i>c</i> [Å] 19.848(2)	Goodness-of-fit on <i>F</i> ²	1.048
	α [°] 90	<i>R</i> 1 [<i>I</i> > 2 σ (<i>I</i>)]	0.0436
	β [°] 100.75(2)	w <i>R</i> 2 (all data)	0.1055
	γ [°] 90	Max. diff. peak / hole [e · Å ⁻³]	0.230 / -0.168
Volume [Å ³]	2815.7(8)	Absolute structure	--
<i>Z</i>	4	Extinction coefficient	0.0029(4)
$\rho_{\text{calcd.}}$ [Mg · m ⁻³]	1.120		

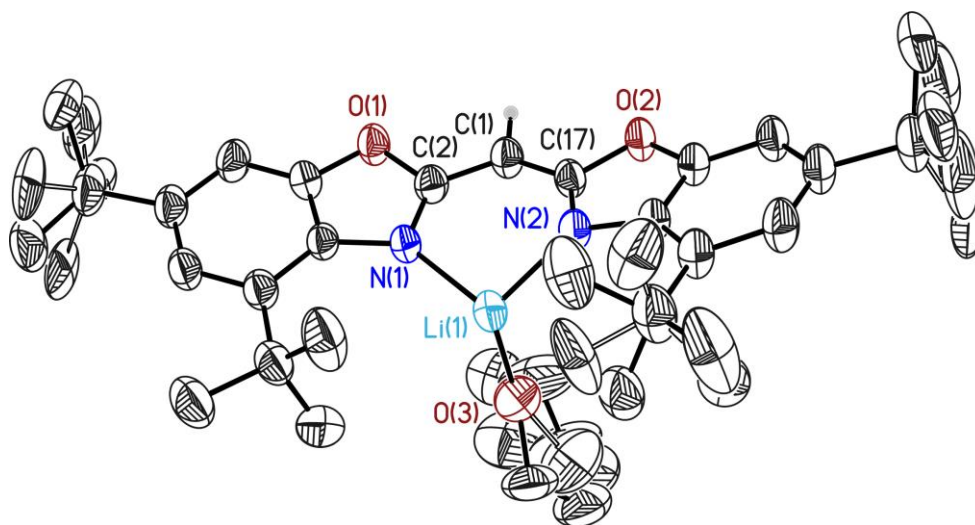
5.1.5 [Li(THF){(4,6-*t*Bu-NCOC₆H₂)₂CH}] (13)

Figure 5-5. Asymmetric unit of **13** containing one molecule. Anisotropic displacement parameters are depicted at the 50% probability level. Hydrogen atoms are omitted for clarity, except for that at the bridging methylene position. Due to a phase transition of the crystal at lower temperatures data collection had to be carried out at an elevated temperature of 180 K causing increased thermal movement and decreased scattering abilities. Thus, three of four *t*Bu substituents and the coordinating THF molecule are disordered about two positions. They are refined with distance restraints and restraints for the anisotropic displacement parameters. The minor positions refined to 0.49(1), 0.321(8), 0.42(1) and 0.39(1). Reprinted with permission from reference^[2]. Copyright 2017, John Wiley and Sons.

Table 5-5. Crystallographic data for **13**.

Structure code	IDK_058	CCDC no.	1551830
Empirical formula	C ₃₅ H ₄₉ LiN ₂ O ₃	μ [mm ⁻¹]	0.069
Formula weight [g · mol ⁻¹]	552.70	<i>F</i> (000)	2400
Temperature [K]	180(2)	Crystal size [mm]	0.126 x 0.116 x 0.091
Wavelength [Å]	0.71073	θ range [°]	1.219 to 25.510
Crystal system	Monoclinic	Reflections collected	49428
Space group	<i>C</i> 2/ <i>c</i>	Unique Reflections	6154
Unit cell parameters		<i>R</i> _{int}	0.0905
	<i>a</i> [Å] 34.402(6)	Completeness to θ_{\max} [%]	100.0
	<i>b</i> [Å] 12.474(2)	Restraints / parameters	1712 / 494
	<i>c</i> [Å] 15.983(3)	Goodness-of-fit on <i>F</i> ²	1.074
	α [°] 90	<i>R</i> 1 [<i>I</i> > 2 σ (<i>I</i>)]	0.0805
	β [°] 103.89(2)	<i>wR</i> 2 (all data)	0.2347
	γ [°] 90	Max. diff. peak / hole [e · Å ⁻³]	0.328 / -0.351
Volume [Å ³]	6658(2)	Absolute structure	--
<i>Z</i>	8	Extinction coefficient	--
$\rho_{\text{calcd.}}$ [Mg · m ⁻³]	1.103		

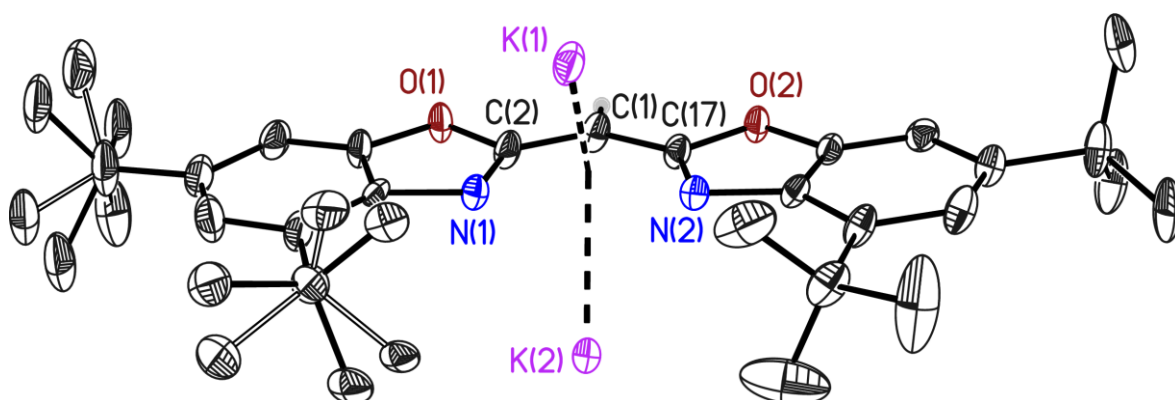
5.1.6 $[K\{\eta^5-(4,6-tBu-NCOC_6H_2)_2CH\}]_\infty$ (**14**)

Figure 5-6. Asymmetric unit of **14** containing one ligand molecule and two potassium ions, which both lie on an inversion center. Anisotropic displacement parameters are depicted at the 50% probability level. Hydrogen atoms are omitted for clarity, except for that at the bridging methylene position. The data were collected from a four-fold non-merohedral twin. The fractional contributions of the minor domains refined to 0.296(4), 0.202(3) and 0.193(3), respectively. The crystal diffract very weakly. Therefore the data are cut to a resolution of 0.9 Å. Two of four *t*Bu substituents are disordered about two positions. They are refined with distance restraints and restraints for the anisotropic displacement parameters. The occupancy of the minor positions refined to 0.48(1) and 0.088(9), respectively. Reprinted with permission from reference ^[2]. Copyright 2017, John Wiley and Sons.

Table 5-6. Crystallographic data for **14**.

Structure code	IDK_073		
Empirical formula	C ₃₁ H ₄₁ KN ₂ O ₂	CCDC no.	1551831
Formula weight [g · mol ⁻¹]	512.76	μ [mm ⁻¹]	0.210
Temperature [K]	100(2)	<i>F</i> (000)	552
Wavelength [Å]	0.71073	Crystal size [mm]	0.098 x 0.046 x 0.033
Crystal system	Triclinic	θ range [°]	2.353 to 23.301
Space group	<i>P</i> $\bar{1}$	Reflections collected	37614
Unit cell parameters		Unique Reflections	4010
	<i>a</i> [Å] 9.242(2)	<i>R</i> _{int}	0.1275
	<i>b</i> [Å] 9.733(2)	Completeness to θ_{\max} [%]	96.2
	<i>c</i> [Å] 17.430(3)	Restraints / parameters	712 / 393
	α [°] 86.98(2)	Goodness-of-fit on <i>F</i> ²	1.059
	β [°] 88.01(2)	<i>R</i> 1 [<i>I</i> >2 σ (<i>I</i>)]	0.0859
	γ [°] 69.48(2)	<i>wR</i> 2 (all data)	0.2061
Volume [Å ³]	1466.1(5)	Max. diff. peak / hole [e · Å ⁻³]	0.378 / -0.384
<i>Z</i>	2	Absolute structure	--
$\rho_{\text{calcd.}}$ [Mg · m ⁻³]	1.161	Extinction coefficient	--

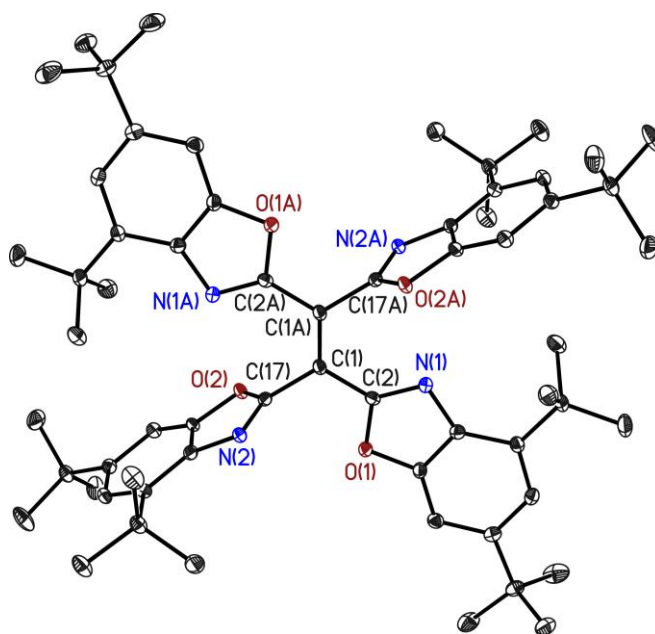
5.1.7 1,1,2,2-tetrakis(4,6-*t*Bu-benzoxazol-2-yl)ethene (15)

Figure 5-7. Asymmetric unit of **15** containing one molecule. Anisotropic displacement parameters are depicted at the 50% probability level. Hydrogen atoms are omitted for clarity.

Table 5-7. Crystallographic data for **15**.

Structure code	IDK_079	CCDC no.	1576653
Empirical formula	C ₆₂ H ₈₀ N ₄ O ₄	μ [mm ⁻¹]	0.070
Formula weight [g · mol ⁻¹]	945.30	$F(000)$	1024
Temperature [K]	100(2)	Crystal size [mm]	0.157 x 0.137 x 0.127
Wavelength [Å]	0.71073	θ range [°]	1.542 to 27.482
Crystal system	Monoclinic	Reflections collected	134577
Space group	$P2_1/c$	Unique Reflections	6383
Unit cell parameters		R_{int}	0.0364
a [Å]	9.974(2)	Completeness to θ_{max} [%]	100.0
b [Å]	26.406(2)	Restraints / parameters	0 / 328
c [Å]	11.263(3)	Goodness-of-fit on F^2	1.020
α [°]	90	$R1$ [$I > 2\sigma(I)$]	0.0372
β [°]	110.20(2)	$wR2$ (all data)	0.0938
γ [°]	90	Max. diff. peak / hole [$e \cdot \text{Å}^{-3}$]	0.387 / -0.215
Volume [Å ³]	2783.9(8)	Absolute structure	--
Z	2	Extinction coefficient	--
$\rho_{\text{calcd.}}$ [Mg · m ⁻³]	1.128		

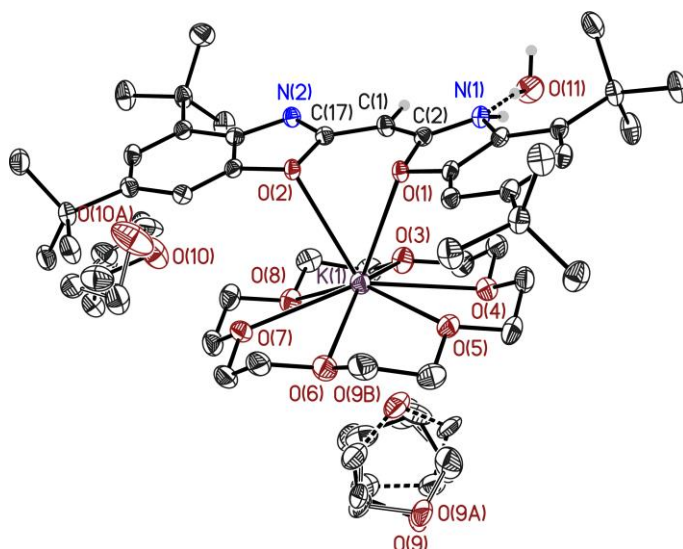
5.1.8 [K(18-crown-6)]{(4,6-*t*Bu-OCNC₆H₂)₂CH}·(H₂O)_{0.35}·(THF)₂ (**16**)

Figure 5-8. Asymmetric unit of **16** containing one molecule of the potassium complex and additionally a co-crystallized H₂O as well as two THF molecule. Anisotropic displacement parameters are depicted at the 50% probability level. Hydrogen atoms are omitted for clarity, except for those at the bridging methylene position and the water molecule. One of the co-crystallized THF molecules is disordered about two, the other about three positions. They are refined with distance restraints and restraints for the anisotropic displacement parameters. The occupancy of the minor position of the single disordered THF refined to 0.395(9), while these for the two-fold disordered THF refined to 0.057(2) and 0.346(3), respectively. Additionally, the occupancy of the water molecule was fixed to 0.35 to give sensible displacement parameters. One of its hydrogen atoms is partly protonating the nitrogen atom N(1). These hydrogen atoms were refined with distance restraints and U-values of 1.5 U(eq) of the O or the N atom, respectively. The H(O) position refined to 21% and the H(N) position to 14 %. Reprinted with permission from reference^[3]. Copyright 2017, John Wiley and Sons.

Table 5-8. Crystallographic data for **16**.

Structure code	IDK_084	CCDC no.	1555630
Empirical formula	C ₅₁ H ₈₁ KN ₂ O ₁₀ ·(H ₂ O) _{0.35}	μ [mm ⁻¹]	0.159
Formula weight [g · mol ⁻¹]	927.58	<i>F</i> (000)	2014
Temperature [K]	100(2)	Crystal size [mm]	0.180 x 0.110 x 0.100
Wavelength [Å]	0.71073	θ range [°]	1.487 to 25.323
Crystal system	Monoclinic	Reflections collected	61760
Space group	<i>P</i> 2 ₁ / <i>c</i>	Unique Reflections	9419
Unit cell parameters		<i>R</i> _{int}	0.0424
<i>a</i> [Å]	10.413(2)	Completeness to θ_{\max} [%]	100.0
<i>b</i> [Å]	15.047(2)	Restraints / parameters	1833 / 750
<i>c</i> [Å]	33.190(4)	Goodness-of-fit on <i>F</i> ²	1.059
α [°]	90	<i>R</i> ₁ [<i>I</i> >2 σ (<i>I</i>)]	0.0411
β [°]	95.48(2)	w <i>R</i> ₂ (all data)	0.0967
γ [°]	90	Max. diff. peak / hole [e · Å ⁻³]	0.254 / -0.294
Volume [Å ³]	5176.6(14)		

Z	4	Abs. struct. parameter	--
$\rho_{\text{calcd.}} [\text{Mg} \cdot \text{m}^{-3}]$	1.190	Extinction coefficient	--

5.1.9 [MgCl(THF)₂{(4,6-*t*Bu-NCOC₆H₂)₂CH}]·pentane (18)

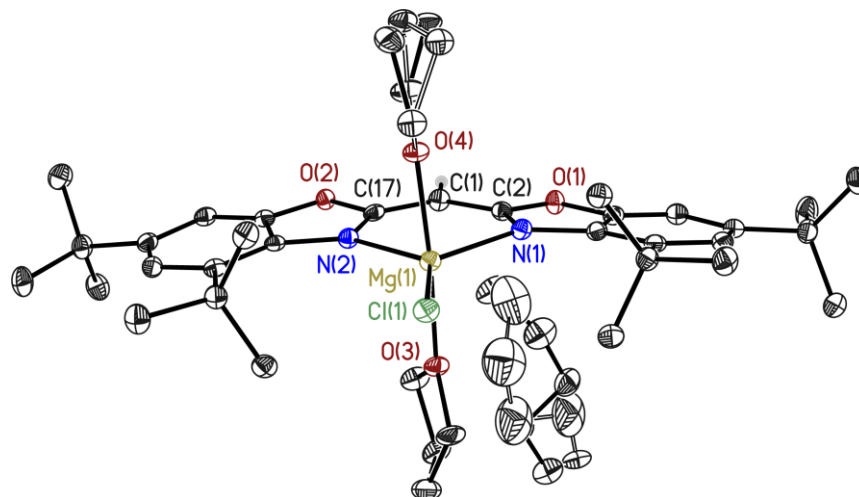


Figure 5-9. Asymmetric unit of **18** containing one molecule and co-crystallized lattice pentane molecule. Anisotropic displacement parameters are depicted at the 50% probability level. Hydrogen atoms are omitted for clarity, except for that at the bridging methylene position. The four carbon atoms of an attached THF molecule and a co-crystallized pentane molecule are disordered about two positions. They are refined with distance restraints and some of the anisotropic displacement parameters are constrained to be the same. The occupancy of the minor positions refined to 0.067(6) and 0.079(5), respectively. Reprinted with permission from reference^[2]. Copyright 2017, John Wiley and Sons.

Table 5-9. Crystallographic data for **18**.

Structure code	IDK_059	CCDC no.	1551832
Empirical formula	C ₄₄ H ₆₉ ClMgN ₂ O ₄	μ [mm ⁻¹]	0.145
Formula weight [g · mol ⁻¹]	749.77	<i>F</i> (000)	1632
Temperature [K]	100(2)	Crystal size [mm]	0.226 x 0.196 x 0.129
Wavelength [Å]	0.71073	θ range [°]	1.507 to 26.103
Crystal system	Monoclinic	Reflections collected	64634
Space group	<i>P</i> 2 ₁ / <i>n</i>	Unique Reflections	8491
Unit cell parameters		<i>R</i> _{int}	0.0410
<i>a</i> [Å]	10.775(3)	Completeness to θ_{max} [%]	99.9
<i>b</i> [Å]	27.033(7)	Restraints / parameters	771 / 546
<i>c</i> [Å]	14.765(4)	Goodness-of-fit on <i>F</i> ²	1.157
α [°]	90	<i>R</i> 1 [<i>I</i> >2 σ (<i>I</i>)]	0.0438
β [°]	90.92(2)	<i>wR</i> 2 (all data)	0.1024
γ [°]	90	Max. diff. peak / hole [e · Å ⁻³]	0.345 / -0.293
Volume [Å ³]	4300(2)	Absolute structure parameter	--
Z	4	Extinction coefficient	--
$\rho_{\text{calcd.}} [\text{Mg} \cdot \text{m}^{-3}]$	1.158		

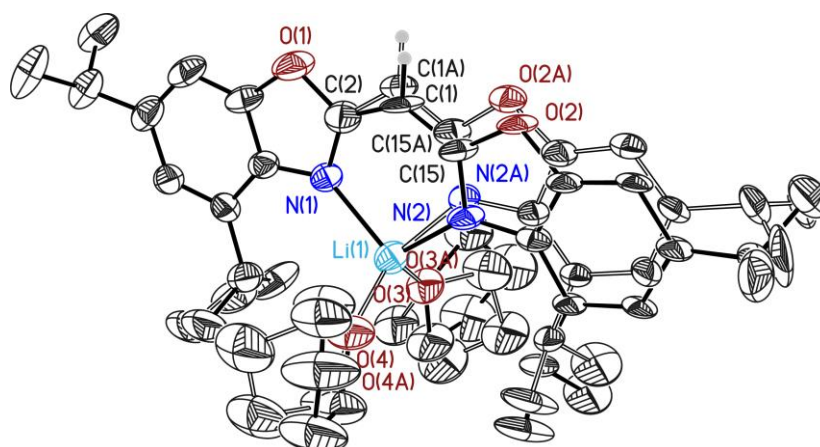
5.1.10 [Li(THF)₂{(4,6-*i*Pr-NCOC₆H₂)₂CH}] (27)

Figure 5-10. Asymmetric unit of **27** containing one molecule. Anisotropic displacement parameters are depicted at the 50% probability level. Hydrogen atoms are omitted for clarity, except for that at the bridging methylene position. One of the benzoxazol side arms of the ligand molecule as well as both attached THF donor molecules are disordered about two positions. They are refined with distance restraints and restraints for the anisotropic displacement parameters. The occupancy of the minor position of the heteroaromatic side arm refined to 0.370(13), while the minor positions of the THF molecules refined to 0.428(13) and 0.332(13), respectively. In the other side arm, one of the *i*Pr substituents is disordered about two positions. They are refined with distance restraints and partially with restraints for the anisotropic displacement parameters, since those of one of the methyl carbons are constraint to be the same. The minor position refined to 0.33(2). The disorder leads to a poor data-to-parameter ratio, but the restraints stabilize the refinement. *Reprinted with permission from reference* ^[4]. Copyright 2017, American Chemical Society.

Table 5-10. Crystallographic data for **27**.

Structure code	IDK_086	CCDC no.	1572042
Empirical formula	C ₃₅ H ₄₉ LiN ₂ O ₄	μ [mm ⁻¹]	0.074
Formula weight [g · mol ⁻¹]	568.70	<i>F</i> (000)	1232
Temperature [K]	100(2)	Crystal size [mm]	0.275 x 0.225 x 0.100
Wavelength [Å]	0.71073	θ range [°]	1.763 to 25.328
Crystal system	Monoclinic	Reflections collected	19040
Space group	<i>Cc</i>	Unique Reflections	5877
Unit cell parameters		<i>R</i> _{int}	0.0380
<i>a</i> [Å]	15.234(2)	Completeness to θ_{\max} [%]	100.0
<i>b</i> [Å]	9.324(2)	Restraints / parameters	2088 / 613
<i>c</i> [Å]	23.111(4)	Goodness-of-fit on <i>F</i> ²	1.079
α [°]	90	<i>R</i> ₁ [<i>I</i> > 2 σ (<i>I</i>)]	0.0751
β [°]	91.92(2)	<i>wR</i> ₂ (all data)	0.1933
γ [°]	90	Max. diff. peak / hole [e · Å ⁻³]	0.283 / -0.244
Volume [Å ³]	3280.9(10)	Absolute structure parameter ^[319]	-0.2(5)
<i>Z</i>	4	Extinction coefficient	--
$\rho_{\text{calcd.}}$ [Mg · m ⁻³]	1.151		

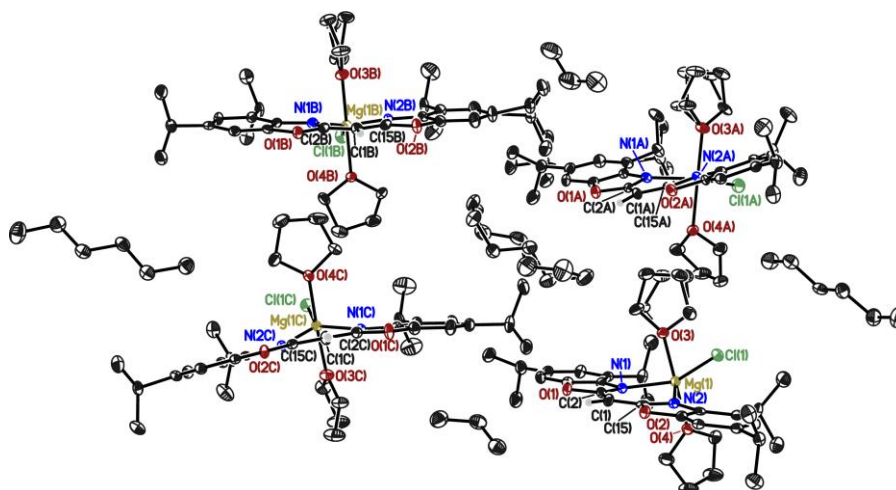
5.1.11 [MgCl(THF)₂{(4,6-*i*Pr-NCOC₆H₂)₂CH}]·hexane (29)

Figure 5-11. Asymmetric unit of **29** containing four equivalents of the complex as well as four lattice hexane molecules. Anisotropic displacement parameters are depicted at the 50% probability level. Hydrogen atoms are omitted for clarity, except for that at the bridging methylene position. The compound crystallized as a four-fold non-merohedral twin with the twin laws $1\ 0\ 0 / -1\ -1\ 0 / 0\ 0\ -1$; $-1\ 0\ 0 / 1\ 1\ 0.630 / 0\ 0\ -1$; $-1\ 0\ 0 / 0\ -1\ -0.630 / 0\ 0\ 1$. The fractional contributions of the minor components refined to 0.4290(8), 0.0132(11) and 0.0135(11), respectively. Three of the eight THF donor molecules are disordered about two positions. They are refined with distance restraints and restraints for the anisotropic displacement parameters. The occupancies of the minor positions refined to 0.307(8), 0.464(11) and 0.156(13), respectively. Additionally, three of the sixteen *i*Pr groups are disordered about two positions. They are refined with distance restraints and partially with restraints for the anisotropic displacement parameters, since those of four methyl group carbons are constrained to be the same. The minor positions refined to 0.293(10), 0.47(2) and 0.39(2), respectively. Additionally, one of the four lattice hexane molecules is disordered about two positions. They are refined with distance restraints and partially with restraints for the anisotropic displacement parameters, since those of a terminal methyl group are constrained to be the same. The minor position refined to 0.376(6). Reprinted with permission from reference ^[4]. Copyright 2017, American Chemical Society.

Table 5-11. Crystallographic data for **29**.

Structure code	IDK_063		
Empirical formula	C ₄₁ H ₆₃ ClMgN ₂ O ₄	CCDC no.	1572043
Formula weight [g · mol ⁻¹]	707.69	μ [mm ⁻¹]	0.150
Temperature [K]	100(2)	$F(000)$	3072
Wavelength [Å]	0.71073	Crystal size [mm]	0.221 x 0.125 x 0.085
Crystal system	Triclinic	θ range [°]	1.251 to 25.409
Space group	$P\bar{1}$	Reflections collected	82492
Unit cell parameters		Unique Reflections	29794
a [Å]	10.538(2)	R_{int}	0.0634
b [Å]	27.580(3)	Completeness to θ_{max} [%]	100.0
c [Å]	30.525(3)	Restraints / parameters	3278 / 2000
α [°]	110.40(2)	Goodness-of-fit on F^2	1.007
β [°]	90.04(2)	$R1$ [$I > 2\sigma(I)$]	0.0507
γ [°]	101.00(2)	$wR2$ (all data)	0.1128

Volume [\AA^3]	8141.(2)	Max. diff. peak / hole [$e \cdot \text{\AA}^{-3}$]	0.335 / -0.325
Z	8	Absolute structure parameter	--
$\rho_{\text{calcd.}}$ [$\text{Mg} \cdot \text{m}^{-3}$]	1.155	Extinction coefficient	--

5.1.12 $[\text{Mg}\{(\text{4,6-}i\text{Pr-NCOC}_6\text{H}_2)_2\text{CH}\}_2] \cdot \text{hexane}$ (30)

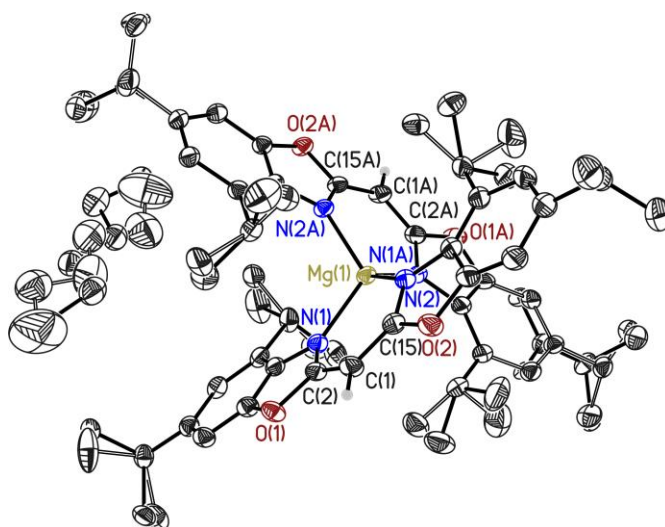


Figure 5-12. Asymmetric unit of **30**, additionally containing a lattice hexane molecule. Anisotropic displacement parameters are depicted at the 50% probability level. Hydrogen atoms are omitted for clarity, except for those at the bridging methylene positions. The co-crystallized hexane molecule, seven of the eight *iPr* groups as well as parts of one benzene perimeter are disordered about two positions. They are refined with distance restraints and restraints for the anisotropic displacement parameters. The occupancy of the minor position of the hexane molecule refined to 0.328(4). The minor positions of six of the *iPr* groups refined to 0.43(2), 0.344(7), 0.048(4), 0.251(13), 0.160(7), 0.38(2), respectively, while the minor position of the *iPr* group in combination with the disordered benzene perimeter refined to 0.489(6). Reprinted with permission from reference [4]. Copyright 2017, American Chemical Society.

Table 5-12. Crystallographic data for **30**.

Structure code	IDK_088	CCDC no.	1572044
Empirical formula	$\text{C}_{60}\text{H}_{80}\text{MgN}_4\text{O}_4$	μ [mm^{-1}]	0.083
Formula weight [$\text{g} \cdot \text{mol}^{-1}$]	945.59	$F(000)$	1024
Temperature [K]	100(2)	Crystal size [mm]	0.316 x 0.175 x 0.139
Wavelength [\AA]	0.71073	θ range [$^\circ$]	1.161 to 26.092
Crystal system	Triclinic	Reflections collected	113528
Space group	$P\bar{1}$	Unique Reflections	10686
Unit cell parameters		R_{int}	0.0480
a [\AA]	12.893(2)	Completeness to θ_{max} [%]	99.9
b [\AA]	13.337(2)	Restraints / parameters	2594 / 859
c [\AA]	18.684(2)	Goodness-of-fit on F^2	1.012
α [$^\circ$]	80.17(2)	R_1 [$I > 2\sigma(I)$]	0.0441
β [$^\circ$]	69.85(2)	wR_2 (all data)	0.1191
γ [$^\circ$]	63.48(2)		

Volume [\AA^3]	2698.2(9)	Max. diff. peak / hole [$e \cdot \text{\AA}^{-3}$]	0.317 / -0.234
Z	2	Absolute structure parameter	--
$\rho_{\text{calcd.}}$ [$\text{Mg} \cdot \text{m}^{-3}$]	1.164	Extinction coefficient	--

5.1.13 [Ca(THF){(4,6-*i*Pr-NCOC₆H₂)₂CH₂}₂] (31)

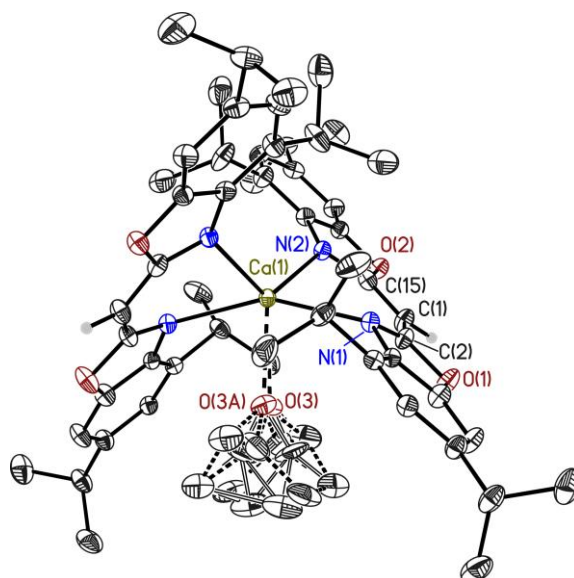


Figure 5-13. Molecular structure of **31**. Anisotropic displacement parameters are depicted at the 50% probability level. Hydrogen atoms are omitted for clarity, except for those at the bridging methylene positions. The compound crystallizes in space group $P4_32_12$ containing half a molecule in the asymmetric unit. The other half is generated by a two-fold rotation axis. The attached THF donor molecule is disordered about two positions as well as along the two-fold rotation axis. They are refined with distance restraints and partially with restraints for the anisotropic displacement parameters, since two of the ring CH₂ units are constrained to be the same. The minor position refined to 0.235(13). *Reprinted with permission from reference* ^[4]. Copyright 2017, American Chemical Society.

Table 5-13. Crystallographic data for **31**.

Structure code	IDK_089	CCDC no.	1572045
Empirical formula	C ₅₈ H ₇₄ CaN ₄ O ₅	μ [mm^{-1}]	0.174
Formula weight [g · mol ⁻¹]	974.29	$F(000)$	2040
Temperature [K]	100(2)	Crystal size [mm]	0.185 x 0.120 x 0.066
Wavelength [\AA]	0.71073	θ range [$^\circ$]	1.694 to 25.360
Crystal system	Tetragonal	Reflections collected	67625
Space group	$P4_12_12$	Unique Reflections	4755
Unit cell parameters		R_{int}	0.0672
a [\AA]	13.112(2)	Completeness to θ_{max} [%]	100.0
b [\AA]	13.112(2)	Restraints / parameters	243 / 358
c [\AA]	30.088(6)	Goodness-of-fit on F^2	1.045
α [$^\circ$]	90	$R1$ [$I > 2\sigma(I)$]	0.0330
β [$^\circ$]	90		

	γ [°]	90	wR2 (all data)	0.0786
Volume [Å ³]		5172.9(19)	Max. diff. peak / hole [e · Å ⁻³]	0.171 / -0.230
Z		4	Absolute structure parameter ^[319]	0.021(14)
$\rho_{\text{calcd.}}$ [Mg · m ⁻³]		1.216	Extinction coefficient	0.0023(3)

5.1.14 [Sr(THF){(4,6-*i*Pr-NCOC₆H₂)₂CH₂}₂] (32)

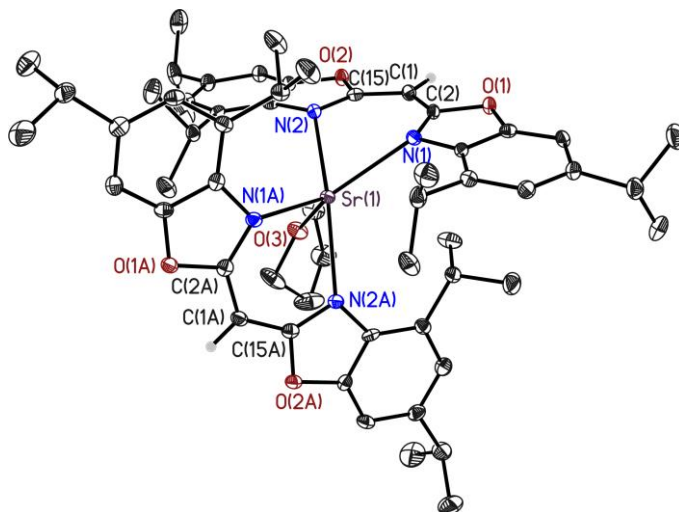


Figure 5-14. Asymmetric unit of **32** containing one molecule. Anisotropic displacement parameters are depicted at the 50% probability level. Hydrogen atoms are omitted for clarity, except for those at the bridging methylene positions. The compound crystallized as a two-fold non-merohedral twin with the twin law $-1\ 0\ 0 / 0\ -1\ 0 / 0.61\ 0\ 1$. The fractional contribution of the minor component refined to 0.2851(5). Reprinted with permission from reference ^[4]. Copyright 2017, American Chemical Society.

Table 5-14. Crystallographic data for **32**.

Structure code	IDK_090	CCDC no.	1572046
Empirical formula	C ₅₈ H ₇₄ SrN ₄ O ₅	μ [mm ⁻¹]	1.090
Formula weight [g · mol ⁻¹]	994.83	$F(000)$	2112
Temperature [K]	100(2)	Crystal size [mm]	0.240 x 0.129 x 0.105
Wavelength [Å]	0.71073	θ range [°]	2.187 to 26.454
Crystal system	Monoclinic	Reflections collected	174741
Space group	$P2_1/c$	Unique Reflections	11737
Unit cell parameters		R_{int}	0.0814
a [Å]	13.202(2)	Completeness to θ_{max} [%]	99.3
b [Å]	13.261(2)	Restraints / parameters	0 / 630
c [Å]	29.928(2)	Goodness-of-fit on F^2	1.084
α [°]	90	$R1$ [$I > 2\sigma(I)$]	0.0412
β [°]	97.72(2)	wR2 (all data)	0.0793
γ [°]	90	Max. diff. peak / hole [e · Å ⁻³]	0.393 / -0.288
Volume [Å ³]	5192.1(12)	Absolute structure parameter	--
Z	4		

$\rho_{\text{calcd.}}$ [$\text{Mg} \cdot \text{m}^{-3}$]	1.273	Extinction coefficient	--
--	-------	------------------------	----

5.1.15 $[\text{Ba}(\text{THF})\{(\text{4,6-}i\text{Pr-NCOC}_6\text{H}_2)_2\text{CH}\}_2]_2$ (**33**)

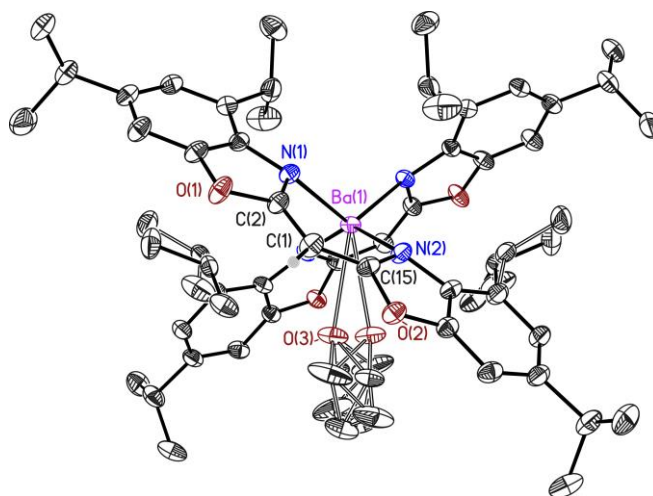


Figure 5-15. Molecular structure of **33**. Anisotropic displacement parameters are depicted at the 50% probability level. Hydrogen atoms are omitted for clarity, except for those at the bridging methylene positions. The compound crystallizes in space group $C2/c$ containing half a molecule in the asymmetric unit. The other half is generated by a two-fold rotation axis. Additionally, the attached THF donor molecule is disordered along this two-fold axis. Furthermore, one of the *i*Pr groups is disordered about two positions. They are refined with distance restraints and restraints for the anisotropic displacement parameters. The minor position refined to 0.475(5). Reprinted with permission from reference ^[4]. Copyright 2017, American Chemical Society.

Table 5-15. Crystallographic data for **33**.

Structure code	IDK_091	CCDC no.	1572047
Empirical formula	$\text{C}_{58}\text{H}_{74}\text{BaN}_4\text{O}_5$	μ [mm^{-1}]	0.809
Formula weight [$\text{g} \cdot \text{mol}^{-1}$]	1044.55	$F(000)$	2184
Temperature [K]	100(2)	Crystal size [mm]	0.237 x 0.144 x 0.104
Wavelength [\AA]	0.71073	θ range [$^\circ$]	1.931 to 26.384
Crystal system	Monoclinic	Reflections collected	154533
Space group	$C2/c$	Unique Reflections	5379
Unit cell parameters		R_{int}	0.0282
a [\AA]	19.286(2)	Completeness to θ_{max} [%]	100.0
b [\AA]	18.480(2)	Restraints / parameters	204 / 364
c [\AA]	14.984(2)	Goodness-of-fit on F^2	1.060
α [$^\circ$]	90	$R1$ [$I > 2\sigma(I)$]	0.0197
β [$^\circ$]	100.79(2)	wR2 (all data)	0.0503
γ [$^\circ$]	90	Max. diff. peak / hole [$\text{e} \cdot \text{\AA}^{-3}$]	0.586 / -0.322
Volume [\AA^3]	5246.0(11)	Absolute structure parameter	--
Z	4	Extinction coefficient	--
$\rho_{\text{calcd.}}$ [$\text{Mg} \cdot \text{m}^{-3}$]	1.323		

5.2 DOSY NMR Data

TMB was used as internal reference for all measurements with $\log D_{\text{ref,fix}}(\text{TMB}) = -8.7771$ (C_6D_6) and $\log D_{\text{ref,fix}}(\text{TMB}) = -8.7749$ ($[\text{D}_8]\text{THF}$). For C_6D_6 , the accuracy of the ECC (ED) is in the range of $MW_{\text{dif}} \leq \pm 8\%$, for ECC (DSE) in the range of $MW_{\text{dif}} \leq \pm 6\%$ and for ECC (Merge) in the range of $MW_{\text{dif}} \leq \pm 20\%$. For $[\text{D}_8]\text{THF}$, the accuracy of the ECC's is in a range of $MW_{\text{dif}} \leq \pm 3\%$ (ED), $MW_{\text{dif}} \leq \pm 8\%$ (DSE) and $MW_{\text{dif}} \leq \pm 18\%$ (Merge).

Table 5-16. ECC-parameters for DOSY measurements in $[\text{D}_8]\text{THF}^{[281]}$ and $\text{C}_6\text{D}_6^{[282]}$

	logK	error	α	error
$\text{ECC}_{\text{Merge}}^{[\text{D}_8]\text{THF}}$	-7.60	0.0407	-0.553	0.0180
$\text{ECC}_{\text{CS}}^{[\text{D}_8]\text{THF}}$	-7.74	0.0397	-0.494	0.0187
$\text{ECC}_{\text{DSE}}^{[\text{D}_8]\text{THF}}$	-7.54	0.0285	-0.582	0.0124
$\text{ECC}_{\text{ED}}^{[\text{D}_8]\text{THF}}$	-7.12	0.0449	-0.752	0.0191
	logK	error	α	error
$\text{ECC}_{\text{Merge}}^{\text{C}_6\text{D}_6}$	-7.58	0.0380	-0.572	0.0172
$\text{ECC}_{\text{CS}}^{\text{C}_6\text{D}_6}$	-7.75	0.0545	-0.494	0.0260
$\text{ECC}_{\text{DSE}}^{\text{C}_6\text{D}_6}$	-7.47	0.0284	-0.622	0.0124
$\text{ECC}_{\text{ED}}^{\text{C}_6\text{D}_6}$	-7.06	0.0861	-0.787	0.0365

Table 5-17. ^1H -DOSY-ECC-MW estimation of $[\text{Li}(\text{THF})\{(4,6\text{-}t\text{Bu-NCOC}_6\text{H}_2)_2\text{CH}\}]$ (**13**) in C_6D_6 at 25 °C. Hypothetical aggregates are $[\text{Li}(\text{THF})_n\{(4,6\text{-}t\text{Bu-NCOC}_6\text{H}_2)_2\text{CH}\}]$ with $n = 0 - 2$ in **A** to **C**.

^1H -DOSY		25 °C		
		Aggregate	MW_{calc} [g/mol]	MW_{dif} [%]
D_x [m^2/s]	6.357E-09	A	481	-16 (DSE)
$\log D_x$	-9.1967			-4 (ED)
$\log D_{x,\text{norm}}$	-9.1863			-25 (Merge)
$D_{\text{ref}}(\text{TMB})$ [m^2/s]	1.631E-09	B	553	-4 (DSE)
$\log D_{\text{ref}}(\text{TMB})$	-8.7875			10 (ED)
MW_{det} [g/mol] (ED)	503			-14 (Merge)
ΔMW_{det} [g/mol] (%) (ED)	± 64 (13)	C	625	9 (DSE)
MW_{det} [g/mol] (DSE)	575			24 (ED)
ΔMW_{det} [g/mol] (%) (DSE)	± 32 (6)			-3 (Merge)
MW_{det} [g/mol] (Merge)	643			
ΔMW_{det} [g/mol] (%) (Merge)	± 55 (9)			

Table 5-18. ^1H -DOSY-ECC-MW estimation of $[\text{K}\{\eta^5\text{-}(4,6\text{-}t\text{Bu-NCOC}_6\text{H}_2)_2\text{CH}\}]_{\infty}$ (**14**) in C_6D_6 at 25 °C. Hypothetical aggregates are $[\text{K}(\text{benzene})_n\{\eta^5\text{-}(4,6\text{-}t\text{Bu-NCOC}_6\text{H}_2)_2\text{CH}\}]$ with $n = 0 - 2$ in **A** to **C**.

^1H -DOSY		25 °C		
		Aggregate	MW_{calc} [g/mol]	MW_{dif} [%]
D_x [m^2/s]	7.050E-09	A	513	-8 (DSE)
$\log D_x$	-9.1518			5 (ED)
$\log D_{x,\text{norm}}$	-9.1774			-17 (Merge)
$D_{\text{ref}}(\text{TMB})$ [m^2/s]	1.772E-09	B	591	6 (DSE)
$\log D_{\text{ref}}(\text{TMB})$	-8.7515			21 (ED)
MW_{det} [g/mol] (ED)	490			-5 (Merge)
ΔMW_{det} [g/mol] (%) (ED)	± 62 (13)	C	669	20 (DSE)
MW_{det} [g/mol] (DSE)	556			37 (ED)
ΔMW_{det} [g/mol] (%) (DSE)	± 31 (6)			8 (Merge)
MW_{det} [g/mol] (Merge)	620			
ΔMW_{det} [g/mol] (%) (Merge)	± 52 (8)			

Table 5-19. ¹H-DOSY-ECC-MW estimation of K(18-crown-6){(4,6-*t*Bu-OCNC₆H₂)₂CH}·(H₂O)_{0.35}·(THF)₂ (**16**) in [D₈]THF at 25 °C. Hypothetical aggregates are [K(18-crown-6)(THF)_n{(4,6-*t*Bu-NCOC₆H₂)₂CH}] with n = 0 – 2 in **A** to **C**.

¹ H-DOSY		25 °C		
		Aggregate	MW _{calc} [g/mol]	MW _{dif} [%]
<i>D</i> _x [m ² /s]	5.782E-10	A	777	-11 (DSE)
log <i>D</i> _x	-9.2312			14 (ED)
log <i>D</i> _{x,norm}	-9.2509			-20 (Merge)
<i>D</i> _{ref} (TMB) [m ² /s]	1.757E-09	B	849	-2 (DSE)
log <i>D</i> _{ref} (TMB)	-8.7552			25 (ED)
MW _{det} [g/mol] (ED)	682			-12 (Merge)
ΔMW _{det} [g/mol] (%) (ED)	±56 (8)	C	921	6 (DSE)
MW _{det} [g/mol] (DSE)	870			35 (ED)
ΔMW _{det} [g/mol] (%) (DSE)	±64 (7)			-5 (Merge)
MW _{det} [g/mol] (Merge)	967			
ΔMW _{det} [g/mol] (%) (Merge)	±112 (12)			

Table 5-20. ¹H-DOSY-ECC-MW estimation of [MgCl(THF)₂{(4,6-*t*Bu-NCOC₆H₂)₂CH}] (**18**) in C₆D₆ at 25 °C. Hypothetical aggregates are [MgCl(THF)_n{(4,6-*t*Bu-NCOC₆H₂)₂CH}] with n = 0 – 2 in **A** to **C**.

¹ H-DOSY		25 °C		
		Aggregate	MW _{calc} [g/mol]	MW _{dif} [%]
<i>D</i> _x [m ² /s]	5.845E-09	A	533	-12 (DSE)
log <i>D</i> _x	-9.2332			1 (ED)
log <i>D</i> _{x,norm}	-9.2020			-22 (Merge)
<i>D</i> _{ref} (TMB) [m ² /s]	1.555E-09	B	606	0 (DSE)
log <i>D</i> _{ref} (TMB)	-8.8083			15 (ED)
MW _{det} [g/mol] (ED)	527			-12 (Merge)
ΔMW _{det} [g/mol] (%) (ED)	±67 (13)	C	678	11 (DSE)
MW _{det} [g/mol] (DSE)	609			29 (ED)
ΔMW _{det} [g/mol] (%) (DSE)	±34 (6)			-1 (Merge)
MW _{det} [g/mol] (Merge)	685			
ΔMW _{det} [g/mol] (%) (Merge)	±59 (9)			

Table 5-21. ¹H-DOSY-ECC-MW estimation of [MgBr(THF)₂{(4,6-*t*Bu-NCOC₆H₂)₂CH}] (**18a**) in C₆D₆ at 25 °C. Hypothetical aggregates are [MgBr(THF)_n{(4,6-*t*Bu-NCOC₆H₂)₂CH}] with n = 0 – 2 in **A** to **C**.

¹ H-DOSY		25 °C		
		Aggregate	MW _{calc} [g/mol]	MW _{dif} [%]
<i>D</i> _x [m ² /s]	5.476E-09	A	578	-9 (DSE)
log <i>D</i> _x	-9.2616			6 (ED)
log <i>D</i> _{x,norm}	-9.2127			-19 (Merge)
<i>D</i> _{ref} (TMB) [m ² /s]	1.493E-09	B	649	2 (DSE)
log <i>D</i> _{ref} (TMB)	-8.8259			19 (ED)
MW _{det} [g/mol] (ED)	544			-9 (Merge)
ΔMW _{det} [g/mol] (%) (ED)	±70 (13)	C	720	14 (DSE)
MW _{det} [g/mol] (DSE)	634			32 (ED)
ΔMW _{det} [g/mol] (%) (DSE)	±36 (6)			1 (Merge)
MW _{det} [g/mol] (Merge)	715			
ΔMW _{det} [g/mol] (%) (Merge)	±62 (9)			

Table 5-22. ¹H-DOSY-ECC-MW estimation of [Mg{(4,6-*t*Bu-NCOC₆H₂)₂CH}₂] (**19**) in C₆D₆ at 25 °C.

¹ H-DOSY		25 °C		
		Aggregate	MW _{calc} [g/mol]	MW _{dif} [%]
<i>D</i> _x [m ² /s]	4.548E-09	Homoleptic	972	14 (DSE)
log <i>D</i> _x	-9.3422			41 (ED)
log <i>D</i> _{x,norm}	-9.2942			-2 (Merge)
<i>D</i> _{ref} (TMB) [m ² /s]	1.496E-09			
log <i>D</i> _{ref} (TMB)	-8.8251			
MW _{det} [g/mol] (ED)	690			
ΔMW _{det} [g/mol] (%) (ED)	±92 (13)			
MW _{det} [g/mol] (DSE)	857			
ΔMW _{det} [g/mol] (%) (DSE)	±50 (6)			
MW _{det} [g/mol] (Merge)	993			
ΔMW _{det} [g/mol] (%) (Merge)	±90 (9)			

5.3 Spectra of ^1H NMR Water Titration Experiments

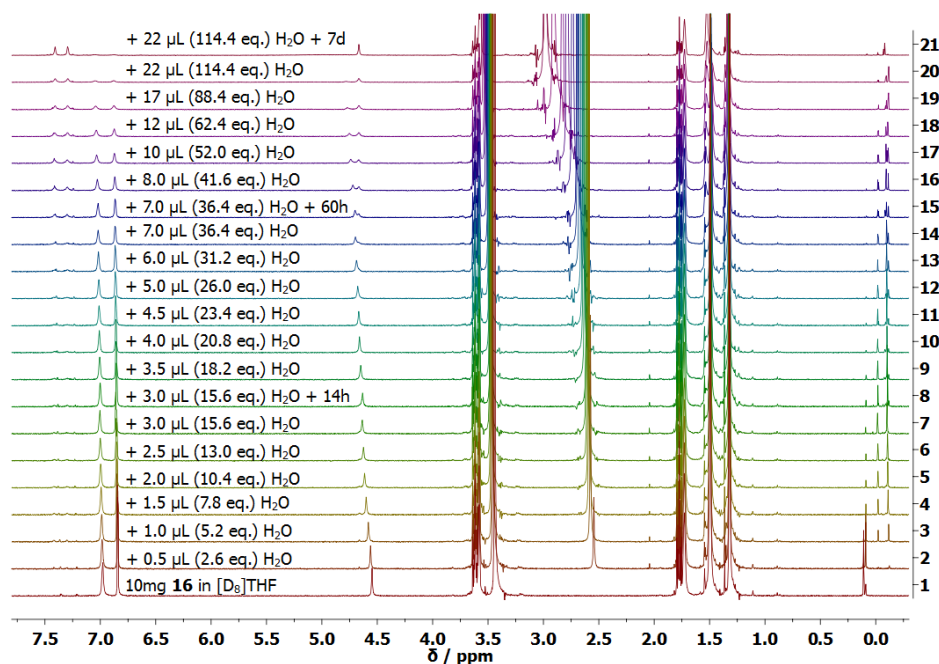


Figure 5-16. Full Stacked ^1H NMR spectra of a water titration experiment of **16** in $[\text{D}_8]\text{THF}$. Note that the resonances around 0 ppm which are obviously also affected by the successive addition of water belong to an impurity. Adapted with permission from reference^[3]. Copyright 2017, John Wiley and Sons.

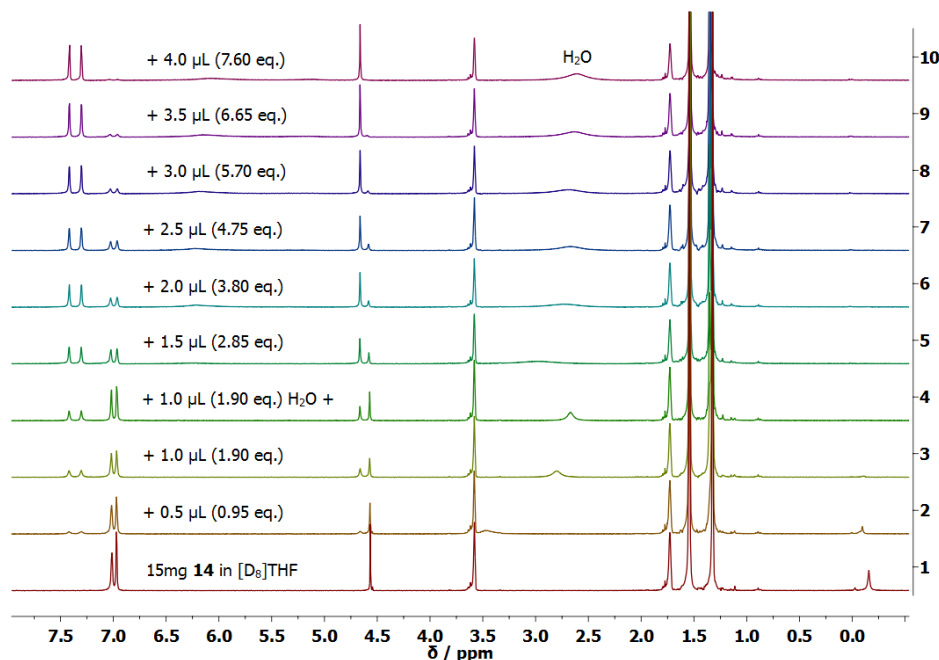


Figure 5-17. Full stacked ^1H NMR spectra of a water titration experiment of $[\text{K}\{\eta^5-(4,6-t\text{Bu-NCOC}_6\text{H}_2)_2\text{-CH}\}]_\infty$ (**14**) in $[\text{D}_8]\text{THF}$. Note that the resonances around 0 ppm which are obviously also affected by the successive addition of water belong to an impurity. Adapted with permission from reference^[3]. Copyright 2017, John Wiley and Sons.

5.4 Structural Models of 19 and 19a

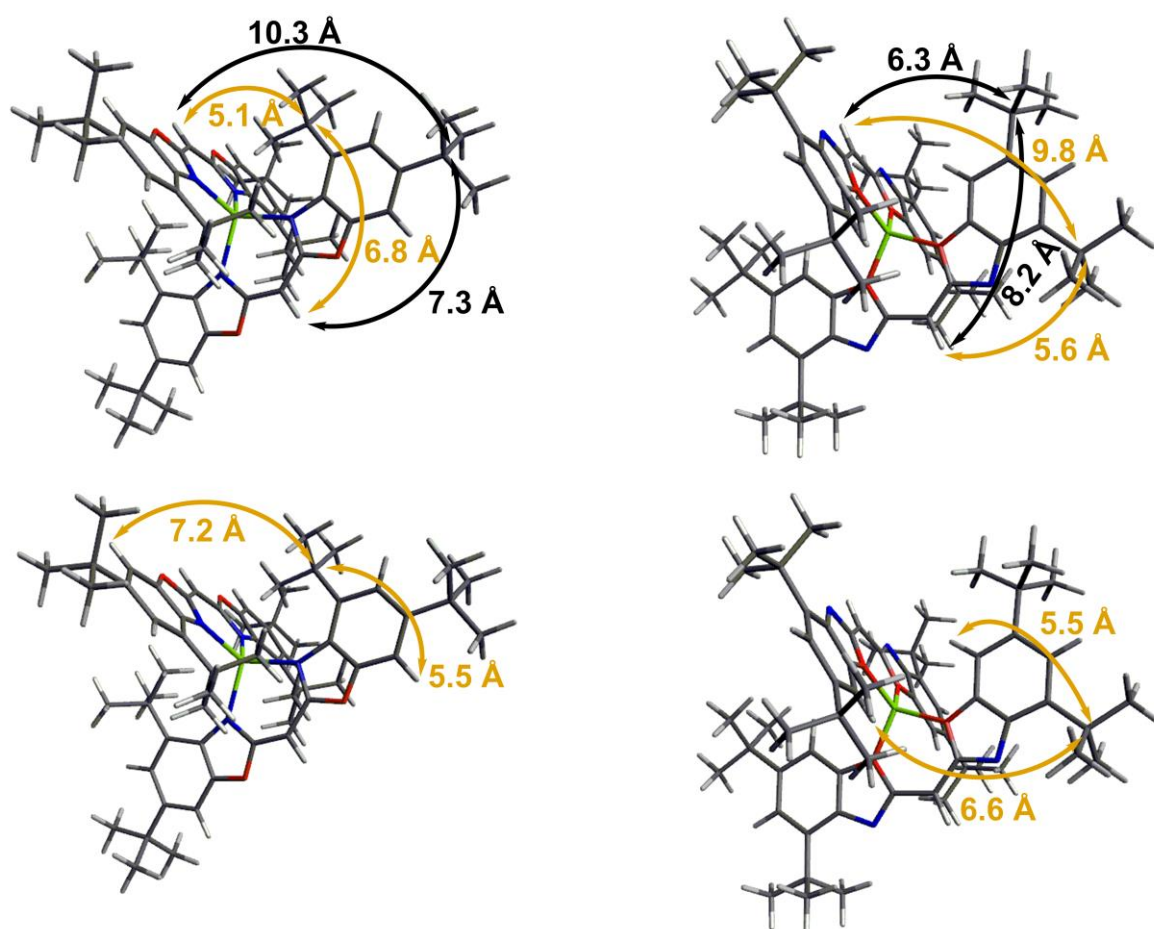


Figure 5-18. Force field optimized structural models to illustrate approximate distances. Top: Between H_{bridge} and the corresponding 4-*t*Bu substituents (quaternary C atom). Bottom: Between the hydrogen atom H7 and the corresponding 4-*t*Bu substituents (quaternary C atom). Left: N-bound **19**. Right: O-bound **19a**.

6 REFERENCES

- [1] I. Koehne, R. Herbst-Irmer, D. Stalke; *Eur. J. Inorg. Chem.* **2017**, 2017, 3322.
- [2] I. Koehne, S. Bachmann, T. Niklas, R. Herbst-Irmer, D. Stalke; *Chem. Eur. J.* **2017**, 23, 13141.
- [3] I. Koehne, S. Bachmann, R. Herbst-Irmer, D. Stalke, *Angew. Chem.* **2017**, 129, 15337; *Angew. Chem., Int. Ed.* **2017**, 56, 15141.
- [4] I. Koehne, N. Graw, T. Teuteberg, R. Herbst-Irmer, D. Stalke; *Inorg. Chem.* **2017**, 56, 14968.
- [5] B. Cornils, W. A. Herrmann, M. Muhler, C.-H. Wong (Eds.), *Catalysis from A to Z. A Concise Encyclopedia*, Wiley-VCH, Weinheim, **2007**.
- [6] F. Baier, Z. Fei, H. Gornitzka, A. Murso, S. Neufeld, M. Pfeiffer, I. Rüdener, A. Steiner, T. Stey, D. Stalke; *J. Organomet. Chem.* **2002**, 661, 111.
- [7] J. R. Khusnutdinova, D. Milstein, *Angew. Chem.* **2015**, 127, 12406; *Angew. Chem., Int. Ed.* **2015**, 54, 12236.
- [8] D. G. A. Verhoeven, M.-E. Moret; *Dalton Trans.* **2016**, 45, 15762.
- [9] C. Camp, J. Arnold; *Dalton Trans.* **2016**, 45, 14462.
- [10] T. Kottke, D. Stalke; *Chem. Ber.* **1997**, 130, 1365.
- [11] M. S. Hill, D. J. Liptrot, C. Weetman; *Chem. Soc. Rev.* **2016**, 45, 972.
- [12] R. L. Webster; *Dalton Trans.* **2017**, 46, 4483.
- [13] S. G. McGeachin; *Can. J. Chem.* **1968**, 46, 1903.
- [14] R. Bonnett, D. C. Bradley, K. J. Fisher; *Chem. Commun.* **1968**, 886.
- [15] J. E. Parks, R. H. Holm; *Inorg. Chem.* **1968**, 7, 1408.
- [16] L. Bourget-Merle, M. F. Lappert, J. R. Severn; *Chem. Rev.* **2002**, 102, 3031.
- [17] L. C. Dorman; *Tetrahedron Lett.* **1966**, 7, 459.
- [18] H. Meerwein, G. Hinz, P. Hofmann, E. Kroning, E. Pfeil; *J. Prakt. Chem.* **1937**, 147, 257.
- [19] W. J. Barry, I. L. Finar, E. F. Mooney; *Spectrochim. Acta* **1965**, 21, 1095.
- [20] J. Feldman, S. J. McLain, A. Parthasarathy, W. J. Marshall, J. C. Calabrese, S. D. Arthur; *Organometallics* **1997**, 16, 1514.
- [21] M. Asay, C. Jones, M. Driess; *Chem. Rev.* **2011**, 111, 354.
- [22] N. J. Hardman, R. J. Wright, A. D. Phillips, P. P. Power; *J. Am. Chem. Soc.* **2003**, 125, 2667.
- [23] M. Stender, A. D. Phillips, R. J. Wright, P. P. Power, *Angew. Chem.* **2002**, 114, 1863; *Angew. Chem., Int. Ed.* **2002**, 41, 1785.
- [24] M. Cheng, D. R. Moore, J. J. Reczek, B. M. Chamberlain, E. B. Lobkovsky, G. W. Coates; *J. Am. Chem. Soc.* **2001**, 123, 8738.
- [25] M. Stender, R. J. Wright, B. E. Eichler, J. Prust, M. M. Olmstead, H. W. Roesky, P. P. Power; *J. Chem. Soc., Dalton Trans.* **2001**, 3465.
- [26] Di Zhu, P. H. M. Budzelaar; *Dalton Trans.* **2013**, 42, 11343.

- [27] P. H. M. Budzelaar, A. B. van Oort, A. G. Orpen; *Eur. J. Inorg. Chem.* **1998**, 1998, 1485.
- [28] D. C. H. Do, A. Keyser, A. V. Protchenko, B. Maitland, I. Pernik, H. Niu, E. L. Kolychev, A. Rit, D. Vidovic, A. Stasch et al.; *Chem. Eur. J.* **2017**, 23, 5830.
- [29] H. G. Viehe, Z. Janousek, *Angew. Chem.* **1971**, 83, 615; *Angew. Chem., Int. Ed.* **1971**, 10, 574.
- [30] C. Chen, S. M. Bellows, P. L. Holland; *Dalton Trans.* **2015**, 44, 16654.
- [31] N. Carrera, N. Savjani, J. Simpson, D. L. Hughes, M. Bochmann; *Dalton Trans.* **2011**, 40, 1016.
- [32] L. Ferro, M. P. Coles, I. J. Day, J. R. Fulton; *Organometallics* **2010**, 29, 2911.
- [33] D. J. Doyle, P. B. Hitchcock, M. F. Lappert, G. Li; *J. Organomet. Chem.* **2009**, 694, 2611.
- [34] X. Tian, R. Goddard, K.-R. Pörschke; *Organometallics* **2006**, 25, 5854.
- [35] R. J. Wright, P. P. Power, B. L. Scott, J. L. Kiplinger; *Organometallics* **2004**, 23, 4801.
- [36] L. Kakaliou, Scanlon, B. Qian, S. W. Baek, M. R. Smith, D. H. Motry; *Inorg. Chem.* **1999**, 38, 5964.
- [37] H. M. El-Kaderi, M. J. Heeg, C. H. Winter; *Organometallics* **2004**, 23, 4995.
- [38] T. R. Dugan, X. Sun, E. V. Rybak-Akimova, O. Olatunji-Ojo, T. R. Cundari, P. L. Holland; *J. Am. Chem. Soc.* **2011**, 133, 12418.
- [39] I.-Z. El-Zoghbi, A. Ased, P. O. O. O. Oguadinma, E. Tchirioua, F. Schaper; *Can. J. Chem.* **2010**, 88, 1040.
- [40] D. J. Mindiola, *Angew. Chem.* **2009**, 121, 6314; *Angew. Chem., Int. Ed.* **2009**, 48, 6198.
- [41] T. B. Rauchfuss (Ed.) *Inorg. Synth., Vol. 35*, John Wiley & Sons, Inc; Wiley, Hoboken, NJ, USA, **2010**.
- [42] Y.-C. Tsai; *Coord. Chem. Rev.* **2012**, 256, 722.
- [43] A. D. Phillips; *Organomet. Chem.* **2014**, 39, 72.
- [44] S. Hohloch, B. M. Kriegel, R. G. Bergman, J. Arnold; *Dalton Trans.* **2016**, 45, 15725.
- [45] O. Eisenstein, P. B. Hitchcock, A. V. Khvostov, M. F. Lappert, L. Maron, L. Perrin, A. V. Protchenko; *J. Am. Chem. Soc.* **2003**, 125, 10790.
- [46] S. Harder (Ed.) *Topics in Organometallic Chemistry, Vol. 45*, Springer-Verlag, Berlin Heidelberg, **2013**.
- [47] Z. Rappoport, I. Marek (Eds.), *Lead structures in lithium organic chemistry*, John Wiley & Sons, Chichester (GB), **2004**.
- [48] R. Luisi, V. Capriati (Eds.), *Lithium Compounds in Organic Synthesis - From Fundamentals to Applications*, Wiley-VCH, Weinheim, **2014**.
- [49] D. T. Carey, E. K. Cope-Eatough, E. Vilaplana-Mafe, F. S. Mair, R. G. Pritchard, J. E. Warren, R. J. Woods; *Dalton Trans.* **2003**, 1083.
- [50] Y. Xiong, S. Yao, M. Driess; *Chem. Asian J.* **2009**, 4, 1323.
- [51] W. Clegg, E. K. Cope, A. J. Edwards, F. S. Mair; *Inorg. Chem.* **1998**, 37, 2317.
- [52] A. J. Wooles, W. Lewis, A. J. Blake, S. T. Liddle; *Organometallics* **2013**, 32, 5058.

- [53] S. J. Bonyhady, C. Jones, S. Nembenna, A. Stasch, A. J. Edwards, G. J. McIntyre; *Chem. Eur. J.* **2010**, *16*, 938.
- [54] H. M. El-Kaderi, M. J. Heeg, C. H. Winter; *Polyhedron* **2006**, *25*, 224.
- [55] J. Prust, K. Most, I. Müller, E. Alexopoulos, A. Stasch, I. Usón, H. W. Roesky; *Z. Anorg. Allg. Chem.* **2001**, *627*, 2032.
- [56] S. P. Sarish, S. Nembenna, S. Nagendran, H. W. Roesky; *Acc. Chem. Res.* **2011**, *44*, 157.
- [57] S. P. Sarish, A. Jana, H. W. Roesky, T. Schulz, D. Stalke, M. John; *Inorg. Chem.* **2010**, *49*, 3816.
- [58] S. Hong, T. J. Marks; *Acc. Chem. Res.* **2004**, *37*, 673.
- [59] G. A. Molander, J. A. C. Romero; *Chem. Rev.* **2002**, *102*, 2161.
- [60] S. Sarish, S. Nembenna, S. Nagendran, H. W. Roesky, A. Pal, R. Herbst-Irmer, A. Ringe, J. Magull; *Inorg. Chem.* **2008**, *47*, 5971.
- [61] M. H. Chisholm, J. Gallucci, K. Phomphrai; *Chem. Commun.* **2003**, 48.
- [62] M. H. Chisholm, J. C. Gallucci, K. Phomphrai; *Inorg. Chem.* **2004**, *43*, 6717.
- [63] M. R. Crimmin, M. Arrowsmith, A. G. M. Barrett, I. J. Casely, M. S. Hill, P. A. Procopiou; *J. Am. Chem. Soc.* **2009**, *131*, 9670.
- [64] M. Arrowsmith, M. R. Crimmin, A. G. M. Barrett, M. S. Hill, G. Kociok-Köhn, P. A. Procopiou; *Organometallics* **2011**, *30*, 1493.
- [65] A. G. M. Barrett, I. J. Casely, M. R. Crimmin, M. S. Hill, J. R. Lachs, M. F. Mahon, P. A. Procopiou; *Inorg. Chem.* **2009**, *48*, 4445.
- [66] A. G. M. Barrett, M. R. Crimmin, M. S. Hill, P. A. Procopiou; *Proc. R. Soc. A* **2010**, 466, 927.
- [67] S. Harder, J. Brettar; *Angew. Chem.* **2006**, *118*, 3554; *Angew. Chem., Int. Ed.* **2006**, *45*, 3474.
- [68] S. P. Green, C. Jones, A. Stasch; *Angew. Chem.* **2008**, *120*, 9219; *Angew. Chem., Int. Ed.* **2008**, *47*, 9079.
- [69] J. Spielmann, S. Harder; *Chem. Eur. J.* **2007**, *13*, 8928.
- [70] M. Arrowsmith, M. S. Hill, D. J. MacDougall, M. F. Mahon; *Angew. Chem.* **2009**, *121*, 4073; *Angew. Chem., Int. Ed.* **2009**, *48*, 4013.
- [71] J. Intemann, J. Spielmann, P. Sirsch, S. Harder; *Chem. Eur. J.* **2013**, *19*, 8478.
- [72] S. Harder; *Chem. Commun.* **2012**, 48, 11165.
- [73] B. Maitland, M. Wiesinger, J. Langer, G. Ballmann, J. Pahl, H. Elsen, C. Färber, S. Harder; *Angew. Chem.* **2017**, *129*, 12042; *Angew. Chem., Int. Ed.* **2017**, *56*, 11880.
- [74] S. Harder; *Chem. Rev.* **2010**, *110*, 3852.
- [75] J. Spielmann, S. Harder; *Eur. J. Inorg. Chem.* **2008**, 2008, 1480.
- [76] J. Spielmann, G. Jansen, H. Bandmann, S. Harder; *Angew. Chem.* **2008**, *120*, 6386; *Angew. Chem., Int. Ed.* **2008**, *47*, 6290.
- [77] M. Arrowsmith, M. S. Hill, T. Hadlington, G. Kociok-Köhn, C. Weetman; *Organometallics* **2011**, *30*, 5556.
- [78] I. Resa, E. Carmona, E. Gutierrez-Puebla, A. Monge; *Science* **2004**, *305*, 1136.

- [79] Y. Wang, B. Quillian, P. Wei, H. Wang, X.-J. Yang, Y. Xie, R. B. King, P. v. R. Schleyer, H. F. Schaefer, G. H. Robinson; *J. Am. Chem. Soc.* **2005**, *127*, 11944.
- [80] E. Carmona, A. Galindo, *Angew. Chem.* **2008**, *120*, 6626; *Angew. Chem., Int. Ed.* **2008**, *47*, 6526.
- [81] S. P. Green, C. Jones, A. Stasch; *Science* **2007**, *318*, 1754.
- [82] C. Jones; *Nat. Rev. Chem.* **2017**, *1*, 0059 EP -.
- [83] A. Stasch, C. Jones; *Dalton Trans.* **2011**, *40*, 5659.
- [84] A. J. Boutland, I. Pernik, A. Stasch, C. Jones; *Chem. Eur. J.* **2015**, *21*, 15749.
- [85] Y. Liu, S. Li, X.-J. Yang, P. Yang, B. Wu; *J. Am. Chem. Soc.* **2009**, *131*, 4210.
- [86] A. J. Boutland, D. Dange, A. Stasch, L. Maron, C. Jones, *Angew. Chem.* **2016**, *128*, 9385; *Angew. Chem., Int. Ed.* **2016**, *55*, 9239.
- [87] M. Westerhausen, *Angew. Chem.* **2008**, *120*, 2215; *Angew. Chem., Int. Ed.* **2008**, *47*, 2185.
- [88] J. Overgaard, C. Jones, A. Stasch, B. B. Iversen; *J. Am. Chem. Soc.* **2009**, *131*, 4208.
- [89] J. A. Platts, J. Overgaard, C. Jones, B. B. Iversen, A. Stasch; *J. Phys. Chem A* **2011**, *115*, 194.
- [90] L.-C. Wu, C. Jones, A. Stasch, J. A. Platts, J. Overgaard; *Eur. J. Inorg. Chem.* **2014**, *2014*, 5536.
- [91] R. D. Rieke, M. V. Hanson; *Tetrahedron* **1997**, *53*, 1925.
- [92] W. Uhlig; *Z. Naturforsch., B* **1995**, 1674.
- [93] N. G. Connelly, W. E. Geiger; *Chem. Rev.* **1996**, *96*, 877.
- [94] B. Bogdanovic; *Acc. Chem. Res.* **1988**, *21*, 261.
- [95] C. L. Raston, G. Salem; *J. Chem. Soc., Chem. Commun.* **1984**, 1702.
- [96] W. J. Evans; *Coord. Chem. Rev.* **2000**, *206-207*, 263.
- [97] M. Szostak, M. Spain, D. J. Procter; *Chem. Soc. Rev.* **2013**, *42*, 9155.
- [98] M. Szostak, M. Spain, D. J. Procter; *J. Org. Chem.* **2014**, *79*, 2522.
- [99] C. Jones, L. McDyre, D. M. Murphy, A. Stasch; *Chem. Commun.* **2010**, *46*, 1511.
- [100] S. J. Bonyhady, S. P. Green, C. Jones, S. Nembenna, A. Stasch, *Angew. Chem.* **2009**, *121*, 3017; *Angew. Chem., Int. Ed.* **2009**, *48*, 2973.
- [101] J. O. Moilanen, B. M. Day, T. Pugh, R. A. Layfield; *Chem. Commun.* **2015**, *51*, 11478.
- [102] C. Bakewell, A. J. P. White, M. R. Crimmin; *J. Am. Chem. Soc.* **2016**, *138*, 12763.
- [103] R. Lalrempuia, A. Stasch, C. Jones; *Chem. Sci.* **2013**, *4*, 4383.
- [104] R. Lalrempuia, C. E. Kefalidis, S. J. Bonyhady, B. Schwarze, L. Maron, A. Stasch, C. Jones; *J. Am. Chem. Soc.* **2015**, *137*, 8944.
- [105] A. Stasch, *Angew. Chem.* **2014**, *126*, 10364; *Angew. Chem., Int. Ed.* **2014**, *53*, 10200.
- [106] H. Braunschweig, A. Damme, R. D. Dewhurst, A. Vargas; *Nat. Chem.* **2012**, *5*, 115 EP -.
- [107] S. J. Bonyhady, D. Collis, G. Frenking, N. Holzmann, C. Jones, A. Stasch; *Nat. Chem.* **2010**, *2*, 865.
- [108] S. J. Bonyhady, N. Holzmann, G. Frenking, A. Stasch, C. Jones, *Angew. Chem.* **2016**, *129*, 8647; *Angew. Chem., Int. Ed.* **2016**, *56*, 8527.

- [109] A. Sidiropoulos, C. Jones, A. Stasch, S. Klein, G. Frenking, *Angew. Chem.* **2009**, *121*, 9881; *Angew. Chem., Int. Ed.* **2009**, *48*, 9701.
- [110] C. Jones, A. Sidiropoulos, N. Holzmann, G. Frenking, A. Stasch; *Chem. Commun.* **2012**, *48*, 9855.
- [111] P. P. Power; *Nature* **2010**, *463*, 171.
- [112] Y. Mizuhata, T. Sasamori, N. Tokitoh; *Chem. Rev.* **2009**, *109*, 3479.
- [113] C. Osuch, R. Levine; *J. Am. Chem. Soc.* **1956**, *78*, 1723.
- [114] H. Schödel, C. Näther, H. Bock, F. Butenschön; *Acta Crystallogr. B* **1996**, *52*, 842.
- [115] M. Elie, F. Sguerra, F. Di Meo, M. D. Weber, R. Marion, A. Grimault, J.-F. Lohier, A. Stallivieri, A. Brosseau, R. B. Pansu et al.; *ACS Appl. Mater. Interfaces* **2016**, *8*, 14678.
- [116] H. Gornitzka, D. Stalke; *Organometallics* **1994**, *13*, 4398.
- [117] H. Gornitzka, D. Stalke, *Angew. Chem.* **1994**, *106*, 695; *Angew. Chem., Int. Ed.* **1994**, *33*, 693.
- [118] H. Gornitzka, C. Hemmert, G. Bertrand, M. Pfeiffer, D. Stalke; *Organometallics* **2000**, *19*, 112.
- [119] M. Pfeiffer, F. Baier, T. Stey, D. Leusser, D. Stalke, B. Engels, D. Moigno, W. Kiefer; *J. Mol. Model.* **2000**, *6*, 299.
- [120] M. Pfeiffer, A. Murso, L. Mahalakshmi, D. Moigno, W. Kiefer, D. Stalke; *Eur. J. Inorg. Chem.* **2002**, *2002*, 3222.
- [121] H. Gornitzka, D. Stalke; *Eur. J. Inorg. Chem.* **1998**, *3*, 311.
- [122] A. Steiner, D. Stalke; *J. Chem. Soc., Chem. Commun.* **1993**, 444.
- [123] A. Steiner, D. Stalke; *Organometallics* **1995**, *14*, 2422.
- [124] J. Henn, K. Meindl, A. Oechsner, G. Schwab, T. Koritsanszky, D. Stalke, *Angew. Chem* **2010**, *122*, 2472; *Angew. Chem., Int. Ed.* **2010**, *49*, 2422.
- [125] M. Pfeiffer, T. Stey, H. Jehle, B. Klüpfel, W. Malisch, V. Chandrasekhar, D. Stalke; *Chem. Commun.* **2001**, 337.
- [126] B. A. McKeown, H. E. Gonzalez, T. B. Gunnoe, T. R. Cundari, M. Sabat; *ACS Catal.* **2013**, *3*, 1165.
- [127] P. Vasko, V. Kinnunen, J. O. Moilanen, T. L. Roemmele, R. T. Boere, J. Konu, H. M. Tuononen; *Dalton Trans.* **2015**, *44*, 18247.
- [128] N. S. Sommerfeld, J. Gülzow, A. Roller, K. Cseh, M. A. Jakupec, A. Grohmann, M. Galanski, B. K. Keppler; *Eur. J. Inorg. Chem.* **2017**, *2017*, 3115.
- [129] E. Sauvageot, R. Marion, F. Sguerra, A. Grimault, R. Daniellou, M. Hamel, S. Gaillard, J.-L. Renaud; *Org. Chem. Front.* **2014**, *1*, 639.
- [130] E. S. Donovan, B. M. Barry, C. A. Larsen, M. N. Wirtz, W. E. Geiger, R. A. Kemp; *Chem. Commun.* **2016**, *52*, 1685.
- [131] A. Kobayashi, T. Hasegawa, M. Yoshida, M. Kato; *Inorg. Chem.* **2016**, *55*, 1978.
- [132] A. K. Ghosh, P. Mathivanan, J. Cappiello; *Tetrahedron: Asymmetry* **1998**, *9*, 1.

- [133] H. A. McManus, P. J. Guiry; *Chem. Rev.* **2004**, *104*, 4151.
- [134] R. Rasappan, D. Laventine, O. Reiser; *Coord. Chem. Rev.* **2008**, *252*, 702.
- [135] G. Desimoni, G. Faita, K. A. Jørgensen; *Chem. Rev.* **2011**, *111*, PR284-PR437.
- [136] Q.-J. Liu, L. Wang, Q.-K. Kang, X. P. Zhang, Y. Tang, *Angew. Chem.* **2016**, *128*, 9366; *Angew. Chem., Int. Ed.* **2016**, *55*, 9220.
- [137] T. Ollevier; *Catal. Sci. Technol.* **2016**, *6*, 41.
- [138] S. Dagorne, S. Bellemin-Lapponnaz, R. Welter; *Organometallics* **2004**, *23*, 3053.
- [139] H. Arai, F. Nakadate, K. Mochida, T. Kawashima; *Organometallics* **2011**, *30*, 4471.
- [140] J. F. Kögel, S. Kusaka, R. Sakamoto, T. Iwashima, M. Tsuchiya, R. Toyoda, R. Matsuoka, T. Tsukamoto, J. Yuasa, Y. Kitagawa et al., *Angew. Chem.* **2016**, *128*, 1399; *Angew. Chem., Int. Ed.* **2016**, *55*, 1377.
- [141] E. Marchi, M. Locritani, M. Baroncini, G. Bergamini, R. Sinisi, M. Monari, C. Botta, W. Mroz, M. Bandini, P. Ceroni et al.; *J. Mater. Chem. C* **2014**, *2*, 4461.
- [142] J. M. Takacs, D. S. Reddy, S. A. Moteki, Di Wu, H. Palencia; *J. Am. Chem. Soc.* **2004**, *126*, 4494.
- [143] E. Le Roux, N. Merle, K. W. Tornroos; *Dalton Trans.* **2011**, *40*, 1768.
- [144] H. Arai, M. Matsuo, F. Nakadate, K. Mochida, T. Kawashima; *Dalton Trans.* **2012**, *41*, 11195.
- [145] F. Buch, S. Harder; *Z. Naturforsch., B Chem. Sci.* **2008**, *63b*, 169.
- [146] M. G. Davidson, P. R. Raithby, R. Snaith, D. Stalke, D. S. Wright, *Angew. Chem.* **1991**, *103*, 1696; *Angew. Chem., Int. Ed.* **1991**, *30*, 1648.
- [147] A. Walli, S. Dechert, M. Bauer, S. Demeshko, F. Meyer; *Eur. J. Inorg. Chem.* **2014**, *2014*, 4660.
- [148] V. E. Goswami, A. Walli, M. Forster, S. Dechert, S. Demeshko, M. C. Holthausen, F. Meyer; *Chem. Sci.* **2017**, *8*, 3031.
- [149] A. Walli, S. Dechert, F. Meyer; *Eur. J. Org. Chem.* **2013**, *2013*, 7044.
- [150] B. Ramalingam, M. Neuburger, A. Pfaltz; *Synthesis* **2007**, *2007*, 572.
- [151] H. Werner, R. Vicha, A. Gissibl, O. Reiser; *J. Org. Chem.* **2003**, *68*, 10166.
- [152] J. Li, S.-H. Liao, H. Xiong, Y.-Y. Zhou, X.-L. Sun, Y. Zhang, X.-G. Zhou, Y. Tang, *Angew. Chem.* **2012**, *124*, 8968; *Angew. Chem., Int. Ed.* **2012**, *51*, 8838.
- [153] H. Xiong, H. Xu, S. Liao, Z. Xie, Y. Tang; *J. Am. Chem. Soc.* **2013**, *135*, 7851.
- [154] V. L. Rendina, S. A. Goetz, A. E. Neitzel, H. Z. Kaplan, J. S. Kingsbury; *Tetrahedron Lett.* **2012**, *53*, 15.
- [155] W. H. Mills; *J. Chem. Soc., Trans.* **1922**, *121*, 455.
- [156] C. Rai, J. B. Braunwarth; *J. Org. Chem.* **1961**, *26*, 3434.
- [157] A. Abbotto, S. Bradamante, A. Facchetti, G. A. Pagani; *J. Org. Chem.* **2002**, *67*, 5753.
- [158] A. Abbotto, S. Bradamante, G. A. Pagani; *J. Org. Chem.* **1996**, *61*, 1761.

- [159] A. Abbotto, S. Bradamante, N. Capri, H. Rzepa, D. J. Williams, A. White; *J. Org. Chem.* **1996**, *61*, 1770.
- [160] S. Bradamante, G. A. Pagani; *J. Chem. Soc., Perkin Trans. 2* **1986**, 1035.
- [161] A. Abbotto, V. Alanzo, S. Bradamante, G. A. Pagani; *J. Chem. Soc., Perkin Trans. 2* **1991**, 481.
- [162] C. Gatti, A. Ponti, A. Gamba, G. Pagani; *J. Am. Chem. Soc.* **1992**, *114*, 8634.
- [163] A. Abbotto, S. Bradamante, G. A. Pagani; *J. Org. Chem.* **1993**, *58*, 444.
- [164] F. Ragaini, M. Pizzotti, S. Cenini, A. Abbotto, G. A. Pagani, F. Demartin; *J. Organomet. Chem.* **1995**, *489*, 107.
- [165] A. Abbotto, A. Facchetti, S. Bradamante, G. A. Pagani; *J. Org. Chem.* **1998**, *63*, 436.
- [166] D.-R. Dauer, D. Stalke; *Dalton Trans.* **2014**, *43*, 14432.
- [167] D.-R. Dauer, M. Flügge, R. Herbst-Irmer, D. Stalke; *Dalton Trans.* **2016**, *45*, 6149.
- [168] D.-R. Dauer, I. Koehne, R. Herbst-Irmer, D. Stalke; *Eur. J. Inorg. Chem.* **2017**, *2017*, 1966.
- [169] C. Cui, H. W. Roesky, H.-G. Schmidt, M. Noltemeyer, H. Hao, F. Cimpoesu, *Angew. Chem.* **2000**, *112*, 4444; *Angew. Chem., Int. Ed.* **2000**, *39*, 4274.
- [170] N. J. Hardman, B. E. Eichler, P. P. Power; *Chem. Commun.* **2000**, 1991.
- [171] M. S. Hill, P. B. Hitchcock; *Chem. Commun.* **2004**, 1818.
- [172] M. S. Hill, P. B. Hitchcock, R. Pongtavornpinyo; *Dalton Trans.* **2005**, 273.
- [173] D.-R. Dauer, M. Flügge, R. Herbst-Irmer, D. Stalke; *Dalton Trans.* **2016**, *45*, 6136.
- [174] D. R. Armstrong, D. Barr, R. Snaith, W. Clegg, R. E. Mulvey, K. Wade, D. Reed; *J. Chem. Soc., Dalton Trans.* **1987**, 1071.
- [175] R. E. Mulvey; *Chem. Soc. Rev.* **1991**, *20*, 167.
- [176] K. Gregory, P. v. R. Schleyer, R. Snaith; *Adv. Inorg. Chem.* **1991**, *Volume 37*, 47.
- [177] R. E. Mulvey; *Chem. Soc. Rev.* **1998**, *27*, 339.
- [178] T. Stey, M. Pfeiffer, J. Henn, S. K. Pandey, D. Stalke; *Chem. Eur. J.* **2007**, *13*, 3636.
- [179] R. G. Parr, R. G. Pearson; *J. Am. Chem. Soc.* **1983**, *105*, 7512.
- [180] R. G. Pearson; *J. Am. Chem. Soc.* **1985**, *107*, 6801.
- [181] R. G. Pearson; *J. Am. Chem. Soc.* **1963**, *85*, 3533.
- [182] J. Hey, D. Leusser, D. Kratzert, H. Fliegl, R. A. Mata, J. M. Dieterich, D. Stalke; *Phys. Chem. Chem. Phys.* **2013**.
- [183] T. Stey, J. Henn, D. Stalke; *Chem. Commun.* **2007**, 413.
- [184] C. Kling, D. Leusser, T. Stey, D. Stalke; *Organometallics* **2011**, *30*, 2461.
- [185] T. Stey, D. Stalke; *Z. Anorg. Allg. Chem.* **2005**, *631*, 2931.
- [186] H. Ben Ammar, J. Le Nôtre, M. Salem, M. T. Kaddachi, P. H. Dixneuf; *J. Organomet. Chem.* **2002**, *662*, 63.
- [187] P. Rademacher, *Strukturen organischer Moleküle*. 1, Wiley-VCH, Weinheim, **1987**.

- [188] P. Müller, R. Herbst-Irmer, A. L. Spek, T. R. Schneider, M. R. Sawaya, *Crytal Structure Refinement A Crystallographer's Guide to SHELXL*. 1st, Oxford University Press, New York, **2006**.
- [189] U. Pieper, D. Stalke; *Organometallics* **1993**, *12*, 1201.
- [190] S. Harder; *Organometallics* **2002**, *21*, 3782.
- [191] R. Shannon; *Acta Crystallogr. A* **1976**, *32*, 751.
- [192] D. Kratzert, D. Leusser, D. Stern, J. Meyer, F. Breher, D. Stalke; *Chem. Commun.* **2011**, *47*, 2931.
- [193] J. W. Elder, R. P. Mariella; *Can. J. Chem.* **1963**, *41*, 1653.
- [194] T. Steiner, *Angew. Chem.* **2002**, *114*, 50; *Angew. Chem., Int. Ed.* **2002**, *41*, 48.
- [195] S. Wu, N. Deligonal, J. D. Protasiewicz; *Dalton Trans.* **2013**, *42*, 14866.
- [196] H. Zhang, F. Y. Kwong, Y. Tian, K. S. Chan; *J. Org. Chem.* **1998**, *63*, 6886.
- [197] B. Dhawan, D. Redmore; *J. Org. Chem.* **1984**, *49*, 4018.
- [198] B. Dhawan, D. Redmore; *J. Org. Chem.* **1986**, *51*, 179.
- [199] M. Hesse, H. Meier, B. Zeeh, *Spektroskopische Methoden in der organischen Chemie*. 7th, Thieme, Stuttgart, New York, **2005**.
- [200] R. Neufeld, M. John, D. Stalke, *Angew. Chem.* **2015**, *127*, 7100; *Angew. Chem., Int. Ed.* **2015**, *54*, 6994.
- [201] C. Lambert, P. v. R. Schleyer, *Angew. Chem.* **1994**, *106*, 1187; *Angew. Chem., Int. Ed.* **1994**, *33*, 1129.
- [202] W.-P. Leung, Q. W.-Y. Ip, T.-W. Lam, T. C. W. Mak; *Organometallics* **2004**, *23*, 1284.
- [203] D. Hoffmann, W. Bauer, F. Hampel, van Eikema Hommes, Nicolaas J. R., P. v. R. Schleyer, P. Otto, U. Pieper, D. Stalke, D. S. Wright, R. Snaith; *J. Am. Chem. Soc.* **1994**, *116*, 528.
- [204] G. Rabe, H. W. Roesky, D. Stalke, F. Pauer, G. M. Sheldrick; *J. Organomet. Chem.* **1991**, *403*, 11.
- [205] E. Klemm, D. Klemm, H. H. Hörhold; *Synthesis* **1977**, *1977*, 342.
- [206] G. R. Newkome, Y. J. Joo, D. W. Evans, F. R. Fronczek, G. R. Baker; *J. Org. Chem.* **1990**, *55*, 5714.
- [207] C. Shimokawa, S. Itoh; *Inorg. Chem.* **2005**, *44*, 3010.
- [208] D. R. Lide, *CRC handbook of chemistry and physics. a ready-reference book of chemical and physical data*, CRC Press, Boca Raton, **2006**.
- [209] J. Zhang, Z. Zhang, Z. Chen, X. Zhou; *Dalton Trans.* **2012**, *41*, 357.
- [210] T. L. Rathman, J. A. Schwindeman; *Org. Process Res. Dev.* **2014**, *18*, 1192.
- [211] J. García-Álvarez, E. Hevia, V. Capriati; *Eur. J. Org. Chem.* **2015**, *31*, 6779.
- [212] J. Clayden, *Organolithiums. Selectivity for Synthesis*, Elsevier Science (Pergamon), Oxford, **2002**.
- [213] R. Taylor; *Tetrahedron Lett.* **1975**, *16*, 435.

- [214] S.-C. Kuo, F. Chen, D. Hou, A. Kim-Meade, C. Bernard, J. Liu, S. Levy, G. G. Wu; *J. Org. Chem.* **2003**, 68, 4984.
- [215] P. Wipf, S. Lim, *Angew. Chem.* **1993**, 105, 1095; *Angew. Chem., Int. Ed.* **1993**, 32, 1068.
- [216] D. Barr, P. R. Raithby, P. v. R. Schleyer, R. Snaith, D. S. Wright; *J. Chem. Soc., Chem. Commun.* **1990**, 643.
- [217] D. R. Armstrong, D. Barr, P. R. Raithby, P. v. R. Schleyer, R. Snaith, D. S. Wright; *Inorg. Chim. Acta* **1991**, 185, 163.
- [218] P. Mikulcik, P. R. Raithby, R. Snaith, D. S. Wright, *Angew. Chem.* **1991**, 103, 452; *Angew. Chem., Int. Ed.* **1991**, 30, 428.
- [219] C. Lambert, P. v. R. Schleyer, U. Pieper, D. Stalke, *Angew. Chem.* **1992**, 104, 78; *Angew. Chem., Int. Ed.* **1992**, 31, 77.
- [220] V. Capriati, F. M. Perna, A. Salomone; *Dalton Trans.* **2014**, 43, 14204.
- [221] C. Vidal, J. García-Álvarez, A. Hernán-Gómez, A. R. Kennedy, E. Hevia, *Angew. Chem.* **2014**, 126, 6079; *Angew. Chem., Int. Ed.* **2014**, 53, 5969.
- [222] C. Vidal, J. García-Álvarez, A. Hernán-Gómez, A. R. Kennedy, E. Hevia, *Angew. Chem.* **2016**, 128, 16379; *Angew. Chem., Int. Ed.* **2016**, 55, 16145.
- [223] V. Mallardo, R. Rizzi, F. C. Sassone, R. Mansueto, F. M. Perna, A. Salomone, V. Capriati; *Chem. Commun.* **2014**, 50, 8655.
- [224] F. C. Sassone, F. M. Perna, A. Salomone, S. Florio, V. Capriati; *Chem. Commun.* **2015**, 51, 9459.
- [225] L. Cicco, S. Sblendorio, R. Mansueto, F. M. Perna, A. Salomone, S. Florio, V. Capriati; *Chem. Sci.* **2016**, 7, 1192.
- [226] E. Massolo, S. Palmieri, M. Benaglia, V. Capriati, F. M. Perna; *Green Chem.* **2016**, 18, 792.
- [227] L. Cicco, M. J. Rodriguez-Alvarez, F. M. Perna, J. Garcia-Alvarez, V. Capriati; *Green Chem.* **2017**, 19, 3069.
- [228] C. L. Boldrini, N. Manfredi, F. M. Perna, V. Trifiletti, V. Capriati, A. Abbotto; *Energy Technol.* **2017**, 5, 345.
- [229] P. Vitale, V. M. Abbinante, F. M. Perna, A. Salomone, C. Cardellicchio, V. Capriati; *Adv. Synth. Catal.* **2017**, 359, 1049.
- [230] F. Milano, L. Giotta, M. R. Guascito, A. Agostiano, S. Sblendorio, L. Valli, F. M. Perna, L. Cicco, M. Trotta, V. Capriati; *ACS Sus. Chem. Eng.* **2017**, 5, 7768-7776.
- [231] G. Dilauro, M. Dell'Aera, P. Vitale, V. Capriati, F. M. Perna, *Angew. Chem.* **2017**, 129, 10334; *Angew. Chem., Int. Ed.* **2017**, 56, 10200.
- [232] K. E. Horner, P. B. Karadakov; *J. Org. Chem.* **2015**, 80, 7150.
- [233] A. Abbotto, S. Bruni, F. Cariati, G. A. Pagani; *Spectrochim. Acta Part A: Mol. Biomol. Spectr.* **2000**, 56, 1543.
- [234] S. T. H. Willems, J. C. Russcher, P. H. M. Budzelaar, B. d. Bruin, R. d. Gelder, J. M. M. Smits, A. W. Gal; *Chem. Commun.* **2002**, 148.

- [235] B. D. Ward, L. H. Gade; *Chem. Commun.* **2012**, 48, 10587.
- [236] A. Falcicchio, S. O. Nilsson Lill, F. M. Perna, A. Salomone, D. I. Coppi, C. Cuocci, D. Stalke, V. Capriati; *Dalton Trans.* **2015**, 44, 19447.
- [237] C. R. Groom, I. J. Bruno, M. P. Lightfoot, S. C. Ward; *Acta Crystallogr. B* **2016**, 72, 171.
- [238] Y. Gimbert, D. Lesage, C. Fressigné, J. Maddaluno; *J. Org. Chem.* **2017**, 82, 8141.
- [239] B. Durham, T. J. Anderson, J. A. Switzer, J. F. Endicott, M. D. Glick; *Inorg. Chem.* **1977**, 16, 271.
- [240] J. R. Bleeke, Y. F. Xie, L. Bass, M. Y. Chiang; *J. Am. Chem. Soc.* **1991**, 113, 4703.
- [241] M. L. Scheuermann, U. Fekl, W. Kaminsky, K. I. Goldberg; *Organometallics* **2010**, 29, 4749.
- [242] R. Neufeld, T. L. Teuteberg, R. Herbst-Irmer, R. A. Mata, D. Stalke; *J. Am. Chem. Soc.* **2016**, 138, 4796.
- [243] A. W. Addison, T. N. Rao, J. Reedijk, J. van Rijn, G. C. Verschoor; *J. Chem. Soc.: Dalton Trans.* **1984**, 1349.
- [244] F. Kramer, M. V. Deshmukh, H. Kessler, S. J. Glaser; *Concept. Magn. Reson. A* **2004**, 21A, 10.
- [245] G. Cornilescu, J. L. Marquardt, M. Ottiger, A. Bax; *J. Am. Chem. Soc.* **1998**, 120, 6836.
- [246] V. Diemer, H. Chaumeil, A. Defoin, A. Fort, A. Boeglin, C. Carré; *Eur. J. Org. Chem.* **2006**, 2006, 2727.
- [247] M. Basauri-Molina, D. G. A. Verhoeven, A. J. van Schaik, H. Kleijn, R. J. M. Klein Gebbink; *Chem. Eur. J.* **2015**, 21, 15676.
- [248] K. P. C. Vollhardt, N. E. Schore, *Organische Chemie*. 4th, Wiley-VCH, Weinheim, **2005**.
- [249] M. Arrowsmith, M. R. Crimmin, M. S. Hill, G. Kociok-Kohn; *Dalton Trans.* **2013**, 42, 9720.
- [250] N. Merle, K. W. Törnroos, V. R. Jensen, E. Le Roux; *J. Organomet. Chem.* **2011**, 696, 1691.
- [251] H. M. El-Kaderi, A. Xia, M. J. Heeg, C. H. Winter; *Organometallics* **2004**, 23, 3488.
- [252] P. Bailey, S. Parsons, Messenger D., S. Liddle; *CSD Communication (Private Communication)* **2005**, CCDC 276761.
- [253] H. Ott, U. Pieper, D. Leusser, U. Flierler, J. Henn, D. Stalke, *Angew. Chem.* **2009**, 121, 3022; *Angew. Chem., Int. Ed.* **2009**, 48, 2978.
- [254] R. Fleischer, D. Stalke; *Inorg. Chem.* **1997**, 36, 2413.
- [255] M. Westerhausen, H. D. Hausen, W. Schwarz; *Z. Anorg. Allg. Chem.* **1992**, 618, 121.
- [256] M. Westerhausen, W. Schwarz; *Z. Anorg. Allg. Chem.* **1993**, 619, 1455.
- [257] M. Westerhausen, H.-D. Hausen; *Z. Anorg. Allg. Chem.* **1992**, 615, 27.
- [258] M. Westerhausen, W. Schwarz; *Z. Naturforsch., Sect. b* **1992**, 47, 453.
- [259] R. Fleischer, D. Stalke; *J. Organomet. Chem.* **1998**, 550, 173.
- [260] M. Seitz, C. Capacchione, S. Bellemin-Laponnaz, H. Wadepohl, B. D. Ward, L. H. Gade; *Dalton Trans.* **2006**, 193.

- [261] C. Jones, S. J. Bonyhady, N. Holzmann, G. Frenking, A. Stasch; *Inorg. Chem.* **2011**, *50*, 12315.
- [262] B. Sedai, M. J. Heeg, C. H. Winter; *Organometallics* **2009**, *28*, 1032.
- [263] S. Harder, F. Feil, K. Knoll, *Angew. Chem.* **2001**, *113*, 4261; *Angew. Chem., Int. Ed.* **2001**, *40*, 4261.
- [264] W. Schlenk, A. Thal; *Chem. Ber.* **1913**, *46*, 2840.
- [265] T. T. Tidwell, *Angew. Chem.* **2001**, *113*, 343; *Angew. Chem., Int. Ed.* **2001**, *40*, 331.
- [266] Georg-August-University, "Virtuelles Labor I", http://www.stalke.chemie.uni-goettingen.de/virtuelles_labor/advanced/13_de.html, 1st January 2018.
- [267] M. Westerhausen; *Inorg. Chem.* **1991**, *30*, 96.
- [268] R. Fischer, M. Gärtner, H. Görls, M. Westerhausen; *Organometallics* **2006**, *25*, 3496.
- [269] M. Westerhausen; *Coord. Chem. Rev.* **1998**, *176*, 157.
- [270] M. Westerhausen, M. Gärtner, R. Fischer, J. Langer, L. Yu, M. Reiher; *Chem. Eur. J.* **2007**, *13*, 6292.
- [271] A. F. Burchat, J. Michael Chong, N. Nielsen; *J. Organomet. Chem.* **1997**, *542*, 281.
- [272] H. J. Svec; *Int. J. Mass Spectrom. Ion Processes* **1985**, *66*, 3.
- [273] J. F. de la Mora., G. J. van Berkel, C. G. Enke, R. B. Cole, M. Martinez-Sanchez, J. B. Fenn; *J. Mass Spectrom.* **2000**, *35*, 939.
- [274] H. B. Linden; *Eur. J. Mass Spectrom.* **2004**, *10*, 459.
- [275] J. H. Gross, N. Nieth, H. B. Linden, U. Blumbach, F. J. Richter, M. E. Tauchert, R. Tompers, P. Hofmann; *Anal. Bioanal. Chem.* **2006**, *386*, 52.
- [276] G. R. Fulmer, Alexander J. M. Miller, N. H. Sherden, H. E. Gottlieb, A. Nudelman, B. M. Stoltz, J. E. Bercaw, K. I. Goldberg; *Organometallics* **2010**, *29*, 2176.
- [277] Georg-August-University, "Virtuelles Labor II", http://www.stalke.chemie.uni-goettingen.de/virtuelles_labor/nmr/de.html, 1st January 2018.
- [278] G. Bodenhausen, D. J. Ruben; *Chem. Phys. Lett.* **1980**, *69*, 185.
- [279] A. Bax, M. F. Summers; *J. Am. Chem. Soc.* **1986**, *108*, 2093.
- [280] H. Friebolin, *Basic One- and Two-Dimensional NMR Spectroscopy*. 5th, WILEY-VCH Verlag, Weinheim, **2011**.
- [281] R. Neufeld, D. Stalke; *Chem. Sci.* **2015**, *6*, 3354.
- [282] S. Bachmann, R. Neufeld, M. Dzemski, D. Stalke; *Chem. Eur. J.* **2016**, *22*, 8462.
- [283] S. Bachmann, B. Gernert, D. Stalke; *Chem. Commun.* **2016**, *52*, 12861.
- [284] A. Jerschow, N. Müller; *J. Magn. Reson., Ser. A* **1996**, *123*, 222.
- [285] A. Jerschow, N. Müller; *J. Magn. Reson.* **1997**, *125*, 372.
- [286] A. Enthart, J. C. Freudenberger, J. Furrer, H. Kessler, B. Luy; *J. Magn. Reson.* **2008**, *192*, 314.
- [287] A.-C. Pöppler, H. Keil, D. Stalke, M. John, *Angew. Chem.* **2012**, *124*, 7963; *Angew. Chem., Int. Ed.* **2012**, *51*, 7843.

- [288] F. Neese; *Wiley Interdiscip. Rev.: Comput. Mol. Sci.* **2012**, 2, 73.
- [289] A. E. Reed, R. B. Weinstock, F. Weinhold; *J. Chem. Phys.* **1985**, 83, 735.
- [290] J. P. Foster, F. Weinhold; *J. Am. Chem. Soc.* **1980**, 102, 7211.
- [291] E. D. Glendening, F. Weinhold; *J. Comput. Chem.* **1998**, 19, 610.
- [292] E. D. Glendening, J. K. Badenhop, F. Weinhold; *J. Comput. Chem.* **1998**, 19, 628.
- [293] E. D. Glendening, J. K. Badenhop, A. E. Reed, J. E. Carpenter, J. A. Bohmann, C. M. Morales, F. Weinhold, *GenNBO 5.9*, University of Wisconsin, Madison, **2009**.
- [294] A. D. Becke; *Phys. Rev. A* **1988**, 38, 3098.
- [295] A. D. Becke; *J. Chem. Phys.* **1993**, 98, 5648.
- [296] F. Weigend, R. Ahlrichs; *Phys. Chem. Chem. Phys.* **2005**, 7, 3297.
- [297] S. Grimme, J. Antony, S. Ehrlich, H. Krieg; *J. Chem. Phys.* **2010**, 132, 154104.
- [298] A. D. Becke, E. R. Johnson; *J. Chem. Phys.* **2005**, 123, 154101.
- [299] E. R. Johnson, A. D. Becke; *J. Chem. Phys.* **2005**, 123, 24101.
- [300] E. R. Johnson, A. D. Becke; *J. Chem. Phys.* **2006**, 124, 174104.
- [301] J. L. Whitten; *J. Chem. Phys.* **1973**, 58, 4496.
- [302] B. I. Dunlap, J. W. D. Connolly, J. R. Sabin; *J. Chem. Phys.* **1979**, 71, 3396.
- [303] F. Neese, F. Wennmohs, A. Hansen, U. Becker; *Chem. Phys.* **2009**, 356, 98.
- [304] A. Poater, B. Cosenza, A. Correa, S. Giudice, F. Ragone, V. Scarano, L. Cavallo; *Eur. J. Inorg. Chem.* **2009**, 1759.
- [305] L. Falivene, R. Credendino, A. Poater, A. Petta, L. Serra, R. Oliva, V. Scarano, L. Cavallo; *Organometallics* **2016**, 35, 2286.
- [306] T. Kottke, D. Stalke; *J. Appl. Crystallogr.* **1993**, 26, 615.
- [307] D. Stalke; *Chem. Soc. Rev.* **1998**, 27, 171.
- [308] Georg-August-University, "Virtuelles Labor III", <http://www.stalke.chemie.uni-goettingen.de/virtuelleslabor/special/22de.html>, 1st January 2018.
- [309] T. Schulz, K. Meindl, D. Leusser, D. Stern, J. Graf, C. Michaelsen, M. Ruf, G. M. Sheldrick, D. Stalke; *J. Appl. Crystallogr.* **2009**, 42, 885.
- [310] Bruker AXS Inc., *APEX2 v2012/2*, APEX2, WI, USA, Madison, **2012**.
- [311] Bruker AXS Inc., *SAINT v8.30C*, Madison, USA, **2013**.
- [312] L. Krause, R. Herbst-Irmer, G. M. Sheldrick, D. Stalke; *J. Appl. Crystallogr.* **2015**, 48, 3.
- [313] G. M. Sheldrick, *TWINABS 2012/1*, Göttingen, **2012**.
- [314] L. Krause, R. Herbst-Irmer, D. Stalke; *J. Appl. Crystallogr.* **2015**, 48, 1907.
- [315] G. M. Sheldrick, *XPREP in SHELXTL 2014/2*, WI, USA, Madison, **2014**.
- [316] G. M. Sheldrick; *Acta Crystallogr. A* **2015**, 71, 3.
- [317] G. M. Sheldrick; *Acta Crystallogr. C* **2015**, 71, 3.
- [318] C. B. Hübschle, B. Dittrich; *J. Appl. Crystallogr.* **2011**, 44, 238.
- [319] S. Parsons, H. D. Flack, T. Wagner; *Acta Crystallogr. B* **2013**, 69, 249.

Danksagung

Zunächst möchte ich meinem Doktorvater Prof. Dr. Dietmar Stalke herzlich für die Aufnahme in seinem Arbeitskreis und die Möglichkeit und das Vertrauen für das Anfertigen dieser Arbeit danken. Zu jeder Zeit habe ich mich durch fachliche und persönliche Gespräche mit Ihnen sehr gut beraten und gefördert gefühlt. Zudem bedanke ich mich bei Prof. Dr. Franc Meyer für die Übernahme des Korreferats und bei Prof. Dr. Matthias Tamm als drittes Mitglied des Betreuungsausschusses. Allen Mitgliedern des Prüfungskomitees sei für das entgegengebrachte Interesse an meiner Forschung und die Zeit, die sie für das Lesen dieser Arbeit investiert haben gedankt.

Prof. Stalke und dem Bundesland Niedersachsen danke ich zudem für die finanzielle Förderung meiner Arbeit durch die Vergabe eines Promotionsstipendiums im Rahmen des CaSuS Programms.

Bei der Lösung aller in dieser Arbeit präsentierten Kristallstrukturen wurde ich durch Dr. Regine Herbst-Irmer mit hilfreichen Tipps, Ratschlägen und vor allem großem Engagement unterstützt. Ihr und den Strahlenbiegern des ED-Raumes, die mich in die Welt der Röntgendiffraktometerbedienung eingeführt haben, gebührt mein aufrichtiger und herzlicher Dank. In diesem Kontext sind vor allem Dr. Benedikt Niepötter und Christian Schürmann zu erwähnen. Weiterer Dank gilt meinen Kooperationspartnern Sebastian Bachmann (¹H-DOSY-ECC-MW), Thomas Niklas (NOESY, CLIP-HSQC) und Thorsten Teuteberg. (electronic structure analyses). Für letzteres sei zudem Prof. Dr. Ricardo A. Mata für die Bereitstellung der EDV-Infrastruktur gedankt. Nico Graw danke ich für das Nachziehen von Ligand während seiner Masterarbeit.

Für das Korrekturlesen dieser Arbeit und hilfreiche Verbesserungsvorschläge sei von Herzen gedankt: Claudia Schremmer, Dr. Thomas Niklas, Dr. Sebastian Bachmann und Niklas Ruth.

Eine sehr angenehme, und dadurch kurzweilige Zeit in der Uni und dem Labor und Büro habe ich Claudia Schremmer, Dr. Thomas Niklas, Janine Wegner, Dr. Sebastian Bachmann, Nico Graw, Anne Kreyenschmidt und Annika Münch zu verdanken. Zudem danke ich den Kicker Jungs und Mädels für die harten Matches in der Mittagspause. Euch allezeit ein kräftiges „pjiu-pjiu“ und lasst euch nicht „napfen“. Bei allen Arbeitskreismitgliedern möchte ich mich noch für die entspannte Atmosphäre, das gute Teamwork und die ein oder andere gesellige Grillung bedanken.

Meiner ACF Praktikantin Linda Eijsink aus Groningen und meinen beiden Lehramts-Bachelor Kandidaten Ann-Ki Roever und Daniel Lüert danke ich für ihren Einsatz und hoffe, dass sie unter meiner Anleitung etwas gelernt haben. Der guten Seele unserer Chemikalienlager, Martin Schlote, möchte ich zudem für die prompte Versorgung mit den nötigen Edukten und Glasgeräten danken.

Meiner Familie (M. S. V. D. F.) und allen lieben Menschen, die mich bis hierhin begleitet haben danke ich für ihre immerwährende Motivation und Unterstützung. Vor allem Du, liebe Nicole, hast die letzten zwei Jahre zu den besten meines Lebens gemacht! Danke!

CURRICULUM VITAE

Ingo Köhne

Humboldtallee 18
37073 Göttingen
Phone: +49 (0)176 / 84542042
E-mail: ikoehne@chemie.uni-goettingen.de

Date / place of birth: 24.01.1987 in Soltau

Nationality: german

EDUCATION

- | | |
|-------------------|---|
| 01/2014 – 03/2018 | <i>Ph.D. in Chemistry</i> at the Georg-August-University Göttingen
Thesis: “ <i>Novel Bulky Bis(benzoxazol-2-yl)methane Ligands in s-Block Metal Coordination</i> “ with Prof. Dr. D. Stalke and Prof. Dr. F. Meyer within the “ <i>Catalysis for Sustainable Synthesis</i> ” (CaSuS) Ph. D. program |
| 04/2011 – 09/2013 | <i>M.Sc. in Chemistry</i> (1.7, „gut“) at the Georg-August-University Göttingen |
| 03/2013 – 09/2013 | Master thesis under supervision of Prof. Dr. S. Schneider
“ <i>Synthese und Charakterisierung von Pinzettenkomplexen des Eisens für die homogene Katalyse</i> “ (1.3, „sehr gut“) |
| 10/2007 – 03/2011 | <i>B.Sc. in Chemistry</i> (2.1, „gut“) at the Georg-August-University Göttingen |
| 10/2010 – 01/2011 | Bachelor thesis under supervision of Prof. Dr. F. Meyer “ <i>Synthese sterisch anspruchsvoller Liganden zur Herstellung biomimetischer [2Fe-2S]-Cluster</i> “ (1.3, „sehr gut“) |
| 08/1999 – 07/2006 | <i>A-level</i> (2.2, „gut“) at the Kooperative Gesamtschule (KGS) Schneeverdingen |

EXPERIENCE AT UNIVERSITY

- | | |
|-------------------|---|
| 01/2014 – 03/2018 | Scientific researcher in the group of Prof. Dr. D. Stalke |
| 10/2014 – 03/2018 | Supervision of basic and advanced lab courses for chemistry teacher trainees as part of their Bachelor- and Master of Education studies |

04/2010 – 07/2010 Research student in the group of Prof. Dr. F. Meyer (Göttingen) within the “*International Research Training Group*” (IRTG) program

VOLUNTEER WORK, FELLOWSHIPS AND AWARDS

10/2014 – 03/2018 *Ph.D.* fellowship within the “*Catalysis for Sustainable Synthesis*“ (CaSuS) *Ph.D.* program provided by the state of Lower Saxony

06/2016 Award for the best oral presentation at the 8. Göttinger Chemie-Forum organized by “*JungChemikerForum*” (JCF) Göttingen

10/2014 Admission to the government-funded (State of Lower Saxony) *Ph.D.* program “*Catalysis for Sustainable Synthesis*“ (CaSuS)

11/2010 – 10/2012 Elected students council speaker within the student self-administration at the *Max-Kade* students hostel Göttingen

PERSONAL SKILLS

Languages German (mother tongue)
English, fluent (ZESS Göttingen, Scientific English I, C1)
Spanish, basic (ZESS Göttingen, A1)

Computer applications MS-Word, Power Point
Excel, Adobe Photoshop (basic knowledge)
Scientific data handling: ChemDraw, Origin, MestreNova, Avogadro, Mercury
Bruker APEXIII, SHELXTL bundle, ShelXle, PLATON (basic knowledge)

Additional qualifications *IDEASxSKILLS* Workshop “*Führungsexzellenz in der globalen Wissensgesellschaft*” (02/2015)
IDEASxSKILLS Workshop “*Interkulturelle Zusammenarbeit*” (10/2015)

KC-Klein&Collegen Workshop “*Betriebswirtschaft kompakt (Business Management Fundamentals) – European Business Competence Licence (EBC*L Level A)*“ (12/2015)
Training as “*Brandschutzhelfer*” (11/2016)

Expertise According to §5 Chemikalienverbotsverordnung

CONFERENCES AND WORKSHOPS

- “Catalysis for Sustainable Synthesis“ (CaSuS) kick-off workshop, 01–02. 2014 in Holle (Poster)
- “Center of Materials Crystallography” (CMC) meeting, 09.–10. 10. 2014 in Aarhus (Talk)
- “Niedersächsisches Katalyse Symposium“ (NiKaS), 16.–17. 10. 2014 in Göttingen (Poster; Talk-session chairman)
- 18. “Norddeutsches Doktorandenkolloquium” (NDDK), 07.–08. 09. 2015 in Goslar (Poster)
- “Center of Materials Crystallography” (CMC) meeting, 26. 04. 2016 in Aarhus (Talk)
- 8. Göttinger Chemie-Forum, 21. 06. 2016 in Göttingen (Talk; Award for best oral presentation)
- “Niedersächsisches Katalyse Symposium“ (NiKaS), 19.–20. 10. 2016 in Braunschweig (Poster)

SCIENTIFIC PUBLICATIONS

1. I. Koehne, T. J. Schmeier, E. A. Bielinsky, C. J. Pan, P. O. Lagaditis, W. H. Bernskoetter, M. K. Takase, Ch. Würtele, N. Hazari, S. Schneider, “Synthesis and Structure of Six-Coordinate Iron Borohydride Complexes Supported by PNP Ligands“, *Inorg. Chem.* **2014**, 53, 2133-2143.
2. D. Ganapathy, J. R. Reiner, L. E. Löffler, L. Ma, B. Gnanaprakasam, B. Niepötter, I. Koehne, L. F. Tietze, “Enantioselective Total Synthesis of Secalonic Acid E“, *Chem. Eur. J.* **2015**, 21, 16807-16810.
3. D.-R. Dauer, I. Koehne, R. Herbst-Irmer, D. Stalke, “From Bis(imidazol-2-yl)methanes to Asymmetrically Substituted Bis(heterocyclo)methanides in Metal Coordination“, *Eur. J. Inorg. Chem.* **2017**, 2017, 1966-1978.
4. I. Koehne, R. Herbst-Irmer, D. Stalke, “Bis(4-methylbenzoxazol-2-yl)methanide in s-Block Metal Coordination“, *Eur. J. Inorg. Chem.* **2017**, 2017, 3322-3326.
5. I. Koehne, S. Bachmann, T. Niklas, R. Herbst-Irmer, D. Stalke, “A Novel Bulky Heteroaromatic-Substituted Methanide Mimicking NacNac: Bis(4,6-tert-butylbenzoxazol-2-yl)methanide in s-Block Metal Coordination“, *Chem. Eur. J.* **2017**, 23, 13141-13149.
6. I. Koehne, S. Bachmann, R. Herbst-Irmer, D. Stalke, “A Water-Containing Organopotassium Compound Based on Bis(4,6-tBu-benzoxazol-2-yl)methanide and Its Unexpected Stability to Hydrolysis“, *Angew. Chem.* **2017**, 129, 15337-15342; *Angew. Chem. Int. Ed.* **2017**, 56, 15141-15145.
7. I. Koehne, N. Graw, T. Teuteberg, R. Herbst-Irmer, D. Stalke, “Introducing NacNac-Like Bis(4,6-isopropylbenzoxazol-2-yl)methanide in s-Block Metal Coordination“, *Inorg. Chem.* **2017**, 56, 14968-14978.

Göttingen, 28.02.2018